Universidade de Aveiro Departamento de Física
2011

Sandra Marta Nobre Plecha

Contribuição para o Estudo da Morfodinâmica da Embocadura da Ria de Aveiro

Contribution to the Study of the Ria de Aveiro Inlet Morphodynamics

Universidade de Aveiro Departamento de Física
2011

Sandra Marta Nobre Plecha

Contribuição para o Estudo da Morfodinâmica da Embocadura da Ria de Aveiro

Contribution to the Study of the Ria de Aveiro Inlet Morphodynamics

Dissertação apresentada à Universidade de Aveiro para cumprimento dos requisitos necessários à obtenção do grau de Doutor em Física, realizada sob a orientação científica do Prof. Doutor João Miguel Dias, Professor Auxiliar do Departamento de Física da Universidade de Aveiro, e co-orientação científica do Prof. Doutor Paulo Silva, Professor Auxiliar do Departamento de Física da Universidade de Aveiro e da Doutora Anabela Oliveira do Laboratório Nacional de Engenharia Civil.

Este trabalho foi realizado no âmbito dos Projectos:
EMERA - POCI/ECM/59958/2004
G-Cast – GRID/GRI/81733/2006
ADAPTARia – PTDC/AAC-CLI/100953/2008
com o apoio financeiro da Fundação para a Ciência e a Tecnologia no âmbito do III Quadro Comunitário de Apoio.

O autor foi financiado pela Fundação para a Ciência e a Tecnologia – FCT e do FSE no âmbito do III Quadro Comunitário de Apoio através da Bolsa de Doutoramento FRH/BD/29368/2006.

To my parents and sister

o júri

Presidente

Doutor António Carlos Matias Correia
Professor Catedrático da Universidade de Aveiro

Vogais

Doutora Anabela Pacheco de Oliveira
Investigadora Principal do Núcleo de Tecnologias da Informação do Laboratório Nacional de Engenharia Civil

Doutor Xavier Pierre Jean Bertin
Investigador Auxiliar do Centre National de La Recherche Scientifique, Université de La Rochelle - França

Doutor Rui Pires de Matos Taborda
Professor Auxiliar da Faculdade de Ciências da Universidade de Lisboa

Doutor João Miguel Sequeira Silva Dias
Professor Auxiliar da Universidade de Aveiro

Doutor Paulo Manuel Cruz Alves da Silva
Professor Auxiliar da Universidade de Aveiro

Doutor Nuno Alexandre Firmino Vaz
Investigador Auxiliar do CESAM – Centro de Estudos do Ambiente e do Mar da Universidade de Aveiro

Acknowledgements

This work was supported by the FCT through a PhD grant - $FRH/BD/29368/2006$ and partly supported by FCT and by European Union (COMPETE, QREN, FEDER) in the frame of the research projects: $POCI/ECM/59958/2004$: EMERA - Study of the Morphodynamics of the Ria de Aveiro Lagoon Inlet; $GRID/GRI/81733/2006$: G-cast - Application of GRID-computing in a coastal morphodynamics nowcast-forecast system and $PTDC/AAC-CLI/100953/2008$: ADAPTARia - Climate Change Modelling on Ria de Aveiro Littoral - Adaptation Strategy for Coastal and Fluvial Flooding.

In the first place, a special thank to my supervisors Professor João Miguel Dias, Professor Paulo Silva and Anabela Oliveira for all the scientific support and patience along the years in my journey for sediments.

To André Fortunato and Nicolas Bruneau from LNEC and Xavier Bertin from Université de La Rochelle thank so much for all the help with the numerical model MORSYS2D and readiness in clarifying the questions. A thanks also to Francisco Sancho from LNEC for the help provided in the initial work.

Thanks to Professor Manuel Barroso, Doctor Martinho Almeida and Mr. Franscisco Reis for all the technical support.

A big thanks for all my colleagues at the "Laboratório de Atmosfera" for the friendly environment and fellowship, especially to my senior Nuno Vaz and my "younger twin" Ana Picado.

To my parents and nephew a giant thanks for all the love. To my sister, thanks for being an angel always present.

To Nuno, thanks for all the support and for the last boring months.

palavras-chave

Morfodinâmica; embocadura de laguna; modelação; forçamento de maré; forçamento de ondas.

resumo

Ao longo dos anos observou-se junto ao quebramar norte da embocadura da *Ria de Aveiro* um aumento da profundidade, que poderá colocar em perigo a estabilidade desta mesma estrutura. É igualmente observada uma tendência de acreção no canal de navegação desta laguna, colocando em risco a navegabilidade nesta região. Para compreender a causa destas tendências e de outras observadas, é necessário um conhecimento do transporte de sedimentos nesta região de estudo. Este trabalho tem assim como objectivo principal a compreensão dos processos físicos dominantes no transporte de sedimentos na embocadura e área adjacente da *Ria de Aveiro*, aumentando os conhecimentos da morfodinâmica desta região.

A metodologia seguida neste estudo consistiu na análise de levantamentos topo-hidrográficos realizados pela Administração do Porto de Aveiro e de resultados de simulações numéricas efectuadas com o sistema de modelos morfodinâmico MORSYS2D. A análise dos levantamentos foi feita através do estudo de evolução temporal da batimetria. A análise numérica teve como base a implementação do modelo para a área de estudo, análises de sensibilidade das fórmulas de cálculo do transporte de sedimentos à variação de parâmetros de entrada (por exemplo: profundidade, diâmetro médio do sedimento, velocidade da corrente de maré), e análise dos resultados numéricos de fluxos de sedimentos e de variações batimétricas. As simulações efectuadas consideraram apenas o forçamento de correntes de maré e o forçamento conjunto de maré e ondas no transporte de sedimentos. No caso do forçamento de ondas foram efectuadas simulações com ondas monocromáticas e com um regime de agitação real.

Os resultados revelaram que os padrões observados para o transporte residual de sedimentos têm origem na configuração do canal. Verificou-se também que no interior da laguna os fluxos são maioritariamente induzidos pela acção do campo de correntes de maré, restringindo-se a acção do campo de agitação à embocadura e costa adjacente.

No canal de navegação são previstos fluxos residuais de sedimentos direccionados para o exterior da laguna que oscilam entre 7 e 40 m^3/dia e originam acreções na ordem de 10 m^3/dia na região menos profunda e de 35 m^3/dia para a região entre o *marégrafo* e o *triângulo das marés*. Na região da embocadura os fluxos residuais de sedimentos são de aproximadamente 30 m^3/dia gerando tendências de erosão de aproximadamente 20 m^3/dia. Na área exterior da embocadura é prevista acreção a Norte da embocadura e erosão a Sul às taxas de 250 e 1500 m^3/dia, respectivamente.

Concluiu-se ainda que as ondas com maior contributo para o fluxo residual de sedimentos têm alturas compreendidas entre 4 e 5 m. No entanto, as ondas de tempestade, com alturas superiores a 5 m, apesar de terem apenas 10% de frequência de ocorrência são responsáveis por 25% do transporte de sedimentos observado.

keywords Morphodynamic; lagoon inlet; modeling; tidal forcing; wave forcing.

abstract

Over the years it was observed at the *Ria de Aveiro* lagoon inlet, near the head of the north breakwater, a depth increase that might threaten the stability of this structure. A trend of accretion in the navigation channel of this lagoon is observed, endangering the navigation in this region. In order to understand the origin of these and other trends observed, the knowledge of the sediment transport in the study area is imperative. The main aim of this work is understanding the dominant physical processes in the sediment transport of sediment at the *Ria de Aveiro* lagoon inlet and adjacent area, improving knowledge of this region morphodynamics.

The methodology followed in this study consisted in the analyzes of the topo-hydrographic surveys performed by the Administration of the Aveiro Harbor, and in the numerical simulations results performed with the morphodynamic modeling system MORSYS2D. The analysis of the surveys was performed by studying the temporal evolution of the bathymetry. The numerical analysis was based on the implementation of the model at the study area, sensitivity analysis of the formulations used to compute the sediment transport to the variation of input parameters (e.g. depth, sediment size, tidal currents) and analysis of the sediment fluxes and bathymetric changes predicted. The simulations considered as sediment transport forcing the tidal currents only and the coupled forcing of tides and waves. Considering the wave effect as sediment transport forcing, both monochromatic waves and a wave regime were simulated.

The results revealed that the observed residual sediment transport patterns are generated due to the channel configuration. Inside the lagoon the fluxes are mainly induced by the tidal currents action, restricting the action of waves to the inlet and adjacent coast.

In the navigation channel the residual sediment fluxes predicted are directed offshore with values between 7 and 40 m^3/day generating accretions of approximately 10 m^3/day for the shallower region and 35 m^3/day for the region between the *tidal gauge* and the *triângulo das marés*. At the inlet, the residual fluxes are approximately 30 m^3/day inducing trends of erosion of approximately 20 m^3/day. At the North side of the nearshore accretion is predicted, while at the South side is predicted erosion, at the rates of 250 and 1500 m^3/day, respectively.

It was also concluded that the waves with higher contribution to the residual sediment fluxes are those with heights between 4 and 5 m. However, the storm waves with heights bigger than 5 m, despite their 10% of frequency of occurrence are responsible for 25% of the observed sediment transport.

Contents

Acknowledgements **i**

Resumo **iii**

Abstract **v**

List of Figures **xi**

List of Tables **xix**

List of Symbols **xxi**

1 Introduction **1**

1.1 Motivation 1

1.2 Literature review 4

1.3 Structure of this work 10

1.4 Prior Dissemination 11

2 Theoretical Background on Lagoons and Tidal Inlets **13**

2.1 Introduction 13

2.2 Classification 14

2.3 Lagoons Hydrodynamics 16

2.4 Lagoon inlets 17

2.5 Sediment transport 20

2.5.1 Sediment transport formulations 20

2.5.2 Longshore sediment transport formulations 29

2.6 Morphological evolution 32

2.7 Conclusions 33

3 Characterization of the Ria de Aveiro Lagoon and Adjacent Coastal Zone **35**

3.1 Introduction 35

3.2 Origin of the Ria de Aveiro lagoon and its inlet 36

3.3 Morphological characterization 39
3.4 Distribution of bottom sediments 46
3.5 Hydrodynamic characterization 49
3.6 Wave regime 52
3.7 Representative waves and longitudinal sediment transport 53
3.7.1 Wave regime considered 53
3.7.2 Simplifications of the wave regime 56
3.8 Conclusions 67

4 MORSYS2D and Models Setup 69
4.1 Introduction 69
4.2 Methodology 69
4.3 Numerical model 70
4.3.1 ELCIRC 70
4.3.2 SWAN 73
4.3.3 SAND2D 74
4.4 Models setup and hydrodynamic validation 76
4.4.1 ELCIRC 76
4.4.2 SAND2D 86
4.4.3 SWAN 86

5 Morphodynamic Simulations Forced by Tidal Currents 91
5.1 Sensitivity analysis 91
5.1.1 Numerical filters 91
5.1.2 Influence of the choice of the sediment transport formula 93
5.1.3 Impacts of spring/neap tide 98
5.1.4 Depth and bottom sediment size distribution 101
5.2 Period June 2001 - March 2003 103
5.3 Period June 2001 - September 2005 107
5.4 Discussion 108

6 Morphodynamic Simulations Forced by Tidal Currents and Waves 113
6.1 Sensitivity analysis 114
6.1.1 Influence of the choice of the sediment transport formula 114
6.2 Simulations forced with a single wave 116
6.2.1 Simulation considering a regular monochromatic wave with height 0 m 116
6.2.2 Simulations forced with a regular monochromatic wave 118
6.3 Simulations forced with a wave regime 126
6.3.1 Storm events 126
6.3.2 Period June 2001 - March 2003 129

6.3.3 Period June 2001 - September 2005 134
6.4 Discussion 138

7 Conclusions and Future Work **141**

8 Appendix **147**

Bibliography **151**

List of Figures

1.1 Location and bathymetry of the Ria de Aveiro lagoon and offshore area. . . . 2
1.2 Bathymetry of the study area. 10

2.1 Hydrodynamic classification of lagoons. From Hayes [1979]. 15
2.2 Schematization of (a) tide and (b) wave dominated lagoons. From Heap et al. [2001]. 16
2.3 Schematic diagram of flood and ebb currents outside an inlet [O'Brien, 1969]. 17
2.4 Three models of inlet behavior and sediment bypassing for mixed-energy coasts (from Fitzgerald [1988]). 19
2.5 Computed transport rate q_s ($\mathrm{kgm^{-1}s}$) in function of d_{50} (mm), considering (a) only the tidal currents and (b) tidal currents coupled to a regular monochromatic wave. 26
2.6 Computed transport rate q_s ($\mathrm{kgm^{-1}s}$) in function of d_{50} (millimetre) for a tidal cycle forced by tidal currents only (a) and (b) and forced by tidal currents coupled with a wave regime (c) and (d), for a depth of (a) and (c) 10 m and (b) and (d) 20 m. The left (right) columns in (a), (b), (c) and (d) represent the transport rates at neap (spring) tide condition. 27
2.7 Locations of the points where the velocity is used to perform the sensitivity analysis presented. 28
2.8 Values of the ratio q/q_{mean} for a tidal cycle forced by tidal currents only (a) and (b) and forced by tidal currents coupled with a wave regime (c) and (d), for a depth of (a) and (c) 10 m and (b) and (d) 20 m. The left (right) columns in (a), (b), (c) and (d) represent the transport rates at neap (spring) tide condition. The middle (bottom) panel in (a), (b), (c) and (d) represent the transport rates considering a sediment size of $d_{50} = 0.3$ mm ($d_{50} = 1.5$ mm). . 29

3.1 Probable evolution of the coastline between Espinho and Mira, with reference to main salt ponds and islands and showing the position of the river mouth. The 1808 inlet was artificially open. (-) Possible shoreline position in IX-XII centuries; (-) Possible shoreline position in XIV-XV centuries; (△) Salt pans in X-XIII centuries; (⇒) inlet localization in the years specified. From Bastos [2009]. 36
3.2 Bathymetry in meters of the Ria de Aveiro lagoon inlet corresponding to the surveys of (from left to right, top to bottom): 1987/88, June 2001, March 2003, July 2003, September 2003, November 2003, March 2004, September 2004 and October 2004. The values in the axis are in metres. 41
3.3 Bathymetry in meters of the Ria de Aveiro lagoon inlet corresponding to the surveys of (from left to right, top to bottom): March 2005, September 2005, October 2006, May 2007, September 2007, January 2008, June 2008, December 2008 and June 2010. The values in the axis are in metres. 42
3.4 Observed bathymetric changes (metre) in the study area between 1987/88 and June 2001. The negative (positive) values represent erosion (accretion). Solid lines represent the bathymetry in 1987/88. The values in the axis are in metres. 43
3.5 Observed bathymetric changes (metre) in the study area between June 2001 and March 2003. The negative (positive) values represent erosion (accretion). Solid lines represent the bathymetry in June 2001. The values in the axis are in metres. 43
3.6 Observed bathymetric changes (metre) in the study area between June 2001 and September 2005. The negative (positive) values represent erosion (accretion). Solid lines represent the bathymetry in June 2001. The values in the axis are in metres. 44
3.7 Sections location where transport of sediments is computed and regions where sedimentation rates are computed. The sections and regions were defined in order to be coincident with variations in the bathymetric or lagoon inlet geometry. 44
3.8 Depth along the sections illustrated in Figure 3.7 observed in June 2001 (-) and September 2005 (-) surveys. The lower panel figure illustrates the depth along the longitudinal section (dashed line in Figure 3.7). The y (x) values in the x-axis increases from South to North (West to East). 45
3.9 Observed bathymetric changes (metre) in the study area between September 2005 and 2010. The negative (positive) values represent erosion (accretion). Solid lines represent the bathymetry in September 2005. The values in the axis are in metres. 46

3.10 Observed bathymetric changes (metre) in the study area between (a) March-November 2003, (b) November 2003-March 2004, (c) March-October 2004 and (d) October 2004-March 2005. The negative (positive) values represent erosion (accretion). The values in the axis are in metres. 47
3.11 Sediment size (a) classes for the study area considered in the numerical simulations (millimetre). (b) Location of the sediment data samples with the corresponding sediment size color (millimetre). (c) Sediment size distribution for the study area (millimetre). 48
3.12 (a) Sea surface elevation (m) relative to ZH and (b) velocity intensity (ms^{-1} in the Ria de Aveiro lagoon inlet. The vertical bars in (a) delimit one neap and one spring tide period. 50
3.13 Top panel: Sea surface elevation (m) relative to ZH and velocity. Center and lower panels corresponds to ebb and flood velocities, respectively (dots in the upper panel). In the left and right panels are illustrated the velocities for neap and spring neap tide, respectively. 51
3.14 Offshore wave regime at Aveiro. (a) Wave directions and heights (metre) and (b) wave periods (seconds). 52
3.15 Number of wave records in function of the month, for the two buoys located in Figueira da Foz ($40^o11'08''N - 9^o8'44''$W, depth 92 m ZH) and Leixões ($41^o19'00''N - 8^o59'00''$W, depth 83 m ZH) [Capitão et al., 1997; Costa et al., 2003]. 54
3.16 Sensitivity analysis of the longshore sediment transport formulations to (a) d_{50} (mm) and (b) the bottom slope (m). 55
3.17 Frequency of occurrence of the (a) incident wave angles and (b) wave heights of the complete wave regime at deepwater (+) and at the breaker line (o). . . 60

4.1 Schematic diagram of the MORSYS2D morphodynamic model system. 71
4.2 Unstructured grid of the Ria de Aveiro lagoon. 77
4.3 Bathymetry imposed as initial condition of the Ria de Aveiro lagoon. 78
4.4 Ria de Aveiro lagoon bathymetry and location of the stations where data field data are available. 79
4.5 Comparison between predicted and observed SSE. Solic line: model results from this study (red) and from Oliveira et al. (2007) (blue) simulations; black circles: measurements. In the panels is referred the day of each compared period. 80
4.6 Distributions of tidal amplitude and phase for M_2, S_2, O_1, K_1 and M_4 constituents. Measurements (dark green); model results obtained in this study (light green) and using the Oliveira et al. [2007] grid (yellow). 83

4.7 Asymmetric coefficients: amplitude ratio, relative phase (^{o}) and difference between ebb and flood duration (hours) along the axis of the four main channels of the Ria de Aveiro lagoon. Results obtained in this study (blue) and Oliveira et al. [2007] (green). 85
4.8 Computational (a) regular and (b) curvilinear grids used in the wave model SWAN. 87
4.9 Data and model wave parameter comparisons from the wave directional buoy located at Leixões (red) and from WW3 model offshore Aveiro (blue), for the year of 1998. 89
4.10 Scatter diagrams of modeled H_s versus measured H_s for the entire data set. The green line corresponds to $y = x$ and the red line the linear regression for the data represented. 90

5.1 (a) Final bathymetry (metre) of the Ria de Aveiro lagoon inlet computed after 1 year for EH formulation. (b) Difference between the computed final and initial bathymetries (metre) for a 1 years simulation. From top to bottom: Considering the influence of: a non-linear bathymetric filter, a gradient filter, a global filter, a flux filter and a diffusive filter (Section 5.1.1). In (b) the solid lines illustrate the 2001 bathymetry. The negative (positive) values represent erosion (accretion). The values in axes are in metres. 92
5.2 (a) and (b) Residual sediment flux (m^2s^{-1}) for SvR formulation. (c) Final bathymetry (metre) of the Ria de Aveiro lagoon inlet computed after 1 year for SvR formulation. (d) Difference between the computed final and initial bathymetries (metre) for a 1 year simulation. In (d) the solid lines illustrate the 2001 bathymetry. The negative (positive) values represent erosion (accretion). The values in axes are in metres. 94
5.3 Same as Figure 5.2 for Bha formulation. Black areas represents data out of the scale represented. 95
5.4 Same as Figure 5.2 for EH formulation. 95
5.5 Same as Figure 5.2 for kk formulation. 96
5.6 Same as Figure 5.2 for Bi formulation. 96
5.7 Same as Figure 5.2 for MPM formulation. 97
5.8 Same as Figure 5.2 for vR formulation. Black areas represents data out of the scale represented. 97
5.9 Same as Figure 5.2 for AW formulation. 98
5.10 Sediment flux (m^2s^{-1}) for EH formulation (top) and AW formulation (bottom) for neap tide (left) and spring tide (right) conditions. 99

5.11 (a) and (b) Residual sediment flux (m^2s^{-1}) for EH formulation considering d_{50} constant in space. (c) Final bathymetry (metre) of the Ria de Aveiro lagoon inlet computed after 60 days for EH formulation. (d) Difference between the computed final and initial bathymetries (metre) for a 60 days simulation. In (d) the solid lines illustrate the initial bathymetry. The negative (positive) values represent erosion (accretion). The values in axes are in metres. 102
5.12 (a) and (b) Residual sediment flux (m^2s^{-1}) for EH formulation considering d_{50} and h initially constant in space. (c) Final bathymetry (metre) of the Ria de Aveiro lagoon inlet computed after 60 days for EH formulation. (d) Difference between the computed final and initial bathymetries (metre) for a 60 days simulation. In (d) the solid lines illustrate the initial bathymetry. The negative (positive) values represent erosion (accretion). The values in axes are in metres. 103
5.13 Left: Final bathymetry (metre) of the Ria de Aveiro lagoon inlet computed after 1.75 years for (from top to bottom) SvR, EH, kk and AW formulations. Right: Difference between the computed final and initial bathymetries (metre) for a 1.75 year simulation (the solid lines illustrate the 2001 bathymetry). The negative (positive) values represent erosion (accretion). The values in axes are in metres. 104
5.14 Depth along the sections illustrated in Figure 3.7 observed in June 2001 (o) and March 2003 (+) surveys and simulated with the formulations: SvR, EH, kk and AW. The set of figures at the top panel correspond to the sections 1-7 and the figure at the bottom panel correspond to the longitudinal section (dashed line in Figure 3.7). The y (x) values in the x-axis increases from South to North (West to East). 105
5.15 Sedimentation rate between June 2001 and March 2003 obtained using the sediment transport formulations of SvR, EH, kk and AW. 106
5.16 (a) Final bathymetry (metre) of the Ria de Aveiro lagoon inlet computed after 4.25 years for EH formulation. (b) Difference between the computed final and initial bathymetries (metre) for a 4.25 years simulation. In (b) the solid lines illustrate the 2001 bathymetry. The negative (positive) values represent erosion (accretion). The values in axes are in metres. 107
5.17 Depth along the sections illustrated in Figure 3.7 observed in September 2005 (+) and predicted using EH formulation (-). The set of figures at the top panel correspond to the sections 1-7 and the figure at the bottom panel correspond to the longitudinal section (dashed line in Figure 3.7). The y (x) values in the x-axis increases from South to North (West to East). 109
5.18 Observed and predicted sedimentation rate between June 2001 and September 2005 110

6.1 (a) and (b) Residual sediment flux (m^2s^{-1}) for AW formulation. (c) Final bathymetry (metre) of the Ria de Aveiro lagoon inlet computed after 1 year for AW formulation. (d) Difference between the computed final and initial bathymetries (metre) for a 1 year simulation. In (d) the solid lines illustrate the 2001 bathymetry. The negative (positive) values represent erosion (accretion). The values in axes are in metres. 115
6.2 Same as Figure 6.1 for Bi formulation. Black areas represents data out of the scale represented. 116
6.3 Same as Figure 6.1 for SvR formulation. Black areas represents data out of the scale represented. 117
6.4 (a) and (b) Residual sediment flux (m^2s^{-1}) for AW formulation considering the wave height equal to 0 m. 117
6.5 (a) and (b) Residual sediment flux (m^2s^{-1}) for Wave #1. (c) Final bathymetry (metre) of the Ria de Aveiro lagoon inlet computed after 60 days. (d) Difference between the computed final and initial bathymetries (metre) for a 60 days simulation. In (d) the solid lines illustrate the 2001 bathymetry. The negative (positive) values represent erosion (accretion). The values in axes are in metres. 119
6.6 Same as Figure 6.5 for Wave #2. 120
6.7 Same as Figure 6.5 for Wave #3. 120
6.8 Same as Figure 6.5 for Wave #4. 121
6.9 Same as Figure 6.5 for Wave #5. 121
6.10 Same as Figure 6.5 for Wave #6. 122
6.11 Same as Figure 6.5 for Wave #7. 122
6.12 Same as Figure 6.5 for Wave #8. 123
6.13 Residual sediment flux (m^3day^{-1}) for the 8 representative waves. 124
6.14 Sedimentation rate m^3day^{-1} for 60 days obtained for the 8 representative waves. 125
6.15 Characteristics of the period chosen enclosing a storm event: from 1 October to 31 December 2001. Offshore (a) waves height (metre) and (b) distribution of wave height and direction. 126
6.16 (a),(c) Significant wave height and (b),(d) wave orbital velocity for a day in normal conditions (01 Oct, top panel) and in a storm event (09 Oct, bottom panel). 127
6.17 Bathymetric changes (metre) computed after 1.5 months simulation enclosing a storm event, for simulations forced by tidal currents coupled with a wave regime. The solid lines illustrate the initial bathymetry. The negative (positive) values represent erosion (accretion). The values in axes are in metres. . 128
6.18 Relative frequency of H, H^2 and H^2T, considering the wave data between June 2001-2001. 128

6.19 (a) Residual sediment fluxes (m^3day^{-1}) in the seven sections defined at the inlet and navigation channel, only with tidal currents forcing (■) and for tidal currents coupled with a wave regime forcing (■). (b) Residual sediment fluxes (m^2day^{-1}) for the sections located at the offshore area of the inlet Ext1-5. . . 130
6.20 Sedimentation rate (m^3day^{-1}) in the nine regions defined (a) at the inlet and navigation channel and (b) nearshore region. 131
6.21 (a) Final bathymetry (metre) of the Ria de Aveiro lagoon inlet computed after 1.75 years and (b) Difference between the computed final and initial bathymetries (metre) for a 1.75 years simulation for simulations forced by tidal currents coupled with a wave regime. In (b) the solid lines illustrate the initial bathymetry. The negative (positive) values represent erosion (accretion). The values in axes are in metres. 133
6.22 Depth along the sections illustrated in Figure 3.7 observed in June 2001 (o) and March 2003 (+) surveys and simulated with the AW formulation for tidal currents and wave regime forcing. The set of figures at the top panel correspond to the sections 1-7 and the figure at the bottom panel correspond to the longitudinal section (dashed line in Figure 3.7). The y (x) values in the x-axis increases from South to North (West to East). 135
6.23 (a) Final bathymetry (metre) of the Ria de Aveiro lagoon inlet computed after 4.25 years and (b) Difference between the computed final and initial bathymetries (metre) for a 4 years simulation forced by tidal currents coupled with a wave regime. In (b) the solid lines illustrate the initial bathymetry. The negative (positive) values represent erosion (accretion). The values in axes are in metres. 136
6.24 Depth along the sections illustrated in Figure 3.7 observed in September 2005 (+) and predicted using AW formulation for coupled forcing of tidal currents and wave regime(-). The set of figures at the top panel correspond to the sections 1-7 and the figure at the bottom panel correspond to the longitudinal section (dashed line in Figure 3.7). The y (x) values in the x-axis increases from South to North (West to East). 137
6.25 Sedimentation rate (m^3day^{-1}) in the nine regions defined (a) at the inlet and navigation channel and (b) nearshore region. 138

8.1 Bathymetry in meters of the Ria de Aveiro lagoon inlet corresponding to the interpolated surveys of (from left to right, top to bottom): 1987/88, June 2001, March 2003, July 2003, September 2003, November 2003, March 2004, September 2004 and October 2004. The values in the axis are in metres. . . . 148

8.2 Bathymetry in meters of the Ria de Aveiro lagoon inlet corresponding to the interpolated surveys of (from left to right, top to bottom): March 2005, September 2005, October 2006, May 2007, September 2007, January 2008, June 2008, December 2008 and June 2010. The values in the axis are in metres. 149

List of Tables

3.1 Longshore sediment transport formulations where K represents each formulation dependency on d_{50} and bottom slope i. 54
3.2 Longshore sediment transport results ($\times 10^6$ m^{3}year^{-1}). 55
3.3 Longshore sediment transport results for wave regime simplification 1a. ($Q_\ell = \times 10^6$ m^{3}year^{-1}). 62
3.4 Longshore sediment transport normalized results for wave regime simplification 1a. ($Q_\ell = \times 10^6$ m^{3}year^{-1}). 62
3.5 Longshore sediment transport results for wave regime simplification 1b. ($Q_\ell = \times 10^6$ m^{3}year^{-1}). 62
3.6 Longshore sediment transport normalized results for wave regime simplification 1b. ($Q_\ell = \times 10^6$ m^{3}year^{-1}). 63
3.7 Longshore sediment transport results for wave regime simplification 2a. ($Q_\ell = \times 10^6$ m^{3}year^{-1}). 63
3.8 Longshore sediment transport normalized results for wave regime simplification 2a. ($Q_\ell = \times 10^6$ m^{3}year^{-1}). 63
3.9 Longshore sediment transport results for wave regime simplification 2b. ($Q_\ell = \times 10^6$ m^{3}year^{-1}). 64
3.10 Longshore sediment transport normalized results for wave regime simplification 2b. ($Q_\ell = \times 10^6$ m^{3}year^{-1}). 64
3.11 Longshore sediment transport results for wave regime simplification 2c. ($Q_\ell = \times 10^6$ m^{3}year^{-1}). 64
3.12 Longshore sediment transport normalized results for wave regime simplification 2c. ($Q_\ell = \times 10^6$ m^{3}year^{-1}). 65
3.13 Longshore sediment transport mormalized results for all wave regime simplifications tested. ($Q_\ell = \times 10^6$m^{3}year^{-1}). 66
3.14 Wave simplified regime computed through the K91 longshore sediment transport formula. Simplification 2b 67

4.1 *RMSE* and predictive *skill* for 11 stations obtained with this study and with Oliveira et al. [2007] grids. 82

5.1 Sediment transport ($m^3 day^{-1}$) through sections illustrated in Figure 3.7 at neap tide, spring tide and residual conditions. 100
5.2 Sediment transport ($m^3 day^{-1}$) at the downstream (1), upstream (6+7) sections and resultant budget. 100

6.1 Wave simplified regime computed through a longshore sediment transport formula. $H_{0,eq}$ is the wave height at deep water of the equivalent wave in meters, $\alpha_{0,eq}$ is the wave angle at deep water of the equivalent wave in degrees and $T_{p,eq}$ is the period of the equivalent wave in seconds. 118

List of Symbols

a	Reference level
A_{sb}	Term for bedload
A_{ss}	Term for suspended load
C	Chézy coefficient
C_{90}	Chézy coefficient based on d_{90}
c_a	Reference concentration
C_b	Wave breaking parameter
C_d	Drag coefficient
c_f	Friction coefficient
c_g	Wave group velocity
d_*	Dimensionless grain size, related with d_{50}
d_{35}	Particle diameter exceeded by 65% of the weight
d_{50}	Particle for which 50% of the sediments are finner
d_{90}	Particle diameter for which 90% is finer
d_{gr}	Dimensionless particle size, related with d_{35}
E	Wave energy
f	Wave frequency
f_c	Current friction factor
f_w	Wave friction factor
f_w	Wave friction coefficient (using r as bed roughness)
f'_w	Wave friction coefficient (using d_{35} as bed roughness)
g	Gravity
H	Wave height
H_0	Wave height in deep water
$H_{0,eq}$	Wave height at deep water of the equivalent wave
H_b	Wave height at breaker point
$H_{b,eq}$	Wave height at breaker point of the equivalent wave
H_{rms}	Root mean square wave height
H_s	Significant wave height
i	Bottom slope

I_ℓ	Longshore transport rate (with units of Ns^{-1})
I_1, I_2	Einstein integrals
K'	Dimensionless coefficient
L_0	Deepwater wavelength
M_{tot}	Total drift per year
P	Tidal prism
Q_ℓ	Longshore transport rate (with units of m^3s^{-1})
q_s	Total load transport/ Sediment flux
$\vec{q_s}$	Sediment flux vector
q_{sb}	Bedload
q_{ss}	Suspended load
q_{st}	Total load
r	Bed roughness
r'	By-pass capacity of the inlet
R_c	Constant
s	Dimensionless sand density
s_d	Specific density
T	Transport stage parameter
T	Transport stage parameter
$T_{b,eq}$	Wave period at breaker point of the equivalent wave
T_p	Peak wave period
T_{sp}	Transport stage parameter
T_z	Zero-upcrossing wave period
$\vec{u}$	Velocity vector
U	Modulus of the depth-averaged velocity
u_*	Stress velocity
u_{*cr}	Critical stress velocity
U_c	Current velocity
U_{cr}	Threshold current velocity
U_{cw}	Current velocity modified
U_{*cw}	Shear velocity modified
U_w	Wave orbital velocity
U_w	Wave orbital velocity
U_{wrms}	Root mean square wave orbital velocity
W	Total width of the cross-section
Z	Suspension parameter
z_0	Bed roughness length
α_0	Wave angle in deepwater
$\alpha_{0,eq}$	Wave angle at deep water of the equivalent wave

α_b	Wave angle at breaker point
$\alpha_{b,eq}$	Wave angle at breaker point of the equivalent wave
β	Local bottom slope
Δ	Dune height
κ	Von Karman constant
λ	Sediment porosity
Λ	Dune length
μ	Ripple factor
ν	Kinematic viscosity of the water
ρ	Water density
ρ_s	Sand density
τ_b	Current bed shear stress
τ_c	Bed shear stress due to currents only
τ_{cw}	Combined shear stress due to waves and currents
θ	Shields parameter
θ_{cr}	Shield critical shear stress
θ_c	Threshold Shields parameter
ζ	Parameter for wave-current interaction

Chapter 1

Introduction

1.1 Motivation

Tidal inlets are a common feature of lowland coasts all around the world. In fact, a significant part of the world's coastlines consists of barriers interrupted by tidal inlets giving access to estuaries and lagoons [Schwartz, 1973]. These coastal features play an important role in the water exchange between the inner water bodies and the outer ocean, provide the navigational access to inner harbors, and modify the sediment budget of a coastal zone, influencing the long-term coastal evolution. Due to its importance, human interventions are common in the tidal inlets to improve the navigation facilities through for instance the construction of breakwaters to maintain its position and channel dredging to enable the passage of ships. However, and despite the recognized advantage of the artificial inlet construction and channel dredging, these engineering works modify the coastal sediment balance and eventually the entire lagoon or estuary. Therefore it is fundamental to study and understand the consequences of geomorphologic changes on the inlet hydrodynamics and morphodynamics.

There are several works in literature concerning the morphodynamic study of natural inlets, their migration or seasonal closure (e.g. Bertin et al. [2009a]; Pires et al. [2011]). However only a minor number concerns artificially inlets limited by two offshore breakwaters, such as the Ria de Aveiro lagoon inlet, which is located at the northwest of the Iberian Peninsula (illustrated in Figure 1.1). In this inlet there is no migration and the regular dredging activities don't allow its closure.

The Ria de Aveiro lagoon hydrodynamics is mainly tidally driven, but its inlet is also subject to a highly energetic wave condition. These characteristics resulted in several transformations of the inlet, either in geometry either in location, since the formation of the lagoon, resulting in several closures of the inlet along the time. The consequences of these instabilities, sometimes catastrophic, gave rise to poorness and illness in Aveiro region [Dias et al., 1994]. Also, the access conditions to the harbor, located in the inner lagoon, became precarious, with direct consequences to the economy of this region [Teixeira, 1994]. These factors originated

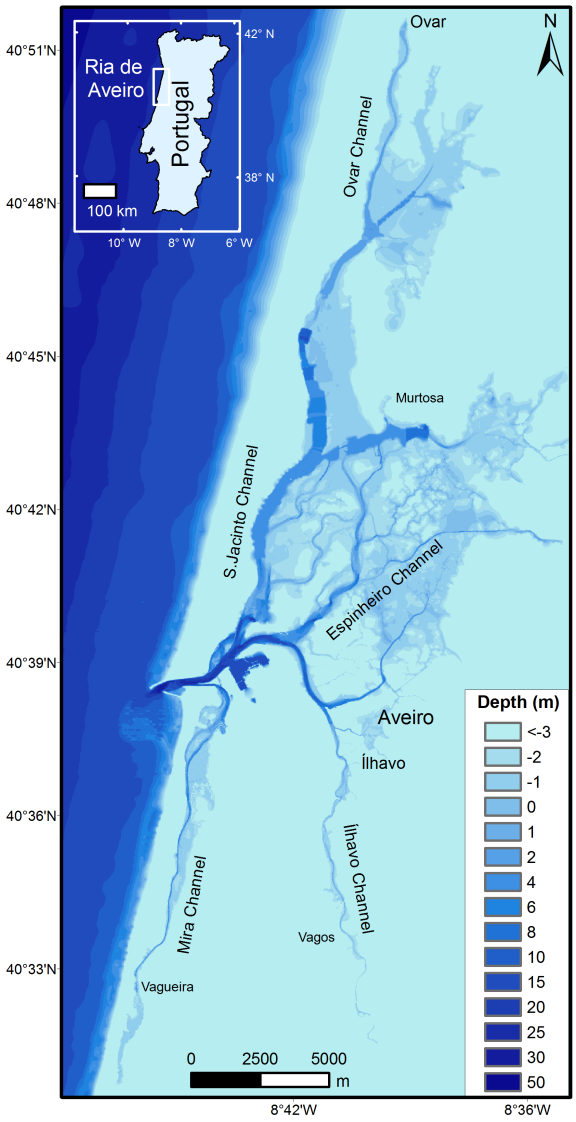

Figure 1.1: Location and bathymetry of the Ria de Aveiro lagoon and offshore area.

the construction of an artificial inlet (actual configuration), initiated in 1802 and completed in 1984/85 after several work phases, resulting in two offshore breakwaters. Several maintenance dredging activities were and are being performed to guaranty the secure navigation and access to the harbor.

However, these dredging activities and sometimes the modifications in the breakwaters configuration alter, not only the inlet dynamics, but also the dynamics of the entire lagoon. Several studies on the hydrodynamics of the Ria de Aveiro lagoon showed that anthropogenic and natural morphologic changes in the inlet and navigation channel depths have impacted the tidal dynamics of the entire lagoon [Araújo et al., 2008; Dias and Mariano, 2011; Dias and Picado, 2011]. These authors concluded that the inlet and navigation channels deepening

increase the tidal amplitude, decrease the tidal phase and raise the tidal prism in the remaining lagoon channels.

One of the inlet's structures, the North breakwater, is the most important and susceptible structure due to its orientation and localization [Moreira and Gomes, 2001]. In the past this structure was already subject to structural maintenance works due to ruptures and to the landslide of the "lighthouse" located at its head. Additionally, surveys performed in 2001 revealed that the 10 m bathymetric contour that in the 80 decade was 600 m far from the head of the breakwater was less than 300 m far at this date, being the wave heights that reach the structure higher than those initially predicted. The surveys performed also revealed the presence of eroded areas with depths higher than 20 m, near the foundation of the breakwater, threatening the stability of this structure. Thus, the erosion in the surrounding area of the head of the North breakwater was already a concern.

Consequently, this work aims to give a contribution to the knowledge of the Ria de Aveiro lagoon inlet morphodynamic characteristics and dominant processes. The relevance of this study arises considering that the morphologic changes of this system and its inlet were found weakly studied, until the present. The studies published are, in general, technical reports requested by Aveiro Harbour Administration (APA) in the frame of the several inlet works carried out over time. In this context Hidroprojecto [1995] proposed solutions to improve the accessibility to the Aveiro harbor and to protect the littoral South coast adjacent to the Ria de Aveiro lagoon from erosion. LNEC [1989] collected data in order to simulate and analyze the coastline evolutions through numerical modeling. Another engineering study reports the maintenance works performed in the North breakwater due to its collapse [Moreira and Gomes, 2001].

The methodology defined to overcome the lack of knowledge about morphodynamic processes in this region consisted in the collection of several information published in the literature and in the analysis of the available data, as well as in the application of the numerical modeling system MORSYS2D to the Ria de Aveiro lagoon inlet. In the present application MORSYS2D is composed by the hydrodynamic model ELCIRC [Zhang et al., 2004], the wave model SWAN [Booij et al., 1999] and the sediment transport and bottom update model SAND2D [Fortunato and Oliveira, 2003, 2007; Bertin et al., 2009c]. This modeling system is applied to the Ria de Aveiro lagoon inlet, following the previous work developed by Oliveira et al. [2007].

It should be pointed out that the implementation of this morphodynamic numerical model gives the opportunity to perform a detailed study of the Ria de Aveiro inlet. The modeling system's results exploitation will help in the understanding of the main processes driving the local morphodynamics and to answer several questions: Are the tides the main responsible forcing for the bathymetric trends observed, or the wave regime surpasses their effect? If the waves have a strong influence, what wave characteristics have higher influence in the sediment transport, the most frequent and with minor wave heights or storm waves? What

is the origin of the strong erosion pattern observed near the North breakwater? Other questions can also be answered, such as: does the diversity of bottom sediment sizes at the inlet and near regions influence the residual sediment fluxes and resulting trends? How different would be the bathymetry of the study area if dredging activities weren't performed? Do the breakwaters have influence in the longshore sediment transport?
To answer these questions, numerical simulations were performed considering only the tidal forcing in the sediment transport and the coupled effect of tidal currents and regular monochromaticwaves or a wave regime.

1.2 Literature review

Morphologic modeling

The reproduction and prediction of the morphologic evolution of estuaries and lagoons inlets are very challenging tasks because it results from the combined action of tides, waves, river discharge and wind in the area of interest. Additionally, an accurate knowledge of the sediment transport, generally complex and a function of both hydrodynamics and bed texture, in combined waves and current flows, is essential to achieve a good morphological characterization. This characterization could be performed using morphological models. These models can be divided in several classes composed by numerical and physical models [Fortunato, 2006]. The numerical models can be based on data, in empirical or semi-empirical formulations, in simplified formulations or systems, or in process based models. All the referred, with exception of the last, have in general the advantages of simplicity and low computational costs, however they need high quality data, provide low spatial and time resolutions results and are limited to simple geometries (with loss of generality). On the other hand, process based models are more suitable for real geometry studies, such as tidal inlets, providing high spatial and time resolution results, but requiring high computational costs. These models are based on physical processes described by numerical formulations to reproduce waves, tidal currents, sediment transports and bottom modifications [Pinto, 2010], as example, the morphodynamic models.
In general, all the morphodynamic modeling systems are composed by three modules: a hydrodynamic model, a wave model and a sediment transport model which performs also the bottom update. The first model simulates all the large scale dynamics of the system, for example the tidal streams. The wave module may take into account a regular monochromaticwave or a wave regime, simulating the wave propagation and the resulting longshore currents through the radiation stress computation. These currents induce a longshore sand drift which might be important for the closure of the tidal inlet. The sediment transport module computes the sediment transport due to the tidal forcing isolated or in coupled wave-current flows. In this module the sediment grain size and the choice of the empirical sediment

transport formulae affect the morphological changes and play a very important role in the accuracy of the results. However, the sediment characteristics and the amount of transported sediment are generally not known with enough precision, due to the scarcity of surveys and data availability. In addition, several formulations to compute sediment transport are available, increasing the uncertainty on the results. All these limitations difficult the validation and accurate evaluation of the numerical predictions. Thus, and due to these uncertainties, several authors develop their own formulations to compute the bed-load and sediment load transport and also sediment transport modules.

Soulsby and Damgaard [2005] developed formulae for bed-load transport of sediments in conditions typical of coastal waters, covering current alone, current plus symmetrical waves, current plus asymmetrical waves and integrated longshore transport. With the aim of predicting the total sediment transport rates (bed-load plus suspended load) in conditions characteristic of the coastal zone (wave or combined wave-current flow), Silva et al. [2006a] developed a semi-unsteady practical model.

Wai et al. [2004] described a 3D sediment transport model with waves and currents directly coupled within the model to continuously account for different-scale activities, especially those that have significant contribution to local sediment transport processes. The model was applied to Pearl River Estuary, China, and it was concluded that the suspended sediment concentration in the estuary increases significantly when waves are present. The authors also concluded that the sediment deposition occurs at the upstream region while erosion takes place mostly at the down-estuary region due to its exposure to wave actions.

Since sand transport models are often based on semi-empirical equilibrium transport formulations that relate sediment fluxes to physical properties, such as velocity, depth and grain size, it is crucial to perform sensitivity analysis of the formulae used. Pinto et al. [2006] compared the sediment transport formulae of Ackers and White [1973]; Engelund and Hansen [1967]; van Rijn [1984a,b,c] and Karim and Kennedy [1990]. These authors concluded that the van Rijn formula is the most sensitive to basic physical properties. Hence, it should only be used when physical properties are known accurately [Silva et al., 2009].

The process based morphodynamic models, required by the complexity of all these processes and interactions, have been emergent in the last years, presenting a strong development over the past 30 years [Nicholson et al., 1997]. MIKE21, developed by the Danish Hydraulic Institute - DHI [Warren and Bach, 1992], DELFT3D, by WL Delft Hydraulics - DH [Roelvink and Banning, 1994] and TELEMAC developed by EDF-DER, France [Laboratoire d'Hydraulique de France, 1997], are widely spread among the scientific community. In Portugal, two morphodynamic modeling systems were developed and are described in literature: MOHID [Neves et al., 2000; Smith et al., 2001; Silva et al., 2004; Aires et al., 2005] and MORSYS2D [Fortunato and Oliveira, 2003, 2007; Bertin et al., 2009c].

Before modeling the real cases is very common the application of numerical models to idealized systems, due to complexity of these numerical tools. In the present case, the idealized

system is usually composed by an inlet area and a lagoon basin and can give insight about the isolated action of different processes that are responsible for the migration and closure of inlets, as example. According to Davidson et al. [2009], that developed a simple 1-D numerical model to simulate the magnitude and non-linearity variability of the tidal flow, there are two main modes of inlet sedimentation: the landward progradation from the mouth and the seaward development of the flood shoal. Tung et al. [2009] applied the DELF2D model to an idealized tidal inlet system to study the closure of the inlet and its migration. The authors concluded that the closure is caused by the prolongation of the inlet channel and infilling with littoral-drift material as consequence of the longshore and cross-shore transport processes, and the migration is originated by the oblique waves, including features such as ebb channel formation, migration and welding to the downdrift barrier. The inlet dynamics was also numerically reproduced by Ranasinghe and Pattiaratchi [1999], that developed a morphodynamic model [Ranasinghe et al., 1999] which simulates the longshore and cross-shore processes. The application of this model to two idealized situations showed that when the longshore sediment transport rates are low, such as under low energy wave conditions, cross-shore processes control the behavior of the tidal inlet. The model was also applied to a real case study, the Wilson inlet located in the Western Australia. The field study and the numerical results confirmed that the sediment transport mechanism governing seasonal closure of the inlet is the onshore transport of sediment, resulting from persistent swell wave conditions [Ranasinghe and Pattiaratchi, 1999].

Synthetic simulations also revealed that the evolution of the configuration of the channel network might be much faster than the bathymetric evolution of the lagoon itself. An example of this behavior was found by Silvio et al. [2010], that applied a long term model of planimetric and bathymetric evolution of Venice lagoon, to a schematic system, considering the interactions between tidal currents, longshore currents and sea waves.

The simplifications performed in the morphodynamic studies goes further than the use of schematic cases. A real case could be researched with simplifications in the different modules that compose the morphodynamic models. For example, forcing the sediment transport only with tidal currents and neglecting the effect of waves [Fortunato and Oliveira, 2003, 2004; Oliveira et al., 2007] or considering representative mean annual wave and tide conditions that induces the same annual transport as real waves [Cayocca, 2001]. In the referred studies, Fortunato and Oliveira [2003], Fortunato and Oliveira [2004] and Oliveira et al. [2007], applied the MORSYS2D to the Guadiana estuary, the Óbidos lagoon and the Ria de Aveiro lagoon, respectively, obtaining good preliminary bathymetric predictions. Cayocca [2001] developed a two-dimensional horizontal morphodynamic model and applied it to Arcachon lagoon, at the French coast, on a side connected to the ocean by a wide inlet between the mainland and an elongated sand pit. The successful results showed that the tide is responsible for the opening of a new channel at the extremity of the sand pit, while waves induce a littoral transport responsible for the longshore drift of sand bodies across the inlet.

When numerical simulations are performed for a real case study, the field experiments play an important role in order to validate the predictions. However they are often scarce, despite their importance. Ranasinghe and Pattiaratchi [2003] used field experiments and the DELF3D model to study a real case, the Wilson Inlet at Western Australia. With this study they identified the morphodynamic processes governing seasonal inlet closure and determined the effect of the seasonal closure of the inlet on the morphodynamic characteristics of the adjacent estuary/lagoon. These authors concluded that the inlet closure is due to the onshore sediment transport induced by persisting swell wave conditions during Summer. Also Work et al. [2001] used observations to analyze numerical predictions. These authors, describe a Mesoscale Inlet Morphology (MIM) modeling system and applied it to the undredged and unstabilized Price Inlet, South California. They concluded that the predicted bathymetric changes were similar in tendency sign (erosion/deposition) and location to the observations, but the model underpredicts the changes magnitude.

Other examples are found in literature for the application of morphodynamic models to real systems. A dredged area evolution in southern Portugal [Rosa et al., 2011], the Aljezur coastal stream morphological variability [Guerreiro et al., 2010] and the Ancão inlet in Ria Formosa [Bertin et al., 2009b] are examples of other studies performed using the numerical modeling system MORSYS2D.

Considering the development of sandbars migration and growth, for example, Grunnet et al. [2004] and Bruneau et al. [2010] used different morphodynamic models, obtaining different accuracy in the predictions. Grunnet et al. [2004] applied the DELFT3D model to hindcast the morphological development of shoreface nourishment along the barrier island of Terschelling, The Netherlands. The morphodynamic results showed a dependency on the spatial scale: on the scale of the bed level evolution with respect to bar migration and growth, model predictions were poor as the nearshore bars were predicted to flatten out. On the other hand, the model satisfactorily predicted the overall effects of the nourishment taking into account the mass volumes integrated over larger spatial scales. Better results were obtained by Bruneau et al. [2010] in the predictions of the development of a meander and the formation of sandbars in the wave dominated inlet of Óbidos lagoon, with the recently partially parallelized MORSYS2D. Xie et al. [2009] used the DELF3D model to analyze the physical processes and mechanisms essential to the formation and evolution of a tidal channel in the macro-tidal Hangzhou Bay, China. In this work model results reproduced accurately the real morphological features. The results showed that spatial gradients of flood dominance, caused by boundary enhancement via current convergence, are responsible for the formation of the channel system, due to, among other effects, the funnel-shaped geometry.

To perform a morphydynamic study it is advisable to previously intercompare the available models, in order to understand their accuracy. Nicholson et al. [1997] performed an intercomparison between the DHI model, a subset of DH model (the DELF2D-MOR), and three other models in order to evaluate their response to the presence of offshore breakwaters.

This comparison revealed that these models produce realistic estimates for the dominant morphodynamic features associated with these structures and that the choice of sediment transport formula on the resulting morphology is essential. Similar conclusions concerning the choice of the sediment transport formulation were obtained by several authors that applied MORSYS2D to the Óbidos lagoon [Oliveira et al., 2005; Fortunato and Oliveira, 2006, 2007; Bertin et al., 2007, 2009a,c; Fortunato et al., 2009]. These authors also concluded that the bottom sediment grain size affect considerably the morphological changes.

Ria de Aveiro

The majority of the studies performed on Ria de Aveiro lagoon are related to the biological and chemical processes of this lagoon. The number of studies concerning its physics and geomorphology are presently significant, but are rare those about its morphodynamics.
In the last decade several studies performed in the Ria de Aveiro lagoon were dedicated to analyze and describe the physical processes occurring in this system. In 1999, Dias et al. [1999] investigated the hydrological features of the lagoon based in two surveys and showed that the lagoon can be considered vertically homogeneous with exception to periods of important rainfalls. These rainfalls originate strong fresh water flows creating some vertical stratification. These hydrological characteristic were also referred by Vaz and Dias [2008], that demonstrated that during wet seasons the stratification induced by the Vouga river flow can be extended up to the inlet. Dias et al. [1999] determined that the tide at the inlet is semidiurnal, generating tidal currents strongly dependent on the local geometry. They also concluded that the tide is the main forcing agent driving water circulation in Ria de Aveiro lagoon and, in addition, Dias [2001] refer that this circulation, during short periods and mostly in shallow waters and wide channels, could also be influenced by extreme conditions of strong wind.
The tide in the entire lagoon was simulated by Dias et al. [2000] using a two-dimensional depth integrated mathematical model with the aim to predict the water level and depth mean current. These authors showed that tides propagate from the inlet and are present in the entire lagoon, decreasing its amplitude with the distance to the mouth while the phase lag increases [Dias et al., 2000]. Dias [2001] revealed that the increase of tidal range along the fortnight neap/spring tide cycle induces a local increase of the high tide level, at the far end of the channels.
The dynamics of the sediment transport in the lagoon were also studied. Lopes et al. [2001] studied the influence of tides and river inputs on suspended sediment concentration (SSC) in Ria de Aveiro lagoon, emphasizing Laranjo Bay from a bio-geophysical point of view. Dias et al. [2003], Lopes et al. [2006] and Abrantes et al. [2006] used numerical models to understand the spatial and temporal variability of SSC. Tidal, wind- and river-induced residual currents contribute to the net exportation of water and sediments seaward which is consistent

with ebb dominance. In Ria de Aveiro lagoon the residual tidal currents are the main forcing process in the transport of suspended sediments, being one or two orders of magnitude higher than the residual currents generated by wind and river runoff [Lopes and Dias, 2007]. The concentration of sediments follows the tidal cycle, being the residual circulation determined by the asymmetries between flood and ebb regimes [Dias et al., 2003; Lopes and Dias, 2007]. Based on surveys performed in sites near the inlet, Martins et al. [2009] determinate the SSC and the bottom sediments characteristics, and studied the influence of the oceanographic regime and the tidal cycles in the sedimentary exchanges between the lagoon and the ocean. They observed that, in general, the higher values of SSC were recorded at the inlet at flood periods during Winter neap tides as well as at Summer regime conditions.

The Ria de Aveiro lagoon is also source of concern when discussing climate changes impacts. Silva and Duck [2001] analyzed the historical changes of bottom topography and tidal amplitude in Ria de Aveiro since the construction of the artificial inlet and presented trends for future evolutions. These authors concluded that any future increase of the mean sea level will contribute to an increase of both area and volume of water mass, increasing the speed of tidal propagation. The authors gave an example: an increase of 0.1 m in mean sea level correspond to an increase of 5% in the capacity of the system, resulting in an increase of 22% of the tidal prism, defined as the volumetric flux passing a cross-section between a low-water and subsequent high-water. Lopes et al. [2011] evaluated the impact of sea level rise in lagoon hydrodynamics performing projections of SLR for the end of this century and found an increase of 20% of the lagoon tidal prism for a sea level rise of 0.42 m. This physical property, as well as the tidal asymmetry were also analyzed by Picado et al. [2010] when investigated possible tidal changes induced by local geomorphologic modifications, specifically the flood caused by salt pans walls collapse . These authors concluded that the increase of the lagoon total area (5.6% for extreme destruction) also results in an increase of 5% (for an average tide) of the tidal prism as well as in the tidal asymmetry, with the higher changes found close to the flooded area and in neap tide.

The studies mentioned above reveal that the inlet morphology determines the tidal currents at the lagoon mouth, affecting as a consequence the water circulation inside the lagoon as well as the water renewal. Additionally, the tidal currents have direct influence in the sediment transport and consequently in the local morphodynamic changes. At the inlet region and adjacent nearshore, the wave regime characteristic of the West coast of Portugal also has an influence on the sediment transport that passes through the inlet. Additionally to these physical factors, the Ria de Aveiro has an important harbor inside the lagoon which requires regular maintenance dredging activities of the inlet channel to guaranty its secure access.

Considering all these factors, the inlet is a highly dynamic region with physical and economic interests. Thus, in order to understand the morphodynamic behavior of Ria de Aveiro lagoon inlet, it is essential to analyze past data and to develop and apply adequate tools such as a morphodynamic model to this study area (schematized in Figure 1.2).

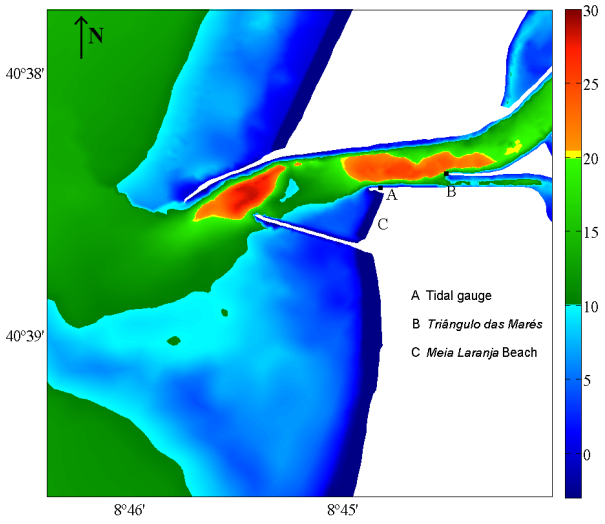

Figure 1.2: Bathymetry of the study area.

1.3 Structure of this work

To perform a morphodynamic study of a coastal lagoon inlet, it is important to review the theoretical background of lagoons and inlets. The information collected in this study is analyzed in Chapter 2, where is presented a classification of the lagoon and inlet under study, considering the tidal range and the mean significant wave height. Also a brief description of lagoons and inlets hydrodynamic and morphological evolutions is performed. In this chapter the sediment transport processes induced by tidal and wave generated currents are equally described. The formulations to compute the amount of sediment that is transported due to the forcing of tidal currents and waves, are also presented and a sensitivity analysis to several characteristics is performed. These later formulations integrate the sediment transport and bottom update model SAND2D used in numerical simulations in Chapters 5 and 6.

After the general theoretical review of lagoons and inlets, is necessary to perform a detailed characterization of the study area. In Chapter 3 the origin of the Ria de Aveiro lagoon and its inlet is described, since the XIII century until nowadays. Additionally, a morphological characterization is performed by analyzing the bathymetric data collected by the Administration of the Ria de Aveiro (A.P.A, S.A.), from 1987/88 to 2010 and the bathymetric changes observed between 1978/88-2001, 2001-2003, 2001-2005 and 2005-2010. To improve the characterization of the study area, the bottom sediment data available in the literature is collected in order to built a distribution of the bottom sediments size. A hydrodynamic characterization of the Ria de Aveiro is also made by considering historical data and numerical simulations performed with the hydrodynamic model ELCIRC. To complete Chapter 3, the wave regime at the nearshore area is analyzed through data collected from two wave directional buoys and a simplified regime is derived. This regime induces a longitudinal sediment

transport at a beach (computed through the formulations presented in Chapter 2) equivalent to that caused by the complete wave regime, and is later used in numerical simulations forced by the tidal current and a regular monochromatic wave (Chapter 6).
The following chapters are related with the numerical modeling system MORSYS2D and the numerical simulations performed to understand the relative importance of tides and waves on the system's morphodynamics.
In Chapter 4, a general overview of MORSYS2D is presented as well as the setup of the used models in the study area.
Chapters 5 and 6 present the results of the morphodynamic simulations forced by tidal currents and by tidal currents coupled with waves, respectively. Both chapters present the results obtained for the sensitivity analysis of the numerical model to several parameters such as: numerical filters, sediment transport formulation, spring and neap tides, depth and bottom sediment size distribution, regular monochromatic waves and storm events.
In the last chapter, general conclusions are presented.

1.4 Prior Dissemination

The work developed in this dissertation gave rise to several publications along its development (bookchapters, scientific journal papers, proceedings) and was presented at several conferences. These publications were used as base for several chapters of this thesis.
Book chapter:

- *Sediment Transport Modelling and Morphological Trends at a Tidal Inlet* - Sandra Plecha, Paulo A. Silva, Anabela Oliveira, João M. Dias, Andrew J. Manning (Eds), INTECH, Chapter 8, 163-186, 2011 (ISBN 978-953-307-586-0) [Plecha et al., 2011e]

- *Trends of Bathymetric Variations at a Tidal Inlet* - Sandra Plecha, Sara Rodrigues, Paulo Silva, João Miguel Dias, Anabela Oliveira, André B. Fortunato, In: River, Coastal and Estuarine Morphodynamics: RCEM2007. C.M. Dohmen-Janssen, S.J.M.H. Hulscher. (eds) Taylor & Francis., Vol 1, pp. 19-23, 2007 [Plecha et al., 2007]

SCI journal papers:

- Establishing the Wave Climate Influence on the Morphodynamics of a Coastal Lagoon Inlet - Sandra Plecha, Paulo A. Silva, Anabela Oliveira, João M. Dias, *Ocean Dynamics*, 2011 (Submitted) [Plecha et al., 2011b]

- Evaluation of Single Waves Effects on the Morphology Evolution of a Coastal Lagoon Inlet - Sandra Plecha, Paulo A. Silva, Anabela Oliveira, João Miguel Dias, *Journal of Coastal Research*, SI64, Vol.II, 1155-1559, 2011 (ISSN 0749-0208) [Plecha et al., 2011c]

- Sensitivity analysis of a morphodynamic modeling system applied to a coastal lagoon inlet - Sandra Plecha, Paulo Silva, Nuno Vaz, Xavier Bertin, Anabela Oliveira, André B. Fortunato, João M. Dias, *Ocean Dynamics*, 60, 275-284, 2010 (DOI 10.1007/s10236-010-0267-5) [Plecha et al., 2010]

- Representative Waves for Morphological Simulations - Sandra Plecha, Francisco Sancho, Paulo Silva, João Miguel Dias, *Journal of Coastal Research*, SI50, 995-999, 2007 (ISSN 0749.0208) [Plecha et al., 2007]

Conference proceedings:

- Evolução Morfodinâmica da Embocadura da Ria de Aveiro - Sandra Plecha, Carina L. Lopes, Paulo Alves Silva, Anabela Oliveira and João Miguel Dias, *Jornadas da Ria de Aveiro*, University of Aveiro, 187-196, 2011 (ISBN 978-972-789-337-9) [Plecha et al., 2011a]

Conference communications:

- Modelação morfodinâmica da embocadura da Ria de Aveiro - Sandra Plecha, Paulo A. Silva, Anabela Oliveira e João M. Dias, *Conferência sobre Morfodinâmica Estuarina e Costeira*, Lisbon, Portugal, $3^{rd} - 4^{th}$ February, 2011 [Plecha et al., 2011d]

Chapter 2

Theoretical Background on Lagoons and Tidal Inlets

2.1 Introduction

In this chapter, a review of the theoretical background of lagoons and inlets is performed. These systems are classified according to the tidal range and mean significant wave height. Also a brief description of the lagoons and inlets hydrodynamic and morphological evolutions is performed. The sediment transport processes induced by tidal and wave generated currents are equally described, as well as several formulations to compute the sediment transport.
There are several definitions and classifications of lagoons. According to Dyer [1997] "a lagoon is a semi-enclosed coastal body of water which has a free connection to the open sea, extending into the river as far as the limit of tidal influence, and within which sea water is measurably diluted with freshwater derived from land drainage". Barnes [1980] defined coastal lagoons as saline water bodies separated or partially-isolated from the sea. They may be enclosed by several barrier islands as well as sand spits, or linked to the sea by one or more channels, which are small relative to the lagoon.
There is no restrictive definitions of inlet, almost any opening in the coast can be called an inlet. According to the CEM [2002], inlets are openings in coastal barriers through which water, sediments, nutrients, planktonic organisms and pollutants are exchanged between the open sea and the protected embayments behind the barriers. The flow in the inlets provides natural flushing to maintain good water quality and reasonable salinity levels. Inlets also have the important assignment of connect the harbours with the ocean, maintaining the commercial navigation. Due to this, navigable inlets are essential to the local economy. To maintain adequate depths, are frequently necessary dredging works in the navigation channels of access to the harbour.
Due to its characteristics, tidal lagoons attract a variety of human activities, such as navigation, recreation, fishing and aquaculture, sand exploration and land reclamation. On the

other hand, many lagoons form the basis of highly valuable and sometimes unique ecosystems. Hence human activities which affect the properties of such a system or put the environmental functions otherwise at risk have important consequences, making a sustainable management of these systems a complex task.
Lagoons are also effective traps for sediment in their formative stages, but gradually infill until a balance is achieved between the sediment inputs, the shape of the lagoon, its depth and the scouring of the currents, through a slow morphological development. When the discharge of sediment by the rivers is higher than the transported by the coastal processes, deltas form in the lagoon. If the sediment discharge is low, or the coastal processes active, the lagoon can be a major indentation in the coastline, and there can be an equilibrium shape established by a balance between the sediment inputs and the physical processes [Dyer, 1997].
In the beginning of this Chapter, the physical processes of lagoons and their inlets are described attending to the sediment transport processes. Afterwards, a description of sediment transport processes is performed and different formulations to compute the total load sediment transport and the longshore sediment transport are presented. A sensitivity analysis of the former formulations to the sediment size and current velocity is also performed.

2.2 Classification

Coastal lagoons can be classified concerning topography, river flow, tidal action and mean wave-height, since these factors influence the rate and extent of the mixing of ocean and river waters. Locally, and for short periods, wind may also become significant.
Considering the goals of this study (see Chapter 1), only the classifications concerning the tidal action and the mean wave-height are presented.
Concerning the tidal range, Hayes [1979] used the following classification for lagoons:

Microtidal < 1.0 m
Low Mesotidal: 1.0 - 2.0 m
High Mesotidal: 2.0 - 3.5 m
Low Macrotidal: 3.5 - 5.5 m
High Macrotidal > 5.5 m

Wave action is very important as it moves sediment onshore and limits the area over which the ebb tidal delta can spread out [Hibma, 1999]. The wave climate is generally characterized by the mean significant wave height H_s, on a yearly average basis:

Low wave energy $H_s < 0.6$ m
Medium wave energy $H_s < 1.5$ m
High wave energy $H_s > 1.5$ m

Based on the combination of tidal range and wave energy classification, Hayes [1979] distinguishes five classes with respect to tidal/wave dominance: wave-dominated, low or high

tide-dominated and mixed energy wave or tide dominant, which are illustrated in Figure 2.1. For the case of tide dominance (high), schematized in Figure 2.2(a), the lagoons are characterized by extensive salt marshes and tidal flats. The inlets of this type of lagoon often have large ebb tidal deltas and very deep inlet gorges. The influence of strong ebb currents extends far offshore and only when the flow has dissipated seaward, the wave and tidal forces are equal. This equilibrium zone between incoming waves and the ebb flow occurs along the sides of the ebb delta and at its edge. In this equilibrium zone, ebb tidal delta sediments deposit. In the case of low dominance, inlets occasionally show wave built bars and transitional forms can be recognized.

In wave dominated lagoons (Figure 2.2(b)) the majority of the sand is either pushed through the inlet into the lagoon or is by-passed around the inlet. Because of the high wave energy and the relatively weak ebb flow, the equilibrium zone is close to the beach and approximately parallel to shore. There are only few tidal inlets with long continuous barriers and a lot of washovers.

In mixed energy lagoons, both waves and tide are important. In the wave dominant case, the adjacent coast of the lagoon has a larger number of inlets and a smaller number of washovers. The size of the ebb-tidal delta will became somewhat bigger. For the tide dominant case, the adjacent coast has abundant tidal inlets, larger ebb tidal deltas and usually drumstick barriers.

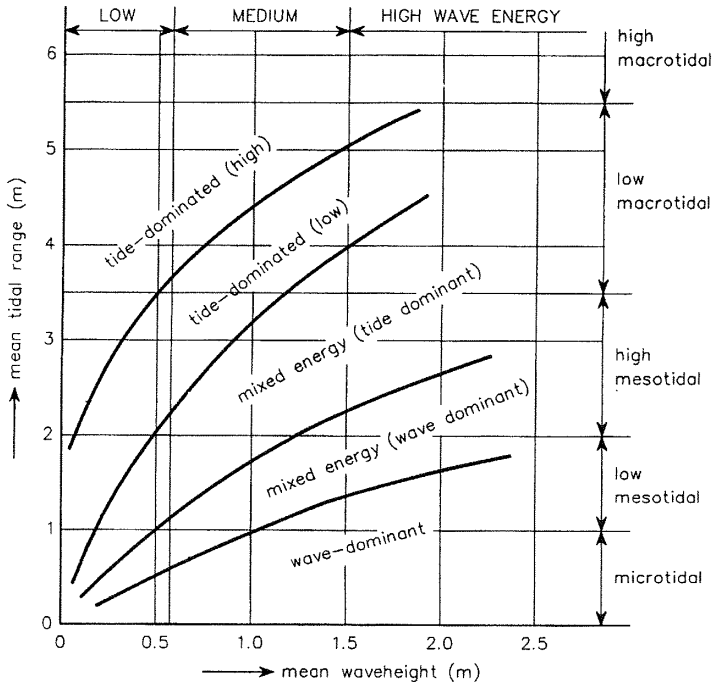

Figure 2.1: Hydrodynamic classification of lagoons. From Hayes [1979].

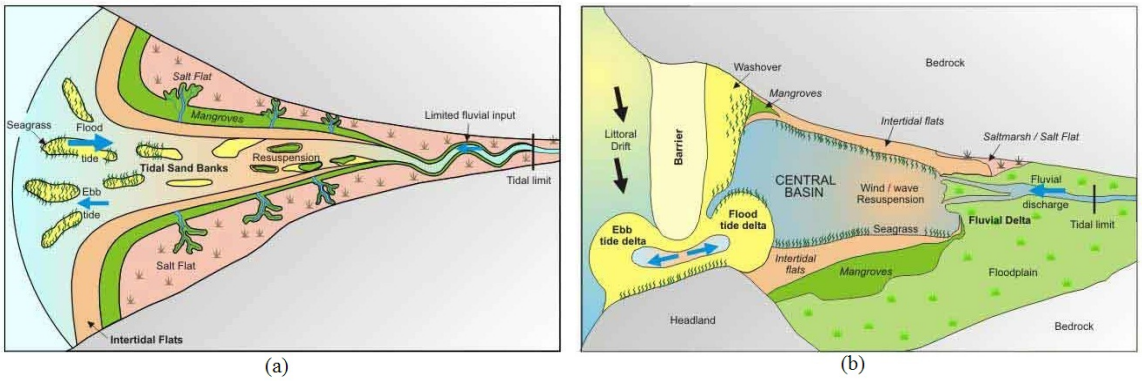

Figure 2.2: Schematization of (a) tide and (b) wave dominated lagoons. From Heap et al. [2001].

2.3 Lagoons Hydrodynamics

When tides propagate into a lagoon, the nonlinear effects of bottom friction and geometry induce distortion in the tidal wave amplitude promoting tidal symmetry and uneven duration of flood and ebb tides. For the case of long lagoons, the friction is the most influent factor, but on the other hand, if the lagoon is shorter the geometry is the most influent factor for tidal deformation. This distortion can be represented by the non-linear growth of the constituents and harmonics of the principal astronomical tidal components [Friedrichs and Aubrey, 1988]. Since the ocean tide is a sum of sinusoidal components, non-linearities produce harmonics and compound constituents.

Along much of the world's coastlines, the dominant astronomical constituent is M_2, the semi-diurnal lunar tide. Because of M_2 dominance, the most significant overtide formed in these well mixed lagoons is M_4, the first harmonic of M_2 [Friedrichs and Aubrey, 1988]. The M_4 constituent is generated through the advective and finite amplitude terms, but friction can also play a minor role [Parker, 1991]. A direct measure of non-linear distortion is given by the ratio between the M_4 and M_2 sea-surface amplitudes and indicates the magnitude of the tidal asymmetry generated within the lagoon. An undistorted tide has an amplitude ratio of zero. The larger the M_4/M_2 ratio, the more distorted is the tide and more strongly flood- or ebb-dominant is the system. The phase of M_4 relative to M_2 is defined as $\phi = 2\theta_{M_2} - \theta_{M_4}$ and determines the orientation of tidal distortion: $0^o < \phi < 180^o$ indicates flood dominance and $180^o < \phi < 360^o$ indicates ebb dominance [Friedrichs and Aubrey, 1988].

A lagoon is referred as flood dominant when the duration of the ebb tide exceeds the flood tide resulting in a larger peak flood current. This is the case of shallow lagoon areas where the influence of the bottom friction is greater in low water than at high water, originating larger flood than ebb velocities [Dronkers and van de Kreeke, 1986], being highly dissipative. For this case, the time delay between the up- and downstream limits of the lagoon in low water is greater than in high water, resulting in longer ebb tides and shorter flood tides,

and consequently in higher velocity currents during flood, due to mass conservation. On the other hand, when the duration of the ebb tide is smaller than the flood tide, strong ebb currents arise and the lagoon is denominated as ebb dominant. According to Robins and Davies [2010], if the asymmetry in the tide causes a net sediment erosion, the lagoon is classified as ebb-dominant, whereas the opposite is flood dominant.
For longer lagoons, the ebb currents are more intense than the flood currents, increasing the capacity to flush out the sediments, representing a more stable condition than in the shorter lagoons [Aubrey and Speer, 1985].
Additionally, the velocity of the tidal currents depends on the tidal magnitude, the channels geometry and the topography of the bottom. According to Woodroffe [2002] there are two types of flow in lagoons: tidal currents induced by the tidal flow, which mainly contribute to the physical processes and residual currents driven by density gradients, by wind stress or by tidal movements. The residual currents are usually one or two orders of magnitude lower than the tidal currents, but they are important because their persistence may allow them to dominate the overall longterm distribution and transport of characteristic water properties or sediments [Pugh, 1987].

2.4 Lagoon inlets

Inlets play a crucial role in the sediment budget of the coastal zone influencing the long-term coastal evolution. The typical flood and ebb current patterns on the ocean side of a tidal inlet are shown in Figure 2.3. The important aspect of this general circulation pattern is that currents usually flow toward the inlet near the shoreline, even on ebb tide. The reason for this apparent paradox is the effect of wave driven currents. On the downdrift side of the inlet, breaking waves are turned toward the inlet due to refraction over the outer bar and on breaking, create currents toward the inlet [CEM, 2002].

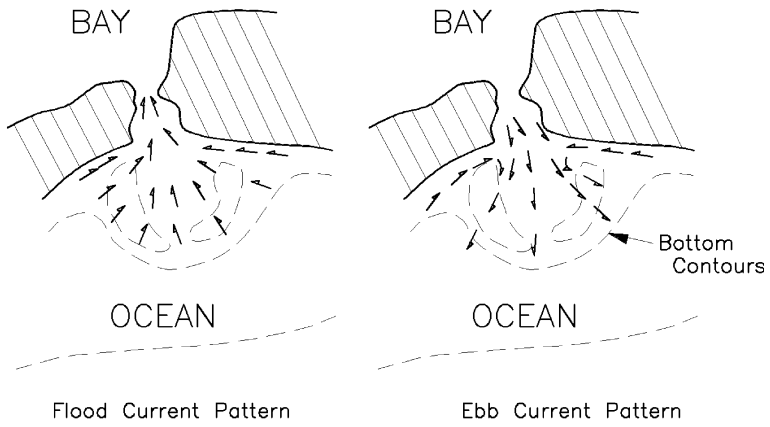

Figure 2.3: Schematic diagram of flood and ebb currents outside an inlet [O'Brien, 1969].

Seaward of the inlet, sand can be accumulated generating an ebb-tide delta. This delta is formed from a combination of sand eroded from the gorge (deepest zone) of the inlet and sand provided by longshore currents and its morphology depends on the interaction of the tidal currents and waves.

At the landward side of the inlet, sand can also be accumulated, generating the flood-tide delta shaped by flood currents (not shown). Inside the inlet, water may diverge into one or more channels created by sand deposition and resulting in a complex pattern of bars, shoal and channels [CEM, 2002].

Inlets can vary significantly in place and time due to the strong differences in the driving parameters and complex interactions between tidal prism, wave energy and sediment supply. The outer delta forms a barrier for the longshore transport of sediment which may enter the inlet via the flood channel or may be transported from the updrift to the downdrift barrier or over the delta. Updrift refers as the coast in the direction from which the majority of offshore wave energy arrives and the opposite as downdrift.

Also, the inlet interrupts the longshore current, which is variable depending on wave conditions. However, not all of the sediments in longshore transport are trapped at the inlet mouths, since some of them, may be transported from the updrift side of the tidal inlet to the downdrift side [Fitzgerald, 1988].

Sediment by-passing is defined as the process which allows material, after a short interruption caused by an inlet, pass, channel, jetty or other type of littoral barrier, to become part again of the normal littoral drift zone a short distance downdrift from the littoral barrier. According to Bruun and Gerritsen [1959] there are two main principles of by-passing by natural action: by-passing via off-shore bars and by-passing by tidal flow action. In the former case the littoral drift continues over the submerged bar to the down-drift barrier maintaining the integrated longshore drift. When tidal flow plays an important part in the by-passing of material, sand transfer can take place by migration of channels and bars or by transport by tidal flow in the channels.

Bruun and Gerritsen [1960] and Bruun et al. [1978] proposed an expression to indicate the type of by-passing:

$$r' = \frac{P}{M_{tot}} \tag{2.1}$$

in which P is the tidal prism per tidal cycle and M_{tot} the total drift per year. The by-pass capacity of the inlet, r', is defined as:

r' $<$ 20; inlets become non-permanent overflow channels

20 $<$ r' $<$ 50; the inlets are typical bar-by-passers

50 $<$ r' $<$ 150; the entrance bars are still pronounced (combination of bar-by-passing and flow-by-passing)

r' $>$ 150; the inlets are predominant flow-by-passers (little bar and good flushing)

Three models to explain inlet sediment by-passing along mixed-energy coasts were proposed by Fitzgerald et al. [1978] and are illustrated in Figure 2.4. The first model describes the tendency of the inlet to migrate downdrift and then shift their course by rupturing the barrier spit. The rate of migration is dependent on several factors, such as wave climate, sediment supply, depth of the main channel and tidal currents. The updrift barrier is subject to accretion by longshore currents, growing and elongating the tidal channel. As the inlet became narrower, the downdrift shore erodes because tidal currents try to maintain the connection open. Over time, the inlet flow between the bay and the ocean becomes more and more inefficient. This process continues until a storm forms a new inlet, breaking the barrier quite often just in front of the ebb channel. The new opened channel is a more direct and efficient pathway for tidal exchange. The older, longer path gradually closes.
The ebb-tidal delta breaching, illustrated in the center of Figure 2.4, occurs at tidal inlets that have stable positions but a variable position of the main ebb tidal channel. The main ebb channel will be downdrift deflected by the longshore sediment transport. A severe deflection of the main channel produces a flow inefficient at the inlet, decreasing the discharge through the old ebb channel. Eventually, this results in a deviation of the ebb discharge to a more direct seaward pathway through the ebb-tidal delta.
The stable inlets, illustrated in the right side of Figure 2.4, have a stable position as well

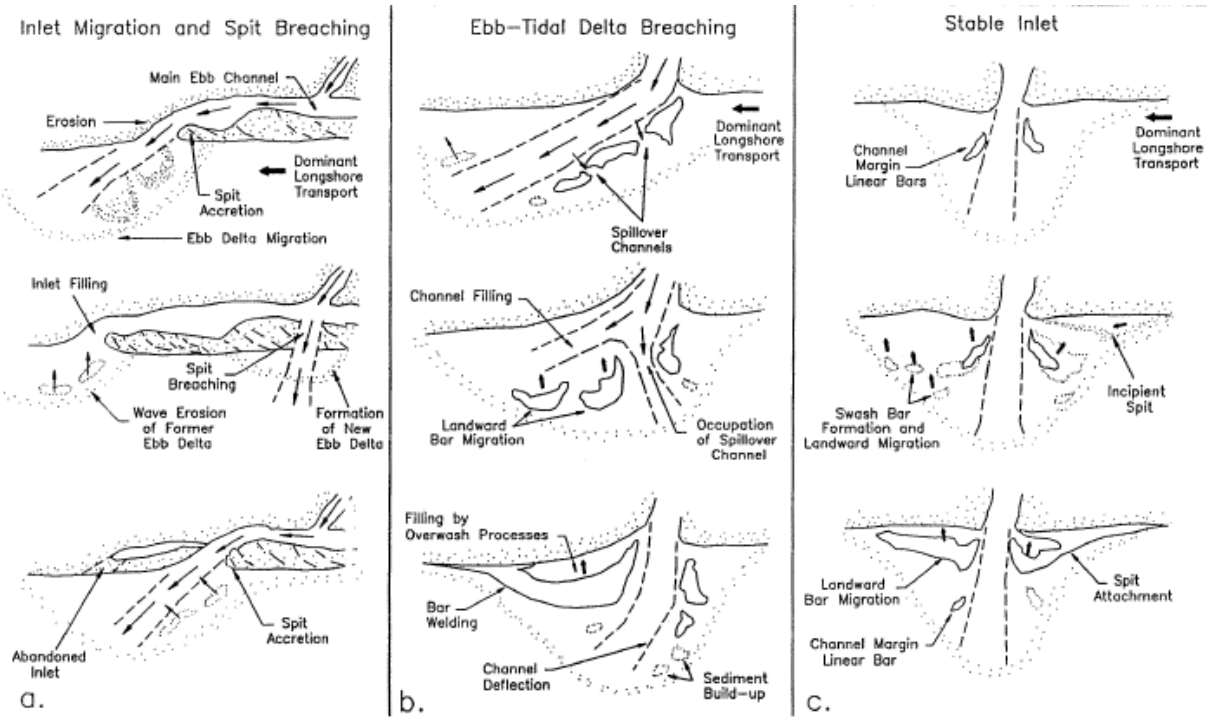

Figure 2.4: Three models of inlet behavior and sediment bypassing for mixed-energy coasts (from Fitzgerald [1988]).

as its main ebb channel. Sand by-passing occur through the constant formation of bars on the ebb tidal delta platform. The dominance of landward flow, coupled with breaking and shoaling waves, move the swash bars onshore, attaching them at the downdrift shoreline. The sediment by-passing depends on sand deliveries through the channel system that form the ebb delta, migrate landward and link to the downdrift shoreline.
Fitzgerald [1988] mentions that, in real tidal inlets, all three by-pass processes can occur simultaneously or may dominate alternately.
The stabilization of migrating inlets is often achieved by the construction of shore perpendicular structures at the mouth, named jetties, to protect the navigation channel from waves or to reduce the amount of dredging required to maintain the navigable depth. These two actions are navigation controls that have the intent of promoting safe passage through the inlet with minimal costs. However, the presence of the jetties affects the local hydrodynamics confining the tidal currents into the channel and restricting the bypassing sediment. In CEM [2002] are found schemes of idealized sediment transport for stabilized inlets and the consequent shore erosion.

2.5 Sediment transport

Sediment transport processes are very important in lagoons and inlets, being essential the good understanding of these processes to describe their morphologic changes. These processes are generally complex and are function of the hydrodynamic circulation and sediment characteristics of the bed. The tidal currents alone or coupled with waves induce sediment transport at a given point as bedload and suspended load. Furthermore, if the waves that approach the coast have an oblique angle, they induce longshore currents that transport sediments. In Sections 2.5.2 and 2.5.1 are presented several formulations to compute the sediment transport and longshore sediment transport. These formulations are then used in later sections to evaluate the sediment transport in the study area.

2.5.1 Sediment transport formulations

The nonlinear dependency of the sediment transport on the current velocity makes the net transport through inlets very sensitive to ebb/flood tidal asymmetries.
The bottom sediments start to move when the driving forces exceed the stabilizing forces. The driving forces are the shear stress between the sediment and the bed while stabilizing forces are the gravity and the frictional forces that holds the sediments on the bed [Fredsøe and Deigaard, 1992]. A critical shear velocity corresponding to the critical shear stress and the sediment size determines the sediment movement.
The rates of sediment transport can be computed by several formulations. In this study, the formulations used integrate the morphodynamic modelling system MORSYS2D and are

presented herein. At the end of this subsection a sensitivity analysis of these formulations is presented.

Bha

Bhattacharya et al. [2007] proposed a formulation to compute the total transport directly:

$$\frac{q_s}{\sqrt{\left(s_d - 1\, g\, d_{50}^3\right)}} = \begin{cases} 0.072078 \frac{T^{0.893}}{d_*^{0.353}} \left(\frac{h}{d_{50}}\right)^{0.486} & T > 2.22 \\ 0.0000782 \frac{T^{0.54}}{d_*^{0.00407}} \left(\frac{h}{d_{50}}\right)^{1.16} & T \leq 2.22 \end{cases} \tag{2.2}$$

where $T = (\theta - \theta_{cr})/\theta_{cr}$, is the transport stage parameter, θ is the Shields parameter, θ_{cr} $= \tau_{cr}/[(\rho_s - \rho)gd_{50}]$ is the Shields critical shear stress where τ_{cr} is the critical shear stress, $d_* = d_{50}((s_d - 1)g/\nu^2)^{1/3}$ is the dimensionless grain size, d_{50} is the medium particle diameter and ν is the Kinematic viscosity of the water, h is the water depth and g is the gravity.

EH

Engelund and Hansen [1967] proposed a formulation that computes the total load directly. The threshold for initiation of motion is not considered. The sediment flux is given by:

$$\vec{q_s} = \frac{0.05}{s^2\, d_{50}\, C^3 \sqrt{g}}\, U^4\, \vec{u} \tag{2.3}$$

where C is the Chézy coefficient given by $\sqrt{c_f/g}$, with c_f the friction coefficient and U is the modulus of the depth-averaged velocity.

kk

Karim and Kennedy [1990] proposed a formulation that computes the total load transport directly. The sediment flux is given by:

$$\vec{q_s} = 10^{-2.821+3.369\log((\nu_1)+0.84\log(\nu_{11}))} \sqrt{(s-1)\, g d_{50}^3}\, \frac{\vec{u}}{U} \tag{2.4}$$

where $\nu_1 = U/\sqrt{(s-1)gd_{50}}$ and $\nu_{11} = (u_* - u_{*cr})/\sqrt{(s-1)gd_{50}}$. u_* is the friction velocity and u_{*cr} is the critical stress velocity and s is the dimensionless sand density.

MPM

Meyer-Peter and Muller [1948] proposed a formulation based on experimental studies only valid for bed-load transport. Carmo [1995] improved this formulation by including the influence of bed-slope. The bed load sand flux is then given by:

$$q_s = \frac{8}{(s-1)\, g} \left(\frac{|\overline{\tau}| - \tau_{cr}}{\rho_s}\right)^{1.5} \tag{2.5}$$

where τ is the bed stress, τ_{cr} is the critical stress and ρ_s is the sand density. The bed roughness in this formulation is proportional to the sediment size and given by $2.5d_{50}$.

vR

van Rijn [1984a,b,c] proposed a formulation valid for bed load and suspended load transport. The bottom slope is considered in the evaluation of the threshold for initiation of motion. The sediment flux is given by:

$$\vec{q_s} = \left(\frac{0.053}{U} \sqrt{g \frac{\rho_s - \rho}{\rho}} \, \frac{d_{50}^{2.1}}{d_*^{0.3}} \, T_{sp}^{2.1} + F h c_a \right) \vec{u} \tag{2.6}$$

where T_{sp} is a transport stage parameter $[= (u_*^2 - \tau_c/\rho)/(\tau_c/\rho)]$, c_a is the reference concentration $(= 0.015 d_{50} T_{sp}^{1.5}/(a d_*^{0.3}))$ where a is the reference level given by:

$$a = \begin{cases} 3d_{90} + 1.1\Delta \left(1 - exp(-25\Delta/\Lambda)\right) & T_{sp} < 25 \\ 3d_{90} & T_{sp} \geq 25 \end{cases}$$

with $\Delta = 0.11 h (d_{50}/h)^{0.3} (1 - exp(-T_{sp}/2))(25 - T_{sp})$ is the dune height and $\Lambda = 7.3h$ is the dune length. A minimum value of a is set to $h/100$. In equation 2.6 F is given by:

$$F = \frac{\left(\frac{a}{h}\right)^Z - \left(\frac{a}{h}\right)^{1.2}}{\left(1 - \frac{a}{h}\right)^Z (1.2 - Z)} \tag{2.7}$$

where $Z = w/(\kappa \beta u_*) + \phi$ is the suspension parameter, where κ is the von Karman constant (=0.4), $\beta = 1 + 2(w^2/u_*^2)$ and $\phi = 1$ if $u_* \geq 100w$ and $\phi = 2.5(w/u_*)^{0.8}(c_a/0.65)^{0.4}$ if $u_* < 100w$.

In this formulation the bed roughness is evaluated through the skin roughness length $z_0 = k_s/30$ where k_s is the Nikuradse grain related roughness height equal to $2d_{50}$.

AW

The formulation presented herein is an adaptation by van de Graaff and van Overeem [1979] of the Ackers and White [1973] formulation for currents to take into account the effect of waves. The total load is given by:

$$q_{st} = U_c \, \frac{1}{1 - \lambda} \, d_{35} \left[\frac{U_{cw}}{U_{*cw}} \right]^n \frac{C_{dgr}}{A^m} \left[\frac{C_d^n \, U_{cw} \left(\frac{U_{*cw}}{U_{cw}} \right)^n}{C_d \, g^{n/2} \sqrt{\left(\frac{\rho_s}{\rho} - 1 \right) d_{35}}} - A \right]^m \tag{2.8}$$

where λ is the sediment porosity, d_{35} the particle diameter exceeded by 65% of the weight, ρ is the density of the water and $A = 0.23/\sqrt{d_{gr}} + 0.14$, $n = 1 - 0.2432 \ln(d_{gr})$, $m = 9.66/d_{gr} + 1.34$, $C_{dgr} = exp(2.86 \ln(d_{gr}) - 0.4343[\ln(d_{gr})]^2 - 8.128)$ are dimensionless parameters and $d_{gr} =$

$d_{35}[g(s_d-1)/\nu^2]^{1/3}$. In equation 2.8, U_{cw} and U_{*cw} are the current velocity and shear velocity modified and are given by:

$$U_{cw} = U_c \sqrt{1 + 0.5 \left(\xi' \frac{U_w}{U_c} \right)^2} \qquad U_{*cw} = U_{*c} \sqrt{1 + 0.5 \left(\xi \frac{U_w}{U_c} \right)^2} \tag{2.9}$$

with

$$\xi = 18 \log \left(\frac{12h}{r} \right) \sqrt{\left(\frac{f_w}{r} \right)} \qquad \xi' = 18 \log \left(\frac{10h}{d_{35}} \right) \sqrt{\left(\frac{f'_w}{2g} \right)} \tag{2.10}$$

where r is the bed roughness and f_w and f'_w are the wave friction coefficient using r and d_{35} as bed roughness, respectively.

Bi

Bijker [1971] derived a formulation for bedload transport where the total load is expressed as the sum of a bedload q_{sb} term and a suspended load q_{ss} term:

$$q_{sb} \quad = C_b \, d_{50} \, \tfrac{U_c}{C} \, \sqrt{g} \, exp \left[\tfrac{-0.27(\rho_s - \rho) \, g \, d_{50}}{\mu \, \tau_{cw}} \right] \tag{2.11a}$$

and

$$q_{ss} \quad = 1.83 \, q_{sb} \left[I_1 \ln \left(\tfrac{33h}{\delta_c} \right) + I_2 \right] \tag{2.11b}$$

where C_b is a wave breaking parameter (1.0 for non breaking waves and 5.0 for breaking waves with a ramp function between the two situations), C is the Chézy coefficient based on d_{50}, μ is a ripple factor ($= (C/C_{90})^{1.5}$, where C_{90} is the Chézy coefficient based on d_{90}), I_1, I_2 are Einstein integrals and τ_{cw} is the combined shear stress due to waves and currents given by:

$$\tau_{cw} = \tau_c \left[1 + 0.5 \left(\zeta \frac{U_c}{U_w} \right)^2 \right] \tag{2.12}$$

where τ_c is the bed shear stress due to currents only, U_w the wave orbital velocity, $\zeta = C\sqrt{f_w/(2g)}$ is a parameter for wave-current interaction, f_w a wave friction factor and U_c is the current velocity. The bed roughness in this formulation is proportional to the sediment size and given by $2.5d_{50}$.

SvR

The formulation of Soulsby and van Rijn [Soulsby, 1997] compute sediment transport under the combined action of wave and currents. The total load is given by:

$$q_{st} = A_s \, U_c \left[\sqrt{U_c^2 + \frac{0.018}{C_d} U_{wrms}} - U_{cr} \right]^{2.4} (1 - 1.6 \tan(\beta)) \tag{2.13}$$

where U_{wrms} is the root mean square wave orbital velocity and β is the local bottom slope and U_{cr} is the threshold velocity. $A_s = A_{sb} + A_{ss}$ with A_{sb} and A_{ss} the terms for bedload and suspended load, respectively, given by:

$$A_{sb} = \frac{0.005\, h \left(\frac{d_{50}}{h}\right)^{1.2}}{\left(\left(\frac{\rho_s}{\rho} - 1\right) g\, d_{50}\right)^{1.2}} \tag{2.14a}$$

and

$$A_{ss} = \frac{0.012\, d_{50}\, d_*^{-0.6}}{\left(\left(\frac{\rho_s}{\rho} - 1\right) g\, d_{50}\right)^{1.2}} \tag{2.14b}$$

where C_d is the drag coefficient ($= (0.40/(ln(h/z_0) - 1))^2$), where z_0 is the bed roughness length. In equation 2.13, U_{cr} is the threshold current velocity equal to $0.19 d_{50}^{0.1} \log(4h/d_{90})$ if 0.1 mm $\leq d_{50} <$ 0.5 mm and to $8.5 d_{50}^{0.6} \log(4h/d_{90})$ if 0.5 mm $\leq d_{50} \leq$ 2.0 mm. The bed roughness in this formulation is considered z_0 =6 mm adapted to moveable bottoms with "ripples".

Some of these formulae consider as input the mean flow velocity calculated from the hydrodynamic model (e.g. AW), while others compute the transport rates as a function of the bed shear stress or the Shields parameter (e.g. Bha). For these, the current bed shear stress is computed from equation 2.15:

$$\tau_b = \frac{1}{2}\, \rho\, f_c\, U^2 \tag{2.15}$$

where f_c is the current friction factor.
All the formulas referred above compute the total load transport, except MPM, which accounts only for the bed load. This formula has a weak dependence on sediment size due to its proportionality to $d_{50}^{3/2}(\theta - \theta_c)$, because θ is proportional to d_{50}^{-1}. The dependency on d_{50} for the MPM formula and the dependency on d_{50}^{-1} for the EH formula are easily identified, in contrast with many other formulae, like the vR formulation. This non-obvious dependency of the formulae on d_{50} and the weak coverage of sediment grain size data available (in general) for sediment transport studies, justifies a sensitivity analysis of the sediment transport formulae in this parameter.

Sensitivity analysis of sediment transport formulations

A sensitivity analysis of the sediment transport rates (q_s), computed from the aforementioned formulae, to the median sediment grain size d_{50}, the water depth h, and depth-averaged velocity U, is performed, to better understand the response of the numerical solutions concerning

bathymetric changes. This analysis is made considering suitable range of current and wave conditions above a sand bed [Silva et al., 2009] and considering values for d_{50}, h and U at several locations within the inlet. For that purpose characteristic values of the Ria de Aveiro inlet were chosen (Chapter 3).

Figure 2.5(a) represents the transport rate q_s as a function of the medium sediment grain size, d_{50}, for a constant water depth of 2, 10 and 20 m and considering a steady current with a depth-averaged velocity value of 1.0, 1.5 and 2.0 ms^{-1}. In Figure 2.5(b) the added effect of a single wave with significant height of 1 m and 7 s of wave period was considered.

The results obtained for all conditions are very similar. The SvR, EH, kk, vR and AW formulations show a decrease of the transport rate with increasing d_{50}, either in presence of tidal currents only (Figure 2.5(a)) or coupled with a regular monochromatic wave (Figure 2.5(b)). Therefore, the dependency of these formulae in d_{50} is very similar. It can be noted that this dependency is non-linear; the range of variation of q_s for the fine and medium grain sizes is higher than for the coarser sand.

In Figure 2.5(a) is visible that the formulation by Bha predicts higher transport rates, except for the higher velocities ($U = 2$ ms^{-1}) or lower depths, where the results are close to those obtained with the other formulations. The MPM formulation predicts systematically lower values of q_s, and changes with d_{50} are not very significant. Note that this formulation only takes into account the bed load transport. The transport rates computed from Bi (in Figure 2.5(a) and (b)) and vR formulations present some oscillations with d_{50} that are not observed with any other formulae, in particular, for the finer sediments. This behavior was also observed by Pinto et al. [2006], that concluded that the vR formulation is more sensitive to the physical properties than kk, EH or AW formulations. When compared to SvR, EH, kk and AW, the vR formula over-predicts the transport rates for finer sediments.

The results predicted, by all the formulations and from the ensemble of tests considered, show a larger spread for the lowest values of U and finer sand than for the highest velocities and coarser sand, respectively. These results stand equally valid for the large range of depth-average tidal flow velocities observed within the inlet.

As an example, Figure 2.6 represents the computed net transport rates for a tidal cycle (for a neap and spring tide periods) forced by tidal currents only and forced by tidal currents coupled with a wave regime, for a local mean depth of 10 m and 20 m (the location of these stations is indicated in Figure 2.7 as P1 and P2, respectively). The concurrent depth-averaged velocity intensity computed from a hydrodynamic model (ELCIRC) at these stations is presented in the upper panel of Figure 2.6(a) to (d). The transport rates were computed considering two values for the d_{50}: 0.3 and 1.5 mm. For any sediment grain size and any sediment transport formulation, the maximum values of q_s increase as the maximum depth-average velocities increase from neap to spring tides, and for small velocities, the transport is null. An exception to this behavior is with EH formulation, because it does not include a threshold velocity for sediment motion. Also, the sediment transport rates

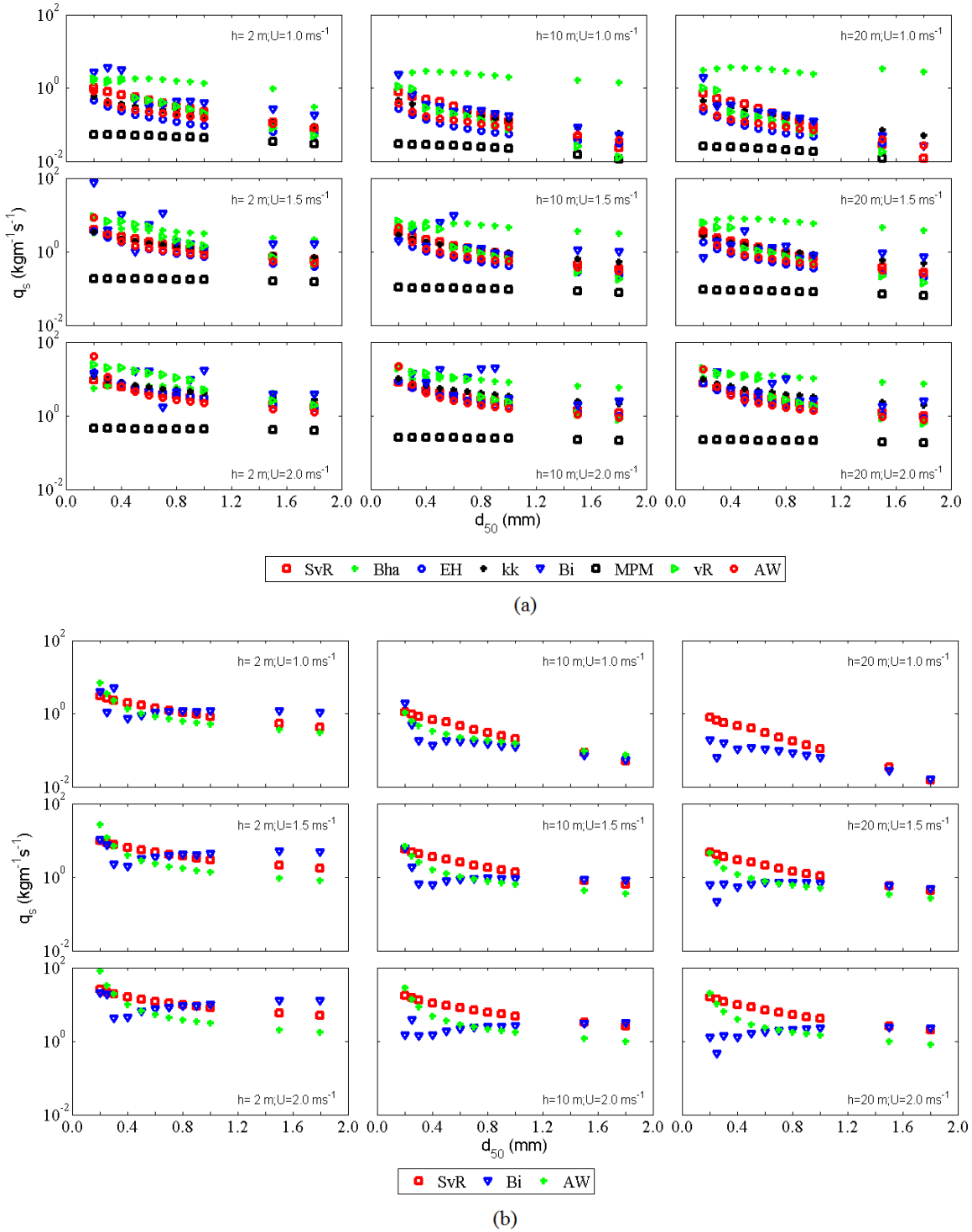

Figure 2.5: Computed transport rate q_s (kgm^{-1}s) in function of d_{50} (mm), considering (a) only the tidal currents and (b) tidal currents coupled to a regular monochromatic wave.

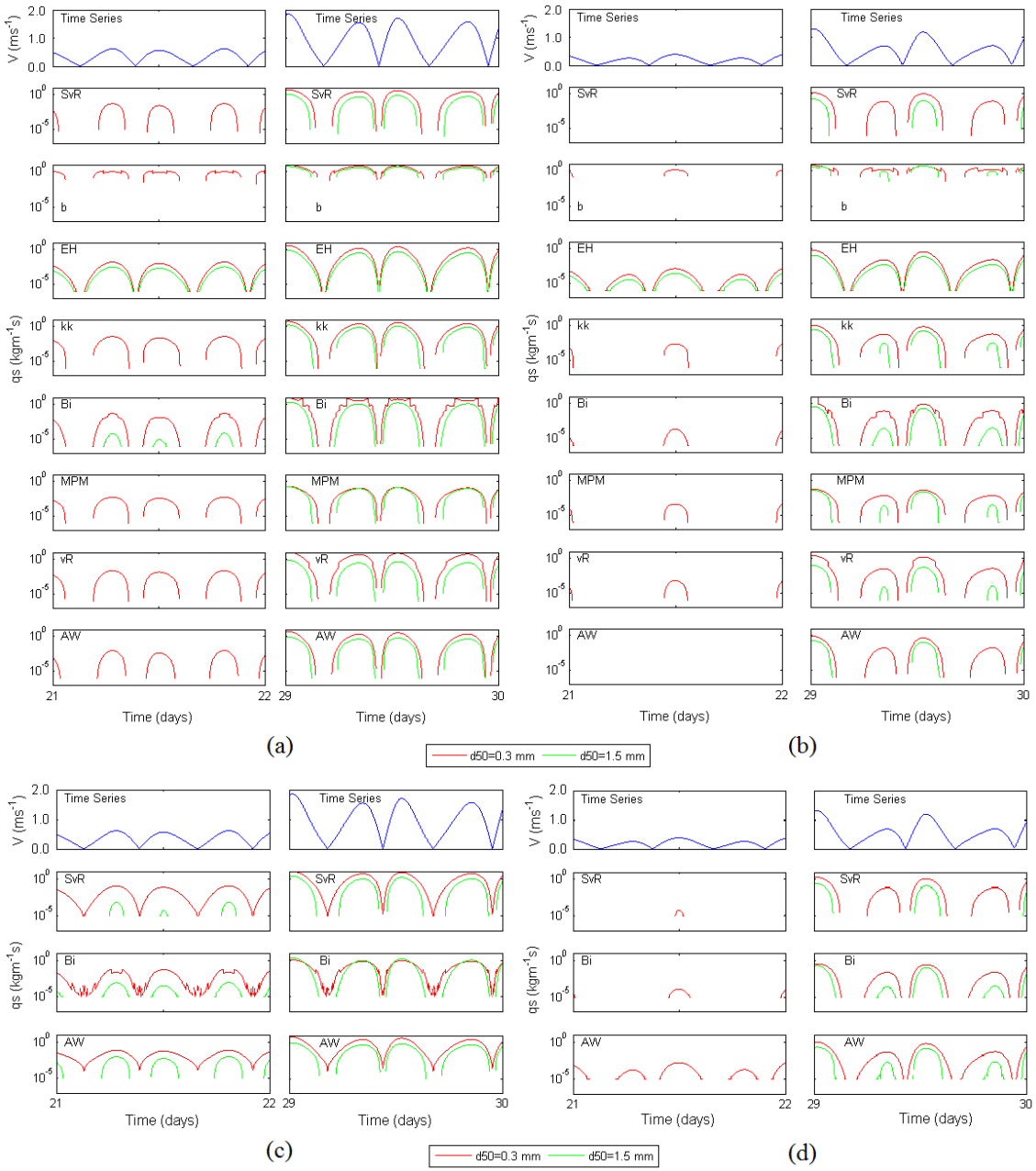

Figure 2.6: Computed transport rate q_s (kgm^{-1}s) in function of d_{50} (millimetre) for a tidal cycle forced by tidal currents only (a) and (b) and forced by tidal currents coupled with a wave regime (c) and (d), for a depth of (a) and (c) 10 m and (b) and (d) 20 m. The left (right) columns in (a), (b), (c) and (d) represent the transport rates at neap (spring) tide condition.

computed from the Bi and vR formulations present some perturbations for the highest velocities. Analyzing Figure 2.6(c) it is possible to perceive that the presence of a regular monochromatic wave induce continuous sediment transport for lower depths (10 m in this

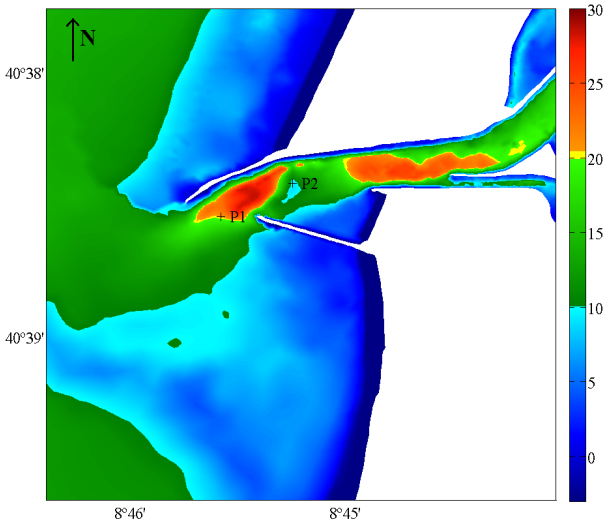

Figure 2.7: Locations of the points where the velocity is used to perform the sensitivity analysis presented.

example). For this water depth, the generated currents have the capacity to move coarser sediments, even in neap tide conditions. For Bi formulation, are observed higher instabilities in the sediment transport rates. For the deeper water case (Figure 2.6(d)), the effect of the wave is not strongly noticeable. However, for neap tide condition exists a slightly increase in the capacity of transporting finer sediments.

To analyze the differences between the several formulations predictions, the ratio between the transport rate computed with a particular formula and the mean value obtained by averaging the fluxes for all formulations was computed (Figure 2.8). This study is analogous to those performed by Sistermans and van der Graaff [2001] and Silva et al. [2009]. It is observed that the higher deviations occur for small flow velocities in particular for the SvR and AW formulations considering only the tidal currents forcing and for the SvR formulation when considering the coupled forcing of the tidal current and the regular monochromatic wave. For the transport predictions with the tidal current forcing (Figure 2.8(a) and (b)) the minor deviations are observed for the EH formulation while for the coupled forcing the minor differences are observed for the AW formulation. In the middle panel of Figures 2.8(c) and (d), where the deviation considering high depth and small median sediment size is illustrated, are observed oscillations in the deviations for small flow velocities and in higher magnitude and extension for the Bi formulation, with oscillations of approximately 0.25.

All the aforementioned formulations are used to computed the sediment transport in the numerical simulations that are performed later in Chapters 5 and 6. Are expected large sediment transport rates by using the Bha formulation and in the opposite, small values of sediment transport by using the MPM formulation. The results when using the Bi and vR formulations are expected to present some numerical oscillations.

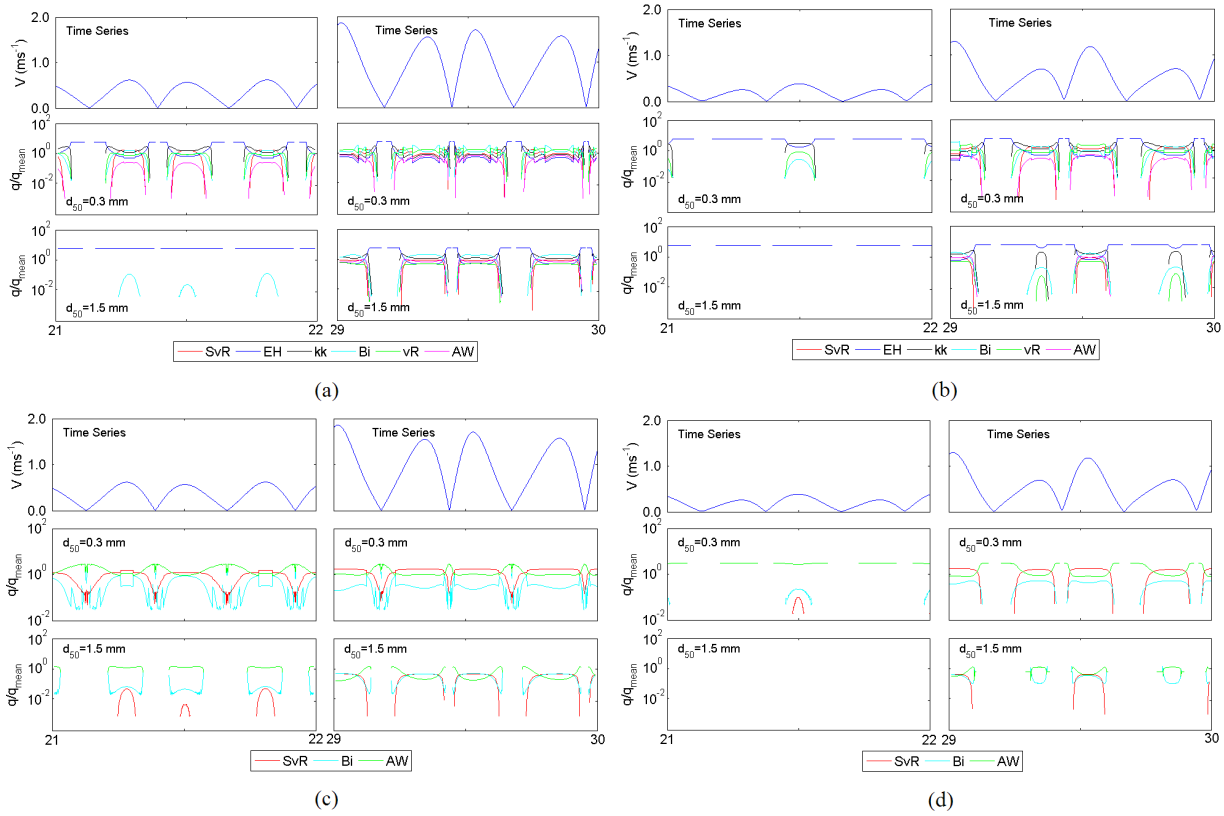

Figure 2.8: Values of the ratio q/q_{mean} for a tidal cycle forced by tidal currents only (a) and (b) and forced by tidal currents coupled with a wave regime (c) and (d), for a depth of (a) and (c) 10 m and (b) and (d) 20 m. The left (right) columns in (a), (b), (c) and (d) represent the transport rates at neap (spring) tide condition. The middle (bottom) panel in (a), (b), (c) and (d) represent the transport rates considering a sediment size of $d_{50} = 0.3$ mm ($d_{50} = 1.5$ mm).

2.5.2 Longshore sediment transport formulations

The sediment transport could be promoted by the longshore currents within and just outside the surf zone. When waves break in the surf zone they release momentum, giving rise to a radiation stress. When waves are obliquely incident to the shoreline, there is a longshore component of the radiation stress, whose gradient give rise to a longshore current which is balanced by friction with the bed [Soulsby, 1997], and promotes longshore transport.

The sediment transport induced by longshore currents along the coast is easily identified through coastal erosion or accretion around structures, such as offshore breakwaters. Considerable amounts of sediment are transported along the coast, depending on the height, period and direction of the waves. Additionally, the sediment size and the beach slope can also determine the amount of transported sediments.

The longshore sediment transport can be calculated through several longshore sediment transport formulations. Herein six of them are presented which will be used in Section

3.7 to quantify the transport in the study area and also to find a simplified wave regime which induces a longitudinal sediment transport at a beach equivalent to that caused by the complete wave regime.
The first five formulations were selected according to Larangeiro and Oliveira [2003]. In these set of formulations the longshore transport rate is proportional to the wave characteristics in the breaker line with different dependencies in wave breaker height, wave period and incident wave breaker angle. The last formulation [CEM, 2002] the longshore sediment transport is proportional to the wave characteristics in deep water.

K&I
Komar and Inman [1970] proposed an empirical formulation for the longshore transport rate base on field data given by:

$$I_\ell = K' \, (E \, c_g)_b \, \cos \alpha_b \, \frac{\overline{V_\ell}}{u_m} \tag{2.16}$$

with

$$\overline{V_\ell} = 20.7 \, i \, (g \, H_b)^{1/2} \, \sin 2 \, \alpha_b \tag{2.17}$$

and

$$u_m = \frac{\gamma}{2} \, (g \, h_b)^{1/2} \tag{2.18}$$

where K' is a dimensionless coefficient, E is the wave energy, c_g is the wave group velocity and i is the bottom slope. By the CEM [2002]:

$$I_\ell = (\rho_s - \rho) \, g \, (1 - n) \, Q_\ell \Leftrightarrow Q_\ell = \frac{I_\ell}{(\rho_s - \rho) \, g \, (1 - n)} \tag{2.19}$$

Thus:

$$Q_\ell = \frac{K' \, (E \, c_g)_b \, \cos \alpha_b \, \frac{\overline{V_\ell}}{u_m}}{(\rho_s - \rho) \, g \, (1 - n)} \tag{2.20}$$

This formulations is proportional to the wave height (power to 2.5) and wave angle at the breaker line, and also proportional to the bottom slope.

K86
Kamphuis et al. [1986] proposed an empirical formulation for the longshore transport rate based on field and laboratory data given by:

$$Q_\ell = \frac{1.28}{(\rho_s - \rho) \, (1 - n)} \, H_b^{7/2} \, i \, d_{50}^{-1} \, \sin 2 \, \alpha_b \tag{2.21}$$

This formulation is proportional to the wave angle and to the wave height (power to 3.5) at the breaker line, to the bottom slope and inversely proportional to the median sediment size.

Kr88

Kraus et al. [1988] proposed an empirical formulation based on linear regression analysis of experiments for the longshore transport rate given by:

$$I_\ell = 2.7\,(R - R_c) \tag{2.22}$$

with $R = \overline{V_l}\,W\,H_b$, being W the total width of the cross section and R_c a constant. By Kraus et al. [1988] it is known that I_ℓ has units of $N\,s^{-1}$ and the coefficient 2.7 is not adimensional. By Larangeiro et al. [2005]:

$$Q_\ell = \frac{2.7\,(R - R_c)}{(\rho_s - \rho)\,g\,(1 - n)} \tag{2.23}$$

This formulation is proportional to the wave height (power 1.5) and to the wave angle at the breaker line, to the bottom slope and to the total width of the cross section.

K91

Kamphuis [1991] based on laboratory data and reanalysis of field data, modified the K86 formulation and proposed a formulation for the longshore transport rate which includes the wave peak period influence:

$$Q_\ell = \frac{2.27}{(\rho_s - \rho)\,(1 - n)}\,H_b^2\,T_p^{1.5}\,i^{0.75}\,d_{50}^{-0.25}\,\sin^{0.6} 2\,\alpha_b \tag{2.24}$$

where the peak period is T_p=1.085T_z+3.058 and T_z is the zero-upcrossing wave period.
In this formulation the dependency on wave height and wave angle at the breaker line is smaller than at K86, also the influence on the median sediment size and bottom slope was reduced. This formulation is proportional to the wave angle and to the square of the wave height at the breaker line, to the bottom slope (power to 0.75) and inversely proportional to the sediment size d_{50} (power to 0.25).

C2

Valle et al. [1993] proposed an empirical formulation for the longshore transport rate given by:

$$Q_\ell = \frac{k}{16\,\sqrt{\gamma}\,(\rho_s - \rho)\,a'}\,\rho\,\sqrt{g}\,H_b^{5/2}\,\sin 2\,\alpha_b \tag{2.25}$$

with $k = 1.4\,e^{-2.5\,d_{50}}$, the medium particle diameter is d_{50} in mm and $a' = 1 - n$. γ is the breaker index, ρ_s is the sand density, ρ is the water density, α_b is the wave angle at breaker point and n is the sediment porosity. The wave height in this formulation is the root mean

square wave height H_{rms} given by:

$$H_{rms} = \sqrt{8\, m_0} => \sqrt{m_0} = \frac{H_{rms}}{\sqrt{8}} \tag{2.26}$$

$$H_s = 4\sqrt{m_0} => \sqrt{m_0} = \frac{H_s}{4} \tag{2.27}$$

$$\frac{H_{rms}}{\sqrt{8}} = \frac{H_s}{4} \Leftrightarrow H_{rms} = \frac{\sqrt{8}}{4} H_s \Leftrightarrow H_{rms} = \frac{\sqrt{2}}{2} H_s \tag{2.28}$$

where H_s is the significant wave height. This formulation is proportional to the root mean square (power to 2.5), to the wave angle at the breaker line and to the exponential of he sediment size d_{50}.

CERC

The CERC formulation was developed in 1966 by the US Army Corps of Engineers based on field works. In 1977 and 1984 this formulation was updated by the Shore Protection Manual. The most recent version of this formulation is presented in CEM [2002]. This formulation is based on the assumption that the longshore transport rate depends on the longshore component of wave energy flux in the surf zone:

$$Q_\ell = 0.064208\, H_0^{5/2}\, F(\alpha_0)\, f \tag{2.29}$$

with

$$F(\alpha_0) = \cos \alpha_0{}^{1/4}\, \sin 2\, \alpha_0 \tag{2.30}$$

where H_0 is the wave height in deep water, α_0 is the wave angle, related to shoreline, in deep water and f is the wave frequency.

The currents effect when significant is a limitation to this empirical formulation.

2.6 Morphological evolution

The continuous interaction between tides, waves and sediments, changes the channels bed and results in a nonsteady lagoon morphology which is modified by hydrodynamic conditions, sediment supply and human interventions [Hibma et al., 2004]. These interactions can result in residual transport currents leading to net sediment erosion or accretion. Over time, these erosion and deposition trends change the lagoon morphology and between others, might threat the navigation in the channels, the stability of structures and the ecological habitat.

The morphological changes in a lagoon take place at different time and spatial scales through complex interactions. Time scales of lagoon morphological evolution may vary from few hours to millennia. de Vriend [1996] presented four groups of scales for changes in morphological

features: micro-, meso-, macro- and mega-scale phenomena. The first group encloses the smallest morphological bedforms, such as ripples, dunes and sandwaves, which takes place at smaller time scales than the corresponding morphodynamic behavior. The meso-scale phenomena encloses the alternating and interacting flood and ebb channels, tidal flats and shoals and are identified as the primary morphodynamic behavior, due to the interaction of tidal processes and bed topography. Features such as inlet gorge and ebb tidal delta, which have much larger scales than the corresponding primary morphodynamic behavior, are included in the macro-scale phenomena. The last one is the mega-scale phenomena which encloses the entire lagoon and the adjacent coastal area.
In lagoon evolutionary processes, morphodynamic and hydrodynamic processes are strongly coupled. The feedback mechanism that comes from the morphological changes affects the hydrodynamic conditions and sediment movement in the lagoons [Moore et al., 2009]. Particularly, changes in the mean water depth and changes in the elevation of the intertidal areas may alter the tidal regime of the lagoons. This feedback mechanism combined with the non-linear interactions have made the lagoon morphological evolution a further complex phenomena to predict.

2.7 Conclusions

In this chapter a classification of lagoons and inlets according to tidal range and wave height, separately or based on a combination of both, was presented. This classification will be used to characterize the study area in the following chapter. Additionally, the system can also be characterized in terms of flood or ebb dominance, evaluated through the magnitude of tidal asymmetry, which is the ratio between the compound harmonic constituent of the dominant harmonic and the dominant harmonic itself. The larger the ratio, the more distorted is the tide and more strongly flood or ebb dominant is the system.
Eight formulations to compute the sediment transport were presented, considering the tidal currents only or coupled with a wave regime. The sensitivity analysis performed allow to conclude that the dependence of sediment transport on the d_{50} is more important for the fine-medium sediments for SvR, EH, kk and AW formulations. As the average sediment at inlet channels is coarser, the uncertainty of the d_{50} does not seem to be crucial for inlet case studies. However it is expected that the morphodynamic simulations performed using Bha formulation over-predict the bathymetric changes. On the opposite, when using the MPM formulation to compute the sediment transport, the bathymetric changes will be under-predicted. The Bi and vR formulations could induce oscillations in bathymetric predictions. For the longshore sediment transport, six formulations were presented. In this case the q_s is proportional to the wave characteristics at deep water and at the breaker line.

Chapter 3

Characterization of the Ria de Aveiro Lagoon and Adjacent Coastal Zone

3.1 Introduction

A characterization of the study area is carried out in this chapter, including the description of the origin of the lagoon and its inlet, of the hydrodynamics and the wave regime at the inlet and adjacent coastal shore, and of the morphology and bottom sediments of the inlet, . The morphologic characterization of the study area is performed by studying the historical bathymetric evolution determined through the analysis of several data collected by surveys performed by the Aveiro Harbour Administration (A.P.A.). This analysis supports the comprehension of the morphology behavior of the inlet and surrounding areas along the years, as well as the identification of areas subject to erosion and accretion.

A characterization of the distribution of the bottom sediments at the inlet and surrounding areas is also performed in this chapter, through the analysis of data collected from surveys carried out by several researchers and published in literature. This characterization allowed the construction of a bottom sediment size distribution variable in space, for the study area, to be used in the modeling studies of Chapters 5 and 6.

At the end of the chapter, a set of waves, that induces the same longshore transport offshore the study area equivalent to that caused by the complete wave regime is derived, through a simplification of the wave regime observed at two nearby wave directional buoys.

3.2 Origin of the Ria de Aveiro lagoon and its inlet

The Ria de Aveiro lagoon is geologically very young. Its origin is related to fluctuations in sea level caused by climatic oscillations [Dias et al., 1994] and to the southward transport of sediments by alongshore currents [Abrantes et al., 2006].

According to Tomás [1995] the origin of the spit South drift that originate the Ria de Aveiro in its actual configuration it is not known precisely. Some authors refer the XI or XII century near Furadouro (Ovar) [Tomás, 1995]. In Figure 3.1 is presented the probable evolution of the shoreline between Espinho and Mira since 1200 until 1808.

In XIII century the spit reached Torreira and remained in this location until the end of this century. Around 1407 the inlet was located a few kilometers North of the actual location, migrating to South until Costa Nova (in the area nowadays known as Mira channel). The

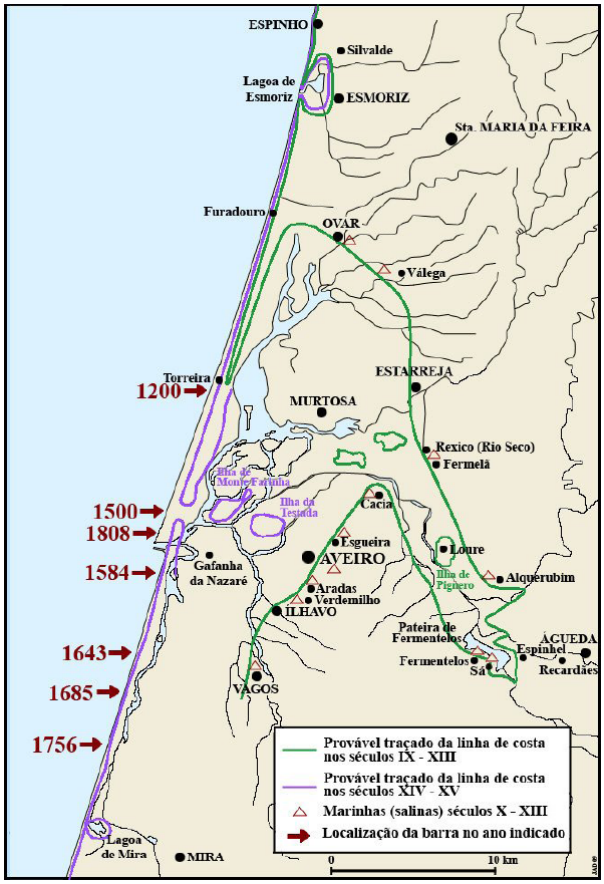

Figure 3.1: Probable evolution of the coastline between Espinho and Mira, with reference to main salt ponds and islands and showing the position of the river mouth. The 1808 inlet was artificially open. (-) Possible shoreline position in IX-XII centuries; (-) Possible shoreline position in XIV-XV centuries; (△) Salt pans in X-XIII centuries; (⇒) inlet localization in the years specified. From Bastos [2009].

spit reached this location in the terminus of the century, remaining there until the beginning of the XVI century. The South movement of the inlet occurred due to the existent strong currents and flooding, as a result of the high temperatures and sea level rise induced by the global warming that took place in the X-XIV centuries (Little Climate Optimum) [Tomás, 1995].

The continuity of the southward evolution of the spit was synchronous with the abrupt climate change in the XIV-XIX centuries (Little Ice Age), characterized by low temperatures and a decrease in mean sea level [Dias et al., 1994]. These changes promoted accretion trends at the inlet and consequently inlet instabilities. Therefore, the access to the harbour located in the inner lagoon became gradually precarious, with direct consequences to the economy of this region [Teixeira, 1994].

After the XVI century the accretion increased and the South movement of the inlet remained. This continuous South movement of the inlet induced a decrease in flood water volume and subsequent decrease in ebb water volume, essential for its maintenance. The lagoon accretion was intensified by the insufficient sediment transport by Vouga river in ebb tidal currents.

Around 1600 the inlet was located South of Costa Nova and in 1643 it lied 18 km South of Aveiro, near Vagueira. In that time the normal access to the lagoon was possible since the inlet depth was between 3 and 6 m in low and high tide, respectively. The South movement of the inlet remained and in 1650 it was located in Vagueira, and in 1685 further South.

During this period the inlet provided bad navigation access to the harbour, alternating periodically between the lagoon closure and stable conditions. At this most southern location the inlet was very far from the Vouga river and the inlet channel between Vagueira and Aveiro had more than 15 km. In this period and to improve the water exchange between the lagoon and the ocean, two Dutch engineers performed the first studies to construct an artificial inlet nearby S. Jacinto. In 1736 the access to the harbour was particularly precarious [Teixeira, 1994].

In the years that follow 1739 the continuous South movement of the spit placed the inlet near Mira, reaching this place in 1741. In this date the inlet was nearly closed being fortuitous the connections between the ocean and the lagoon. The definitive closing of the inlet occurred in 1756. Until 1760 there wasn't any record of commercial ship navigation in the channel. The consequences were catastrophic hitting the populations with illness and poorness [Dias et al., 1994]. Only in 1802 the works to open an artificial inlet in the place where it is presently started, being concluded in 1808 [Teixeira, 1994].

After these works the new inlet already had a depth range between approximately 4 to 6 m, and 264 m width. The structure built embodied a breakwater in E-W direction. Due to the inlet instability, a new breakwater was built 300 m North of the former in 1818, with the works being threatened by the fragility of the structure. In the following years the inlet suffered accretion and, in 1853 it was only 2 m deep. In almost three decades (1858-1886) engineering works were carried out in the inlet, consisting in a reinforcement of the South

breakwater, the construction of a new North breakwater in 1859 and the connection of the Mira channel to the lagoon [Teixeira, 1994]. However, the instability of inlet depth returns until the beginning of the XX century.

In 1932/36 new engineering works were performed in the lagoon: a new North breakwater, a triangular 'dam' to regulate the tidal prism in the inlet and dredging activities in the inlet and navigation channel. At this time the inlet depth was around 5 m.

A new phase of works began in 1948, extending in 710 m the North breakwater and constructing a new South breakwater with 900 m. The works lasted for almost a decade, being performed several dredging operations at the inlet and surrounding areas. In 1958 depths reached 10 m at the inlet.

An extension of 520 m of the North breakwater was performed in 1984/85 [Teixeira, 1994], conducting the ebb sediment transport to regions located southward.

The orientation and localization of the North breakwater turns it into the most important structure and also the most susceptible to damage due to the wave climate characteristic of the Portuguese West coast [Moreira and Gomes, 2001]. Due to its relative inaccessibility, structural maintenance works were not performed for 16 years, despite the evident structure damages. Consequently, a first collapse of the North breakwater (of approximately 20 m) occurred during storms at the end of 1995 and beginning of 1996. The strong wave regime in the Winter of 1997/98 caused a new rupture of more than 47 m in the breakwater and the landslide of the "lighthouse" of this structure.

When the repairing works began in 1999 the breakwater already had a rupture 20 m higher, totalizing a destruction of 87 m. The blocks that fall off the structure lied nearby the inlet, endangering the normal operation of the Aveiro harbor. The repairing works ended in 2001. By that time the erosion in the surrounding area of the head of the North breakwater was already a concern. Surveys performed in that period revealed that the 10 m bathymetric line that in the 80 decade was 600 m far from the head of the breakwater, was in that period in less than 300 m far, making the wave heights that reach the structure higher than those initially predicted. The surveys performed also revealed the presence of eroded areas with depths higher than 20 m, near the foundation of the breakwater, threatening the stability of this structure.

The local harbor authorities were contacted with the purpose of collect information about the dredging activities in Ria de Aveiro lagoon inlet along the last years, namely areas and volumes dredged, as well as dates of these interventions. Unfortunately this information is not available, and therefore cannot be used in order to improve the knowledge about the inlet morphodynamics.

The actual configuration of the Ria de Aveiro lagoon is therefore the result of the long term transport of sediments, modified by the presence and configuration of the inlet. Considering the actual sediments transport in the lagoon, it is crucial to analyze the sediments origin and preferential paths inside the lagoon.

In fact the sediments at the lagoon may have three sources: oceanic, from the rivers and from the margins degradation, which is being presently accelerated by the increase of the tidal currents and the tidal prism [Picado, 2008; Picado et al., 2010].
To study the suspended sediments behavior in the Ria de Aveiro lagoon, Dias et al. [2007] used a lagrangian numerical model to release particles at the inlet and at the Vouga river mouth, and analyzed their trajectories inside the lagoon. The authors observed that the particles of oceanic origin released at the inlet are transported mainly to the S. Jacinto channel and to the Espinheiro and Mira channels during the tidal excursion, however the far end of the channels remains out of oceanic influence. Of all the particles released at the navigation channel and at the four main channels, only those released at the S. Jacinto channel became trapped in the upper lagoon. The particles released at the Ílhavo channel had a small influence area. The remaining emissions reached the inlet and are flushed out of the lagoon during the ebb.
Considering that the Vouga river is the main sediment source of fluvial origin, the particles released at its mouth were analyzed and it was found that they are transported along the Espinheiro channel and exported to the ocean.
In previous works [Dias, 2001; Oliveira et al., 2007; Picado, 2008] was found that the Ria de Aveiro lagoon central area is actually ebb dominant, while the main channels heads are flood dominant. Therefore, and taking into account the particle trajectories described, the sediments of oceanic and fluvial origin are exported to the nearshore, being concluded that the Ria de Aveiro lagoon is characterized by sediments exportation. Nevertheless, at the upper reaches of the lagoon, the sediments, mainly from the channels margins, may became trapped as a result of the flood dominance in that regions.
Comparing the lagoon bathymetry of 1987/88 (general topohydrographic study performed by the Portuguese Hydrographic Institute) with a just performed survey in the frame of the *Polis Litoral da Ria de Aveiro* study, it is observed that the almost overall of the lagoon suffered erosion (with exception at some channels heads with accretion trends). This pattern is in agreement with the overall sediment dynamics previously described, since there are no important sediment sources into the lagoon and it reveals an important trend to export sediments to the ocean.

3.3 Morphological characterization

Nowadays, the Ria de Aveiro is composed of several channels and intertidal areas, resulting in a very complex morphology. The lagoon has a maximum width of 10 km, and its length measured along the longitudinal axis is 45 km, covering an area of 83 km^2 at high tide (spring tide) that is reduced to 66 km^2 at low tide [Dias and Lopes, 2006]. The average depth of the lagoon is approximately 1 m, relative to the chart datum, however higher depths are observed at the inlet and navigable channels that are maintained through dredging operations. The

maximum depths, of approximately 30 m, are observed at the inlet while at the navigable channels 10 m depth are observed [Dias and Lopes, 2006]. The artificial inlet configuration remains since 1984/85, being approximately 350 m wide and 2 km long.

Several topohydrographic surveys of the inlet have been performed through the years by the Portuguese Hydrographic Institute (I.H.) and by the Aveiro Harbour Administration (A.P.A.), and were available for this study. The data analyzed corresponds to surveys performed between 1987 and June 2010 and are irregular in time and area (Figures 3.2 and 3.3). The survey of 1987/88 was performed by the I.H. while the remain surveys where performed by A.P.A.. There is a time span of 14 years between the first two surveys, performed in 1987/1988 and 2001, respectively. The time spans between the following bathymetries vary between several months and 1 year. Comparisons between bathymetric surveys from different periods allow an interpretation of the bottom dynamics. In Figures 3.2 and 3.3 are represented the available bathymetric data.

A first rough analysis shows that the study area, composed by the tidal inlet and the navigation channel, is characterized by two deeper areas separated by a shallower water zone. The deepest area is located at the inlet, between the breakwaters, while the other region with large depths is located between the tidal gauge and the channel bifurcation (called *triângulo das marés*, cf. Figure 1.2). The study area is also characterized by a beach near the South breakwater, the *Meia Laranja* beach. Through the years, the deepest area located at the inlet is becoming deeper and is migrating offshore and slightly inflecting southward (Figures 3.2 and 3.3).

To perform a comparative analysis between bathymetric changes of consecutive surveys, the data illustrated in Figures 3.2 and 3.3 were interpolated through the nearest neighbor method (results in the Appendix) to a regular grid. In the present study, the small bathymetric changes with maximum variations of 0.2 m in absolute value, will be considered negligible. Furthermore, only the bathymetric changes for the regions where data from both surveys were measured are represented.

The bathymetric changes between 1987/88 and June 2001 (Figure 3.4) show a generalized deepening of the inlet channel higher than 4 m (also referred by Moreira and Gomes [2001]). At the entrance zone, near the side walls of the inner North jetty and in the central part of the channel, the erosion show higher rates. Outside the inlet channel, a well defined track showing erosion may reveal dredging activities for navigation purposes. Additionally, accretion is identified in different zones: near the South jetty, at its head (for the higher depths, see Figures 3.2, 3.3) and at the inner "shadow" zones; at the head of the North jetty; in some spots near the side walls of the inlet channel and near the *triângulo das marés* (for the larger depths, see Figures 3.2, 3.3).

In general, all the subsequent bathymetric changes show generalized erosion in the navigation channel. Between June 2001 and March 2003 it is observed a strong erosion pattern near the head of the North breakwater (Figure 3.5). In the navigation channel near the side walls

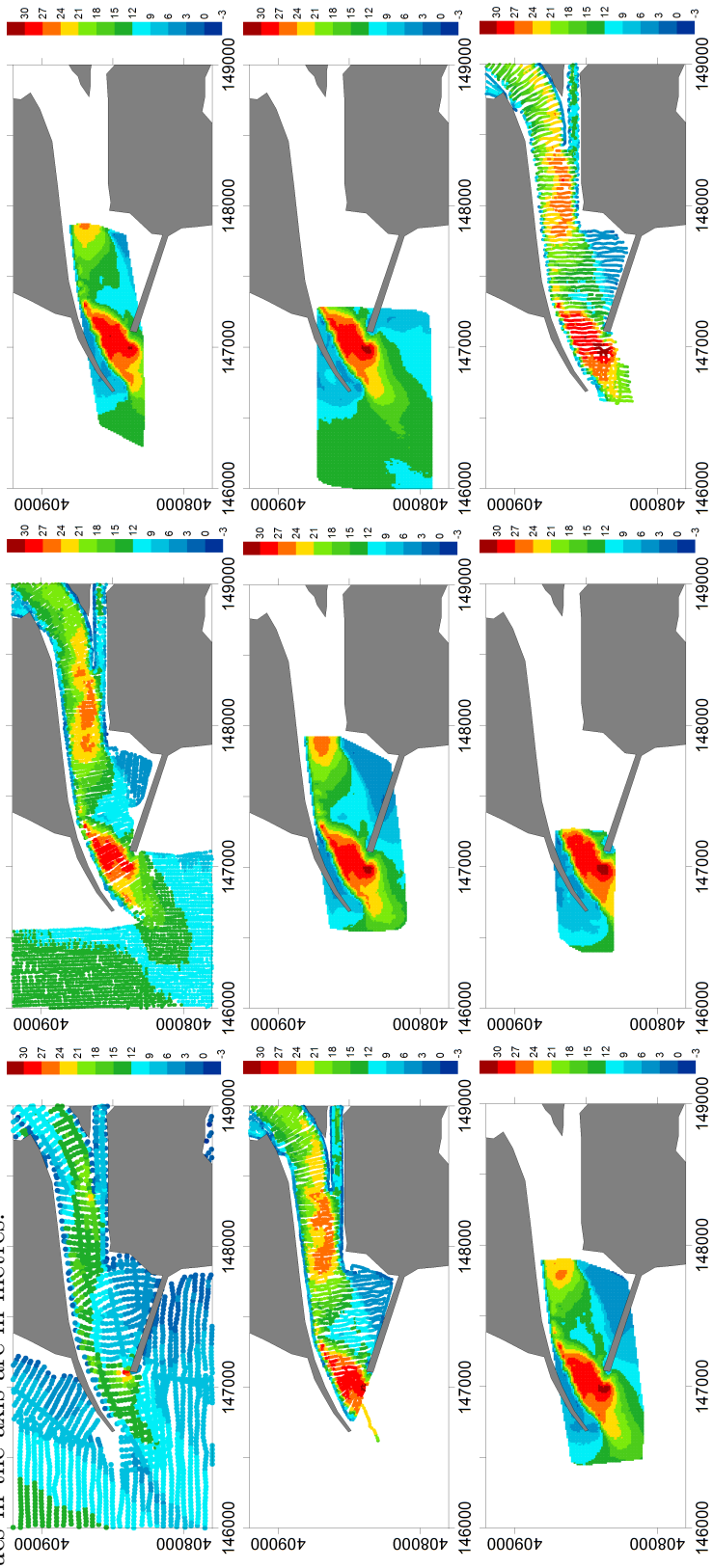

Figure 3.2: Bathymetry in meters of the Ria de Aveiro lagoon inlet corresponding to the surveys of (from left to right, top to bottom): 1987/88, June 2001, March 2003, July 2003, September 2003, November 2003, March 2004, September 2004 and October 2004. The values in the axis are in metres.

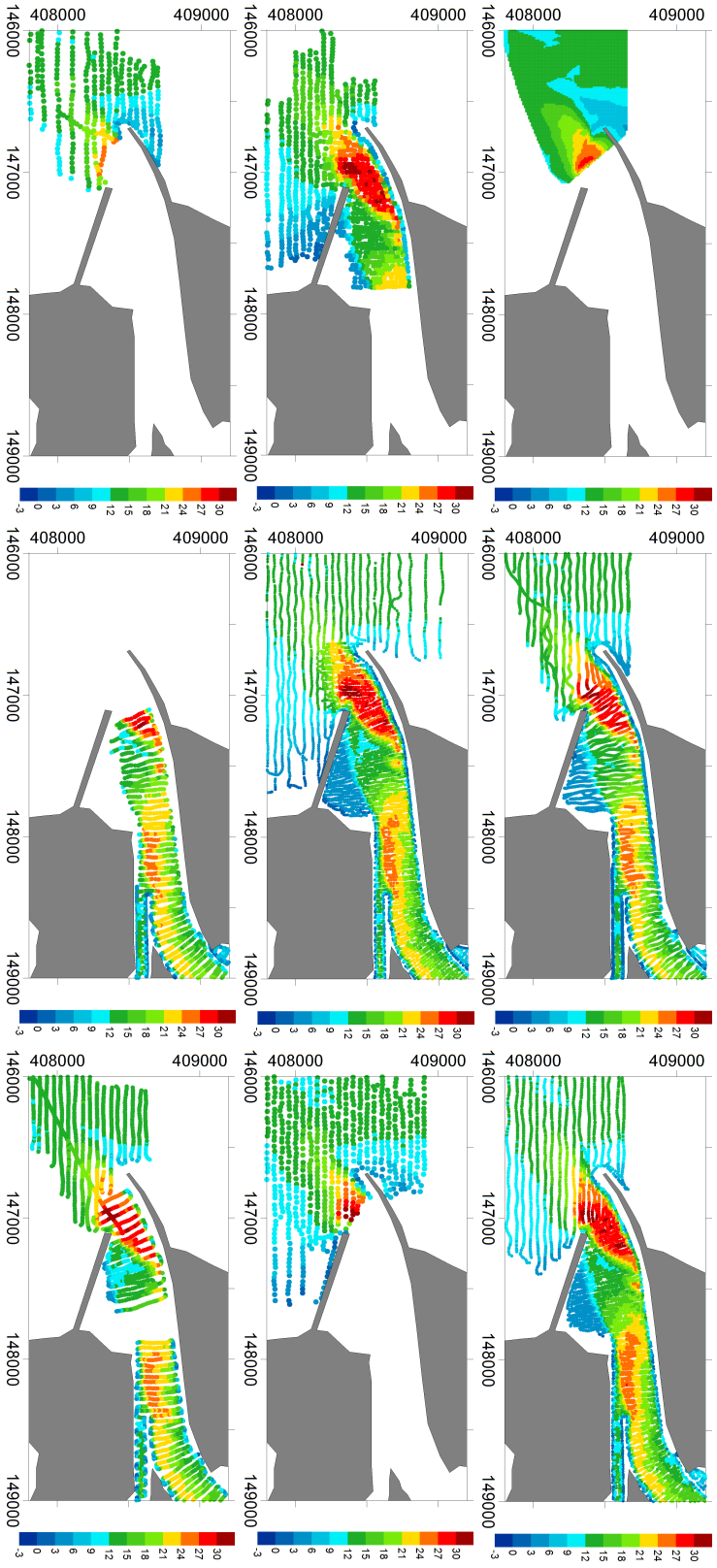

Figure 3.3: Bathymetry in meters of the Ria de Aveiro lagoon inlet corresponding to the surveys of (from left to right, top to bottom): March 2005, September 2005, October 2006, May 2007, September 2007, January 2008, June 2008, December 2008 and June 2010. The values in the axis are in metres.

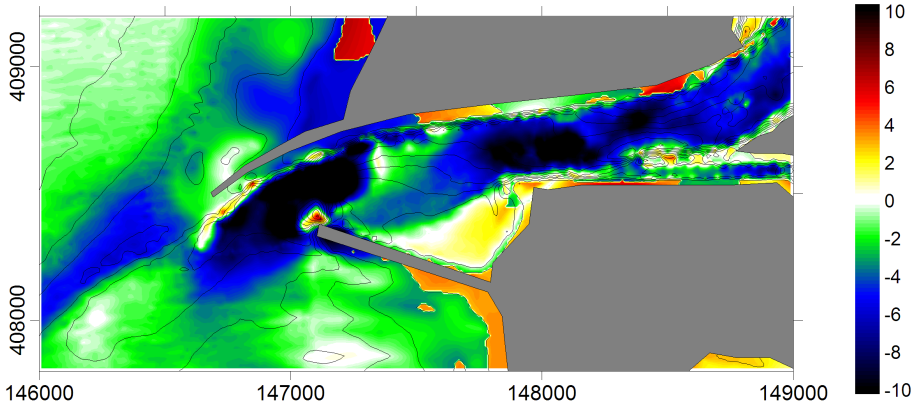

Figure 3.4: Observed bathymetric changes (metre) in the study area between 1987/88 and June 2001. The negative (positive) values represent erosion (accretion). Solid lines represent the bathymetry in 1987/88. The values in the axis are in metres.

of this structure are found accretion patterns, contrarily to the patterns observed in Figure 3.4.

The bathymetric evolution between June 2001 and September 2005 (see Figures 3.2 and 3.3) shows that the deeper area located between the tidal gauge and the *triângulo das marés* is filling in. An offshore and southward movement is observed for the deeper area located between the breakwaters, deepening at the left side of the deeper area and slightly accreting at the right side. An accretion zone is well pronounced in the beach, and the shallower zone between the two deeper zones is eroding. The accretion and erosion trends previously analyzed are represented in Figure 3.6, that shows the bathymetric changes of the inlet between 2005 and 2001. The bathymetric contours of 2001 are also represented in Figure 3.6. In this figure, the regions near the North and South breakwaters show marked changes

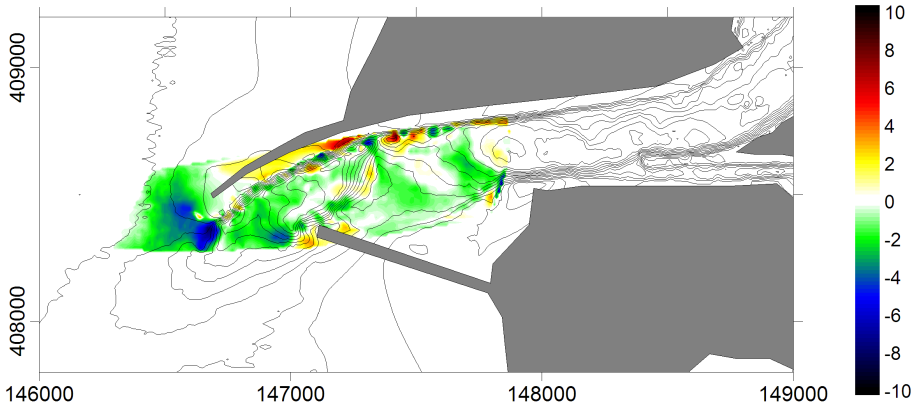

Figure 3.5: Observed bathymetric changes (metre) in the study area between June 2001 and March 2003. The negative (positive) values represent erosion (accretion). Solid lines represent the bathymetry in June 2001. The values in the axis are in metres.

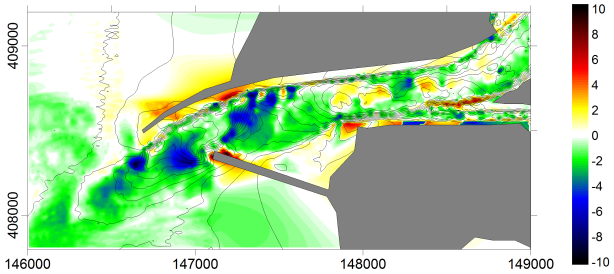

Figure 3.6: Observed bathymetric changes (metre) in the study area between June 2001 and September 2005. The negative (positive) values represent erosion (accretion). Solid lines represent the bathymetry in June 2001. The values in the axis are in metres.

in the bathymetry.

An analysis of the depth along several sections illustrated in Figure 3.7 was performed and the results obtained for the period June 2001-September 2005 are illustrated in Figure 3.8. Its analysis revealed that near the northern breakwater pronounced depth changes within a strip of around 30 m close to the structure are observed (section 1 in Figure 3.8 at the right side). These changes are probably justified by the presence of rocks that collapsed from the breakwater and by the emergency works performed in 2004 to repair this structure. Indeed these works deposited large amount of rocks at the breakwater and near its bottom, observed in recent side-scan sonar images. In Figure 3.8 it is also observed that, in this period, occurred accretion near the structures (more precisely North breakwater and head of South breakwater) and at the upstream sections. On the other hand, erosion is observed at the center of the inlet section (section 1). Also the depth along the longitudinal direction (E-W,

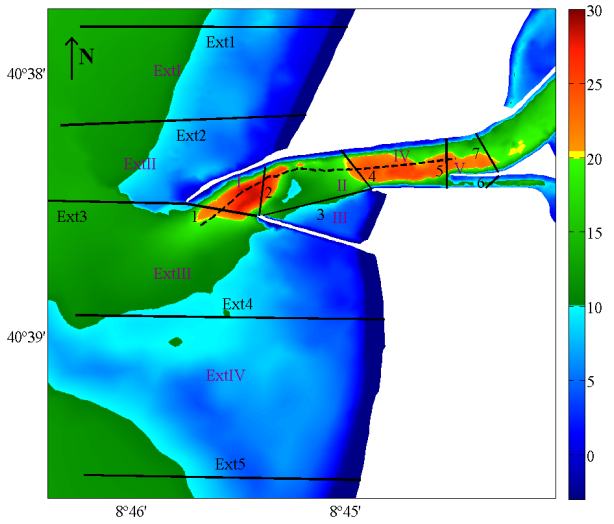

Figure 3.7: Sections location where transport of sediments is computed and regions where sedimentation rates are computed. The sections and regions were defined in order to be coincident with variations in the bathymetric or lagoon inlet geometry.

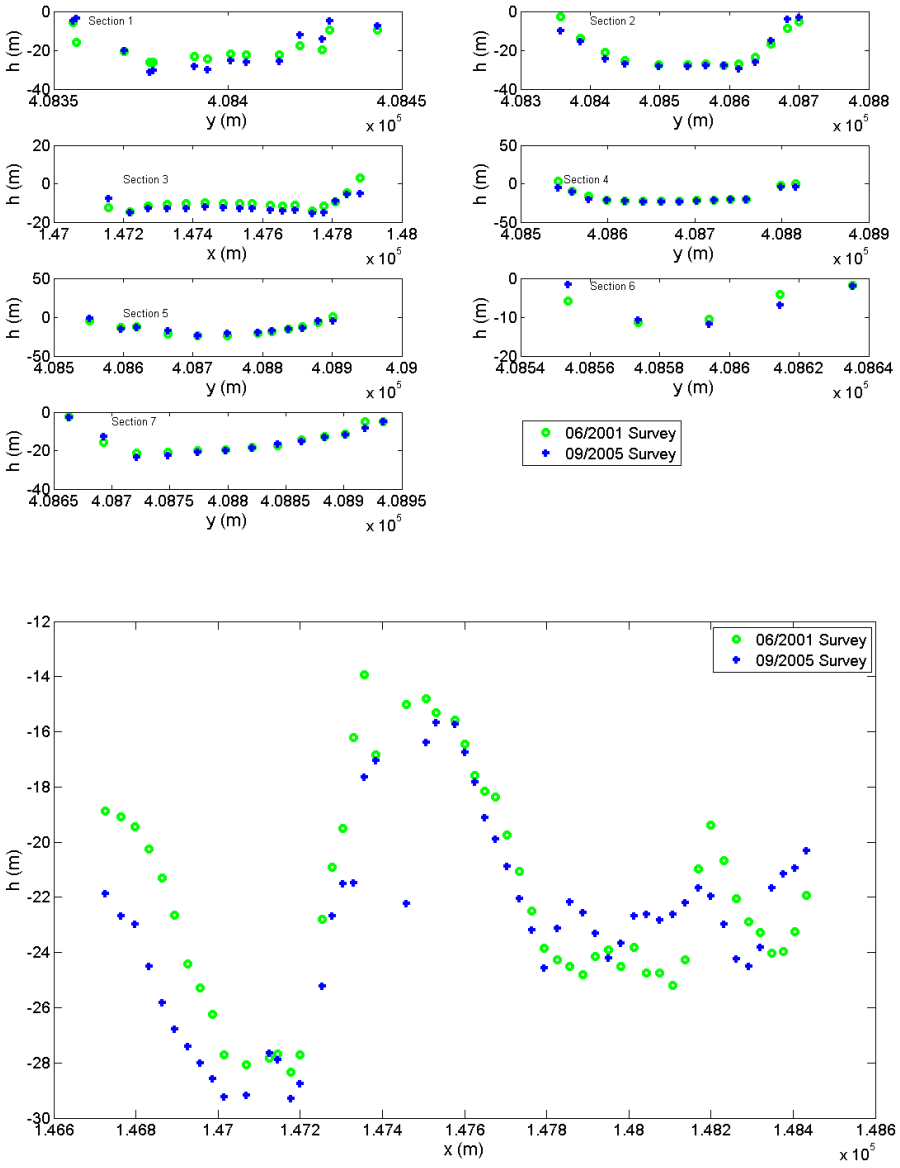

Figure 3.8: Depth along the sections illustrated in Figure 3.7 observed in June 2001 (-) and September 2005 (-) surveys. The lower panel figure illustrates the depth along the longitudinal section (dashed line in Figure 3.7). The y (x) values in the x-axis increases from South to North (West to East).

Figure 3.7) is plotted and presented at the lower panel of Figure 3.8. It is observed in this figure that the deeper area located in the navigation channel is infilling and the bottom features are moving offshore. The deeper area located at the inlet, between the breakwaters, show a slightly erosion pattern and clearly reveals a smooth slope on the downstream direction. Between September 2005 and June 2010 (Figure 3.9) is observed an inversion of the trends

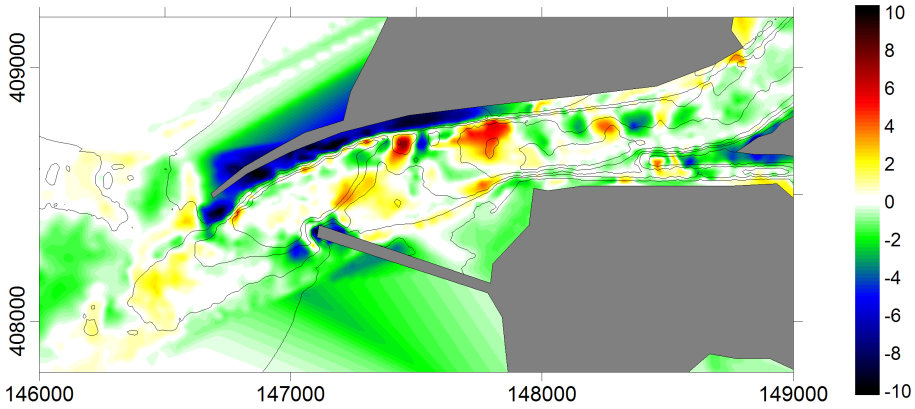

Figure 3.9: Observed bathymetric changes (metre) in the study area between September 2005 and 2010. The negative (positive) values represent erosion (accretion). Solid lines represent the bathymetry in September 2005. The values in the axis are in metres.

near the walls at the navigation channel, with strong erosion patterns at North and South breakwaters. At the navigation channel smaller trends of erosion are observed; furthermore is observed accretion with higher values than those observed between June 2001 and September 2005. These new accretion trends are probably related to the interruption of the regular dredging activities at the navigation channel. The deeper area located between the tidal gauge and the *triângulo das marés* is filling, as well as some spots at the channel. The deeper area located between the head of the breakwaters continues the offshore and South movement observed, identified by the accretion trends at the right side and erosion at the left side. It is important to observed that the survey in June 2010 was performed for very sparse locations.

The seasonal bathymetric variations, maritime Summer (May to October) and Winter (November to April) were also computed and are illustrated in Figure 3.10. It is observed that in the center of the inlet, between the heads of the breakwaters exists erosion, independently of the season. Therefore, a seasonally dependent pattern was not identified.

A correct interpretation of the bathymetric trends from the surveys, disregarding the anthropogenic actions, requires a correlation of the data obtained through surveys with the dredging activities.

3.4 Distribution of bottom sediments

A relevant property for a morphological analysis is the distribution of the bottom sediment, as they have a direct influence in the sediment fluxes. When the flow velocities are high, and velocities gradients exist, the sediments tend to be moved and erosion trends are observed in these locations, remaining at the bottom the coarser sand.

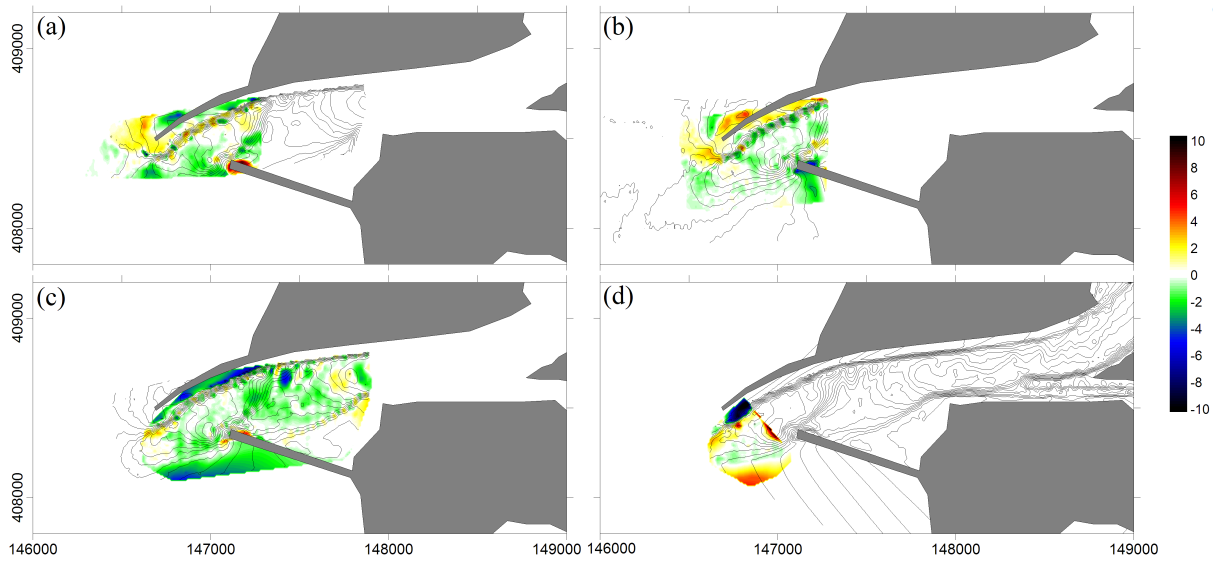

Figure 3.10: Observed bathymetric changes (metre) in the study area between (a) March-November 2003, (b) November 2003-March 2004, (c) March-October 2004 and (d) October 2004-March 2005. The negative (positive) values represent erosion (accretion). The values in the axis are in metres.

The knowledge of the distribution of bottom sediments is also relevant to perform more realistic numerical simulations, however when this study was performed, this was poorly known for the Ria de Aveiro inlet and navigation channel, being frequently assumed a constant bottom sediment size distribution. Therefore the data published in the literature when this study started, namely the data published by Freitas et al. [2005] and the sediment data collected in surveys performed in 2006 in the scope of the FCT funded EMERA research project (Study of the Morphodynamic of the Ria de Aveiro Lagoon Inlet), were compiled and used to create a heterogeneous spatial distribution of the bottom sediments grid. The information about the bottom sediments properties at the lagoon indicates that the sediment distribution is very heterogeneous, combining fine, median and coarse sediment fractions [Martins et al., 2007].

Normally, the sand grains are measured in millimeters (usually denoted by d) or in terms of the phi-scale (ϕ), being possible to perform the conversion between these two units through the following:

$$\phi = -log_2 d \Leftrightarrow d = 2^{-\phi} \tag{3.1}$$

In this work, the sediment characterization performed consisted in the median sieve diameter d_{50}, that denotes the diameter for which 50% of the grains by mass is finer [Soulsby, 1997]. Analyzing the sediment size distribution generated (Figure 3.11(a)), it is observed that on average, the bottom sediment size found at the inlet is mostly composed by medium sand (0.25 mm - 0.5 mm), followed by coarse sand (0.5 mm - 1 mm), fine sand (0.125 mm - 0.25

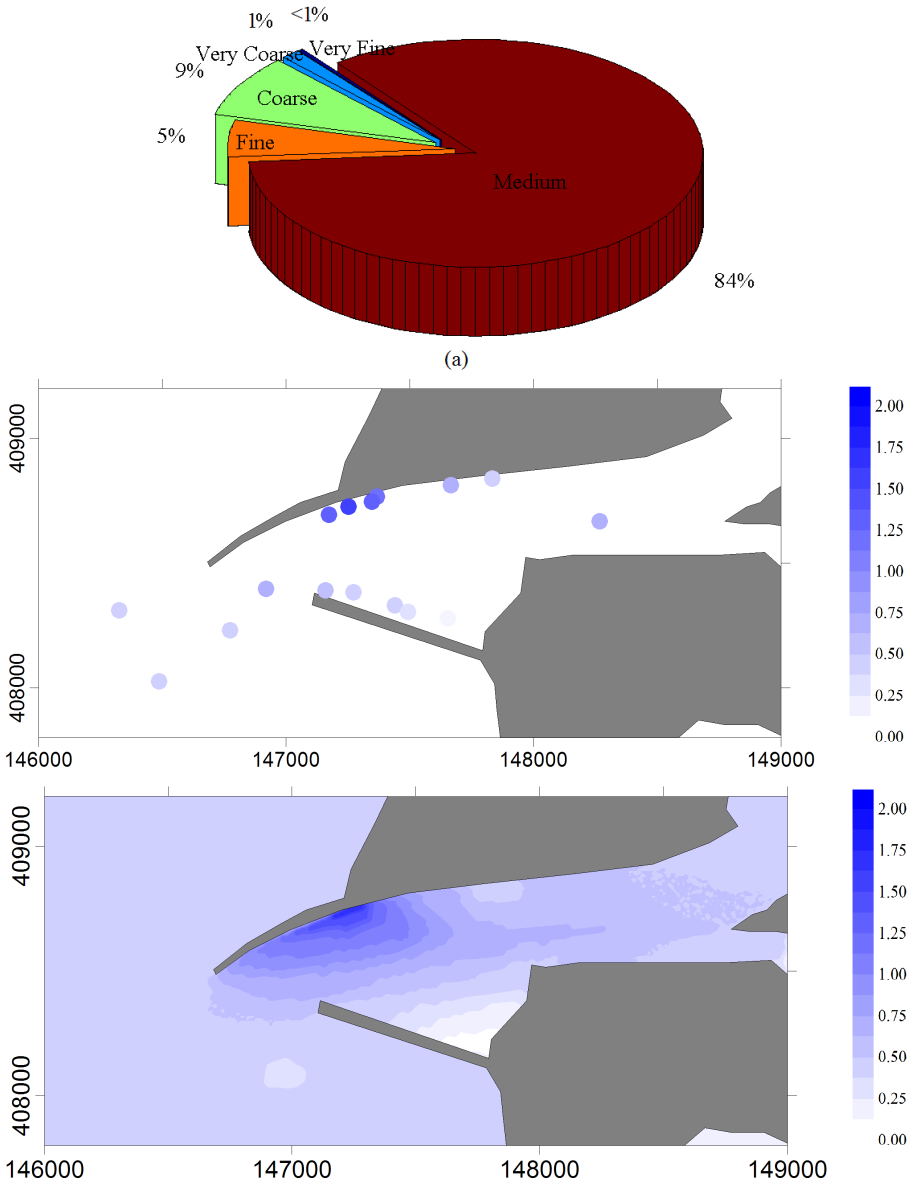

Figure 3.11: Sediment size (a) classes for the study area considered in the numerical simulations (millimetre). (b) Location of the sediment data samples with the corresponding sediment size color (millimetre). (c) Sediment size distribution for the study area (millimetre).

mm), and with 1% and lower by very coarse (1 mm - 2 mm) and very fine sand (0.0625 mm - 0.125 mm), respectively. These dimensional limits and classification are published in the literature (e.g. Soulsby [1997]) and is denoted by Wentworth grain size scale.

The available data samples location is illustrated in Figure 3.11(b) together with the respective sediment size. These data was interpolated through the Nearest Neighbor method being obtained a heterogeneous granulometric distribution grid illustrated in Figure 3.11(c). For

the offshore region the sediment size was considered constant, with 0.4 mm. This value is in agreement with those published for the beaches near Aveiro, that comprises sediment sizes between 0.2 and 0.4 mm [Ferreira, 1998; Coelho, 2005].
Spatially, the sediment size distribution is characterized by finer sediments in the beach located between the tidal gauge and the South breakwater. This area is also characterized by accretion trends that can be observed in Figures 3.4 and 3.6.
Recently, Martins et al. [2009, 2011] analyzed the distribution of bottom sediments considering new data surveys and created a new map of sediment size distribution. The grid made in this work is similar to that obtained by Martins et al. [2011], considering the same range of sediment size. Similarities are found near the North breakwater, which is characterized by coarser sediments and near the *Meia Laranja* beach, characterized by fine sediments. The higher difference is observed near the channels bifurcation, where Martins et al. [2011] identify coarse sediments while in the distribution determined in this study is found medium sand.
In spite of these differences, this analysis is in close agreement with Martins et al. [2007, 2011] that referred that areas with finer sediment correspond to shallow accretion zones characterized by small flow velocities, while coarser sediment corresponds to deeper zones where erosion was found.

3.5 Hydrodynamic characterization

The hydrodynamics of the Ria de Aveiro lagoon has been analyzed through both observational and numerical studies. These studies have shown that tides constitute the main forcing of the water motion in the lagoon [Dias et al., 2000]. They are semidiurnal, with an average range at the inlet of 2 m and maximum and minimum ranges of 3.2 (spring tide) and 0.6 m (neap tides), respectively [Dias et al., 1999, 2000; Sousa and Dias, 2007].
An illustration of the sea surface elevation and velocity time series at the Ria de Aveiro lagoon inlet is presented in Figure 3.12. These series are characteristic of a point located at the inlet (P1 at Figure 2.7) and were obtained through simulations with the ELCIRC, a calibrated hydrodynamic numerical model (described in Chapter 4). The tide generates tidal currents strongly dependent on the local geometry. Tidal amplitudes decrease in the inner parts of the lagoon, while a phase delay is observed comparing to the oceanic tide [Dias et al., 2000; Araújo et al., 2008]. According to the tidal range observed in Figure 3.12(a) and considering the classification presented in Section 2.2, this lagoon is characterized as mesotidal.
Several authors evaluated the tidal prism for the Ria de Aveiro lagoon through different numerical models (considering different bathymetries). Several values were obtained. For maximum spring tide Dias [2001] and Lopes et al. [2006] estimate 136.7×10^6 m^3, Picado et al. [2010] 86.3×10^6 m^3 and Lopes et al. [2010] 87.5×10^6 m^3 and for minimum neap tide

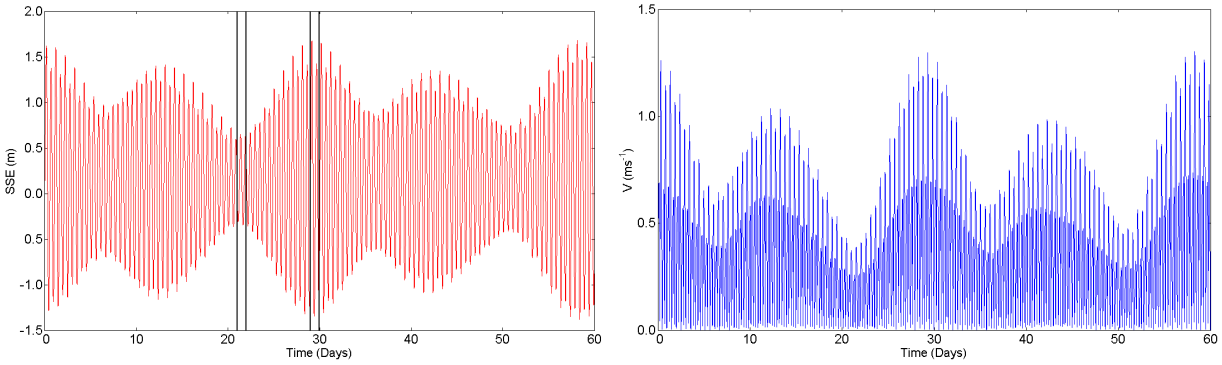

(a) (b)

Figure 3.12: (a) Sea surface elevation (m) relative to ZH and (b) velocity intensity (ms^{-1} in the Ria de Aveiro lagoon inlet. The vertical bars in (a) delimit one neap and one spring tide period.

Dias [2001] and Lopes et al. [2006] estimated 34.9×10^6 m^3, Picado et al. [2010] 31.0×10^6 m^3 and Lopes et al. [2010] 28.9×10^6 m^3. These values of tidal prism were computed in a flooding cycle, thus the flux related to these ranges are 3.87 to 6.12×10^3 m^3s^{-1} for spring tide and 1.30 to 1.56×10^3 m^3s^{-1} for neap tide.

The lagoon receives freshwater from two main rivers: Antuã (5 m^3s^{-1} average discharge) and Vouga (50 m^3s^{-1}) (Moreira et al. [1993]). However, the river discharge is negligible when compared to the flux related to the tidal prism values aforementioned. The influence of rivers discharge is only noticed in the upper parts of the lagoon, where an horizontal density gradient is dynamically active [Vaz and Dias, 2008]. Hence, the water column is well mixed in the study area (lagoon mouth) and a two-dimensional model is adequate to represent the relevant physical processes.

Due to the limited width of the Ria de Aveiro lagoon inlet, the tidal flow velocity has the direction of the channel banks and its magnitude can exceed 2 ms^{-1} at the center of the channel [Vaz et al., 2009], both during the ebb and flood. Velocities are higher on ebb than on flood [Dias et al., 2000] and numerical simulations of the ocean circulation in the vicinity of the channel [Silva et al., 2006b] have also shown that the ebb jet extends into the shelf.

A representation of the velocity field for the inlet and navigation channel is illustrated in Figure 3.13 for neap (left) and spring (right) tide conditions and in ebb (center) and flood (bottom) periods (for the instants indicated with dots in the top panel). The velocities represented are results from numerical simulations with the ELCIRC, a calibrated numerical model (described in Chapter 4). The differences in the velocity magnitude between neap and spring tide periods and flood and ebb conditions can be observed in the figure. Also it can be observed that flood duration is higher than ebb duration, with differences of approximately 2 h and 1.2 h for neap and spring tide conditions, respectively, inducing higher velocities in ebb than in flood. These differences, already referred by Dias et al. [2000], can be visualized

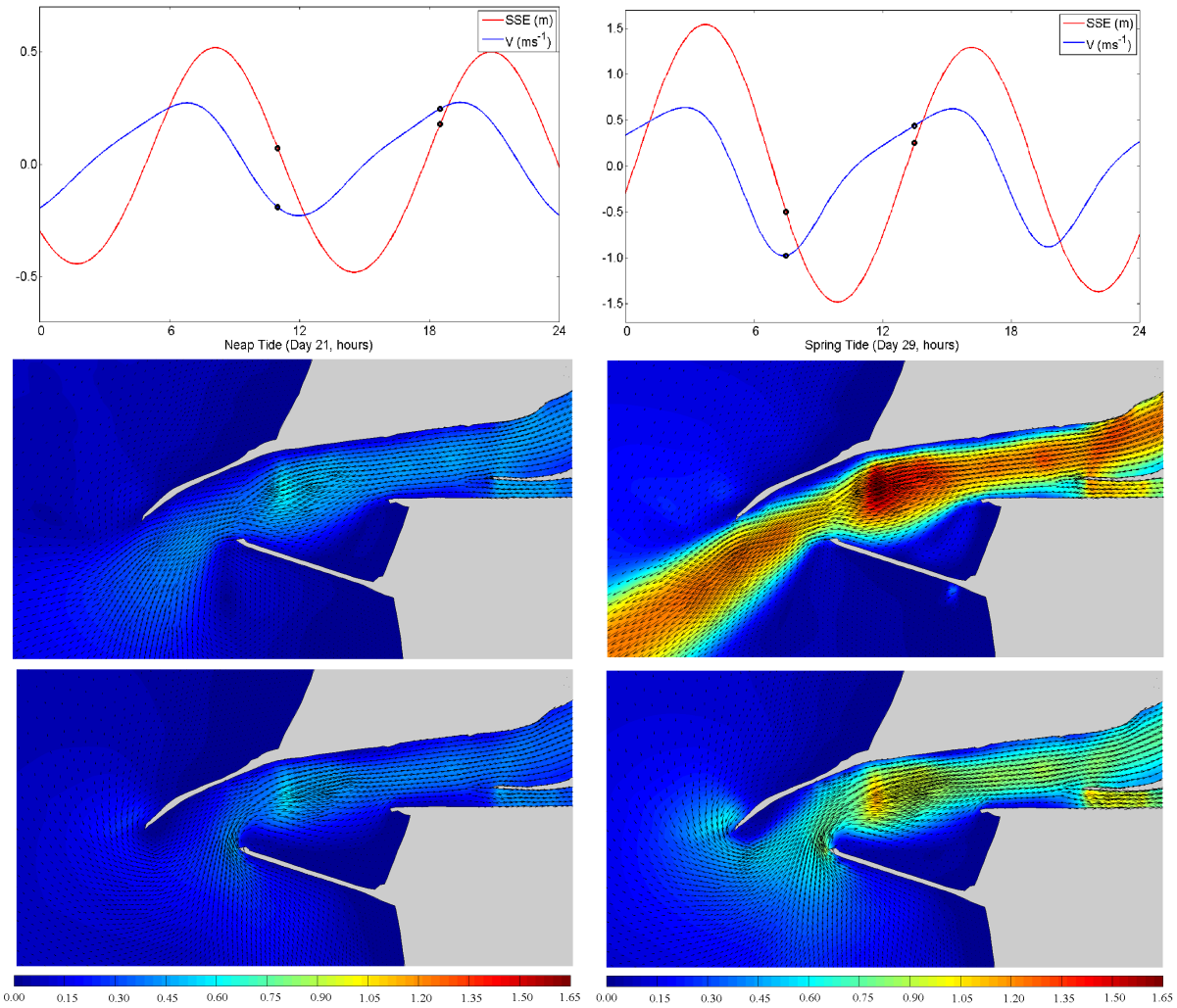

Figure 3.13: Top panel: Sea surface elevation (m) relative to ZH and velocity. Center and lower panels corresponds to ebb and flood velocities, respectively (dots in the upper panel). In the left and right panels are illustrated the velocities for neap and spring neap tide, respectively.

either at the magnitude (upper panel of Figure 3.13) as at the spatial representation of the velocities (at the center and bottom panel of the supracited Figure).

Taking into account the definitions introduced in Section 3.5, it is possible to characterize this lagoon and inlet as ebb-dominant.

The residual currents of the Ria de Aveiro lagoon were analyzed by several authors. According to Dias et al. [2000, 2003], the residual currents in Ria de Aveiro are 2 orders of magnitude lower than the tidal currents and are essentially tidally driven. Nevertheless, in the long-term perspective, they are very important, since they affect the overall exchange of water and particles within the lagoon and between the lagoon and the ocean. Tidal residual currents are stronger at S. Jacinto and Espinheiro channels and are directed downstream

towards Barra, contributing to net water and sediment exportation towards the ocean [Dias et al., 2000, 2003; Abrantes et al., 2006; Dias et al., 2007]. In fact several studies based on Winter and Summer campaigns estimated that the annual mass balance of several properties, such as bacterioplankton [Cunha et al., 2003], mercury [Pato et al., 2008] and organic carbon [Lopes et al., 2008], corresponded to a net exportation, acting the Ria de Aveiro lagoon as an exportation agent.

3.6 Wave regime

The adjacent coastal zone of Ria de Aveiro is subjected to a highly energetic wave climate (according to the definition at Figure 2.1), with a yearly mean significant wave height (H_s) of 2–2.5 m, wave periods of 9–11 s corresponding to WNW to NNW swell [Andrade et al., 2002]. Figure 3.14 illustrates the offshore wave regime at Aveiro obtained through data collected from two wave directional buoy located in Figueira da Foz ($40^o11'08"$N-$9^o8'44"$W, depth 92 m ZH) and Leixões ($41^o19'00"$N-$8^o59'00"$W, depth 83 m ZH) [Capitão et al., 1997; Costa et al., 2003].

During the Winter, North Atlantic storms give rise to high amplitude waves, whose significant height frequently exceeds 5 m, while milder conditions are observed during the Summer [Ferreira et al., 2008]. The northern breakwater protects the channel from the impinging waves. Visual observations of the waves propagating into the lagoon inlet channel reveal that their amplitude is low, being considered that the waves influence is restricted to the outer part of the inlet and the ebb-delta. This wave climatology results in a strong littoral drift southward, which is hard to quantify, being therefore proposed in the literature a wide range of values. Several authors along the years proposed values for the littoral drift in the ranges of 0–3.5×10^6 $m^3 year^{-1}$ directed North-South, while some even estimate a littoral drift directed South-North. A more detailed analysis of these estimations can be found in Oliveira et al.

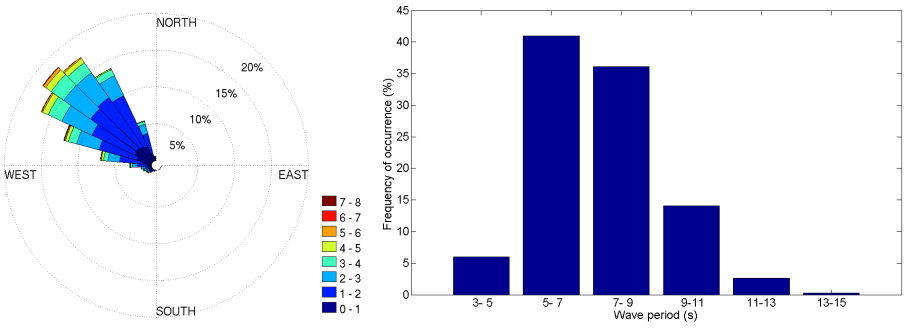

(a) (b)

Figure 3.14: Offshore wave regime at Aveiro. (a) Wave directions and heights (metre) and (b) wave periods (seconds).

[1982] and Teixeira [1994]. As example, Oliveira et al. [1982] evaluated the littoral drift at the range of 1–3.5$\times 10^6$ m^{3}year^{-1}, Teixeira [1994] proposed the range 1.4-1.7$\times 10^6$ m^{3}year^{-1}, Andrade et al. [2002] proposed the range 1-2$\times 10^6$ m^{3}year^{-1}, Larangeiro and Oliveira [2003] proposed 1$\times 10^6$ m^{3}year^{-1} and Coelho [2005] the value of 1.1 $\times 10^6$ m^{3}year^{-1}. This littoral drift, associated with the ebb dominance of the lagoon, generates a submerged ebb tidal delta, that can be observed offshore Costa Nova (identified in Figure 1.1).

3.7 Representative waves and longitudinal sediment transport

This Section presents the study performed to quantify the longshore sediment transport and to find a simplified wave regime which induces a longitudinal sediment transport offshore the study area equivalent to that caused by the complete wave regime. This equivalent wave regime will be used in the morphodynamic simulations in order to understand the effect of each single wave in the complete sediment transport. With this purpose the methodology proposed by Chonwattana et al. [2005] was applied with the modifications described in the next subsection. This method is based on the principles of conservation of wave power and longshore sediment transport capacity between the two sets of wave regimes.
The first step consists in calculate the longshore sediment transport due to the complete wave regime offshore Aveiro. After that, the regime is simplified using different formulae for the sediment transport and new estimates of the longshore transport are calculated. Comparing the results between these wave regimes with the complete one, the best simplification can be chosen.

3.7.1 Wave regime considered

The complete wave regime was obtained based on data from two wave directional buoy located in Figueira da Foz ($40^o11'08''N - 9^o8'44''$W, depth 92 m ZH) and Leixões ($41^o19'00''N - 8^o59'00''$W, depth 83 m ZH) [Capitão et al., 1997; Costa et al., 2003]. In spite of the different locations, the offshore regime for these two buoys can be considered the same [Coli, 2003], that is, these 2 buoys register the same wave climate, and thus their records can be complemented with each other in case one buoy fails. After joining the available data from the buoys, a deep water wave time series was obtained approximately 11 years long (1990-2001) with 18870 observations. The number of occurrences of the wave records is illustrated in Figure 3.15 in function of the month. To calculate the longshore sediment transport due to these set of waves, a cross-shore section 1.5 km northward of Ria the Aveiro lagoon inlet was selected. The wave regime is computed along this section, considering wave refraction and shoaling, and assuming straight and parallel bottom contours.
The longshore sediment transport is calculated by means of the six longshore sediment trans-

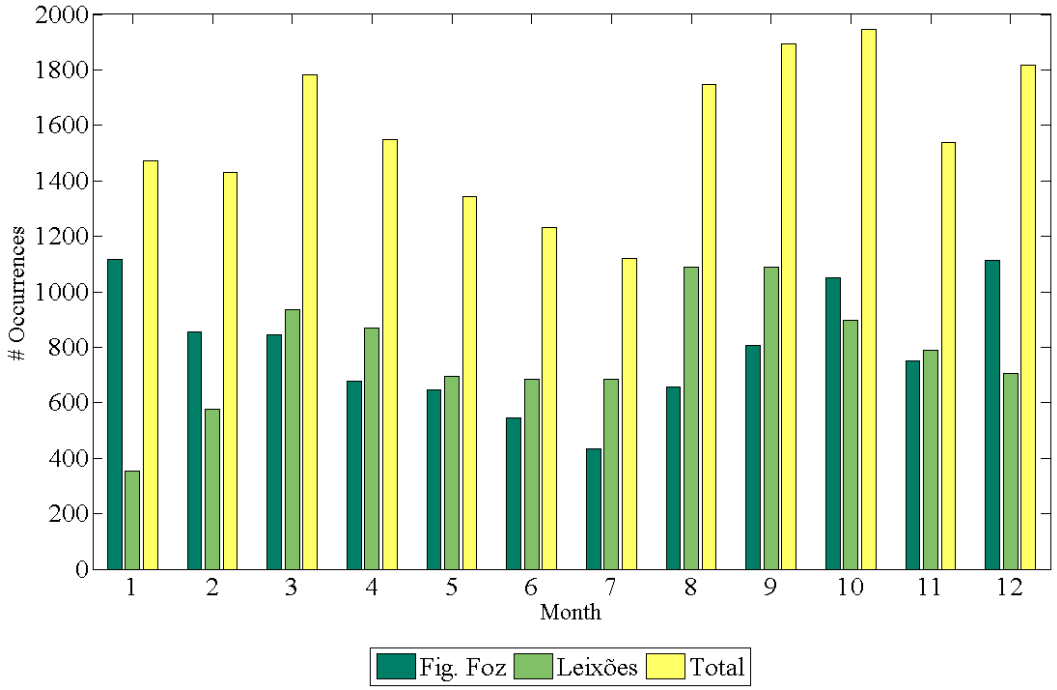

Figure 3.15: Number of wave records in function of the month, for the two buoys located in Figueira da Foz ($40^o11'08''N - 9^o8'44''$W, depth 92 m ZH) and Leixões ($41^o19'00''N - 8^o59'00''$W, depth 83 m ZH) [Capitão et al., 1997; Costa et al., 2003].

port formulations presented in Section 2.5.2. The dependency of each sediment transport formulation on the wave height and angle at the breaker line and the dependency on d_{50} and bottom slope i is presented in Table 3.1. It should be noted that all these formulae make use of the breaking significant wave height, except the C2 formula which accounts for the root mean square wave height, H_{rms}. The longshore sediment transport is computed considering the characteristics of each wave that constitute a wave regime composed by a set of 282 distinct waves, obtained through the 18870 records of the wave directional buoys.
The value for the sediment size and bottom slope has to be chosen considering the range

Table 3.1: Longshore sediment transport formulations where K represents each formulation dependency on d_{50} and bottom slope i.

Formulation	$Q_\ell(\mathrm{m^3 year^{-1}})$	K$\propto$
C2	$K_1\, H_{rms}^{5/2}\, \sin 2\alpha_b$	$e^{d_{50}}$
K&I	$K_2\, H_b^{5/2} \cos\alpha_b\, \sin 2\,\alpha_b$	i
Kr88	$K_3\, H_b^{3/2} \sin 2\,\alpha_b\, W$	i
K86	$K_4\, H_b^{7/2}\, \sin 2\,\alpha_b$	$d_{50}^{-1} i$
K91	$K_5\, H_b^2\, T_p^{1.5}\, \sin^{0.6} 2\,\alpha_b$	$d_{50}^{-0.25} i^{0.75}$

of values presented in bibliography. The values considered are $d_{50} = 0.50$ mm and bottom slope $i = 0.014$ m, computed through the average of slopes at the cross section considered. However, due to the range of these two characteristics values at the nearshore study area, a sensitivity analysis of the formulations to typical values of d_{50} and i is performed. These results are illustrated in Figure 3.16. All formulations, with exception to C2, depend on the bottom slope. Only the C2, K86 and K91 have dependencies on the sediment size d_{50}. The formula K86 revealed to be highly sensitive to the value of d_{50} considered, due to its inverse dependency on the sediment size. The C2 formulation, with an exponential dependency on d_{50} also revealed a strong dependency to this characteristic.

Analyzing the results of the dependency of longshore sediment transport to the bottom slope, again the K86 formulation have the higher dependency due to the linear dependency on i. The same dependency and sensible behavior is obtained when using the K&I formulation to compute the longshore sediment transport.

Considering the supracited values of d_{50} and bottom slope (0.5 mm and 0.014 m, respectively), the values obtained for the longshore sediment transport are presented in Table 3.2. There is a wide spread of results for the longshore sediment transport. The reference value considered for the Portuguese West coast in Aveiro was presented by Larangeiro and Oliveira [2003] and is Q_ℓ=1×10^6 m^{3}year^{-1}. Analyzing the values obtained it is concluded that the longshore sediment transport computed for the complete wave regime by all transport formulae is overestimated when compared with the reference value.

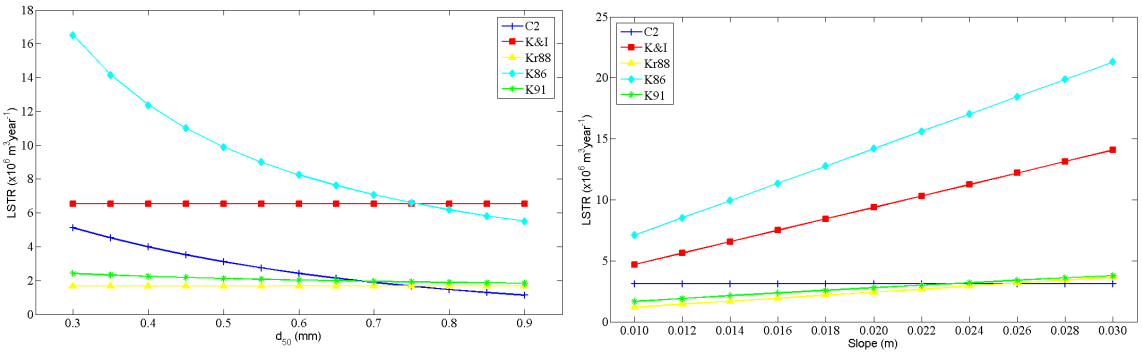

(a) (b)

Figure 3.16: Sensitivity analysis of the longshore sediment transport formulations to (a) d_{50} (mm) and (b) the bottom slope (m).

Table 3.2: Longshore sediment transport results (×10^6 m^{3}year^{-1}).

CERC	C2	K&I	Kr88	K86	K91
8.83	3.11	5.63	1.44	8.52	1.90

3.7.2 Simplifications of the wave regime

To calculate a simplified wave regime the method proposed by Chonwattana et al. [2005] is used. This method is based in the wave energy conservation principle coupled to longshore sediment transport.
Knowing that the conservation of the wave energy flux along the wave radii [CEM, 2002] is given by:

$$H_1^2\, c_{g1} = H_2^2\, c_{g2} \tag{3.2}$$

$$\Leftrightarrow \quad H_1^2\, T_1 = H_2^2\, T_2 \tag{3.3}$$

taking into account that $c_g = (gT_z)/(4\pi)$. We can derive the wave power equations in cross-shore and longshore directions:

$$\text{Power in cross-shore direction} = H_0^2\, T_z\, \cos\alpha_0 \tag{3.4}$$

$$\text{Power in longshore direction} = H_0^2\, T_z\, \sin\alpha_0 \tag{3.5}$$

If the total longshore sediment transport is to be conserved among two different sets of wave regimes, then equation (2.29) yields,

$$H_0^{5/2}\, \cos\alpha_0{}^{1/4}\, \sin 2\,\alpha_0 = \text{constant} \tag{3.6}$$

Now if the wave energy and longshore sediment transport are to be conserved, equations (3.4), (3.5) and (3.6) are constants and form a non-linear system:

$$\begin{cases} C_1 = H_0^2\, T_z\, \cos\alpha_0 \\ C_2 = H_0^2\, T_z\, \sin\alpha_0 \\ C_3 = H_0^{5/2}\, \cos\alpha_0{}^{1/4}\, \sin 2\,\alpha_0 \end{cases} \tag{3.7}$$

The constants C_1, C_2 and C_3 are calculated for each wave of the wave regime, given H_0, T and α_0.
The simplified wave regime is calculated by dividing the complete regime in a few (usually less than 10) directional or wave height classes, each one corresponding to one equivalent wave. Each class has one trio $(C_{1,eq}, C_{2,eq}, C_{3,eq})$ that is a function of the percentage of occurrence of all waves within that new class:

$$(C_{1,eq}, C_{2,eq}, C_{3,eq}) = \left(\frac{\Sigma p_i C_{1,i}}{\Sigma p_i}, \frac{\Sigma p_i C_{2,i}}{\Sigma p_i}, \frac{\Sigma p_i C_{3,i}}{\Sigma p_i} \right) \tag{3.8}$$

where p_i is the probability of occurrence of each wave of the selected class.
Once having computed $(C_{1,eq}, C_{2,eq}, C_{3,eq})$ the system (3.7) is inverted to obtain

$(H_{0,eq}, T_{eq}, \alpha_{0,eq})$ of the equivalent wave, that is:

$$\begin{cases} \alpha_{0,eq} = \arctan \frac{C_2}{C_1} \\ H_{0,eq} = \left(\frac{C_3}{\cos \alpha_{0,eq}{}^{1/4} \sin 2\,\alpha_{0,eq}} \right)^{2/5} \\ T_{z,eq} = \frac{C_1}{H_{0,eq}^2 \cos \alpha_{0,eq}} \end{cases} \tag{3.9}$$

The wave with these characteristics is representative of a certain directional or wave height class and their frequency of occurrence is the sum of the individual frequencies of occurrence within that class (from the complete wave regime).
The longshore sediment transport formulae presented in Table 3.1 depend on the wave characteristics at the breaker line, thus it is important to derive the longshore transport conservation equations for the breaker point. The wave energy flux is given by

$$F = E\,c_g \quad \propto \quad H^2\,c_g \quad \propto \quad H^2\,n\,c \tag{3.10}$$

The wave breaking occurs in shallow water, thus:

$$F_b = H_b^2\,c_b \quad \Leftrightarrow \quad F_b = H_b^2\,\sqrt{g\,h_b} \tag{3.11}$$

Considering that $h_b = H_b/0.78$:

$$F_b = H_b^2 \sqrt{\frac{g\,H_b}{0.78}} = H_b^{5/2} \sqrt{\frac{g}{0.78}} \tag{3.12}$$

Therefore the energy flux in cross-shore and longshore directions, in the breaker line, are:

$$F_{b_{cross}} = const\,H_b^{5/2} \cos \alpha_b \tag{3.13}$$

$$F_{b_{long}} = const\,H_b^{5/2} \sin \alpha_b \tag{3.14}$$

Assuming conservation of the wave energy:

$$C_1 = H_b^{5/2} \cos \alpha_b \tag{3.15}$$

$$C_2 = H_b^{5/2} \sin \alpha_b \tag{3.16}$$

C_1 and C_2 are independent of the wave period (due to wave refraction by Snell's law) and of the transport formulae. The formula to compute the representative wave angle in the breaker line is derived using equations (3.15) and (3.16), independently of the formula used

to compute the longshore sediment transport.

$$\frac{C_2}{C_1} = \frac{H_0^{5/2} \sin \alpha_b}{H_0^{5/2} \cos \alpha_b} = \frac{\sin \alpha_b}{\cos \alpha_b} \Leftrightarrow \frac{C_2}{C_1} = \tan \alpha_b \Leftrightarrow \alpha_{b,eq} = \arctan \frac{C_2}{C_1} \tag{3.17}$$

This formula is used for all formulae presented in Table 3.1.
The C_3 equation depends on the sediment transport formula used, and is derived assuming longshore sediment transport conservation as in equation (3.6).

C2:
Through the equation of Valle et al. [1993] in Table 3.1:

$$Q_\ell \propto K_1 \, H_{rms_b}^{5/2} \sin 2\,\alpha_b$$

$$\Rightarrow C_3(C2) = H_{rms_b}^{5/2} \sin 2\,\alpha_b \tag{3.18}$$

and:

$$\begin{aligned} H_{rms_{b,eq(C2)}} &= \left(\frac{C_{3,eq}}{\sin 2\,\alpha_{b,eq}} \right)^{2/5} = H_{s,eq(C2)} \, \frac{\sqrt{2}}{2} \\ \Rightarrow H_{s,eq(C2)} &= \frac{2}{\sqrt{2}} \, H_{rms_{b,eq(C2)}} \\ \Rightarrow H_{s,eq(C2)} &= \frac{2}{\sqrt{2}} \left(\frac{C_{3,eq}}{\sin 2\,\alpha_{b,eq}} \right)^{2/5} \end{aligned} \tag{3.19}$$

K&I:
Through the equation of Komar and Inman [1970] in Table 3.1:

$$Q_\ell \propto K_2 \, H_b^{5/2} \cos \alpha_b \sin 2\,\alpha_b$$

$$\Rightarrow C_3(K\&I) = H_b^{5/2} \cos \alpha_b \sin 2\,\alpha_b \tag{3.20}$$

and:

$$H_{b,eq(K\&I)} = \left(\frac{C_{3,eq}}{\cos \alpha_{b,eq} \sin 2\,\alpha_{b,eq}} \right)^{2/5} \tag{3.21}$$

Kr88:
Through the equation of Kraus et al. [1988] in Table 3.1:

$$Q_\ell \propto K_3\, H_b^{3/2}\, \sin 2\,\alpha_b\, W \tag{3.22}$$

$$\Rightarrow C_3(Kr88) = H_b^{3/2}\, \sin 2\,\alpha_b\, W \tag{3.23}$$

and:

$$H_{b,eq(Kr88)} = \left(\frac{C_{3,eq}}{\sin 2\,\alpha_{b,eq}\, W}\right)^{2/3} \tag{3.24}$$

K86:
Through the equation of Kamphuis et al. [1986] in Table 3.1:

$$Q_\ell \propto K_4\, H_b^{7/2}\, \sin 2\,\alpha_b$$

$$\Rightarrow C_3(K86) = H_b^{7/2}\, \sin 2\,\alpha_b \tag{3.25}$$

and:

$$H_{b,eq(K86)} = \left(\frac{C_{3,eq}}{\sin 2\,\alpha_{b,eq}}\right)^{2/7} \tag{3.26}$$

K91:
Through the equation of Kamphuis [1991] in Table 3.1:

$$Q_\ell \propto K_5\, H_b^2\, T_p^{1.5}\, \sin^{0.6} 2\,\alpha_b$$

$$\Rightarrow C_3(K91) = H_b^2\, T_p^{1.5}\, \sin^{0.6} 2\,\alpha_b \tag{3.27}$$

and:

$$H_{b,eq(K91)} = \left(\frac{C_{1,eq}}{\cos \alpha_{b,eq}}\right)^{2/5} \tag{3.28}$$

$$T_{p,eq(K91)} = \left(\frac{C_{3,eq}}{H_{b,eq}^2\, \sin^{0.6} 2\,\alpha_{b,eq}}\right)^{2/3} \tag{3.29}$$

To analyze which method of simplification is the most adequate, several waves were grouped by directional and wave height classes. Thus, one has the degree of freedom to, a priori, choose how many waves will have the simplified regime, and how are the individual waves

(or contributions) from the complete set lumped together.

Considering a lumping of the waves by directional classes (that is, grouping together all waves within a certain range of α) were tested two simplifications: one based on the deepwater wave angle (simplification 1a), and the other based on the wave breaker angle (simplification 1b). In the case of grouping the wave regime by wave height classes, were created groups by deepwater wave height (simplification 2a) and breaker wave height (simplifications 2b and 2c). In Figure 3.17 are illustrated the incident wave angles (Figure 3.17a) and wave heights (Figure 3.17b) in deepwater (+) and at the breaker line (o) versus the frequency of occurrence.

With this process to simplify the complete wave regime are obtained several simplified wave regimes, one for each longshore sediment transport formula and simplification procedure (1a, 1b, 2a, 2b and 2c). Each simplified regime will thus consist of a small set of waves (typically less than 10) that yield the same annual total longshore sediment load and wave power as the averaged wave climate. The total annual longshore transport results are presented in Tables 3.3 to 3.12 where the first column of each identifies the formula by which the longshore sediment transport is computed, independently of the wave regime. The results in the second line on Tables 3.3, 3.5, 3.7, 3.9 and 3.11 corresponds to the total annual alongshore transport results previously presented in Table 3.2, whereas the results below this line are the ones obtained through the simplified regimes. These values are compared to the reference value for the Portuguese Aveiro West coast presented by Larangeiro and Oliveira [2003] Q_ℓ=1×10^6 m^{3}year^{-1} . Comparing this value with those obtained with the transport formulae presented above it is possible to conclude which formula performs better.

Analysing the results obtained for the simplified wave regimes, the conclusions are that using CERC formula the results are independent of the simplified wave regime that is used (second column with always the same value).

The most sensitive formula to the (simplified) wave regime is the K86 formula due to its

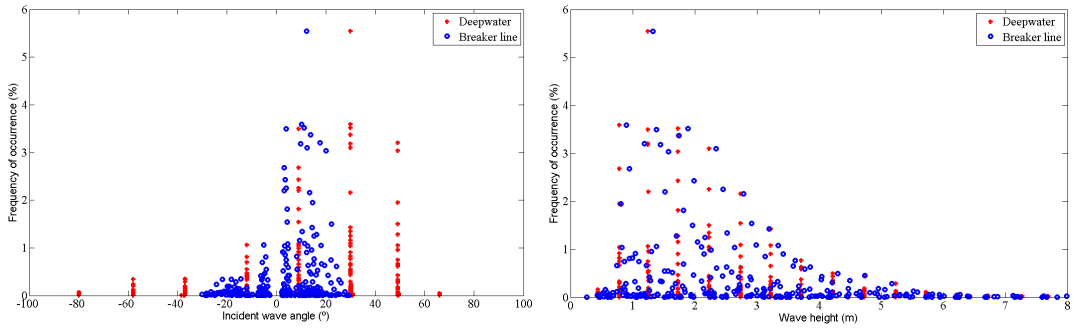

(a) (b)

Figure 3.17: Frequency of occurrence of the (a) incident wave angles and (b) wave heights of the complete wave regime at deepwater (+) and at the breaker line (o).

larger-power dependence of the breaker wave height ($H_b^{7/2}$). The formulae less sensitive to the wave regime are Kr88 ($H_b^{3/2}$) and K91 (H_b^2), which have the smallest wave height dependence.
To analyze which regime simplification performs better, the values of Q_ℓ were normalized taking the ratio between the transport values calculated by the simplified wave regimes and the values obtained by the complete regime: Q_{simpl}/Q_{total}. The average and standard deviation of these normalized ratios has also been calculated.
An example of the normalized values computed from the results in previous tables are presented in Tables 3.4, 3.6, 3.8, 3.10 and 3.12. Also, in this tables are presented the averages and standard deviations of the normalized values of the results by using different wave regimes (vertical averaging), the averages of the results from the several longshore sediment transport formulae (horizontal averaging) and the standard deviations of these.

Thus, looking down a given column one can see how much a certain transport formula is sensitive to variations in computing the simplified wave regime, whereas looking across a given line one concludes how good a simplified wave regime (and methodology) is for all the transport formulae. For instance, column 2 shows that the CERC formula yields precisely the same results for any (properly) simplified wave regime. However, lines 2 and 3 indicate that computing the simplified wave regime using the CERC formula gives rise, on average, to worse results for the total transport than using, for example, C2 to simplify the wave regime.

Simplification 1

The simplification 1 is made by grouping the waves of the complete wave regime in classes with an interval of deepwater wave angle (simplification 1a) and of incident wave breaker angle of 5 degrees each (simplification 1b), resulting in 8 and 12 representative waves respectively (Figure 3.17a).
It is observed that the formula that best predicts the reference value (1×10^6 m^{3}year^{-1}) is Kr88. However, the simplified regimes could yield values of Q_ℓ 20% larger (for simplification 1a) and somewhat larger (35% for simplification 1b) than the value for the complete regime (1.44×10^6 m^{3}year^{-1}).
Analysing the results of the formulae that are a function of the wave characteristics at the breaker line, the Kr88 and K91 formulae for simplification 1a and K91 formula for 1b are the ones that provide the most stable results ($\overline{Q_{\ell,norm}} = 1.05, \sigma = 0.07$, $\overline{Q_{\ell,norm}} = 0.90, \sigma = 0.09$ and $\overline{Q_{\ell,norm}} = 1.14, \sigma = 0.11$, respectively).
Analysing the results of the horizontal averaging in simplification 1a, it is concluded that to compute simplified wave regimes, the formulae Kr88, C2, K&I and K91 are those that provide the best results of the longshore sediment transport computed with simplified regimes, with

Table 3.3: Longshore sediment transport results for wave regime simplification 1a. ($Q_\ell = \times 10^6$ m^{3}year^{-1}).

	CERC	C2	K&I	Kr88	K86	K91
Complete wave regime	8.83	3.11	5.63	1.44	8.52	1.90
CERC	8.83	3.11	5.63	1.44	8.52	1.62
C2	8.83	3.11	5.64	1.48	6.00	1.63
K&I	8.83	3.10	5.63	1.48	5.98	1.63
Kr88	8.83	3.07	5.58	1.44	6.06	1.64
K86	8.83	3.99	7.24	1.72	8.52	2.07
K91	8.83	3.12	5.65	1.48	6.01	1.62

Table 3.4: Longshore sediment transport normalized results for wave regime simplification 1a. ($Q_\ell = \times 10^6$ m^{3}year^{-1}).

Reg \ Form	CERC	C2	K&I	Kr88	K86	K91	$\overline{Q_{\ell,norm}}$	σ
CERC	1.00	1.00	1.00	1.00	1.00	0.85	0.98	0.06
C2	1.00	1.00	1.00	1.03	0.70	0.86	0.93	0.13
K&I	1.00	1.00	1.00	1.03	0.70	0.86	0.93	0.13
Kr88	1.00	0.99	0.99	1.00	0.71	0.86	0.93	0.12
K86	1.00	1.28	1.29	1.19	1.00	1.09	1.14	0.13
K91	1.00	1.00	1.00	1.03	0.71	0.85	0.93	0.13
$\overline{Q_{\ell,norm}}$	1.00	1.04	1.05	1.05	0.80	0.90	0.97	
σ	0.00	0.12	0.12	0.07	0.15	0.09	0.08	

Table 3.5: Longshore sediment transport results for wave regime simplification 1b. ($Q_\ell = \times 10^6$ m^{3}year^{-1}).

	CERC	C2	K&I	Kr88	K86	K91
Complete wave regime	8.83	3.11	5.63	1.44	8.52	1.90
CERC	8.83	3.99	7.22	1.83	11.61	2.09
C2	8.83	3.99	7.23	1.71	8.68	2.02
K&I	8.83	3.98	7.22	1.71	8.66	2.02
Kr88	8.83	4.68	8.49	1.83	11.33	2.35
K86	8.83	4.91	8.91	1.94	11.61	2.48
K91	8.83	4.00	7.24	1.71	8.71	2.09

Table 3.6: Longshore sediment transport normalized results for wave regime simplification 1b. ($Q_\ell = \times 10^6$ m^{3}year^{-1}).

Reg \ Form	CERC	C2	K&I	Kr88	K86	K91	$\overline{Q_{\ell,norm}}$	σ
CERC	1.00	1.28	1.28	1.27	1.36	1.10	1.22	0.14
C2	1.00	1.28	1.28	1.19	1.02	1.07	1.14	0.13
K&I	1.00	1.28	1.28	1.18	1.02	1.06	1.14	0.13
Kr88	1.00	1.50	1.51	1.27	1.33	1.24	1.31	0.19
K86	1.00	1.58	1.58	1.35	1.36	1.30	1.36	0.21
K91	1.00	1.28	1.29	1.19	1.02	1.10	1.15	0.13
$\overline{Q_{\ell,norm}}$	1.00	1.37	1.37	1.24	1.19	1.14	1.22	
σ	0.00	0.14	0.14	0.07	0.18	0.11	0.11	

Table 3.7: Longshore sediment transport results for wave regime simplification 2a. ($Q_\ell = \times 10^6$ m^{3}year^{-1}).

	CERC	C2	K&I	Kr88	K86	K91
Complete wave regime	8.83	3.11	5.63	1.44	8.52	1.90
CERC	8.83	2.37	4.29	1.10	5.95	1.26
C2	8.83	2.37	4.38	1.08	5.41	1.41
K&I	8.83	2.32	4.29	1.06	5.26	1.39
Kr88	8.83	2.49	4.59	1.10	5.80	1.48
K86	8.83	2.52	4.66	1.11	5.95	1.49
K91	8.83	2.42	4.47	1.09	5.57	1.26

Table 3.8: Longshore sediment transport normalized results for wave regime simplification 2a. ($Q_\ell = \times 10^6$ m^{3}year^{-1}).

Reg \ Form	CERC	C2	K&I	Kr88	K86	K91	$\overline{Q_{\ell,norm}}$	σ_{Hor}
CERC	1.00	0.76	0.76	0.77	0.70	0.66	0.77	0.12
C2	1.00	0.76	0.78	0.75	0.64	0.74	0.78	0.12
K&I	1.00	0.75	0.76	0.74	0.62	0.73	0.77	0.13
Kr88	1.00	0.80	0.82	0.77	0.68	0.78	0.81	0.11
K86	1.00	0.81	0.83	0.77	0.70	0.79	0.82	0.10
K91	1.00	0.78	0.79	0.76	0.65	0.66	0.77	0.13
$\overline{Q_{\ell,norm}}$	1.00	0.78	0.79	0.76	0.66	0.73	0.79	
σ	0.00	0.02	0.03	0.01	0.03	0.05	0.04	

Table 3.9: Longshore sediment transport results for wave regime simplification 2b. (Q_ℓ = $\times 10^6$ m^{3}year^{-1}).

	CERC	C2	K&I	Kr88	K86	K91
Complete wave regime	8.83	3.11	5.63	1.44	8.52	1.90
CERC	9.10	3.11	5.63	1.44	8.52	1.62
C2	9.10	3.11	5.74	1.43	8.32	1.83
K&I	9.10	3.05	5.63	1.41	8.10	1.79
Kr88	9.10	3.18	5.87	1.44	8.41	1.87
K86	9.10	3.18	5.87	1.45	8.52	1.86
K91	9.10	3.17	5.86	1.45	8.55	1.62

Table 3.10: Longshore sediment transport normalized results for wave regime simplification 2b. ($Q_\ell = \times 10^6$ m^{3}year^{-1}).

Reg \ Form	CERC	C2	K&I	Kr88	K86	K91	$\overline{Q_{\ell,norm}}$	σ_{Hor}
CERC	1.03	1.00	1.00	1.00	1.00	0.85	0.98	0.06
C2	1.03	1.00	1.02	0.99	0.98	0.96	1.00	0.03
K&I	1.03	0.98	1.00	0.98	0.95	0.94	0.98	0.03
Kr88	1.03	1.02	1.04	1.00	0.99	0.98	1.01	0.02
K86	1.03	1.02	1.04	1.01	1.00	0.98	1.01	0.02
K91	1.03	1.02	1.04	1.01	1.00	0.85	0.99	0.07
$\overline{Q_{\ell,norm}}$	1.03	1.01	1.02	1.00	0.99	0.93	1.00	
σ	0.00	0.02	0.02	0.01	0.02	0.06	0.02	

Table 3.11: Longshore sediment transport results for wave regime simplification 2c. (Q_ℓ = $\times 10^6$ m^{3}year^{-1}).

	CERC	C2	K&I	Kr88	K86	K91
Complete wave regime	8.83	3.11	5.63	1.44	8.52	1.90
CERC	9.24	3.11	5.63	1.44	8.52	1.62
C2	9.24	3.11	5.74	1.23	8.42	1.82
K&I	9.24	3.05	5.63	1.22	8.19	1.79
Kr88	9.24	4.85	8.96	1.44	22.71	2.93
K86	9.24	3.14	5.80	1.24	8.52	1.84
K91	9.24	3.17	5.86	1.25	8.65	1.62

Table 3.12: Longshore sediment transport normalized results for wave regime simplification 2c. ($Q_\ell = \times 10^6$ m^{3}year^{-1}).

Reg \ Form	CERC	C2	K&I	Kr88	K86	K91	$\overline{Q_{\ell,norm}}$	σ
CERC	1.05	1.00	1.00	1.00	1.00	0.85	0.98	0.07
C2	1.05	1.00	1.02	0.86	0.99	0.96	0.98	0.07
K&I	1.05	0.98	1.00	0.85	0.96	0.94	0.96	0.07
Kr88	1.05	1.56	1.59	1.00	2.67	1.54	1.57	0.60
K86	1.05	1.01	1.03	0.86	1.00	0.97	0.99	0.07
K91	1.05	1.02	1.04	0.87	1.01	0.85	0.97	0.09
$\overline{Q_{\ell,norm}}$	1.05	1.10	1.11	0.91	1.27	1.02	1.09	
σ	0.00	0.23	0.23	0.07	0.68	0.26	0.29	

$Q_{\ell,norm}$ equal to 0.93 and standard deviations of 0.12 for Kr88 and 0.13 for the remaining three. For simplification 1b, the formulae C2, K&I and K91 are those that provide the best results of the longshore sediment transport computed with simplified regimes, with $Q_{\ell,norm}$ equal to 1.14 for the first two formulae and 1.15 for the last one, and standard deviations for all three formulae equal to 0.13.

Simplification 2

The simplification 2 is made by grouping the waves of the complete wave regime in classes with an interval of deepwater wave height (simplification 2a), incident wave breaker height of 1 m (simplification 2b) and 0.5 m (simplification 2c), resulting in 16, 8 and 16 representative waves respectively (Figure 3.17b).

One observes that the formula that best predicts the reference value (1×10^6 m^{3}year^{-1}) is Kr88. However, the simplified regimes could yield values of Q_ℓ 26% and 15% lower, for simplification 2a and 2c respectively, than the value for the complete regime (1.44×10^6 m^{3}year^{-1}). For simplification 2b the range of Q_ℓ values is $\pm$ 0.70%.

Analysing the results of the formulae that are a function of the wave characteristics at the breaker line, for simplification 2a, the K&I and C2 formulae are the ones that provide the most stable results ($\overline{Q_{\ell,norm}} = 0.79, \sigma = 0.03$ and $\overline{Q_{\ell,norm}} = 0.78, \sigma = 0.02$). In simplification 2b the formulae are Kr88, C2 and K86 with values of $\overline{Q_{\ell,norm}} = 1.00, \sigma = 0.01$, $\overline{Q_{\ell,norm}} = 1.01, \sigma = 0.02$ and $\overline{Q_{\ell,norm}} = 0.99, \sigma = 0.02$, respectively. Kr88 = $\overline{Q_{\ell,norm}} = 0.91, \sigma = 0.07$ and K91 = $\overline{Q_{\ell,norm}} = 1.02, \sigma = 0.26$ are the results most stable obtained for simplification 2c.

Analysing the results of the horizontal averaging in simplification 2a, we conclude that to compute simplified wave regimes, the formulae K86 and Kr88 are those that provide the best results of the longshore sediment transport computed with simplified regimes, with $Q_{\ell,norm}$ equal to 0.82 and 0.81 and standard deviations of 0.10 and 0.11, respectively. For

simplification 2b, the formulae C2, Kr88 and K86 are those that provide the best results of the longshore sediment transport computed with simplified regimes, with $Q_{\ell,norm}$ equal to 1.00 for the first and 1.01 for both Kr88 and K86, and standard deviations of 0.03 for C2 and 0.02 for the others two. For simplification 2c, the K86 ($Q_{\ell,norm} = 0.99$ and $\sigma = 0.07$) and C2 ($Q_{\ell,norm} = 0.98$ and $\sigma = 0.07$) formulae are those that provide the best results of the longshore sediment transport computed with simplified regimes.

Average of Q_ℓ

To analyze the several simplifications that were made, all the averages of the longshore sediment transport for all the simplifications tested, were joined in one single table (Table 3.13). That is, Table 3.13 contains all the horizontally averaged results of each simplification (in the second last column of Table 3.4 and similar ones). From it we can conclude which method to compute a simplified wave regime is the best one, and which of the computed simplified wave regimes produce longshore transports close to those obtained with the complete wave regime.

Thus, Table 3.13 shows that the best results are provided by simplification 2b (M= 1.00, $\sigma = 0.01$). This wave regime simplification consists in grouping the complete wave regime in wave breaker height classes with intervals of 1 m, resulting in 8 representative waves. The second best tested simplification is 1a (M= 0.97, $\sigma = 0.08$), which corresponds to divide the complete wave regime in directional classes of wave angles in deepwater, resulting in 8 equivalent waves. Analyzing the average and standard deviation of the simplified wave regimes (horizontal average), we conclude that those that are computed through C2, K&I and K91 are the ones that produce results more stable (smaller standard deviation) for longshore sediment transport. The results for all three simplified wave regimes are M= 0.96, $\sigma = 0.13$.

Taking into account the sensitivity analysis of the formulations to d_{50} and to the bot-

Table 3.13: Longshore sediment transport mormalized results for all wave regime simplifications tested. ($Q_\ell = \times 10^6 \mathrm{m}^3\mathrm{year}^{-1}$).

Reg \ Form	1a	1b	2a	2b	2c	M	σ
CERC	0.98	1.22	0.77	0.98	0.98	0.99	0.16
C2	0.93	1.14	0.78	1.00	0.98	0.96	0.13
K&I	0.93	1.14	0.77	0.98	0.96	0.96	0.13
Kr88	0.93	1.31	0.81	1.01	1.57	1.12	0.31
K86	1.14	1.36	0.82	1.01	0.99	1.06	0.20
K91	0.93	1.15	0.77	0.99	0.97	0.96	0.13
M	0.97	1.22	0.79	1.00	1.08	1.08	
σ	0.08	0.10	0.02	0.01	0.24	0.07	

tom slope, it is concluded that among the three formulations, the more stable is K91. Consequently the better simplified regime is obtained using the K91 formulation and the simplification 2b. These representative waves are represented in Table 3.14. This simplified regime induces a longitudinal sediment transport offshore the study area equivalent to that caused by the complete wave regime. This set of waves can be used as boundary condition in morphodynamic simulations, instead of the complete regime, to decrease the computational time. Additionally, these waves can be used separately in order to study and understand the influence of a particular wave height or wave direction in the sediment transport.

Table 3.14: Wave simplified regime computed through the K91 longshore sediment transport formula. Simplification 2b

Wave	Frequency (%)	$H_{0,eq}$ (m)	$\alpha_{0,eq}$ (^{o})	$H_{b,eq}$ (m)	$\alpha_{b,eq}$ (^{o})	$T_{p,eq}$ (s)
#1	0.1429	0.71	20.52	0.87	6.72	8.65
#2	0.4574	1.36	22.10	1.55	8.80	9.28
#3	0.2475	2.23	20.76	2.48	8.25	10.75
#4	0.0971	3.13	19.41	3.39	7.72	11.50
#5	0.0387	4.14	20.22	4.37	8.70	12.19
#6	0.0119	5.10	22.73	5.36	10.19	13.76
#7	0.0023	5.87	18.87	6.31	8.29	14.06
#8	0.0013	6.81	15.25	7.46	4.60	14.88

3.8 Conclusions

Through years the Ria de Aveiro lagoon inlet migrated along the coastline, until its closure around 1741. In 1808 an artificial inlet was constructed, composed by two-breakwaters. The breakwater located at the North side is the most important structure and also the most susceptible to the wave regime. Recently it was subjected to reparation works due to its collapse.

The bathymetric data obtained through surveys performed by I.H. and by A.P.A. in the study area domain were analyzed. It is observed a generalized deepening of the inlet channel between the years 1987/88 and 2001.

The bathymetric evolutions, more pronounced between 2001 and 2005, shows that the deeper area located between the tidal gauge and the *triângulo das marés* is filling in. An offshore and southward movement is observed for the deeper area located between the breakwaters, deepening at the left side of the deeper area and slightly accreting at the right side.

Concerning the bottom sediments size, a heterogeneous distribution was created by merging literature data and observational data. This distribution considers coarser sediments close to the North breakwater decreasing in size up to the *Meia Laranja* beach.

The Ria de Aveiro lagoon was characterized hydrodynamically as mesotidal with a tidal range of 2 m and with semidiurnal tidal forcing. The higher duration of flood currents when compared with the ebb currents, revealed ebb dominance in the lagoon.

A sensitivity analysis of the longshore sediment transport formulations to the sediment size diameter and to bottom slope was performed. It was concluded that the K86 and the K&I formulations have strong dependencies on these domain characteristics. The C2 formulation revealed a strong dependency on d_{50}.

The longshore transport induced by the complete wave regime was computed through several formulations and the results obtained when compared to the reference value presented in literature, revealed over-prediction for all formulations. The formulation of K91 represents the better description of the longshore sediment transport, evaluating the transport as 1.90×10^6 $m^3 year^{-1}$.

In order to find a simplified wave regime which induces a longitudinal sediment transport equivalent to that caused by the complete wave regime, several simplifications were tested by grouping the waves by the correspondent height and incident angle.

The results indicate that to compute the simplified wave regime, the formulations of C2, K&I and K91 are more adequate and accurate than the other formulae (Kr88 and K86). In absolute terms, the K91 seems to be more accurate for this coastal stretch.

To derive a simplified wave regime, among the 5 different alternatives that were tested, the best method is to divide the complete wave regime in wave height classes of intervals of 1m, resulting in 8 equivalent waves, for the wave regime used in this study. The simplified wave regime corresponding to simplification 2b and with Q_ℓ computed from K91 is composed of 8 waves and is presented in Table 3.14. This wave regime will be used as boundary condition in the numerical simulations with the morphodynamic model MORSYS2D (Chapter 6), in order to understand the effect of each single wave in the complete sediment transport.

Chapter 4

MORSYS2D and Models Setup

4.1 Introduction

To identify the processes that govern the sediment transport at the Ria de Aveiro lagoon inlet, the numerical model MORSYS2D is used. The simulations performed take into account different sediment transport forcings: the tidal current and a regular monochromatic wave or a wave regime. With these simulations, bathymetric changes are predicted and the morphodynamic of the inlet is studied.
In this Chapter, the methodology adopted in the numerical modeling study is presented. Also, a general overview of the morphodynamic modeling system used, MORSYS2D, is performed, presenting the main formulations solved by each model component that encompasses this modeling system.
To complete the chapter, the models setup to the Aveiro study case are presented. Also in this section a hydrodynamic validation is performed, by comparing the numerical results obtained in this study with measurements and with the results obtained by Oliveira et al. [2007] . Additionally, a comparison between the wave regime forcing used in this study and the available directional buoy data is made.

4.2 Methodology

The numerical modeling study dedicated to improve the knowledge about the Ria de Aveiro lagoon inlet morphodynamic characteristics and dominant processes is performed by using the modeling system MORSYS2D in two main simulations: forced only by tides (Chapter 5) and forced by coupled tides and waves (Chapter 6). The predicted bathymetry and bathymetric changes are compared with those observed in order to evaluate the models performance. The numerical results allow the analysis of the residual sediment fluxes, obtained by averaging the sand fluxes for two MSf constituent periods (2×14.78 days). These residual fluxes are computed and analyzed at the study area and at nine cross-sections, defined to en-

compass the inlet, navigation channel and nearshore region (Figure 3.7). These nine sections delimit eight regions where the sedimentation rates are computed. Additionally to these, one longitudinally section was defined along the center of the inlet and navigation channel. The choice of the sections and regions locations was made in order to match with the bottom features of the study area, previously analyzed in Chapter 3.
The influence of the tidal currents is analyzed by performing numerical simulations considering the tides as the only sediment transport forcing in the formulations available. Within these simulations the influence of spring and neap tide conditions, bottom depth and distribution of the bottom sediment size is analyzed through the residual sediment fluxes and bathymetric changes.
After understanding the influence of these factors in the morphodynamics, simulations for long periods, 1.75 and 4.25 years are performed in order to validate the numerical results by comparing them with the observations, described in Chapter 3. From these simulations is identified the area of tidal influence at the inlet, concerning the sediment transport.
The influence of the waves in the lagoon inlet morphodynamics is studied through numerical simulations considering the tides and the waves as coupled forcing in the sediment transport. Two separated studies are presented: a regular monochromatic wave and a complete wave regime. The simulations considering a regular monochromatic wave as sediment forcing are performed in order to identify the wave characteristics that induce the largest changes in the inlet morphology. The real wave regime is imposed in order to reproduce the real bathymetric changes observed, validating the results. Long period simulations of 1.75 and 4.25 years are also performed.

4.3 Numerical model

The numerical simulations of the sediment dynamics and morphologic evolution of the Ria de Aveiro inlet were performed with the 2DH morphodynamic modeling system MORSYS2D [Fortunato and Oliveira, 2004, 2007; Bertin et al., 2009c]. This modeling system (schematized in Figure 4.1) integrates the hydrodynamic model ELCIRC, which calculates tidal elevations and currents, the wave model SWAN, which computes wave propagation and the model SAND2D that computes sand transports and updates the bottom topography.
A short description of each model component is presented in the following subsections.

4.3.1 ELCIRC

ELCIRC is an open-source model (www.stccmop.org/CORIE/modeling/elcirc/index.html) developed for the simulation of 3D baroclinic circulation that uses a finite-volume/finite-difference Eulerian-Lagrangian algorithm to solve the set of six hydrostatic equations based on the Boussinesq approximation: mass conservation, momentum conservation and conservation

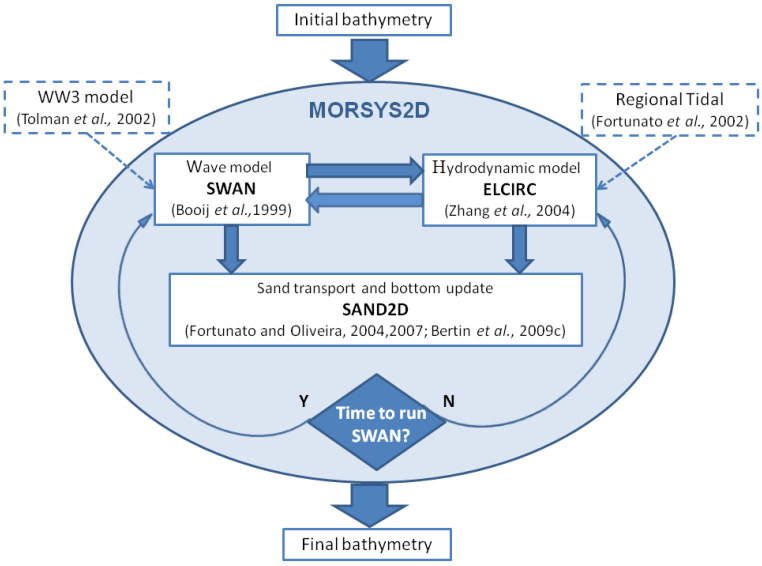

Figure 4.1: Schematic diagram of the MORSYS2D morphodynamic model system.

of salt and heat [Zhang et al., 2004]. The equations for mass and momentum conservation in ELCIRC are given by:

$$\frac{\partial \zeta}{\partial t} + \frac{\partial}{\partial x}\int_{-h}^{\zeta} u\, dz + \frac{\partial}{\partial y}\int_{-h}^{\zeta} v\, dz = 0 \tag{4.1a}$$

$$\frac{Du}{Dt} = f\, v - \frac{\partial}{\partial x}\left\{ g\left(\zeta - \alpha\hat{\psi}\right) + \frac{P_a}{\rho_0}\right\} - \frac{g}{\rho_0}\int_{z}^{\zeta} \frac{\partial \rho}{\partial x}\, dz + \frac{\partial}{\partial z}\left(K_{mv}\frac{\partial u}{\partial z}\right) + F_{mx} \tag{4.1b}$$

$$\frac{Dv}{Dt} = -f\, u - \frac{\partial}{\partial y}\left\{ g\left(\zeta - \alpha\hat{\psi}\right) + \frac{P_a}{\rho_0}\right\} - \frac{g}{\rho_0}\int_{z}^{\zeta} \frac{\partial \rho}{\partial y}\, dz + \frac{\partial}{\partial z}\left(K_{mv}\frac{\partial v}{\partial z}\right) + F_{my} \tag{4.1c}$$

where (x, y) are the horizontal cartesian coordinates, z the vertical coordinate, t the time, ζ the surface water elevation, h the depth, g the gravity, $\hat{\psi}$ the tidal potential, α the effective Earth elasticity factor, ρ the water density, P_a the atmospheric pressure at free surface and K_{mv} the vertical eddy viscosity

Within MORSYS2D, the hydrodynamic model ELCIRC, reverses to a 2D depth-averaged model, by using a single vertical layer. The previous equations for the depth-integrated mode are:

$$\frac{\partial \zeta}{\partial t} + \frac{\partial (HU)}{\partial x} + \frac{\partial (HV)}{\partial y} = 0 \tag{4.2a}$$

$$\frac{\partial U}{\partial t} + U\frac{\partial U}{\partial x} + V\frac{\partial U}{\partial y} = f\, V - g\frac{\partial \zeta}{\partial x} - \frac{\tau_{bx}}{\rho} + \frac{\tau_{sx}}{\rho} + \nu\left(\frac{\partial^2 U}{\partial x^2} + \frac{\partial^2 U}{\partial y^2}\right) \tag{4.2b}$$

$$\frac{\partial V}{\partial t} + U\,\frac{\partial V}{\partial x} + V\,\frac{\partial V}{\partial y} = -f\,U - g\,\frac{\partial \zeta}{\partial y} - \frac{\tau_{by}}{\rho} + \frac{\tau_{sy}}{\rho} + \nu\left(\frac{\partial^2 V}{\partial x^2} + \frac{\partial^2 V}{\partial y^2}\right) \tag{4.2c}$$

where H is the total depth, U, V are the depth averaged velocity components in the x and y directions, τ_{bx}, τ_{by} are the bottom stress in x and y directions, τ_{sx}, τ_{sy} are the surface stress in x and y directions and ν is the horizontal eddy viscosity. In the present application of MORSYS2D, the horizontal diffusion term was not considered.

In the hydrodynamic model these equations are discretized through a volume conservative numerical algorithm, stable and computationally efficient, naturally incorporating wetting and drying. A triangular mesh is used to discretize the horizontal domain.

There are several options of forcing agents in ELCIRC within MORSYS2D: tides, tidal potential, river flow and wind or waves-induced radiation stresses. Only the surface water elevation and waves-induced radiation stresses are considered in this study.

Under the action of tides only, the stress is defined at the bottom according to each horizontal direction:

$$\tau_{bx} = \rho\, C_D\, \sqrt{U^2 + V^2}\, U \tag{4.3a}$$

$$\tau_{by} = \rho\, C_D\, \sqrt{U^2 + V^2}\, V \tag{4.3b}$$

where C_D is the drag coefficient computed using the Manning law and given by:

$$C_D = g\, n^2\, h^{-1/3} \tag{4.4}$$

and the friction coefficient n could be defined constant or variable in space.

According to Longuet-Higgins and Stewart [1964] and Phillips [1977] the effect of short waves on the hydrodynamics is expressed through the forcing by the gradients of wave radiation stresses, which in this 2DH mode can be defined by:

$$\tau_{sx} = -\left(\frac{\partial S_{xx}}{\partial x} + \frac{\partial S_{yx}}{\partial y}\right) \tag{4.5a}$$

$$\tau_{sy} = -\left(\frac{\partial S_{yy}}{\partial y} + \frac{\partial S_{xy}}{\partial x}\right) \tag{4.5b}$$

and $S_{xx}, S_{yy}, S_{xy}, S_{yx}$ are wave radiation stress terms, given by:

$$S_{xx} = \frac{E}{2}\left(2\frac{C_g}{C}\left(\cos^2\alpha + 1\right) - 1\right) \tag{4.6a}$$

$$S_{yy} = \frac{E}{2}\left(2\frac{C_g}{C}\left(\sin^2\alpha + 1\right) - 1\right) \tag{4.6b}$$

$$S_{xy} = S_{yx} = E\frac{C_g}{C}\sin\alpha\cos\alpha \tag{4.6c}$$

where $E = 1/8\rho g H_{rms}^2$ is the wave energy, α is the wave angle to the x axis, C_g is the wave group velocity and C the wave phase velocity.

4.3.2 SWAN

The wave model SWAN [Booij et al., 1999] computes the evolution of the wave spectrum by solving the spectral action balance equation adapted to nearshore zones, given in Cartesian coordinates by Equation 4.7.

$$\frac{\partial}{\partial t}N + \frac{\partial}{\partial x}(c_x\, N) + \frac{\partial}{\partial y}(c_y\, N) + \frac{\partial}{\partial \sigma}(c_\sigma\, N) + \frac{\partial}{\partial \theta}(c_\theta\, N) = \frac{S}{N} \tag{4.7}$$

in which σ is the wave frequency (s^{-1}), θ the wave angle (radians), N the wave action density (m), c_x, c_y the wave propagation speeds in x and y directions (m/s) and S the energy source term (m/s^2).

The first term on the left-hand side of Equation 4.7 represents the local rate of change of action density in time, the second and third terms represent propagation of action in geographical space (with propagation velocities c_x and c_y in x and y space, respectively). The fourth term represents the shifting of the relative frequency due to variations in depths and currents (with propagation velocity c_σ in σ space). The fifth term represents depth induced and current-induced refraction (with propagation velocity c_θ in θ space). The expressions for these propagation speeds are taken from linear wave theory [e.g., Whitham, 1974; Dingemans, 1997]. The term S [$= S(\sigma, \theta)$] at the right-hand side of the action balance equation is the source term represented as energy density, showing the effects of generation, dissipation, and nonlinear wave-wave interactions.

Within MORSYS2D, when interactions with currents or propagation within a non-uniform water level are considered, SWAN is fed by outputs of velocities and elevations from the hydrodynamic model (ELCIRC) linearly interpolated over SWAN's grids. SWAN can be forced at its open boundary by constant wave parameters, time series of wave parameters (e.g. WW3 model [Tolman et al., 2002]), by wave spectra originating from the WW3 model or from oceanic wave buoy data. Depending on the size and the geometry of the modeled domain, several computational grids can be nested, with different spatial resolutions, where the last nested grid is oriented parallel to the coast and includes the whole area where bathymetric changes are being simulated and the bathymetry being updated. The spatial resolution of the finest computational grid is adjusted depending on the wave height and the beach gradient in order to provide a good description of the surf zone.

Significant wave height, period, direction, wavelength, and orbital velocity are outputted from SWAN and used to compute gradients of radiation stresses (Equations 4.6) to force the hydrodynamic model ELCIRC and to compute sand fluxes into SAND2D.

4.3.3 SAND2D

SAND2D, developed by Fortunato and Oliveira [2004, 2007] and Bertin et al. [2009c], computes the sand transport and the bottom update. The sand fluxes due to the effect of currents and waves forcing are simulated by using one of the several formulations presented in Section 2.5.1: Meyer-Peter and Muller [1948] (MPM), citeEH67 (EH), Bijker [1971] (Bi), Ackers and White [1973] (AW), van Rijn [1984a,b,c] (vR), Karim and Kennedy [1990] (kk), Soulsby [1997] (SvR) and Bhattacharya et al. [2007] (Bha) for currents, and Bijker [1971] (Bi), Ackers and White [1973] (AW) and Soulsby [1997] (SvR) for currents coupled with waves. The bottom update is performed through the Exner equation, that describes the conservation of mass between sediment in the bed and the sediment that is being transported.
To deal with the generation of numerical oscillations, a source of constant concern to developers and users of morphodynamic models, different approaches were considered in SAND2D model: a predictor-corrector scheme was implemented in the solution of Exner equation, the inclusion of an additional diffusion term in the referred equation and the inclusion of a morphological factor to adaptatively control the Courant number [Fortunato and Oliveira, 2007]. Additionally, the user may activate five numerical filters: a non-linear bathymetric filter, a gradient filter, a global filter, a flux filter and a diffusive filter. A short description of these approaches is presented here.

Predictor-Corrector Method

After computing the sand fluxes, through the formulations aforementioned, the Exner equation is solved using a predictor corrector method to compute the bathymetry at the next time step:

$$\Delta h^i = \frac{1}{1-\lambda}\nabla Q_*^i \tag{4.8}$$

where Q_* is the sediment flux integrated over the morphological time step, λ is sediment porosity and Δh^i is the bottom variation over a time step. This method is used to cease the stability problems that appear from the explicit discretization of this equation [Fortunato and Oliveira, 2007]. In the predictor-corrector method an estimate of depth at time $n+1$ is first calculated as

$$h^{n+1} = h^n + \frac{1}{1-\lambda}\nabla \int_n^{n+1} q\left(u(t), \zeta(t), h^n\right) dt \tag{4.9}$$

A fully or semi-implicit solution of this equation is then determined in the correction step as

$$h^{n+1} = h^n + \frac{1}{1-\lambda}\nabla \int_n^{n+1} q\left(u(t), \zeta(t), h^*\right) dt \tag{4.10}$$

where $h^* = \alpha h^{n+1} + (1-\alpha)h^n$. The implicitness of the method is determined by the parameter $\alpha \in [0, 1]$. Equations 4.9 and 4.10 can be repeated iteratively, for a user-specified number of correction cycles.

Additional Diffusion Term in the Exner Equation

A simple formula is adopted because the diffusion is added just for stability. Thus, a diffusive term is added to the sediment flux Q, resulting in a new sediment flux formulation Q_* given by:

$$Q_* = Q + \epsilon\,(1-\lambda)\left(|Q_x|\,\frac{\partial h}{\partial x}, |Q_y|\,\frac{\partial h}{\partial y}\right) \tag{4.11}$$

where ϵ is a dimensionless diffusion coefficient specified by the user and Q is the sediment flux, obtained through one of the formulations described in equations 2.2 to 2.13, computed at the center of the elements and integrated in time between steps n and $n+1$.

Adaptive Time Step

Additionally to the predictor-corrector algorithm, the Courant number is used to confine the stability of the solution . The procedure consists in automatically adjust the time step to the maximum Courant number [Bertin et al., 2009c]. The Courant number, Cr, is estimated as:

$$Cr \approx \frac{bQ^*}{H\Delta x} \tag{4.12}$$

where b is the velocity power in the transport formulation (between 3 and 5 considering equations 2.2 to 2.13) and Q^* is the tide averaged transport. As described in Bertin et al. [2009c] the determination of the succeeding morphological time step is based on two assumptions: (1) the logarithm of α_i, the maximum Courant number at time i divided by the time step, varies linearly in time; and (2) the morphological time step varies slowly in time. Assumption (1) and (2) permit to make a prediction of the next Courant number Cr_{n+1}, using a log-linear extrapolation:

$$\frac{\ln(\alpha_{n+1}) - \ln(\alpha_n)}{\Delta t_{n+1}} = \frac{\ln(\alpha_n) - \ln(\alpha_{n-1})}{\Delta t_n} \tag{4.13}$$

According to assumption (2), $\Delta t_{n+1} \approx \Delta t_n$, thus equation 4.13 simplifies to:

$$\alpha_{n+1} = \frac{\alpha_n^2}{\alpha_{n-1}} \tag{4.14}$$

Then, the next morphodynamic time step Δt_{n+1} can be computed as:

$$\Delta t_{n+1} = Cr_{target}\frac{\alpha_{n-1}}{\alpha_n^2} \tag{4.15}$$

depending on a user-specified Courant number Cr_{target}.
Finally, the new morphodynamic time step Δt^*_{n+1} is given by:

$$\Delta t^*_{n+1} = \delta \cdot \Delta t_{n+1} + (1-\delta)\,\Delta t_n \tag{4.16}$$

where δ is a relaxation factor set to 0.7. This adaptative procedure leads to time steps that changes from the maximum sand fluxes, obtained in mid-tide or under the action of very energetic wave conditions (about 2 minutes), to the period when sand fluxes are minimum, around high and low tide or under the influence of small waves (45 minutes) [Bertin et al., 2009c; Fortunato et al., 2009]. The minimum morphodynamic time step is limited by the hydrodynamic model time step.

Numerical filters

The non-linear bathymetric filter smooths the bathymetry errors associated with measurement errors, unresolved bathymetric features and the interpolation algorithms, while preserving the overall domain volume. This filter is applied to eliminate local extrema in the depth followed by a linear filter to smooth all the domain. Fortunato and Oliveira [2000, 2003] tested this filter and obtained an error reduction of the order of 50% at some locations in tidal simulations in a large estuary.
The concept that the sand bottom gradients have to be limited by the stress angle is the basis of the gradient filter. If the gradient is higher than the angle tangent, the equality of these is imposed as well as the volume conservation.
The global filter consists in a linear filter applied to smooth all the domain (cf. SAND2D Fortunato and Oliveira [2004, 2007]; Bertin et al. [2009c]).
The flux filter consists in filtering the fluxes by averaging the flux from the element (where it is computed) to the nodes and back to the elements (cf. SAND2D Fortunato and Oliveira [2004, 2007]; Bertin et al. [2009c]).
The diffusive filter, denoted by ϵ in Exner equation, is used by several authors to minimize numerical fluctuations. SAND2D considers a diffusive coefficient in each flux direction which is proportional to the sediment flux correspondent to that direction. This filter was already introduced and presented in equation 4.11 [Fortunato and Oliveira, 2004].

4.4 Models setup and hydrodynamic validation

To perform the numerical simulations it is necessary to define several input grids and parameters in the numerical models ELCIRC, SAND2D and SWAN. In the next subsections the setup of the models is described as well as the validation of the hydrodynamic and wave models.

4.4.1 ELCIRC

The hydrodynamic model ELCIRC uses a computational domain that extends from the upstream limits of the lagoon to the continental shelf. This domain was discretized with an unstructured grid with 25819 nodes and 43169 elements, illustrated in Figure 4.2. This grid

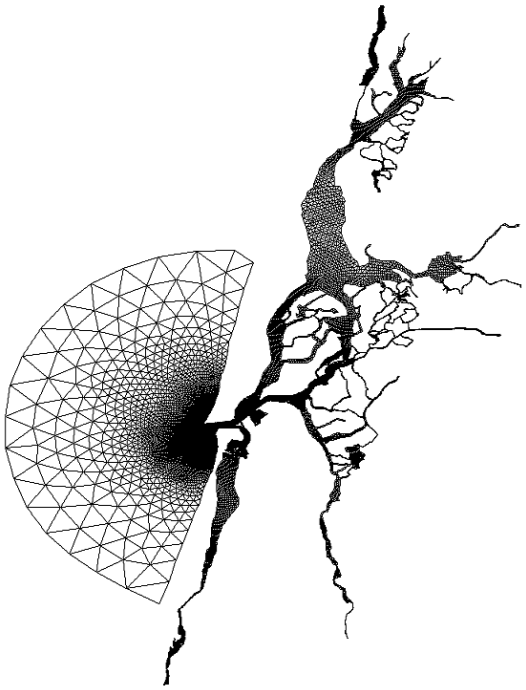

Figure 4.2: Unstructured grid of the Ria de Aveiro lagoon.

is a modification of that presented by Oliveira et al. [2007], with the inlet and nearshore region refined in order to obtain a better prediction of the fluxes at the inlet. The spatial discretization of the grid ranges from 1400 m offshore to 20 m at the inlet and 3 m at the narrow channels upstream.

The bathymetric data considered as initial condition for the numerical simulations is created by coupling bathymetric data collected from two surveys performed by A.P.A.: 1987/88 and 2001, illustrated in Figure 3.2. This is justified because the 2001 survey wasn't performed for all the computational domain defined and represented in Figure 1.1; it was only performed at the inlet, navigation channel and adjacent offshore area. Therefore the bathymetric data collected in 1987/88 was used to complete the computational domain and this coupled grid was used as initial condition in the numerical simulations. A representation of the inlet bathymetry considered as initial condition is illustrated in Figure 4.3.

For all simulations is considered a null horizontal eddy viscosity coefficient and a time step of 90 s.

The calibration of the hydrodynamic model performed by Oliveira et al. [2007] was used as basis. The tide was imposed at the oceanic open boundary of the ELCIRC grid through 11 harmonic constituents (Z_0, MSf, O_1, K_1, N_2, M_2, S_2, M_4, MN_4, MS_4 and M_6) being their amplitude and phase prescribed at the oceanic open boundary of the ELCIRC grid. The amplitude and phase of the harmonic constituents were obtained through the high-resolution finite element model of barotropic tides for the Iberian Atlantic shelf, developed by Fortunato

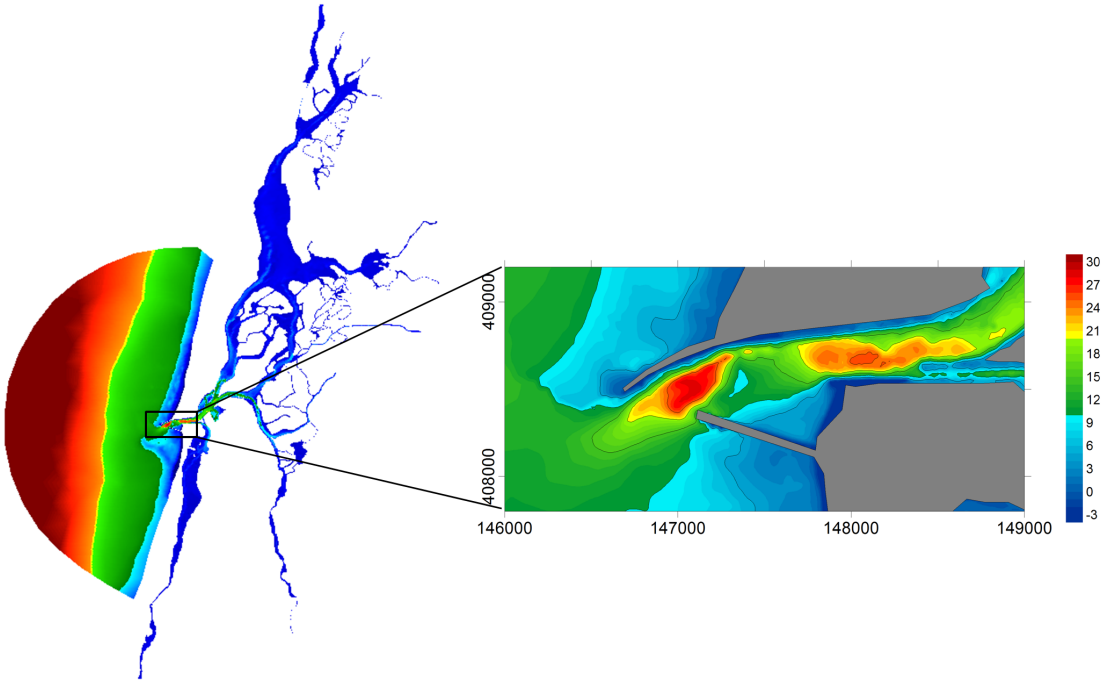

Figure 4.3: Bathymetry imposed as initial condition of the Ria de Aveiro lagoon.

et al. [2002]. The hydrodynamic simulations were performed using the depth-dependent Manning coefficient proposed by Dias and Lopes [2006].

Hydrodynamic validation

The numerical simulations presented in this study are performed using a refinement of the grid used by Oliveira et al. [2007] in the inlet area and nearshore. This refinement was deemed necessary to better resolve the wave-generated currents. This modification justifies a validation of the hydrodynamic model, which is performed at 11 stations within the lagoon and illustrated in Figure 4.4. The data available for this study are from a field campaign of 2003. Sea surface elevations at the eleven stations were measured during a month every 6 min, except at Torreira, where measurements were performed every half-hour. These data were collected in the framework of Araújo [2005].

To evaluate if the modifications performed in the original grid of Oliveira et al. [2007] don't deteriorate the quality of the predictions, numerical simulations considering the grid used by Oliveira et al. [2007] were also performed.

To validate the present version of the hydrodynamic model, qualitative analysis are performed between the numerical predictions obtained in this study and the measurements and also with the predictions obtained using the grid of Oliveira et al. [2007].

The methodology used to validate the hydrodynamic model was based on several studies in

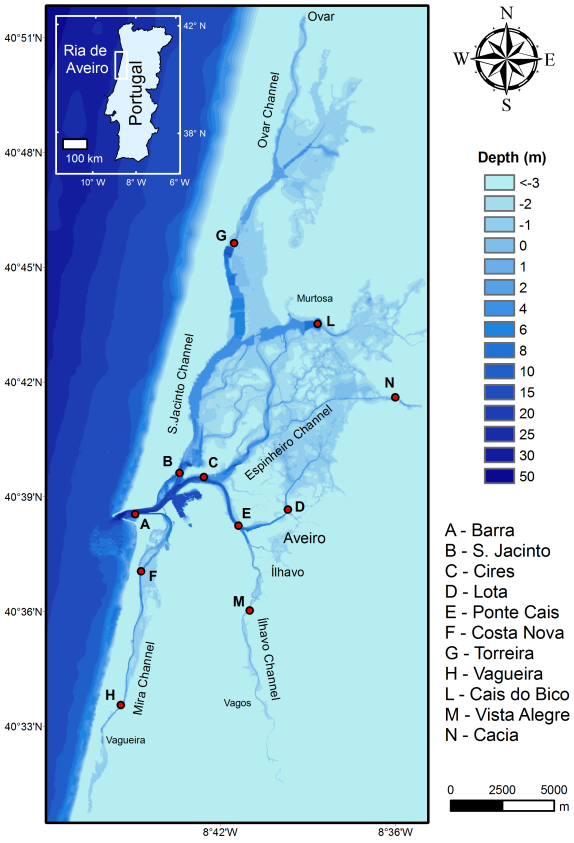

Figure 4.4: Ria de Aveiro lagoon bathymetry and location of the stations where data field data are available.

estuarine systems dominated by tides [Dias et al., 2009; Picado et al., 2010]. In these studies the authors removed the low frequency signal from data and model results, using a cut-off frequency of 0.0000093 Hz (30 h), once the high-frequency domain is the dominant signal intended that the models reproduce with higher accuracy.

The comparison between the model results obtained with this study and the results of Oliveira et al. [2007] and the observed sea surface elevation (SSE) is illustrated in Figure 4.5. It is observed that the model is more accurate at stations close to the inlet (stations A-F) reproducing correctly the amplitudes and phases either in high or low tide. For station N the amplitude is correctly simulated by the model, although it is observed a phase delay, higher for high tide than for low tide. For stations G-M, located at the inner channels of the lagoon is observed that the shape of the SSE evolution is not correctly reproduced (mainly for low tides), what may be justified by the low depths of these channels, which are characterized by wet and drying areas. For stations H-M a phase delay is also observed, being more pronounced for station H.

To quantify these differences and therefore the model's ability to reproduce the data, the root mean square errors ($RMSE$) and the predictive *skill* at each station are computed (Table

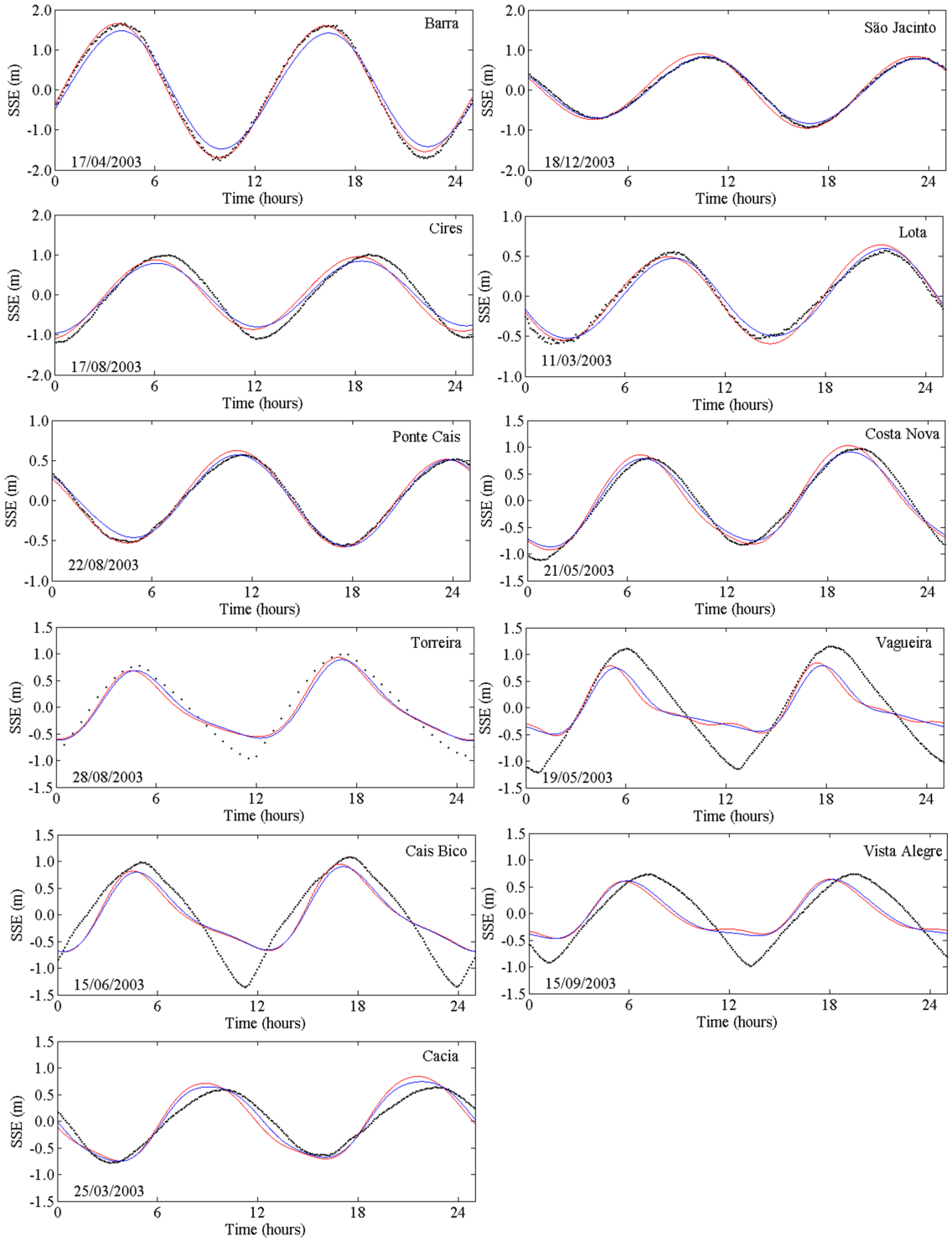

Figure 4.5: Comparison between predicted and observed SSE. Solic line: model results from this study (red) and from Oliveira et al. (2007) (blue) simulations; black circles: measurements. In the panels is referred the day of each compared period.

4.1) through equations 4.17 and 4.18, respectively:

$$RMSE = \left\{ \frac{1}{N} \sum_{i=1}^{n} \left[\zeta_0(t_i) - \zeta_m(t_i) \right]^2 \right\}^{1/2} \tag{4.17}$$

$$skill = 1 - \frac{\sum \left| \zeta_m - \zeta_0 \right|^2}{\sum \left[\left| \zeta_m - \overline{\zeta_0} \right| + \left| \zeta_0 - \overline{\zeta_0} \right| \right]^2} \tag{4.18}$$

where $\zeta_0(t)$ and $\zeta_m(t)$ are the observed and computed SSE, respectively, n is the number of measurements in the time series and the overbar represents the time average.

The *RMSE* should be compared with the local tidal amplitude [Dias et al., 2009]. If they are lower than 5% of the local amplitude, the agreement between model results and observations should be considered excellent. If they range between 5% and 10% of the local amplitude the agreement should be considered very good.

The model predictive *skill*, based on the quantitative agreement between model results and observations, indicates a perfect agreement between model results and observations if the *skill* is 1, a complete disagreement if the *skill* is 0 [Warner et al., 2005] and if the *skill* is higher than 0.95 is considered that there is an excellent agreement between predictions and observations [Dias et al., 2009].

Additionally the harmonic constants determined by the model and the data at the 11 stations are compared, in order to quantify the accuracy of the predicted tidal constituents.

In Table 4.1 are presented the *RMSE* and *skill* determined by comparing the results obtained with the application developed in this study with the observations, as well as comparing the results using Oliveira et al. [2007] grid with the observations.

The *RMS* errors show that the grid used in this study induces similar SSE predictions to those obtained using Oliveira et al. [2007] grid. The refinement performed at the grid generated an improvement of the SSE prediction for the station located at the inlet (A - Barra), when compared to the obtained with the grid used by Oliveira et al. [2007], with an amplitude error of 8 cm at this study and 17 cm for Oliveira et al. [2007]. For the remaining stations there is no evident improvement. For the stations near the inlet (A - F) the *RMSE* values indicate that the predictions are very good ($\leq$10% of the local amplitude) with an excellent agreement between the predictions and observations (*skill*$>$0.95). However, for the remaining stations the *RMS* errors exceed the 10% of local amplitude, being the higher disagreement achieved for the station G, followed by those for stations M, H, L and N.

These errors could be related to possible inaccuracies in the bathymetry as well as to possible uncertainties in the observed data. In fact there is a discrepancy between the dates of the bathymetry and the measurements, since the bathymetry data is from the year of 1987/88 completed with 2001 data and the measurements are from the year 2003. Also the deficient representation of the narrow channels of both grids as well as possible inaccuracies of the

Table 4.1: *RMSE* and predictive *skill* for 11 stations obtained with this study and with Oliveira et al. [2007] grids.

	This study			Oliveira et al. [2007]		
	RMSE (m)	Δ (%)	*skill*	RMSE (m)	Δ (%)	*skill*
Barra	0.08	2.2	1.00	0.17	4.7	0.98
São Jacinto	0.11	6.2	0.99	0.05	2.8	1.00
Cires	0.22	10.0	0.99	0.20	9.1	0.99
Lota	0.06	5.4	0.99	0.06	5.4	0.99
Ponte Cais	0.04	3.5	1.00	0.04	3.5	1.00
Costa Nova	0.16	7.0	0.98	0.12	5.2	0.99
Torreira	0.78	39.6	0.93	0.78	39.6	0.95
Vagueira	0.45	19.1	0.85	0.43	18.3	0.86
Cais Bico	0.36	14.5	0.91	0.36	14.5	0.91
Vista Alegre	0.34	19.5	0.94	0.30	17.2	0.95
Cacia	0.19	13.8	0.94	0.13	9.4	0.97

tidal forcing at the open boundary are likely sources of errors.

The *RMSE* and *skill* values obtained for the grid used in this study are similar to those obtained in previous works concerning the Ria de Aveiro lagoon numerical modeling [Dias and Lopes, 2006; Vaz et al., 2007; Rodrigues et al., 2009; Picado et al., 2010], as well as for other estuaries [Oliveira et al., 2006; Dias et al., 2009], revealing that the numerical model used and the refinement performed in the numerical grid reproduce accurately the lagoon's hydrodynamics.

Considering that the analysis performed evaluates the phase and amplitude errors coupled, a harmonic analysis of the amplitudes and phases for the M_2, S_2, O_1, K_1 and M_4 constituents (major tidal constituents in the Ria de Aveiro), for one month time series of the measurements, for the grids developed for this study and used by Oliveira et al. [2007], was made in order to quantify these errors separately. The results obtained are illustrated in Figure 4.6. The distributions of both observed and computed amplitude and phase (for both grids) are very similar, mainly for M_2, S_2 and O_1 and for the stations located near the inlet. For the stations located far from the inlet (stations G-N), the differences between the observations and the predictions are higher than those obtained for the stations A-F.

The semidiurnal constituents have mean amplitude errors of 19 cm and 5 cm for M_2 and S_2, respectively, corresponding to about 22% of their amplitude for the grid used in this study. A similar value was obtained for the grid used by Oliveira et al. [2007], with mean amplitude errors for M_2 and S_2 of 21%. The mean phase errors are approximately 14^o and 19^o for M_2 and S_2, respectively, corresponding to an average delay between the predicted tide and the observed of about 28 min for M_2 and 39 min for S_2. Similar delays are obtained when using

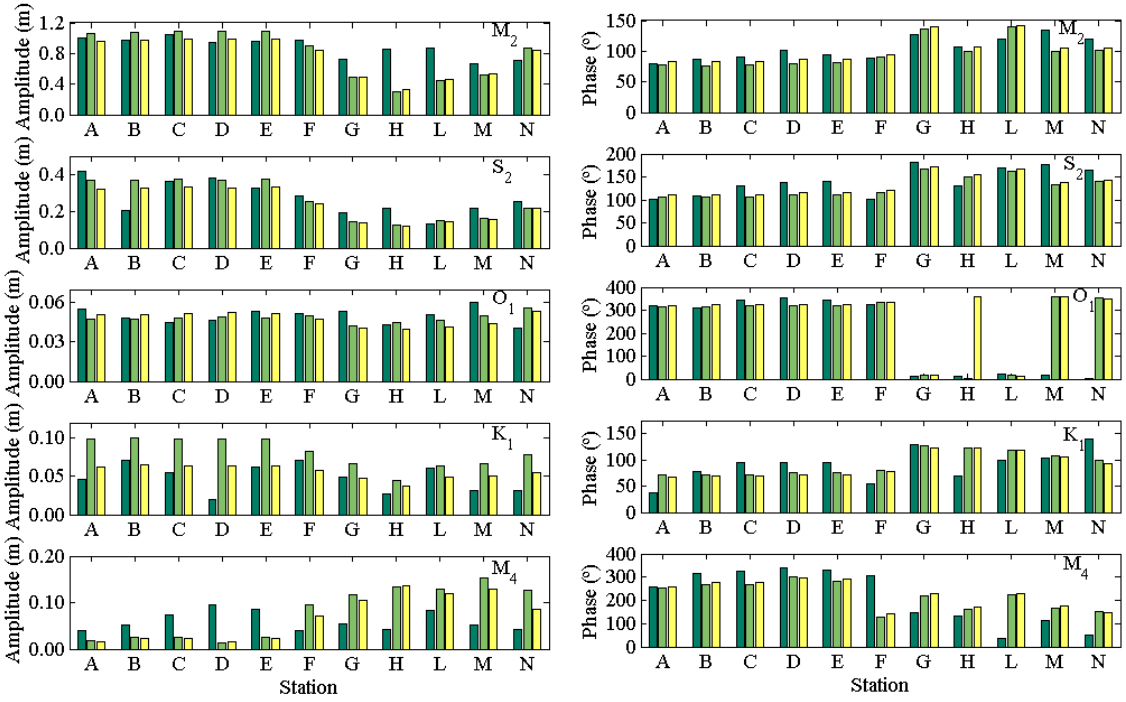

Figure 4.6: Distributions of tidal amplitude and phase for M_2, S_2, O_1, K_1 and M_4 constituents. Measurements (dark green); model results obtained in this study (light green) and using the Oliveira et al. [2007] grid (yellow).

the Oliveira et al. [2007] grid.

For the station A - Barra (located at the study area), is observed that the model predictions are more accurate than for the remaining stations, with amplitude errors of 6 cm (6%) and 5 cm (12%) for the semidiurnal constituents M_2 and S_2, respectively. The phase errors for this station are of approximately 4 min and 8 min, for M_2 and S_2, respectively. Concerning the results for the Oliveira et al. [2007] grid, the amplitude of the main constituent M_2 has a smaller error, 4%, while for S_2 the error is almost twice the obtained in this study (23%). Additionally the phase errors obtained for the Oliveira et al. [2007] grid revealed higher phase delays of 9 min for M_2 and 18 min for S_2.

The predictions for the diurnal constituents reveal a worse agreement between model predictions and observations, with average amplitude errors of about 12% and 97% for the constituents O_1 and K_1, respectively. The results obtained for the grid used in this study, are more (less) accurate for the O_1 (K_1) amplitude, occurring the opposite for the phase.

The results obtained for the M_4 constituent reveal higher accuracy for stations A, B and L than for the remaining stations, being the station A characterized by the higher phase accuracy with an error of approximately 7 min. It is also observed that the M_4 amplitude is underestimated for stations A-E and overestimated for the remaining stations (F-N). At the Barra station (A) the M_4 amplitude underestimation is of about 56% for this study (60%

for Oliveira et al. [2007]), predicting an amplitude of 0.0170 m (0.0157 m for Oliveira et al. [2007]) when the amplitude observed is 0.0388 m. However the comparison with the M_2 constituent amplitude (0.9963 m; approximately 4%) suggests that the influence of the M_4 amplitude underestimation might not be significant. Indeed, these errors have been observed in all hydrodynamic studies performed at the Ria de Aveiro lagoon and could be associated to bathymetric inaccuracies. Additionally, the relatively large errors associated with M_4 are not surprising, as overtides are typically much more difficult to reproduce correctly than the major astronomic constituents [Picado et al., 2010]. Also, as mentioned before, the bathymetry and the tidal data used in this study are not coincident in time; the bathymetry was collected in 1987/88 and 2001 while the tidal data is from 2003.
In summary it is concluded that the numerical results obtained using the grid developed in this study reproduces the observed harmonic constituents with similar accuracy to the results obtained with the grid of Oliveira et al. [2007]. For station A it is observed that the refined grid reproduces better the S_2 constituent while the Oliveira et al. [2007] grid reproduces more accurately the amplitude and phase of the O_1 and K_1 constituents. Analyzing the M_2 and M_4 constituents it is observed that the predictions with both grids are very similar, although the refined grid reproduces more accurately the results for the phase and amplitude of the M_2 and M_4 constituents, respectively.

Tidal asymmetry

In the Ria de Aveiro lagoon the dominant astronomical constituent is M_2, the semidiurnal lunar tide, being the most significant overtide its first harmonic M_4, generated primarily through the advective and finite amplitude terms of momentum equation. The tidal asymmetry evaluates the relative importance of M_2 and M_4, where the amplitude ratio between M_4 and M_2 indicates the magnitude of the tidal asymmetry (cf. Section 3.5). If the ratio is zero, the tide is undistorted; as the amplitude ratio increases, the more distorted the tide is, the higher residual currents are, and more flood or ebb dominant the systems turns into. This asymmetry and consequently the residual sediment fluxes, play a significant role in the sediment transport processes and morphodynamics [Brown and Davies, 2010], since flood dominant estuaries tend to infill their channels with coarser sediments while ebb dominant systems flush bottom sediments seaward more effectively, representing more stable geometry [Aubrey and Speer, 1985].
Therefore the analysis of tidal asymmetry is very important in terms of estuarine morphodynamics, and by this reason is analyzed in this study.
The amplitude ratio, the relative phase and the difference between ebb and flood durations are computed for the four main lagoon channels, along the channels axis, considering the model results obtained using the grid of this study and the one used by Oliveira et al. [2007] (Figure 4.7).

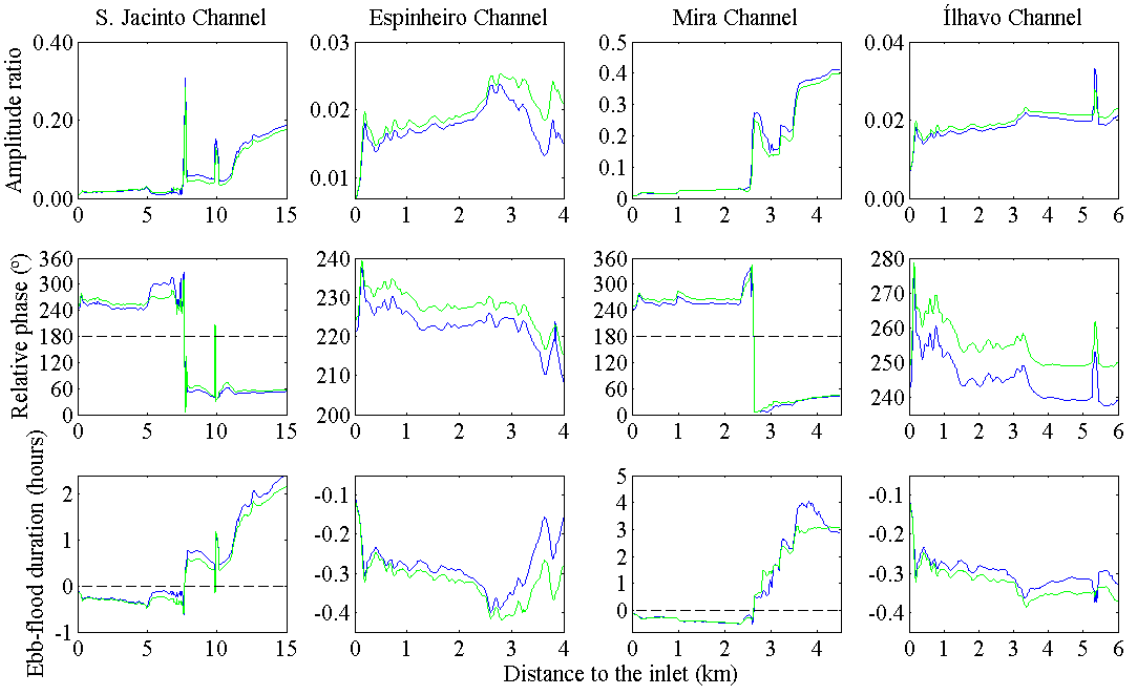

Figure 4.7: Asymmetric coefficients: amplitude ratio, relative phase (^{o}) and difference between ebb and flood duration (hours) along the axis of the four main channels of the Ria de Aveiro lagoon. Results obtained in this study (blue) and Oliveira et al. [2007] (green).

It is observed that the amplitude ratio is very low at the inlet increasing toward the channels heads. Analyzing the relative phase at the S. Jacinto and Mira channels is visible the transition from ebb dominant ($180^o < \phi < 360^o$) at the inlet to flood dominant ($0^o < \phi < 180^o$) at the upper channels. For the Espinheiro and Ílhavo channel this transition occurs far from to the inlet than the distance plotted in this Figure. These results are in agreement with Dias [2001]; Oliveira et al. [2007] and Picado et al. [2010].
In the lower panel of Figure 4.7 is presented the difference between the ebb and flood durations, which indicates ebb (flood) dominance if the value obtained is negative (positive) and consequently ebb currents higher (lower) than flood currents. It is observed that, as for the relative phase, the lagoon has ebb dominance close to inlet and shifts to flood dominance as moving along the channel (visible in this Figure for the S.Jacinto and Mira channels). For the Espinheiro and Ílhavo channels this transition occurs upstream (cf. Oliveira et al. [2007]; Picado [2008]).

With the analysis performed it is concluded that the hydrodynamic model reproduces accurately the lagoon tidal dynamics and produces valid results when compared with the previous studies performed for the Ria de Aveiro lagoon inlet. However the model underestimation of the M_4 amplitude may result in a lower tidal distortion and consequently in

lower ebb dominated residual currents, which in turn underestimate the sediment transport fluxes. Considering that the lagoon export sediments to the adjacent ocean, the model underestimation of the M_4 constituent might induce a reduction of the sediments amount that are flushed out of the inlet over long periods. Therefore, when performing long period morphodynamic simulations, this inaccuracy in the hydrodynamic model may result in the overestimation of the accretion trends and in the underestimation of the erosion trends observed within the inlet and navigation channel.

4.4.2 SAND2D

Considering the SAND2D model, and taking into account that the aim of this thesis is to study the processes at the inlet and adjacent areas, a sub-domain of the ELCIRC grid is used in order to economize computational time. This grid extends from the open ocean boundary of the ELCIRC mesh to the *triângulo das marés*, within the inlet. One of the input parameters of the SAND2D model is the characteristics of the bottom sediment size. In the scope of this thesis a heterogenous distribution of the bottom sediments was created and is illustrated in Figure 3.11, and is used as model input. The morphodynamic time step is adaptive and lies between the hydrodynamic model time step, which is 60 s, and 3600 s.

4.4.3 SWAN

In the present study two nested grids are used in the wave model with different dimensions and characteristics (Figure 4.8). The grid with higher dimensions (Figure 4.8(a)), a regular grid with element area of 125000 m^2, extends from the offshore area with a coarser resolution. In this grid are imposed the waves boundary conditions: a regular monochromatic wave or a wave regime. The second grid (Figure 4.8(b)) encompassing the inlet area is curvilinear in space and with finer resolution, with element area ranging from 1062 m^2 at the inlet to 3500 m^2 farther.
The SWAN wave model is used in stationary mode and several simplifications are performed using the options available in SWAN: the effect of the wave interaction with currents, the energy generation and dissipation by wind, the diffraction, the quadruplet interactions and the whitecapping were neglected. It was considered in this setup the bottom friction, the wave breaking, triad wave-wave interaction and wave propagation within a space and time-varying water level fed up by outputs of water levels from ELCIRC.

Comparison between buoy records and WW3 model results

The waves are imposed at the open boundaries of the grid illustrated in Figure 4.8(a) through two different forcing, the first as regular monochromatic waves and the second as a time series of wave parameters of the WaveWatchIII model run at NCEP/NOAA [Tolman et al., 2002]. The regular monochromatic waves imposed belong to the set of waves obtained in Section

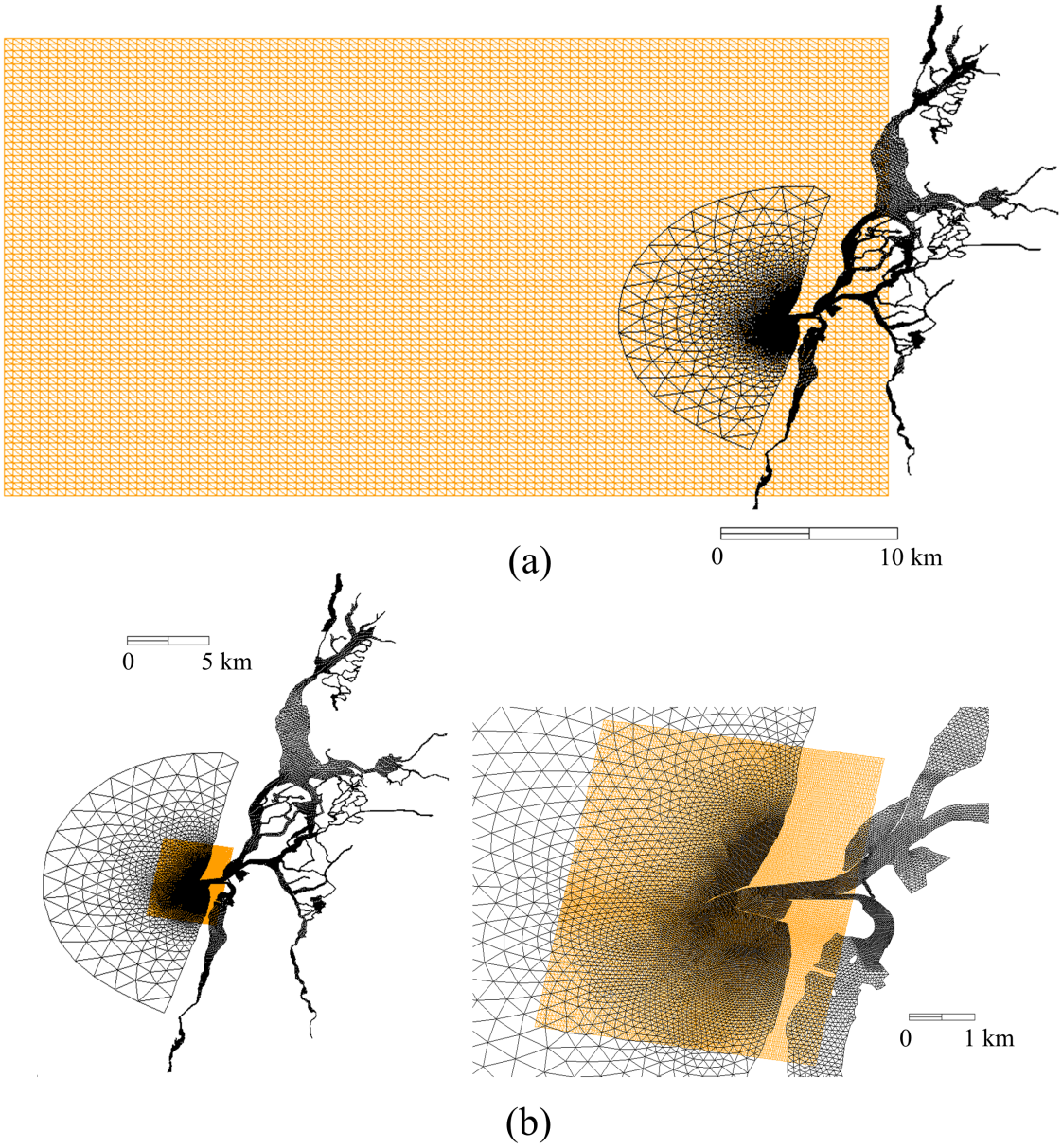

Figure 4.8: Computational (a) regular and (b) curvilinear grids used in the wave model SWAN.

3.7 considered to induce a longshore sediment transport equivalent to that obtained with the complete wave regime. The time series imposed should be validated through comparison with data obtained through a directional wave buoy located close to the study area. However there aren't any buoys located near Aveiro coast and consequently in this study are used the records from the nearest wave buoy, located at Leixões, to validate the WW3 model results. In spite of the different locations, it will be considered that the offshore regime is similar Coli [2003].

The records of the Leixões buoy are available for the period between 1996 and 2001, being the most complete the year of 1998, which will be used to perform the wave parameter comparison between the wave data and ww3 model, illustrated in Figure 4.9. The comparison shows that the time series used as boundary condition are very similar to the records observed in the buoy, reproducing the trends observed. However there are differences in the wave characteristics values, with RMS errors of 0.69 m for the wave height, 18% for wave period relatively to the mean period observed and 28% for the wave direction.

In Figure 4.10 is illustrated the scatter diagram of measured versus modeled H_s for all the entire period available. It is observed that the modeled H_s is overestimated when compared with the H_s observed at the Leixões buoy, with a BIAS of 0.54 m. This trend is inverse to the obtained by Dodet et al. [2010] (BIAS=-0.19 m), however these authors represented the measured H_s for five more buoys than Leixões and for a different period.

The differences obtained between the imposed and observed time series can be justified by the probable noisy nature of the wave records and by the different location and depth of the buoy relative to the WW3 model results.

With this wave heights overestimation it is likely that the radiation stresses are also overestimated, which in turn will originate more intense sediment fluxes in the waves action region. Thus, the erosion (accretion) trends observed at the nearshore region and at the inlet may be overestimated (underestimated) by the numerical model.

The consequences of the 0.7 m wave height overestimation in the morphodynamic predictions, might be analyzed through the numerical simulations with a regular monochromatic wave as sediment transport forcing, performed and described in Chapter 6.

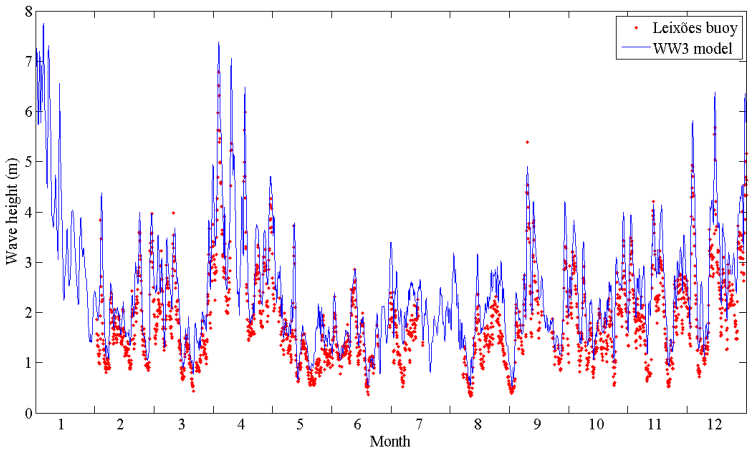

(a)

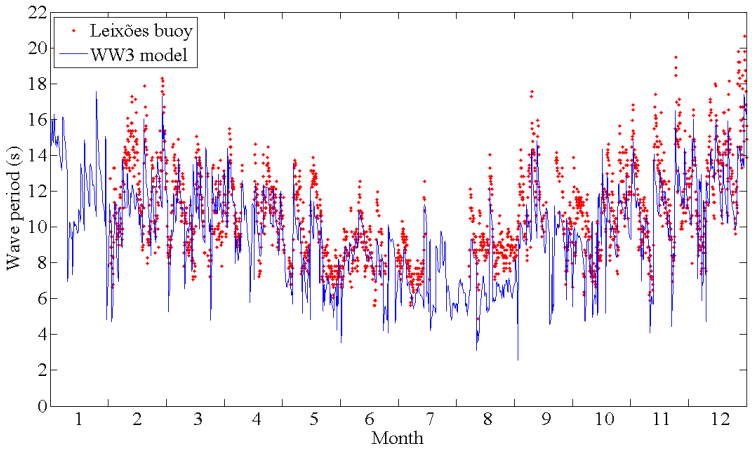

(b)

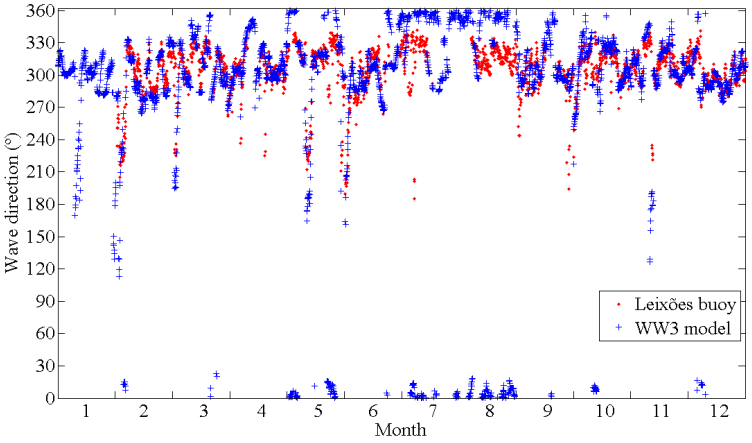

(c)

Figure 4.9: Data and model wave parameter comparisons from the wave directional buoy located at Leixões (red) and from WW3 model offshore Aveiro (blue), for the year of 1998.

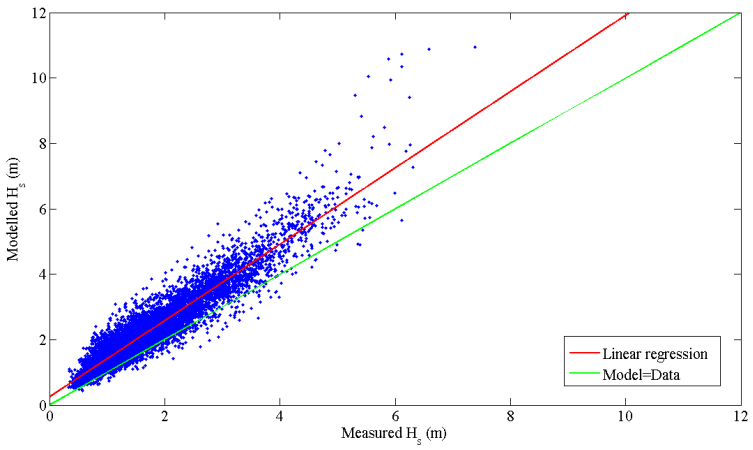

Figure 4.10: Scatter diagrams of modeled H_s versus measured H_s for the entire data set. The green line corresponds to $y = x$ and the red line the linear regression for the data represented.

Chapter 5

Morphodynamic Simulations Forced by Tidal Currents

One of the aims of this thesis is to study the influence of the tidal currents in the sediment budget and in the bottom depth changes of the Ria de Aveiro lagoon inlet, as well as their area of action. In order to achieve these goals, numerical simulations forced only by tidal currents are performed and presented in this Chapter.
A sensitivity analysis of the numerical model to the activation of numerical filters, to the sediment transport formulation considered for transport computations, to spring and neap tide conditions and to depth and bottom sediment size distribution is also performed.
The influence of the currents in the dynamics of the inlet is evaluated by analyzing the numerical results based on residual and total sediment fluxes, bathymetric changes, sediment transport at sections illustrated in Figure 3.7 and sedimentation rates at the regions delimited by these sections (also illustrated in Figure 3.7).

5.1 Sensitivity analysis

5.1.1 Numerical filters

The influence of the numerical filters that are implemented in the numerical model, used to smooth the bathymetry and mitigate local instabilities [Fortunato and Oliveira, 2000], described in Section 4.3.3, is tested and presented in this subsection.
The numerical simulations were performed for periods of 1 year and for all the formulations mentioned in Section 2.5.1. However, only the results obtained by considering the EH sediment transport formulation are presented in Figure 5.1, since the influence of the filters in the remaining formulations is similar. The simulations were performed by activating each one of the filters separately. The simulations considered the heterogeneous bottom sediment size distribution described in Section 3.4 and the model setup described in Section 4.4.

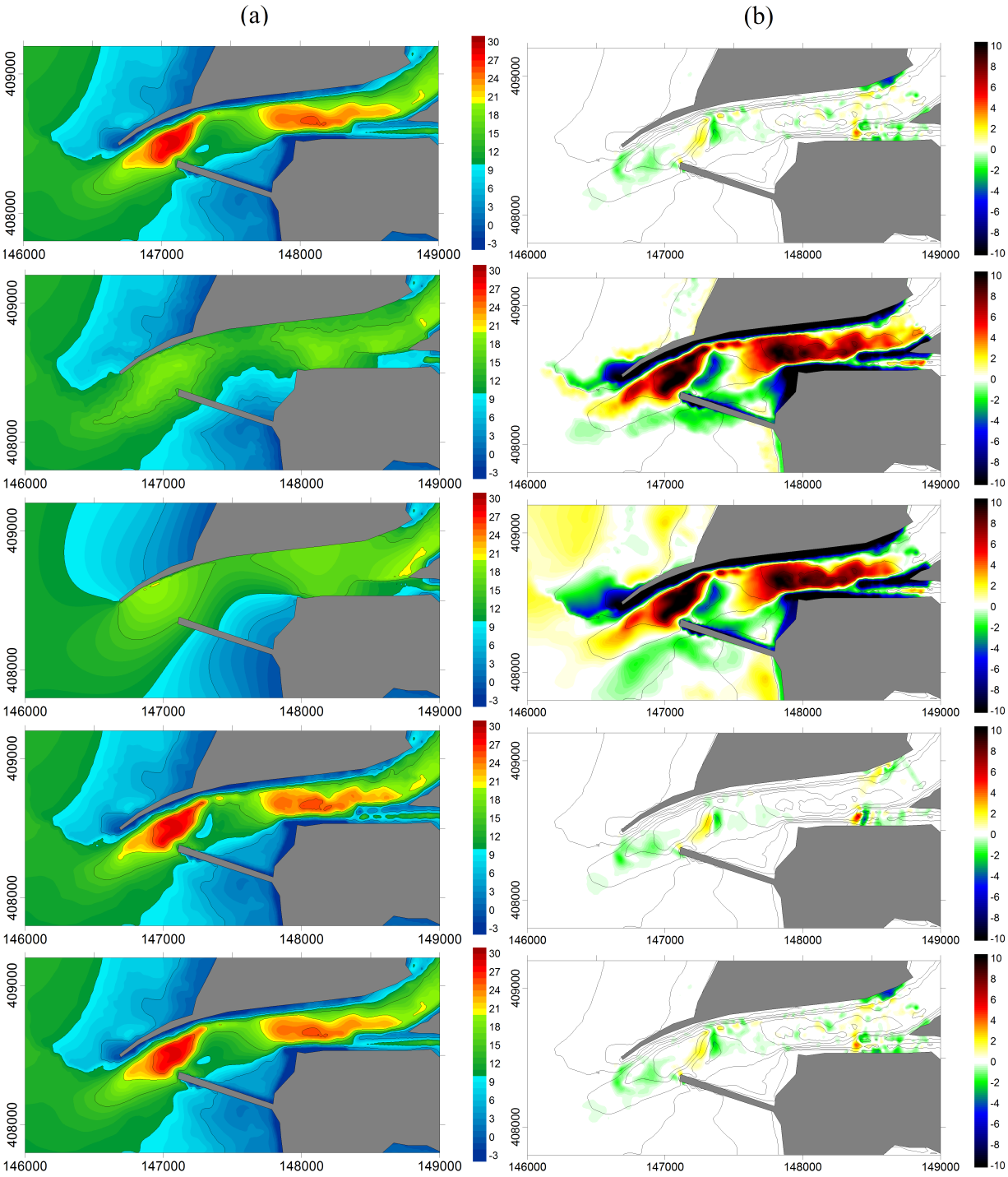

Figure 5.1: (a) Final bathymetry (metre) of the Ria de Aveiro lagoon inlet computed after 1 year for EH formulation. (b) Difference between the computed final and initial bathymetries (metre) for a 1 years simulation. From top to bottom: Considering the influence of: a non-linear bathymetric filter, a gradient filter, a global filter, a flux filter and a diffusive filter (Section 5.1.1). In (b) the solid lines illustrate the 2001 bathymetry. The negative (positive) values represent erosion (accretion). The values in axes are in metres.

The use of the gradient and global filters promote strong bathymetric changes, unrealistic when compared to those expected based on surveys (Section 3.3). The final bathymetries and bathymetric changes obtained when either of the remaining three filters is used, are closer to those expected and observed in Section 3.3. The differences between these three predicted results are not significant.
Considering this analysis, the gradient and global filters will not be used in numerical simulations hereafter. Taking into account previous experiences, the other three filters will be activated with the aim of preventing numerical oscillations.

5.1.2 Influence of the choice of the sediment transport formula

In order to analyze the model predicted bathymetric changes at the tidal inlet computed using the several sediment transport formulations mentioned in Section 4.4, numerical simulations for periods of 1 year were performed, considering the model setup described in Section 4.4.
The residual sediment fluxes, the predicted bathymetry and the bathymetric changes simulated for the 8 sediment transport formulations for the study area are illustrated in Figures 5.2 to 5.9. The white areas in the figures illustrating the difference between the final and initial bathymetry represent unchanged depth, and the solid lines represent the bathymetric initial contours (June 2001).
The results show that the residual fluxes are mostly seaward, with occasional exceptions. One of these exceptions is at the region near the southern breakwater. All the formulations predict similar patterns with exceptions to Bha (Figure 5.3), vR (Figure 5.8) and MPM (Figure 5.7).
The residual sediment fluxes obtained with Bha formulation, Figure 5.3(a) and (b), differ substantially from the other numerical solutions. These higher values obtained with Bha formulation show an over-prediction of the bathymetric annual variations, with maximum rates of accretion of 12 myear^{-1}, which is clearly unrealistic (Figure 5.3(d)). This over-prediction of the morphological changes is consistent with previous studies presented by Fortunato et al. [2009] and Silva et al. [2009].
The vR formulation produce oscillations in the sediment fluxes (Figure 5.8(a) and (b)), visible for finer sediments and intermediate tidal velocities, also observed in the Subsection 2.5.1 when the transport rate was computed and analyzed. These oscillations induce instabilities in bathymetric predictions and variations observed in Figure 5.8(c) and (d). The absence of residual sediment flux in the navigation channel justifies the extreme accretion trend observed in Figure 5.8(d).
Oscillations are also expected for Bi formulation, due to the instabilities obtained in Figures 2.5 and 2.6 for finer sediments and higher flow velocities. However they are not easily noticeable in the residual sediment fluxes and bathymetric predictions for the study area. Despite

the results obtained in Figure 5.6, this formulation will not be considered in the subsequent numerical simulations due to its sensitivity to sediment size d_{50} illustrated in Figures 2.5 and 2.6.

In contrast to the previous results, the solutions obtained with MPM formulation (Figure 5.7) under-predict the sediment fluxes and consequently the maximum observed values of erosion and accretion. This under-prediction is consistent with that obtained in Section 2.5.1 and has been observed in other works [Pinto, 2010].

The numerical results obtained with the SvR (Figure 5.2), EH (Figure 5.4), kk (Figure 5.5) and AW (Figure 5.9) formulations are similar between them and more realistic, predicting maximum accretion values of 6 m and maximum erosion of 4 m.

The residual sediment fluxes pattern highlights four regions with higher values: at the inlet and offshore area, at the center of the navigation channel (Region II in Figure 3.7) and at the beginning of the S. Jacinto and Mira channels. The first two patterns are located in areas of strong bathymetric variation. The first one, which present the largest flux, is located in the transition from the deepest zone located between the breakwaters and shallow zones offshore. At the navigation channel, between the head of the South breakwater and the tidal gauge, an

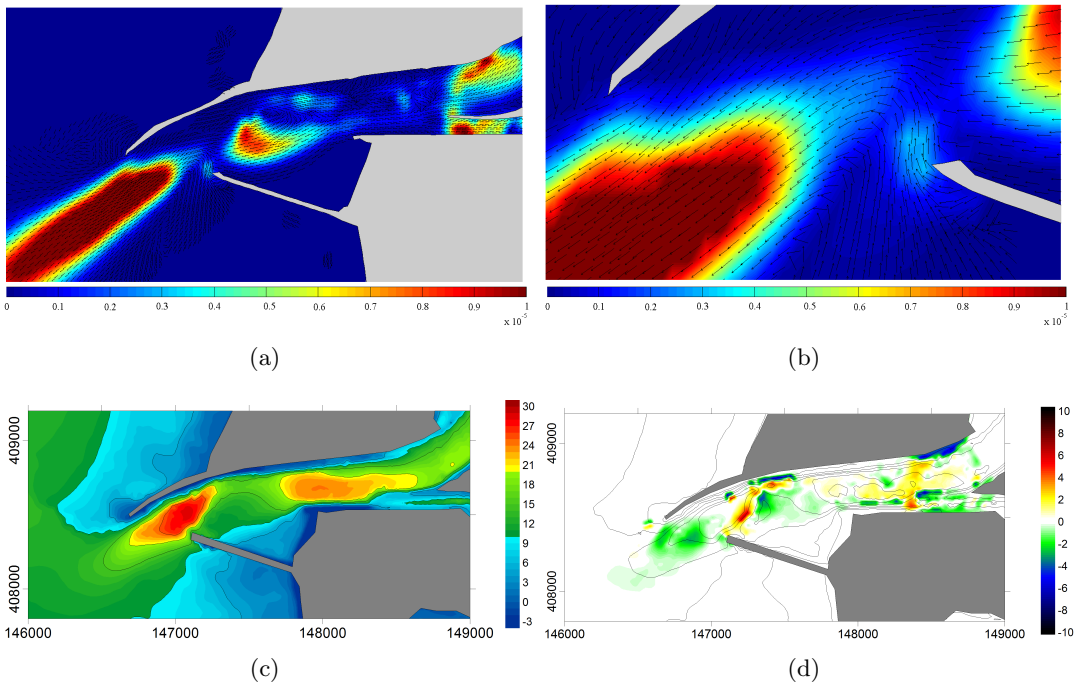

Figure 5.2: (a) and (b) Residual sediment flux (m^2s^{-1}) for SvR formulation. (c) Final bathymetry (metre) of the Ria de Aveiro lagoon inlet computed after 1 year for SvR formulation. (d) Difference between the computed final and initial bathymetries (metre) for a 1 year simulation. In (d) the solid lines illustrate the 2001 bathymetry. The negative (positive) values represent erosion (accretion). The values in axes are in metres.

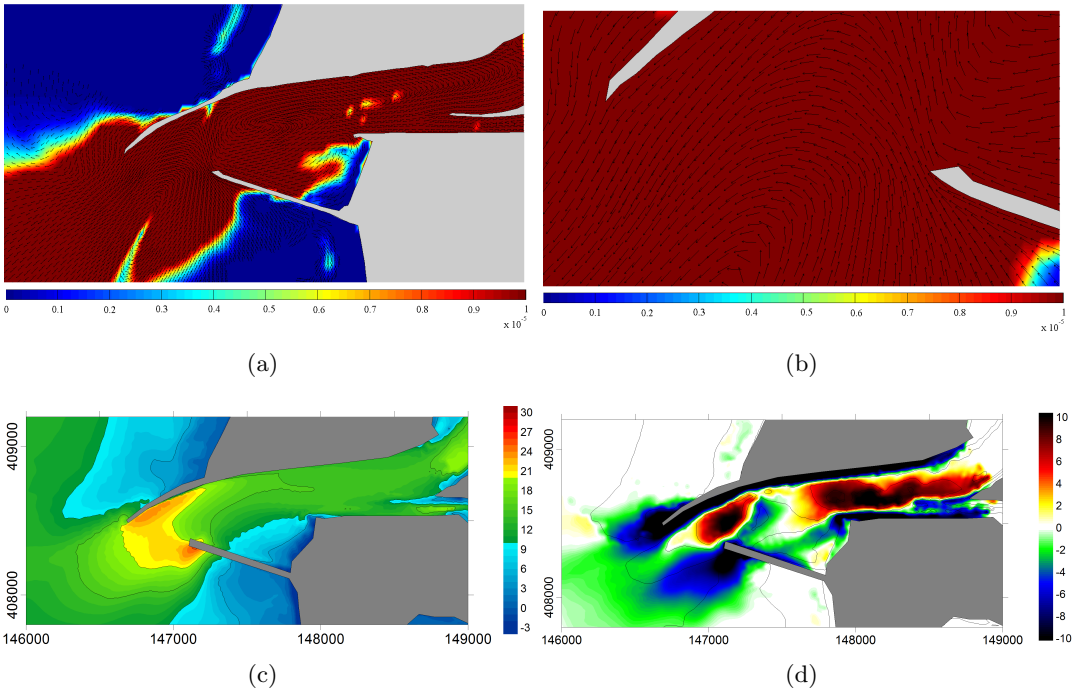

Figure 5.3: Same as Figure 5.2 for Bha formulation. Black areas represents data out of the scale represented.

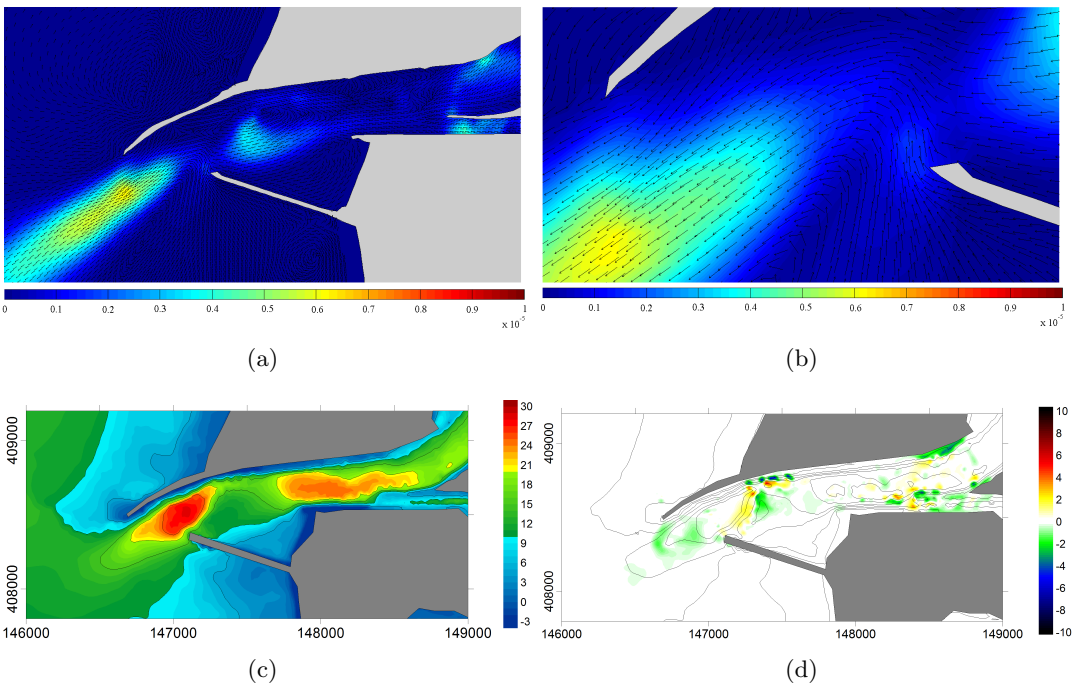

Figure 5.4: Same as Figure 5.2 for EH formulation.

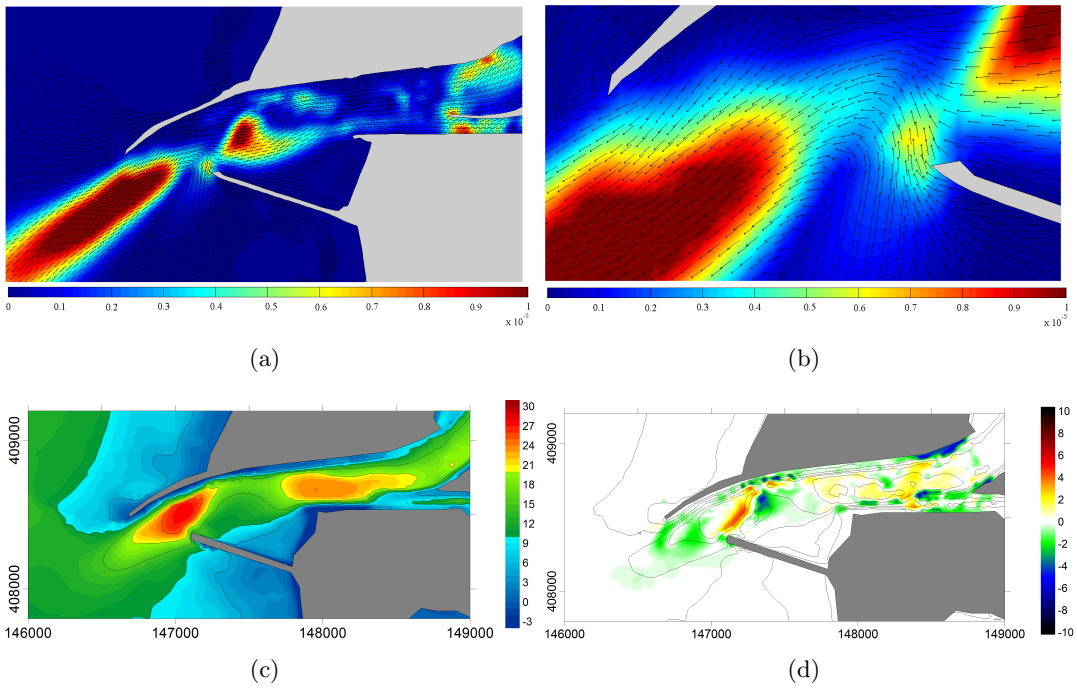

Figure 5.5: Same as Figure 5.2 for kk formulation.

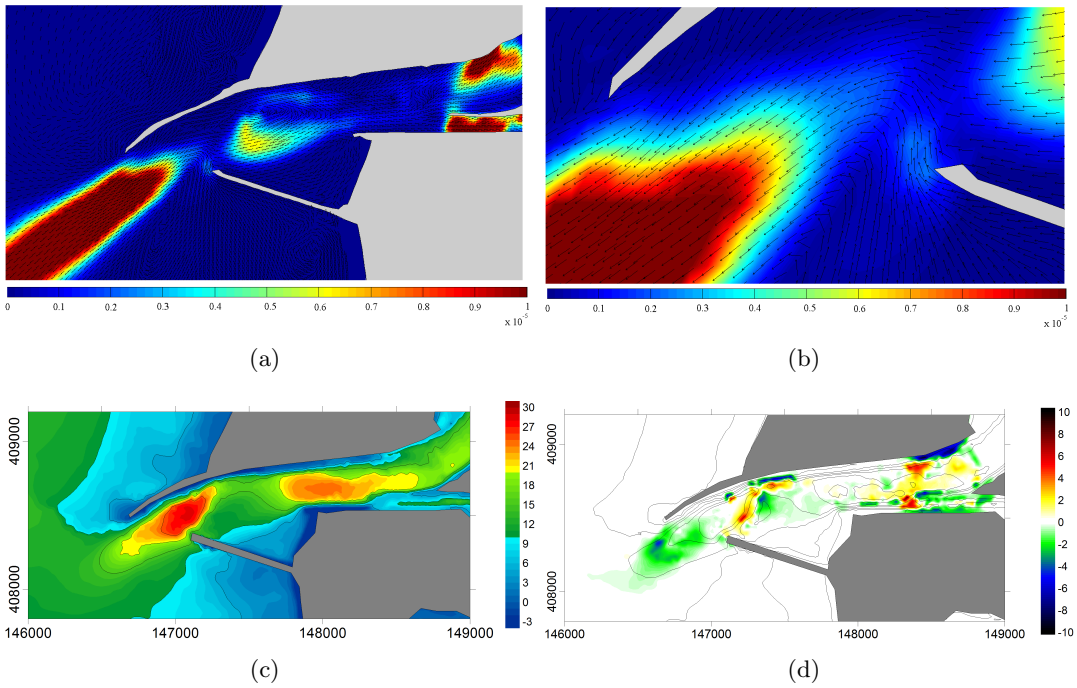

Figure 5.6: Same as Figure 5.2 for Bi formulation.

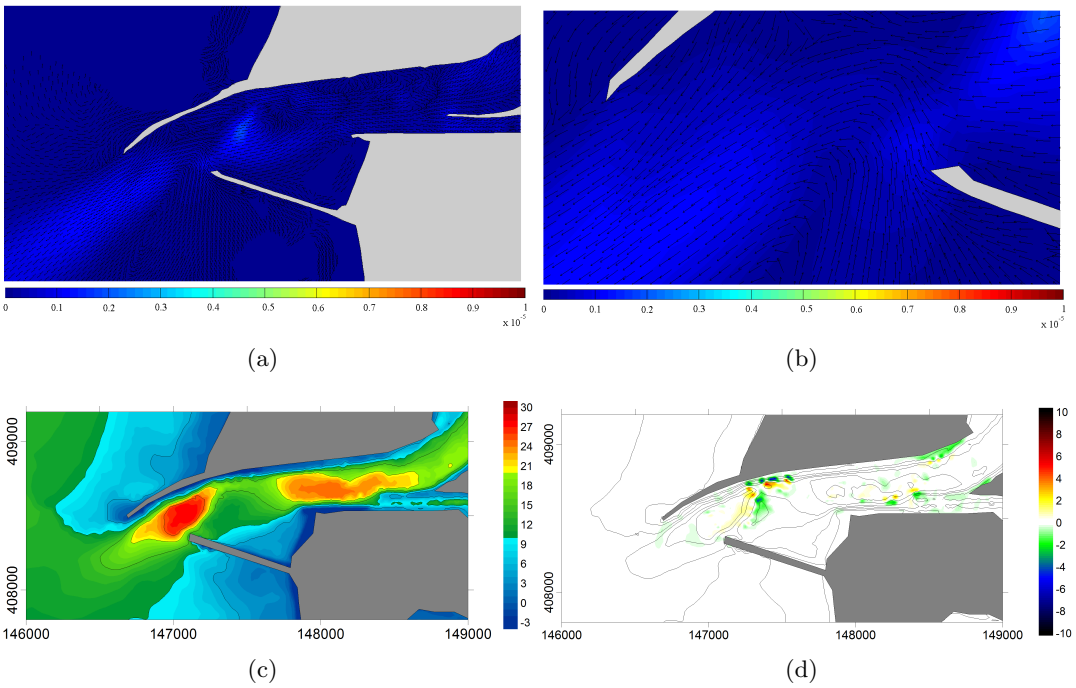

Figure 5.7: Same as Figure 5.2 for MPM formulation.

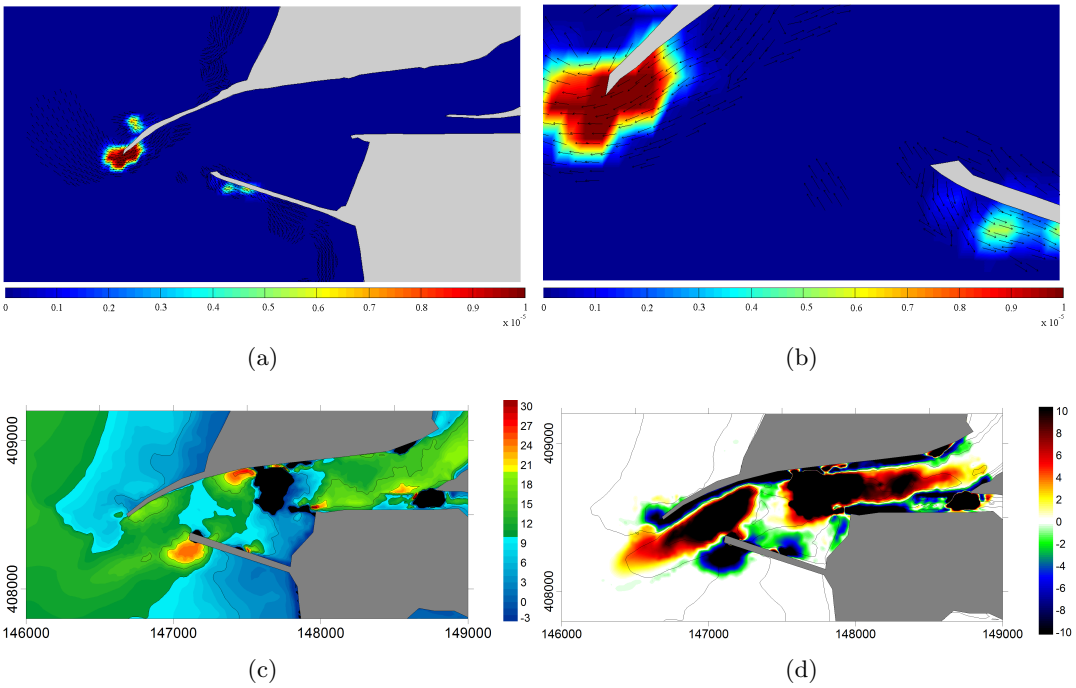

Figure 5.8: Same as Figure 5.2 for vR formulation. Black areas represents data out of the scale represented.

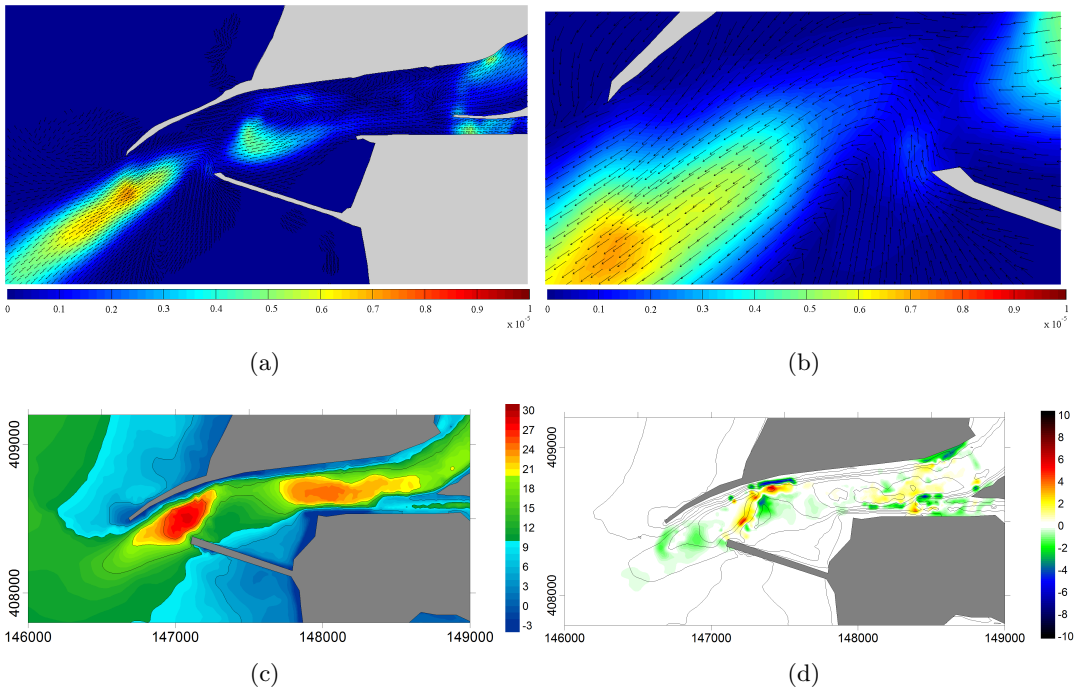

Figure 5.9: Same as Figure 5.2 for AW formulation.

intense residual sediment flux is also observed, although with low intensity when compared to the former. This pattern appears in the shallower area located between the two deeper areas that characterize the study area morphology. Once again, the transition from deeper to shallower bottom originates convergence and consequently an intensification of the residual sediment flux. The residual sediment flux patterns at the inlet generates an erosion trend at the downstream side of the deeper zone located between the heads of the breakwaters. At the upstream side of this bottom feature and due to the decrease in the residual sediment flux, an accretion area is observed. The high magnitude of the residual sediment flux at the beginning of the Mira and S. Jacinto channels (near the side walls) induces erosion trends at these same locations, observed in the Figures illustrating the annual bathymetric changes. At the downstream side of the bifurcation, the orientation and decrease of the fluxes generates accretion trends.

In conclusion, the SvR, EH, kk, and AW formulations are those that a priori best describe the observed tendencies of the bathymetric changes in the Ria de Aveiro lagoon inlet (Figures 3.2 and 3.3).

5.1.3 Impacts of spring/neap tide

In this Section the sediment fluxes for neap and spring tide conditions are computed, averaging the sand fluxes during two M_2 tidal cycles (2×12.42 hours) enclosing the sea surface elevation and velocities illustrated in Figure 3.13. The results obtained using the kk (SvR)

formulation are similar to those obtained using EH (AW) formulation, therefore only the results obtained using the latter formulations are presented in Table 5.1 and Figures 5.10. For all sections, the upstream and downstream sediment transport for each section (see Figure 3.7) was computed and denoted by F_{in} and F_{out}, respectively. Negative (positive) values represent outward (inward) sediment flux. At section 3, negative (positive) values mean sediment flux into (out from) region III. The net transport is denoted by Net. The net sediment flux in neap tide conditions is 3 orders of magnitude lower than in spring tide when the EH formulation is used, having small values of transport. On the other hand, when considering the AW formulation, the transport reaches almost zero in the entire study area, 7 orders magnitude lower than at spring tide.

The sediment fluxes are always negative for all sections, representing downstream fluxes, exporting sediments to the ocean. The higher values are found in section 3, the longest section of the study area. In this section the negative values indicate flux of sediments from the navigation channel to Region III. The analysis will be focused only in sections which have fluxes in up/downstream direction. The higher fluxes are then obtained at sections 1 and 7, the inlet and S. Jacinto channel section, respectively, for the spring tide condition. These higher fluxes occur at spring tide due to the higher velocities occurring at this tidal phase (cf. Figure 3.13).

Comparing the fluxes at the sections that limit the study area, at downstream section 1 and upstream sections 6+7, it is observed that, for all simulations and formulations, accretion

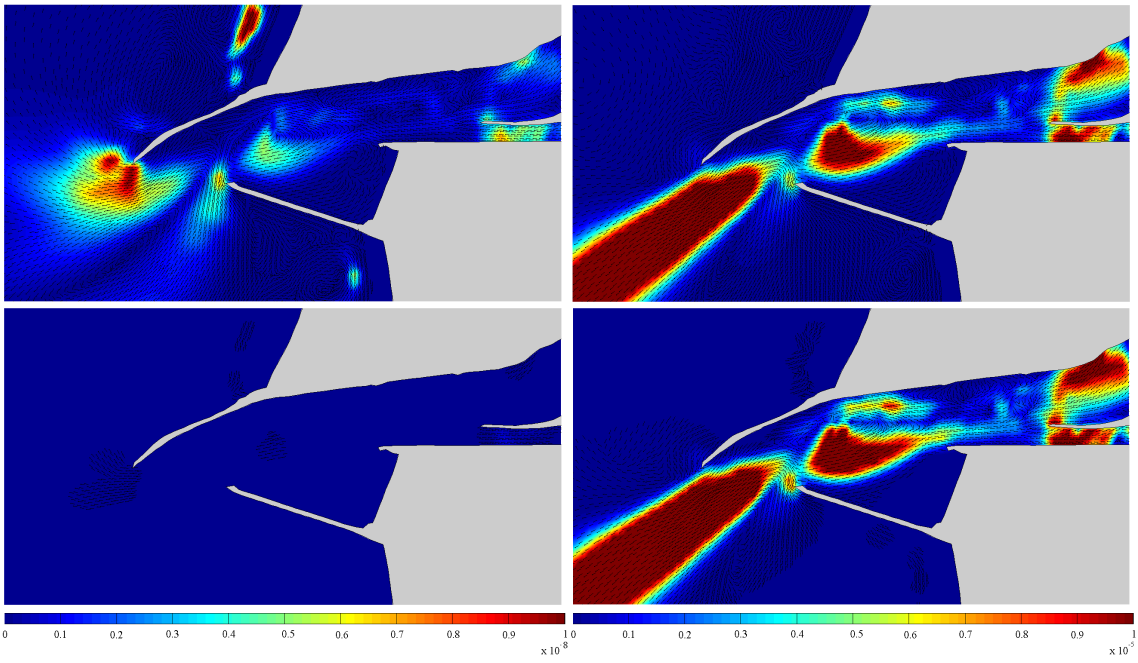

Figure 5.10: Sediment flux (m^2s^{-1}) for EH formulation (top) and AW formulation (bottom) for neap tide (left) and spring tide (right) conditions.

Table 5.1: Sediment transport (m^3day^{-1}) through sections illustrated in Figure 3.7 at neap tide, spring tide and residual conditions.

Form.	Sect	Neap			Spring			Res		
		Net	F_{in}	F_{out}	Net	F_{in}	F_{out}	Net	F_{in}	F_{out}
EH	1	0.0	0.9	-0.9	-135.5	91.4	-226.9	-35.1	25.0	-60.1
	2	0.1	0.5	-0.4	-15.3	101.3	-116.6	-4.5	26.6	-31.1
	3	-1.4	-1.5	0.2	-359.9	-391.9	32.0	-95.2	-104.9	9.7
	4	-0.1	0.8	-0.8	-22.9	213.9	-236.8	-6.8	55.3	-62.1
	5	-0.4	0.8	-1.2	-111.1	208.7	-319.8	-30.1	54.9	-84.9
	6	-0.5	0.6	-1.0	-75.6	205.1	-280.7	-23.2	52.6	-75.8
	7	-0.7	1.2	-2.0	-273.4	281.2	-554.7	-70.2	74.6	-144.8
AW	1	0.0	0.0	0.0	-185.6	101.4	-287.0	-46.3	20.5	-66.9
	2	0.0	0.0	0.0	-24.6	123.8	-148.4	-6.5	24.3	-30.8
	3	0.0	0.0	0.0	-465.9	-487.3	21.4	-105.1	-109.0	3.9
	4	0.0	0.0	0.0	-32.6	274.2	-306.8	-9.0	62.5	-71.5
	5	0.0	0.0	0.0	-148.6	259.2	-407.7	-37.4	57.3	-94.7
	6	0.0	0.0	0.0	-88.1	253.7	-341.8	-27.9	60.6	-88.5
	7	0.0	0.0	0.0	-346.0	336.6	-682.6	-89.9	75.9	-165.8

trends in the region exists flanked by the sections. The calculus performed for this analysis are presented in Table 5.2 for EH and AW formulations. As expected, the sediment budget obtained in spring tide condition is higher (3.5 times) than the residual.

The spatial distribution of the sediment fluxes in Figure 5.10 illustrate very well the magnitude difference between neap and spring tide conditions. The spatial distribution of the current velocity, illustrated in Figure 3.13, with zones of convergence and divergence, originates the sand fluxes pattern illustrated in Figure 5.10. This relation has origin in the proportionality between U and q_s. The sediment fluxes in spring tide are very similar to the residual fluxes illustrated in Figures 5.4 and 5.9 in pattern but different in magnitude.

Table 5.2: Sediment transport (m^3day^{-1}) at the downstream (1), upstream (6+7) sections and resultant budget.

Form.	Sect.	Neap Tide	Spring Tide	Residual
EH	1	0.0	-135.5	-35.1
	6+7	-1.2	-349.0	-93.4
	Budget	-1.2	-213.5	-58.3
AW	1	0.0	-185.6	-46.3
	6+7	0.0	-434.1	-117.8
	Budget	0.0	-248.5	-71.5

In summary, the net sediment flux in neap tide conditions is several orders of magnitude lower than in spring tide. As in the previous section, the sediment fluxes are always negative for all sections, representing downstream fluxes, exporting sediments to the ocean.

5.1.4 Depth and bottom sediment size distribution

In Section 5.1.2 the influence of the formulation used to compute the sediment transport was analyzed. The patterns of the residual fluxes and the bathymetric variations obtained using SvR, EH, kk and AW formulations were very similar. In this Section the origin of the observed patterns is investigated. With this aim, runs for 60 days, considering a constant sediment size distribution (d_{50}=0.5 mm), a initial constant depth at the study area (h=10 m) and the two cases coupled were performed. Only the results obtained using the EH formulation to compute the sediment transport are presented herein, being the results for the remaining three formulations similar.

In Figure 5.11 and 5.12 the residual sediment fluxes, the final bathymetry computed and the bathymetric changes are illustrated considering a constant d_{50} distribution (Figure 5.11) and considering both d_{50} distribution and depth constants (Figure 5.12). The results obtained considering constant depth and a heterogeneous sediment size distribution are similar to those represented in Figure 5.12 and are not shown. This similarity shows that the sediment size heterogeneity does not modify the general residual sediment fluxes pattern.

The analysis of Figure 5.11(a) and (b) reveals that the residual sediment flux is very similar to the obtained using a heterogeneous d_{50} distribution (Figure 5.4(a) and (b)). Thus the sediment size distribution for this system, considered to vary between 0.1 and 1.8 mm, does not has much influence on the residual fluxes pattern, suggesting that they are related to bottom depth changes. The bathymetric variations obtained are almost restricted to the upstream side of the deeper area located between the breakwaters. The smaller variations are located in regions where strong bathymetric changes occur. The erosion trend located at the inlet in Figure 5.4(d) is not perceptible suggesting that it can arise due to the local variation of depth.

To analyze if the fluxes pattern is generated by changes in bathymetry, the initial depth was set to constant in the study area domain. The results obtained considering a constant d_{50} distribution coupled with a constant depth are analyzed and illustrated in Figure 5.12. Comparing the residual fluxes obtained in this simulations with those illustrated in Figures 5.4 and 5.11, it is observed that the fluxes pattern at the inlet and offshore area are similar in shape, however with higher magnitude. This magnitude increase is justified by the modification performed in the bathymetry: in this case (constant depth) the depths are lower than in the reality, inducing higher sediment fluxes. The shape of the fluxes pattern, similar in all simulations, denotes the influence of the North breakwater, guiding the fluxes in a southwestern direction.

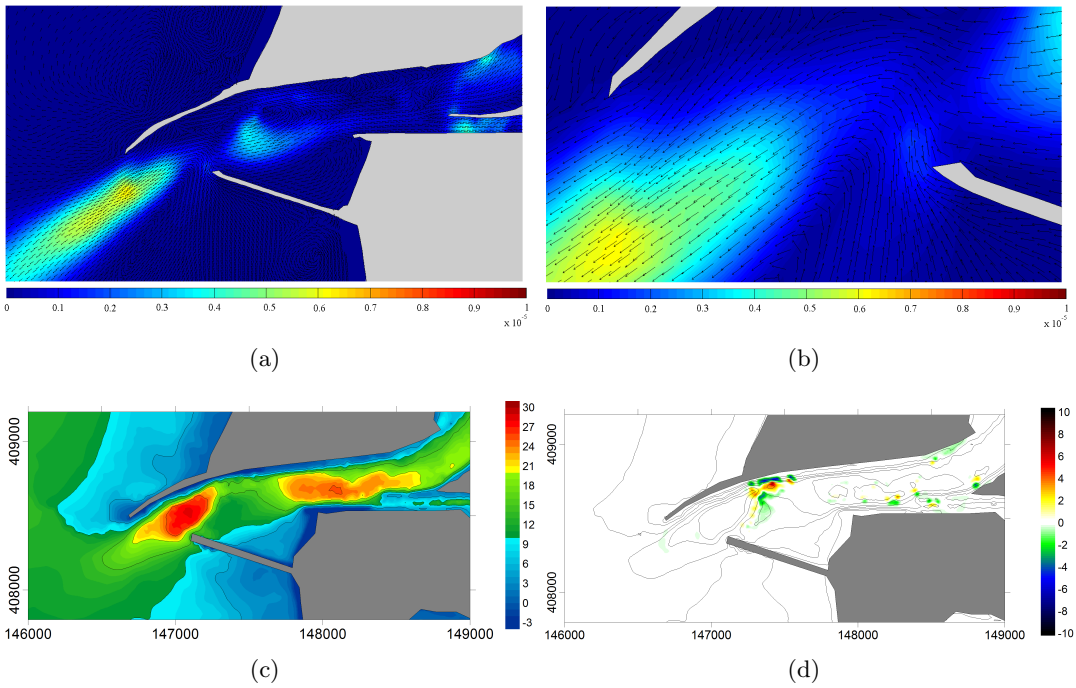

Figure 5.11: (a) and (b) Residual sediment flux (m^2s^{-1}) for EH formulation considering d_{50} constant in space. (c) Final bathymetry (metre) of the Ria de Aveiro lagoon inlet computed after 60 days for EH formulation. (d) Difference between the computed final and initial bathymetries (metre) for a 60 days simulation. In (d) the solid lines illustrate the initial bathymetry. The negative (positive) values represent erosion (accretion). The values in axes are in metres.

In the navigation channel, near the walls of the North breakwater, the residual flux is always oriented W-E. This was not observed when the real bathymetry was used as initial condition. When the real bathymetry was considered, several eddies were observed near the walls, forcing changes in the fluxes direction, related to changes in depth. In this case, due to the constant depth in the study area, an opposite flux is observed all along the domain, generated by the study area configuration.

Therefore, the patterns illustrated in Figure 5.12 are originated by the study area configuration: very strong residual sediment fluxes are observed at the inlet and offshore zone, and with a minor magnitude in the navigation channel. This latter pattern induces erosion between the channel bifurcation and the tidal gauge and accretion downstream. A very relevant pattern is observed near the head of the northern breakwater, where a strong erosion trend is obtained, compromising the stability of that structure. An accretion trend is also formed offshore the inlet.

Furthermore, these fluxes, neglecting the dredging activities, reshape the bottom of the study area, originating the deeper and shallower areas characteristic of the bathymetry of the Ria de Aveiro lagoon inlet.

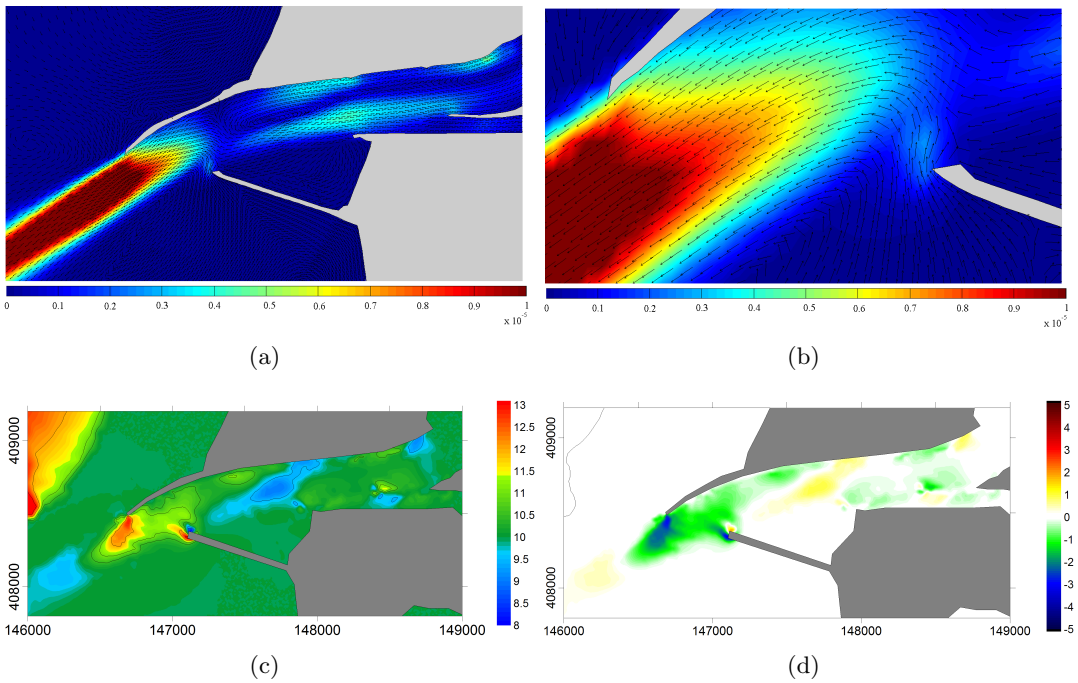

Figure 5.12: (a) and (b) Residual sediment flux (m^2s^{-1}) for EH formulation considering d_{50} and h initially constant in space. (c) Final bathymetry (metre) of the Ria de Aveiro lagoon inlet computed after 60 days for EH formulation. (d) Difference between the computed final and initial bathymetries (metre) for a 60 days simulation. In (d) the solid lines illustrate the initial bathymetry. The negative (positive) values represent erosion (accretion). The values in axes are in metres.

5.2 Period June 2001 - March 2003

In Section 5.1.2 it was concluded that the SvR, EH, kk and AW formulations are those that best describe the observed tendencies. In this section, an additional formulae selection is made, performing numerical simulations for 1.75 years, in order to find the best formulation that produces more realistic results. The predicted bathymetries are analyzed and compared with March 2003 survey data, illustrated in Figure 3.2. The bathymetric changes simulated are compared to those observed and illustrated in Figure 3.5. The numerical results illustrating the simulated bathymetry and the bathymetric changes are illustrated in Figure 5.13. Analyzing the numerical results for the overall study area it is verified that the SvR and the kk formulations over-predict the maximum erosion and accretion trends observed for the areas where strong bathymetric changes are observed. These trends are also identified in Figure 5.14, where the depth observed and simulated are illustrated. The over-prediction referred is more visible in the longitudinal section (bottom of Figure 5.14). On the other hand, the EH and AW formulations slightly under-estimate the depth changes observed.
In Figure 5.13 are identified four zones with different trends, which are directly related to

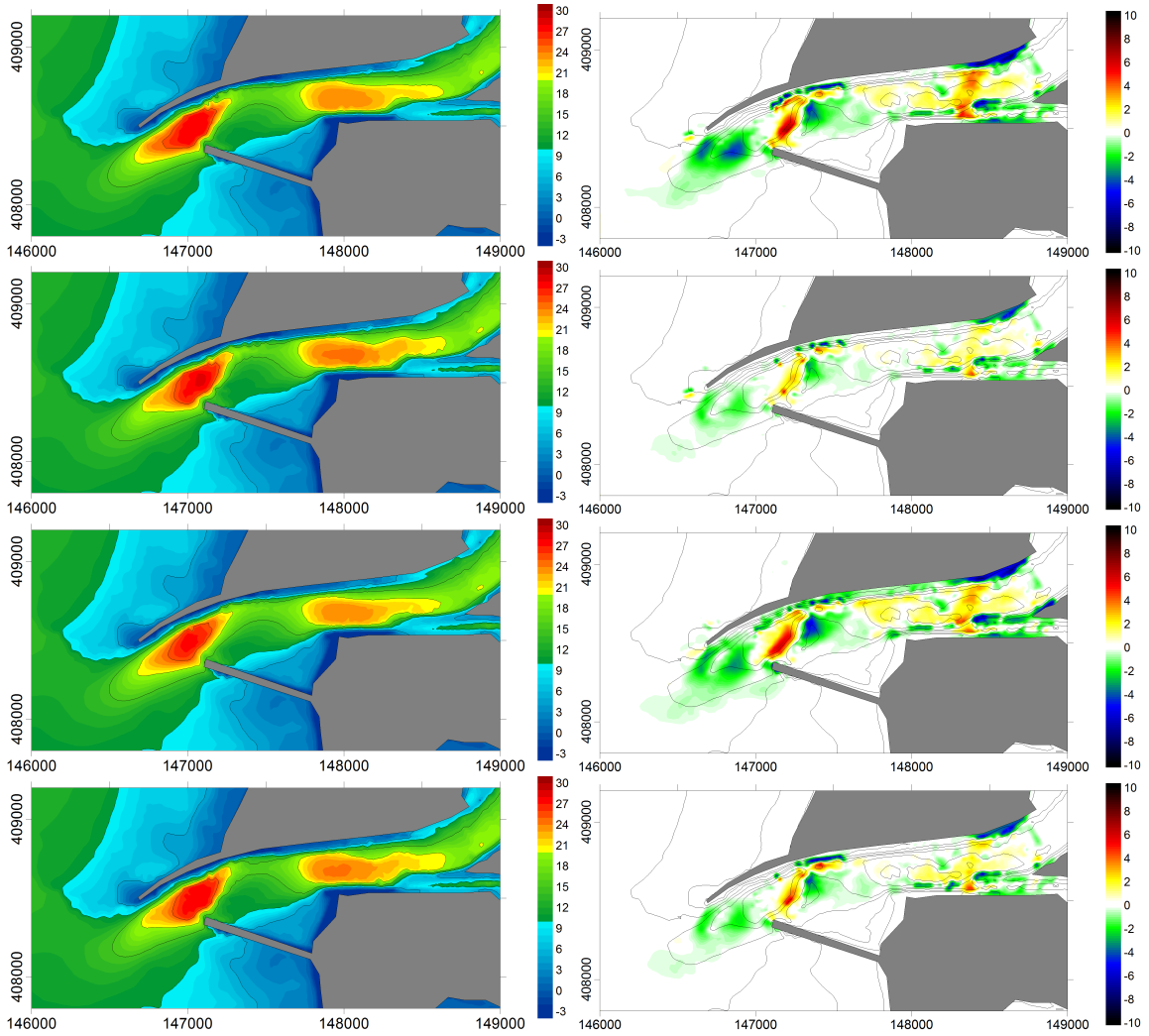

Figure 5.13: Left: Final bathymetry (metre) of the Ria de Aveiro lagoon inlet computed after 1.75 years for (from top to bottom) SvR, EH, kk and AW formulations. Right: Difference between the computed final and initial bathymetries (metre) for a 1.75 year simulation (the solid lines illustrate the 2001 bathymetry). The negative (positive) values represent erosion (accretion). The values in axes are in metres.

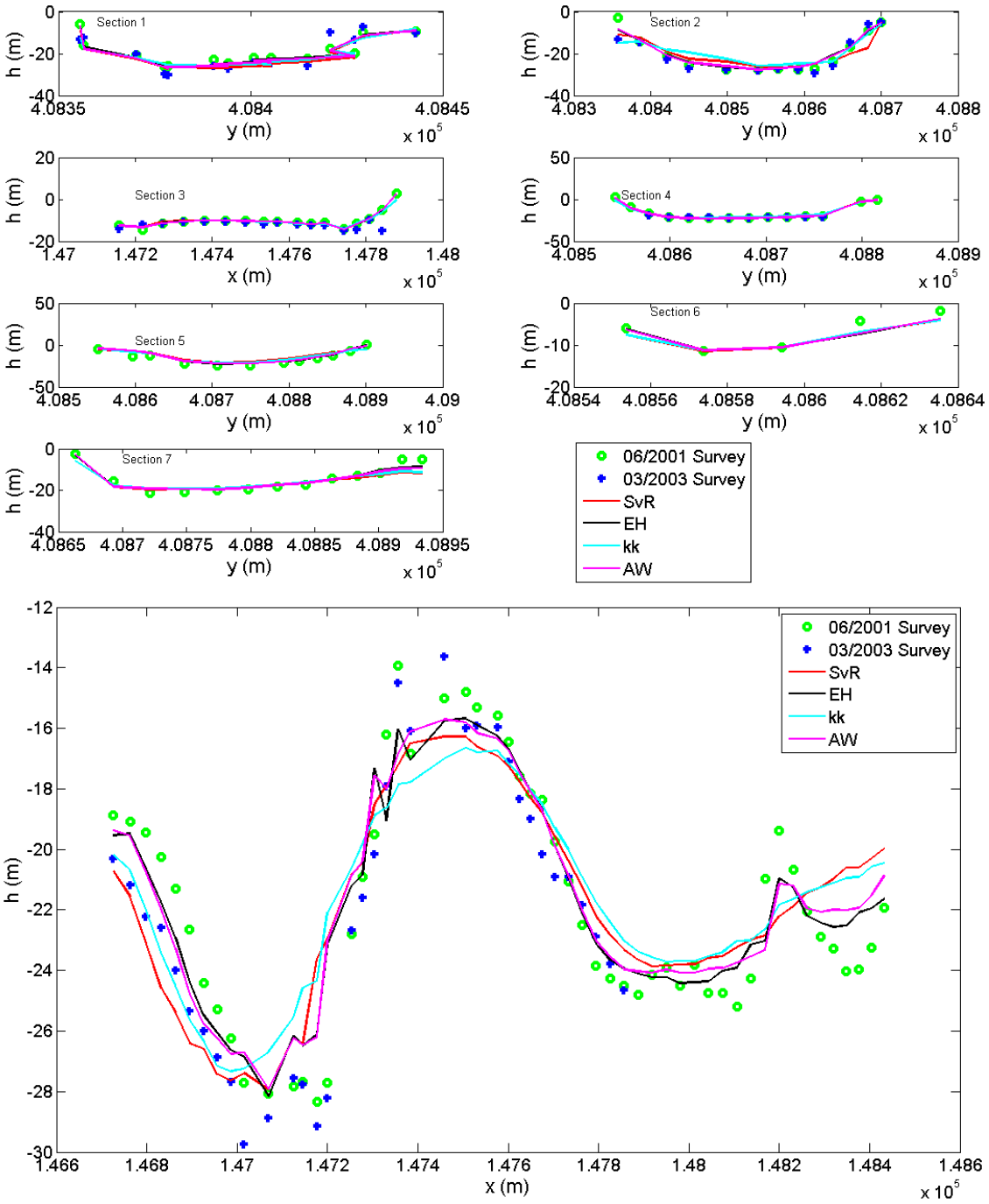

Figure 5.14: Depth along the sections illustrated in Figure 3.7 observed in June 2001 (o) and March 2003 (+) surveys and simulated with the formulations: SvR, EH, kk and AW. The set of figures at the top panel correspond to the sections 1-7 and the figure at the bottom panel correspond to the longitudinal section (dashed line in Figure 3.7). The y (x) values in the x-axis increases from South to North (West to East).

the bottom topography. For the first one, downstream of the deeper area, located between the head of the breakwaters, the numerical simulations predict erosion. The same trend is predicted for the shallower zone located between the two deeper areas in the navigation channel. At the upstream sides of the deeper and shallow areas, accretion is predicted. These alternate patterns are also identified in Figure 3.5, but not so intensely. An opposite trend is obtained in the navigation channel close to the North breakwater, which was also identified in Figure 5.14, sections 1 and 2.

In the longitudinal representation of the depth (Figure 5.14) all the numerical solutions show an offshore movement of the deeper area between the breakwaters that exceeds the observed migration of this area.

The sedimentation rates ($m^3 day^{-1}$) were computed for the regions defined in Figure 3.7 and are illustrated in Figure 5.15. Positive values indicate accretion and negative values erosion. All sediment transport formulations predict the same trends for all sections. For region I, which coincides with the deeper area located at the inlet, all formulations predict erosion. This region is eroding at a rate of approximately 33 $m^3 day^{-1}$ given by EH formulation and 44 $m^3 day^{-1}$ in case of AW formulation. Region II and III also show erosion trends, but with small values, taking into account that SvR and kk formulations over-predict the bathymetric changes, as previously referred. The small value for the sedimentation rate for region II indicates that the predicted erosion and accretion trends (illustrated in Figure 5.13) have almost the same order of magnitude. In region IV, high values of sedimentation rate indicate an infilling of the deeper area located between the tidal gauge and the bifurcation of the channel

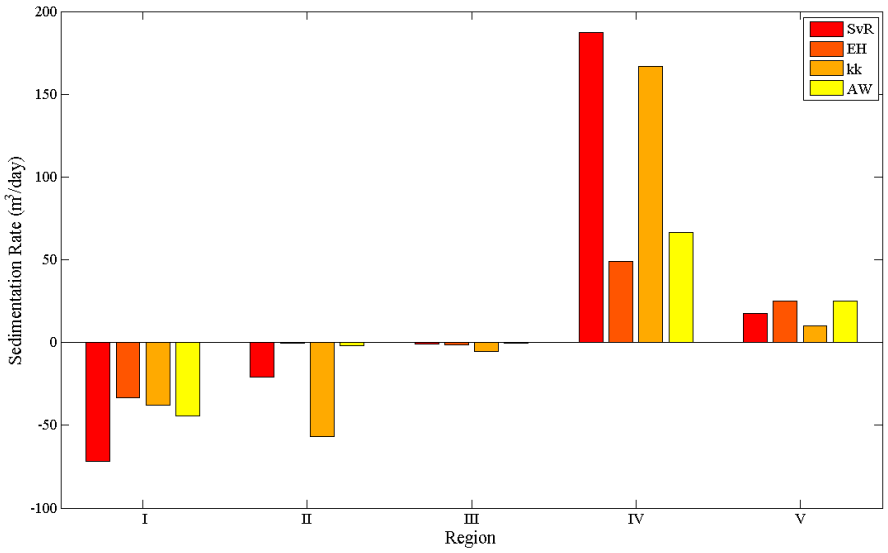

Figure 5.15: Sedimentation rate between June 2001 and March 2003 obtained using the sediment transport formulations of SvR, EH, kk and AW.

at a rate of approximately 49 and 66 $m^3 day^{-1}$ for EH and AW formulations, respectively. Positive values are also obtained for the region that encompasses the S. Jacinto and Mira channels, region V. The rate of sedimentation in this region is nearly 2 and 3 times smaller than at region IV, for EH and AW, respectively.
From the analysis performed it is expected that the SvR and kk formulations will produce, for a longer period of simulation, stronger over-predictions of the bathymetric changes and that AW and EH will be more accurate.

5.3 Period June 2001 - September 2005

A longer set of simulations was then performed, to assess the ability of the morphodynamic model to represent longer periods and to validate the previous conclusions. The simulations performed for a period of 4.25 years using SvR and KK formulations revealed, as expected, an over-prediction of the observed trends. The results obtained with EH and AW formulations are very similar. Taking into account all the analysis performed so far, only the results obtained for the EH formulation are presented in Figure 5.16. In this Figure are illustrated the computed final bathymetry (Figure 5.16(a)) and the bathymetric changes predicted (Figure 5.16(b)).
These results are compared with those presented in Figure 3.6. It turns out that the patterns of erosion and accretion at the inlet are very similar to the numerical solutions obtained for 1 year and for 1.75 years. However, small differences, already observed between the solutions described in previous Sections, are now enhanced and result in increased erosion/accretion rates. In fact, the 4.25 years simulation results show maximum variations of 6 m for erosion and 5 m for accretion. Concerning the patterns observed, the numerical solutions show to some extent the same trends previously identified: the offshore propagation of the deeper zone located between the heads of the South and the North breakwaters, with erosion on the

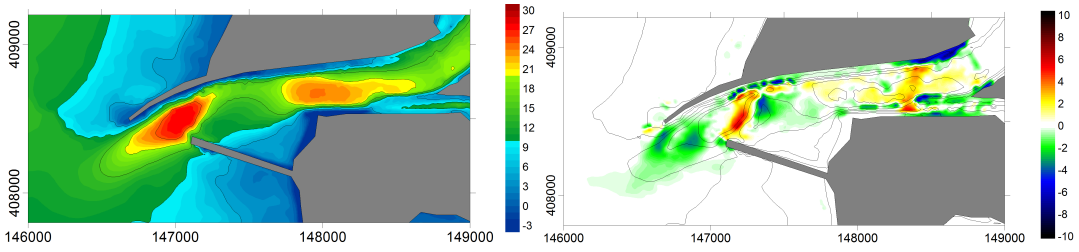

(a) (b)

Figure 5.16: (a) Final bathymetry (metre) of the Ria de Aveiro lagoon inlet computed after 4.25 years for EH formulation. (b) Difference between the computed final and initial bathymetries (metre) for a 4.25 years simulation. In (b) the solid lines illustrate the 2001 bathymetry. The negative (positive) values represent erosion (accretion). The values in axes are in metres.

ocean side and accretion on the inland side; the alternate patterns of erosion and accretion between the tidal gauge and the bifurcation, corresponding to the infilling and downstream movement of this deeper zone; and finally, erosion in the shallow area between the two deeper zones. Qualitatively, at the inlet, these patterns are consistent with the observed bathymetric changes (Figure 3.6). However, the observations northward of the South breakwater show a patch of erosion on the right slope of the outer deep zone, whereas the numerical solutions show accretion. This may be a consequence of the underestimation of the tidal distortion and consequently an overestimation of the accretion trends (referred in Section 4.4.1).
In Figure 5.17 the depth observed in September 2005 and predicted by the numerical model using the sediment transport formulation EH, along the sections presented in Figure 3.7, are illustrated. The predicted depths for each of the section is very similar to those observed, with exception of the zone close to the breakwater structures.
In spite of these results, the longshore section prediction shows that the depth at the upstream side of the two deeper areas is not well reproduced, being overestimated by the model. These differences between the observations and predictions are also illustrated in Figure 5.18, where the observed and simulated sedimentation rates are presented. A good prediction of the bathymetric changes at the inlet is achieved, but the trends found for the navigation channel (regions II and IV) are not consistent with those observed. In these two regions is observed strong erosion, more significant in region II. Observing the residual sediment fluxes at the lagoon inlet, illustrated in Figure 5.4, the substantial sedimentation rate that occurred at region II was not expected as well as the erosion trend at region IV. Taking into account the analysis performed in Section 4.4.1, it was expected that the trends of erosion were underestimated, however and due to the location of these regions, in the navigation channel, it is inevitably to correlate the deepening under prediction with dredging activities that were performed to facilitate the access of large ships to the harbor.

5.4 Discussion

The bathymetric changes in the Ria de Aveiro lagoon inlet were numerically simulated and analyzed, forced only by tidal currents. It was concluded that large modifications in the bottom morphology occurred at the inlet system, showing areas of intense erosion between the two breakwaters. These modifications are supposed to be a natural response of the system to the physical forcing and a consequence of management activities performed over the last 30 years.
It is observed an offshore migration of bedforms as result of the offshore residual sediment transport, characteristic of ebb-dominated coastal systems. It is also observed the lower magnitude of the sediment fluxes in neap tide conditions when compared with the fluxes in spring tide conditions, resulting from the higher magnitudes of the tidal current velocity in this case.

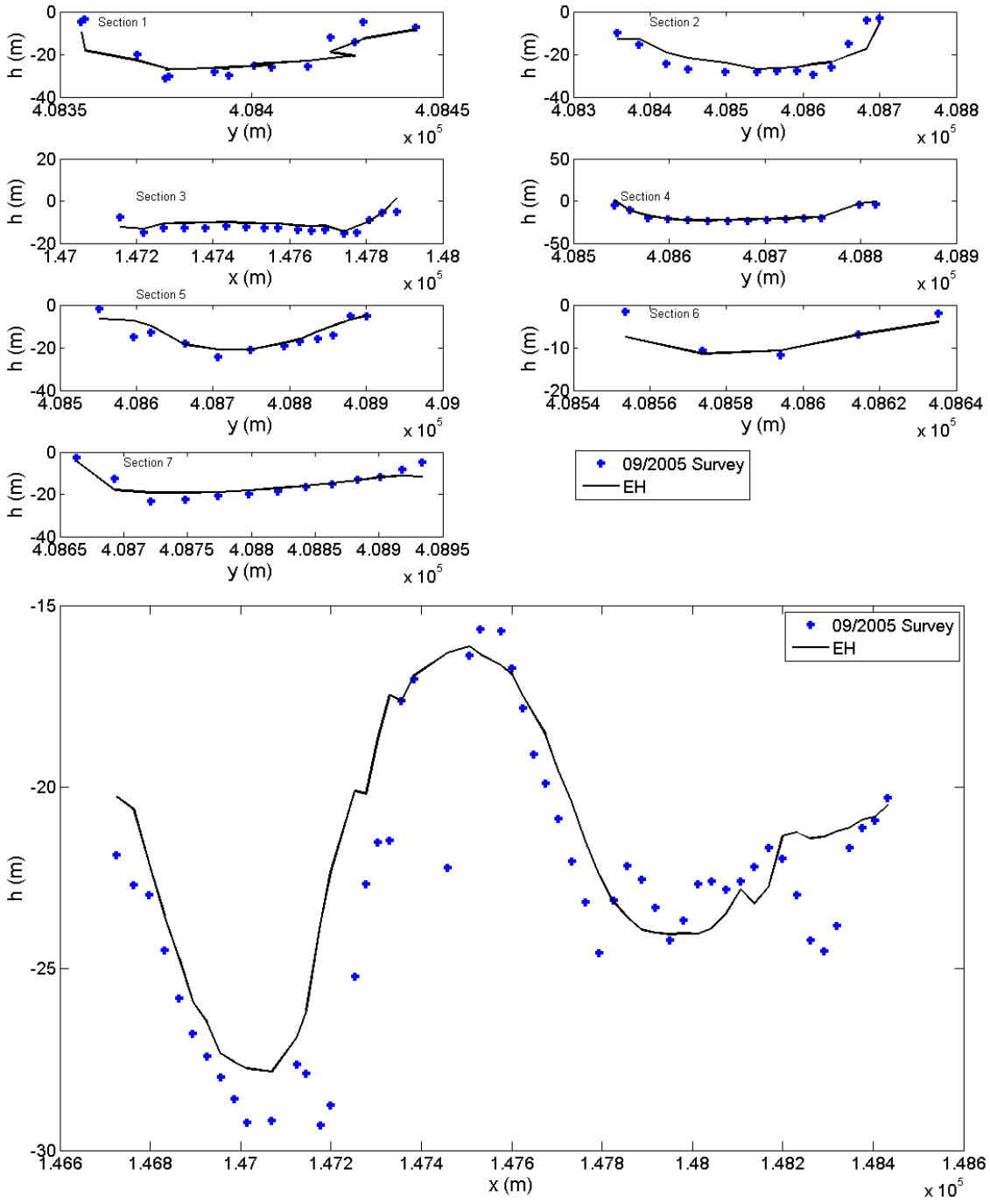

Figure 5.17: Depth along the sections illustrated in Figure 3.7 observed in September 2005 (+) and predicted using EH formulation (-). The set of figures at the top panel correspond to the sections 1-7 and the figure at the bottom panel correspond to the longitudinal section (dashed line in Figure 3.7). The y (x) values in the x-axis increases from South to North (West to East).

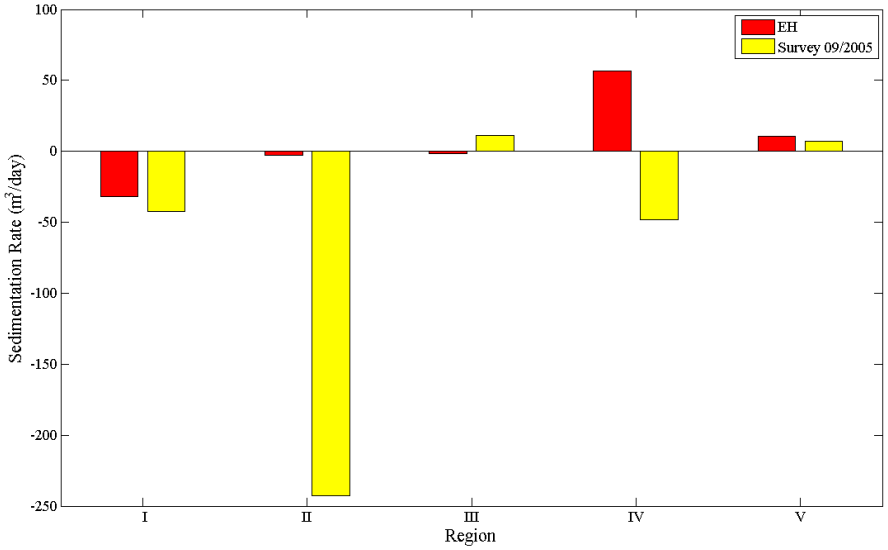

Figure 5.18: Observed and predicted sedimentation rate between June 2001 and September 2005 .

The residual sediment fluxes patterns consist in very strong fluxes at the inlet and offshore zone and in fluxes of lower magnitude in the navigation channel. Defining constant depth and sediment size distribution it was concluded that the sediment size distribution and the bottom morphology are not mandatory on the definition of these patterns, which are essentially induced by the configuration of the study area.

The bathymetric changes obtained when the Bhattacharya et al. [2007] formulation is used to compute the sediment transport are over-predictions of the observations. The Bijker [1967] and van Rijn [1984a,b,c] generate oscillations in sediment transport fluxes, while the formulation of Meyer-Peter and Muller [1948] under-predicts the bathymetric variations. The results obtained with the formulations of Soulsby [1997], Engelund and Hansen [1967], Karim and Kennedy [1990] and Ackers and White [1973] seem to result in predictions more consistent with the observed changes, and among these, the best results considering the overall inlet system, were obtained with the formulations of Engelund and Hansen [1967] and Ackers and White [1973].

Numerical simulations of 4.25 years performed with the EH formulation showed that this formulation is able to reproduce the tendencies of erosion and accretion observed at the inlet channel. However, the underestimation of the M_4 amplitude analyzed in Section 4.4.1, might have influence on the overestimation (underestimation) of the predicted accretion (erosion) trends at the navigation channel.

Analysing the regions where sediment transport occur, it is concluded that the tides induce the bathymetric changes in the navigation channel, also contributing for bottom changes at

the inlet. Consequently, all the solutions show an offshore movement of the deeper areas between the breakwaters, however exceeding the observed trends.
Considering only the tidal forcing, the observed bathymetric changes at the nearshore regions and the southward inflection of the deeper area between the breakwaters, are not numerically predicted. It is expected that with the inclusion of the wave regime as an additional sediment transport forcing a higher accuracy in morphological predictions is reached. It is believed that the wave radiation stress generates sediment transport at the nearshore region and its onshore component pushes the sediment towards the inlet [Bertin et al., 2009a], reproducing the southward inflection of the deeper area located between the breakwaters. Nevertheless, this eventually leads to a reduction of the offshore residual sediment transport in the Ria de Aveiro inlet. Although this process may be inactive in a large part of the time at Aveiro inlet, due to the presence of two long breakwaters, it may be relevant during storms waves, which break over the ebb-delta in front of the inlet.

Chapter 6

Morphodynamic Simulations Forced by Tidal Currents and Waves

To study either the influence of a single wave or a wave regime coupled with the tidal currents in the morphodynamic of the Ria de Aveiro lagoon inlet, the wave forcing was included in the numerical simulations. This represents a step forward in the assessment of the sediment budget and bathymetric changes in the local environment under study.

Similarly to the methodology followed on the study of the tidal effect, the first step in this study consists in performing a sensitivity analysis of the numerical model to the sediment transport formulation. Then, the formulation found to be more adequate is used to compute the sediment transport fluxes induced by the coupled forcing between tidal currents and a regular monochromatic wave or a wave regime.

The sediment transport forcing imposed offshore at the model's open boundary consists in tide and waves properties. The tidal forcing imposed was interpolated from a high-resolution finite element model of barotropic tides for the Iberian Atlantic shelf [Fortunato et al., 2002] as described in Chapter 4. The waves are imposed considering two different approaches: the first considering regular monochromatic waves and the second time series of wave parameters from the WaveWatchIII model run at NCEP/NOAA [Tolman et al., 2002].

The regular monochromatic waves are imposed in order to identify the wave characteristics that induce the largest changes in the inlet morphology. The real wave regime is imposed with the aim of understanding its influence on the morphodynamic of the inlet and to compare model predictions with the real bathymetric changes observed.

The evaluation of single wave effects is performed by analyzing the residual sediment fluxes, the bathymetric changes and the sedimentation rates induced by eight regular monochromatic waves at the inlet. This set of waves was obtained in section 3.7 and is considered that

they induce a longshore sediment transport equivalent to the obtained with the complete wave regime. The real wave climate is imposed as a time series of wave parameters, with a mean wave height of 1.8 m and a mean period of 8.15 s.
The morphodynamics from June 2001 to March 2003 and June 2001 to September 2005 are studied, analyzing the residual sediment fluxes, the bathymetric changes and the sedimentation rates and comparing them with the bathymetric changes observed through local surveys.
As in the previous chapter, the residual fluxes are obtained by averaging the results for 60 days simulations (starting the simulation in 1st June 2001) during two MSf constituent periods (2×14.78 days). The averaging is performed between the 14th and 44th days.

6.1 Sensitivity analysis

6.1.1 Influence of the choice of the sediment transport formula

Three formulations are available in MORSYS2D to compute the sediment transport when the coupled forcing between tidal currents and wave regime is simulated (cf. Chapter 2). A sensitivity analysis of the numerical model to each one of the formulations (AW, Bi and SvR), prior to the model application, should be performed and is presented in the following. The results obtained, considering the tidal currents coupled with a real wave regime as sediment transport forcing, for the three formulations presented (AW, Bi and SvR), for 1 year simulations, are illustrated in Figures 6.1, 6.2 and 6.3, respectively.
The results for the three formulations are very similar. It is observed that, for all numerical formulations, the wave regime inclusion induces residual sediment fluxes magnitudes five times higher than those previously obtained considering only the tidal currents forcing.
The flux pattern in the navigation channel is similar to that obtained for simulations forced only by tidal currents. At the nearshore areas higher residual transport rates are observed, predominantly directed North-South. This flux is induced by the longshore currents generated by the wave regime typical of the study area. At the inlet the fluxes are still dominated by the outward residual tidal currents.
All results show that the presence of the North breakwater induces a discontinuity on the longshore residual sediment fluxes.
As for the case of tidal forcing only, the residual fluxes predicted by the SvR formulation are more intense than those obtained by the AW formulation. The results obtained with the Bi formulation are closer to those obtained with AW formulation. However, and taking into account once more its sensitivity to the sediment size d_{50}, illustrated in Figures 2.5 and 2.6, it was decided not to use this formulation in the numerical simulations for long time periods.
The residual fluxes analyzed induce a strong erosion trend near the head of the North breakwater and an accretion trend at the offshore area of the inlet. The SvR formulation predicts

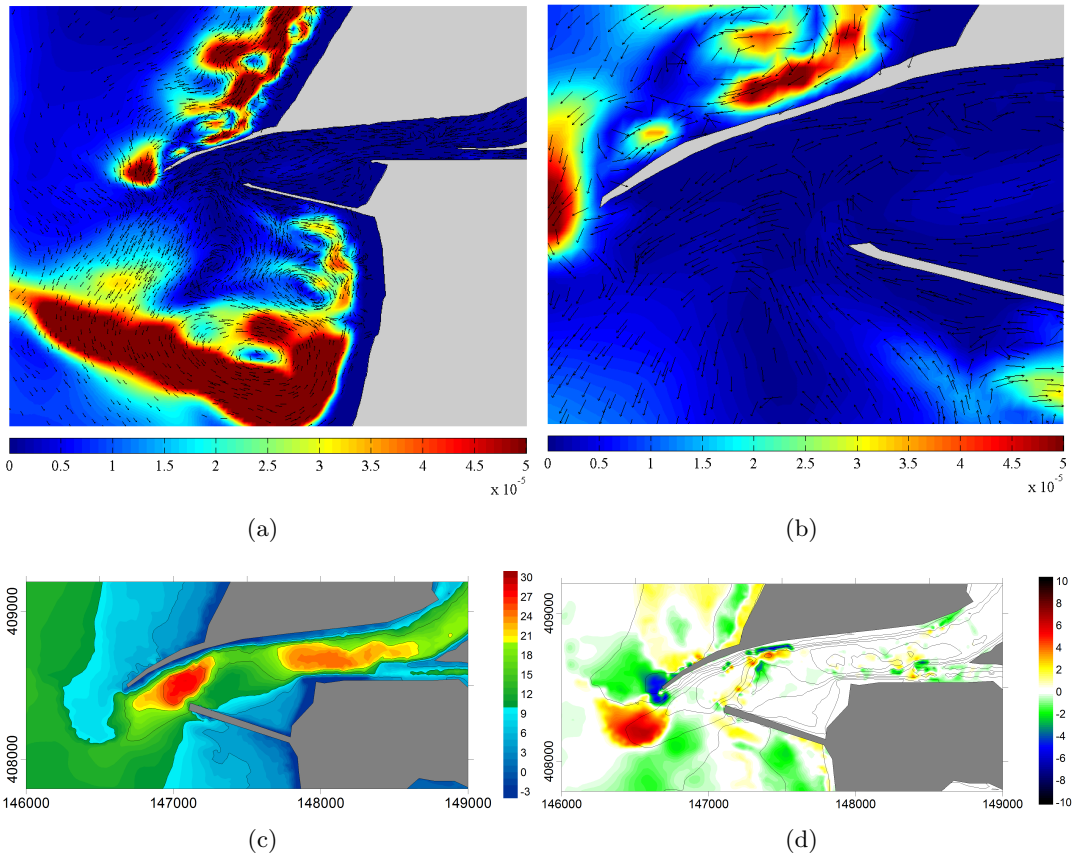

Figure 6.1: (a) and (b) Residual sediment flux (m^2s^{-1}) for AW formulation. (c) Final bathymetry (metre) of the Ria de Aveiro lagoon inlet computed after 1 year for AW formulation. (d) Difference between the computed final and initial bathymetries (metre) for a 1 year simulation. In (d) the solid lines illustrate the 2001 bathymetry. The negative (positive) values represent erosion (accretion). The values in axes are in metres.

also other erosion trend eastern of the accretion trend referred, with higher magnitude than the observed when are used the other two formulations.

These results are in agreement with those obtained by Bertin et al. [2009c] that compared the instantaneous fluxes obtained from these three formulae and concluded that the Bi and the SvR formulae produce 5–10 times larger fluxes than the AW formulation. Also when integrated over a tidal cycle and compared to the transport rates evaluated from tracer experiments, was observed that the SvR formulae produces 5–12 times larger sand fluxes than those observed while the AW formulation gave values in good agreement with tracer results. Comparing the results for the three formulations, the AW formulation is chosen as the more adequate for the remaining analysis.

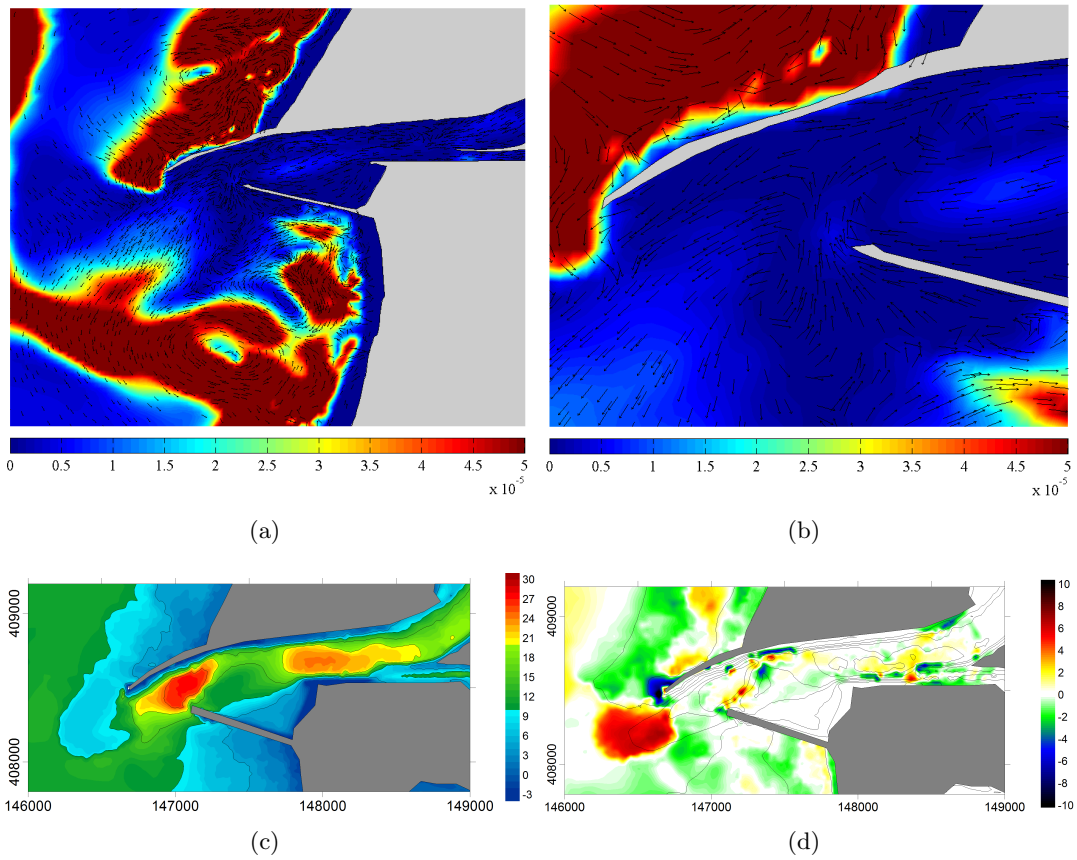

Figure 6.2: Same as Figure 6.1 for Bi formulation. Black areas represents data out of the scale represented.

6.2 Simulations forced with a single wave

6.2.1 Simulation considering a regular monochromatic wave with height 0 m

To understand the influence of the waves in the morphodynamic of the inlet, it is necessary to remove from the results obtained herein (considering the forcing of tidal currents coupled with a wave regime), the effect of the tidal currents forcing. With this aim, are performed numerical simulations considering the tidal currents forcing coupled with a wave with height equal to 0 m. Therefore, the results obtained are considered the result of tidal currents forcing only, using all other conditions equal.

In Figure 6.4 are illustrated the residual sediment fluxes obtained, which are similar to those represented in Figure 5.9 of the previous Chapter.

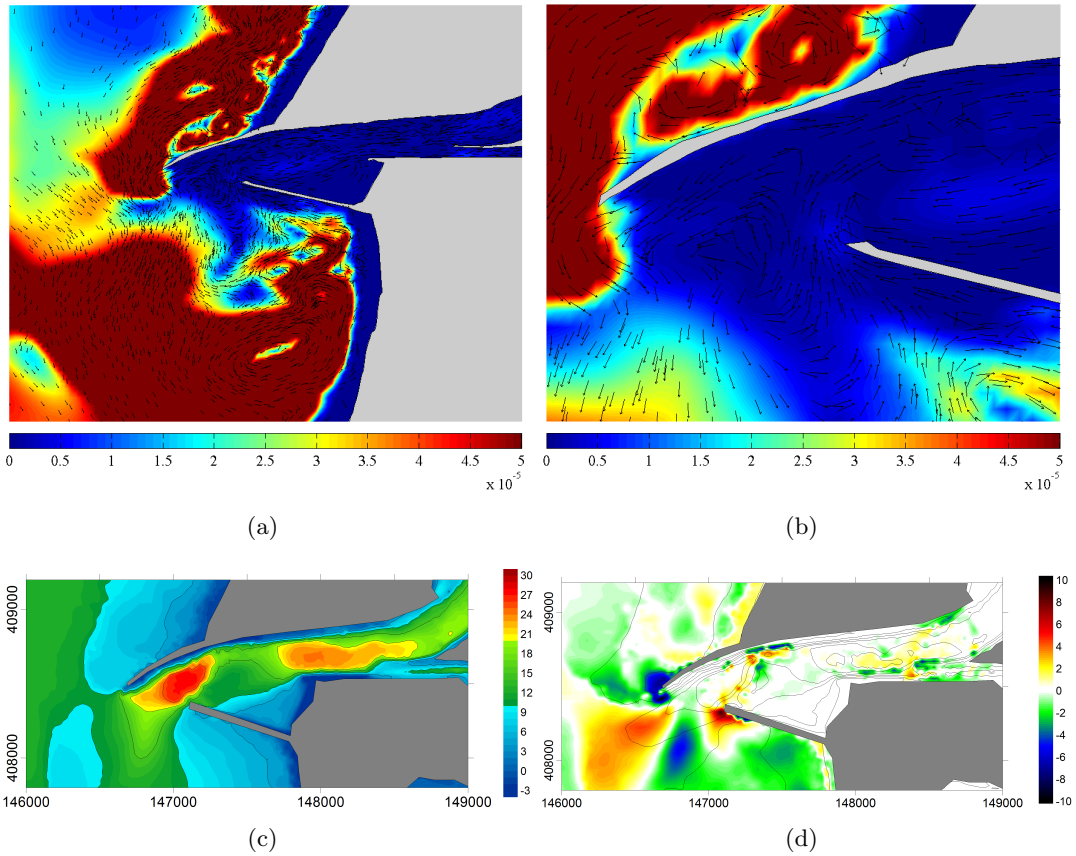

Figure 6.3: Same as Figure 6.1 for SvR formulation. Black areas represents data out of the scale represented.

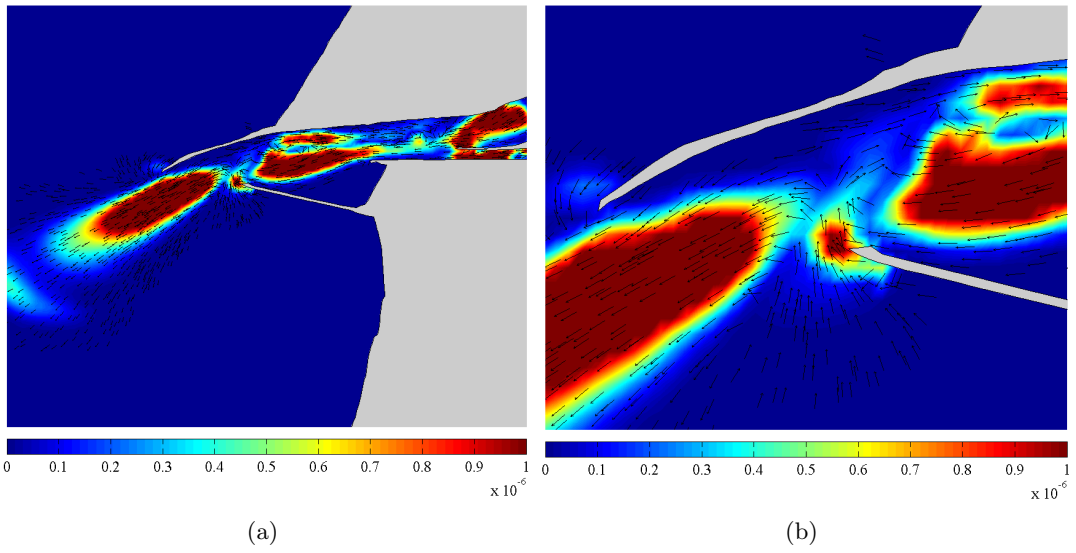

Figure 6.4: (a) and (b) Residual sediment flux (m^2s^{-1}) for AW formulation considering the wave height equal to 0 m.

Table 6.1: Wave simplified regime computed through a longshore sediment transport formula. $H_{0,eq}$ is the wave height at deep water of the equivalent wave in meters, $\alpha_{0,eq}$ is the wave angle at deep water of the equivalent wave in degrees and $T_{p,eq}$ is the period of the equivalent wave in seconds.

Wave	Frequency (%)	$H_{0,eq}$ (m)	$\alpha_{0,eq}$ (^{o})	$T_{p,eq}$ (s)
#1	0.1429	0.71	20.52	8.65
#2	0.4574	1.36	22.10	9.28
#3	0.2475	2.23	20.76	10.75
#4	0.0971	3.13	19.41	11.50
#5	0.0387	4.14	20.22	12.19
#6	0.0119	5.10	22.73	13.76
#7	0.0023	5.87	18.87	14.06
#8	0.0013	6.81	15.25	14.88

6.2.2 Simulations forced with a regular monochromatic wave

In this subsection the results obtained considering the model forced by tidal currents and a regular monochromatic wave are presented. The main aim of this study is to identify the wave characteristics that induce the largest changes in the inlet morphology. The set of waves used was obtained by grouping waves from a complete wave regime in wave height classes of 1 m interval, computed in section 3.7, with the offshore characteristics presented again in Table 6.1. These 8 regular monochromatic waves differ in height, period and direction, and have different frequencies of occurrence. The 0^o incident direction ($\alpha_{b,eq}$) is referenced to the West-East direction and the angles are measured counter-clockwise.

The offshore characteristics of each one of these regular monochromatic waves were imposed as boundary forcing in the morphodynamic modeling system MORSYS2D [Fortunato and Oliveira, 2004; Bertin et al., 2009c].

To compute the sediment transport rate, the Ackers and White [1973] formulation modified by van de Graaff and van Overeem [1979] is used in order to take into account the waves effect. The single wave influence in the morphodynamics is performed by analyzing for each wave the residual fluxes at the entire study area, the residual sediment flux at seven sections (sc1 to sc7), the sedimentation rates in the regions delimited by the sections (regions I-V) and the bathymetric changes at the study area (see Figure 3.7).

To analyze the bathymetric changes generated only by the regular monochromatic waves, the changes obtained only by the tidal current forcing (section 6.2.1) were removed from the bathymetric changes obtained for the coupled forcing.

Waves #1 to #4 are frequent on the adjacent coast of the study area, while waves #6 to #8 are already considered storm waves with a lower frequency of occurrence. In Figures 6.5 to 6.12 the results obtained for these waves are illustrated.

The final bathymetries presented herein are those predicted after 60 days of simulation and are also illustrated the bathymetric changes between the final and the initial bathymetry, induced by the correspondent regular monochromatic wave imposed. Once more, the white areas represent unchanged depths or changes induced by tidal currents only and the contour lines represent the initial bathymetry. Positive values for bathymetric changes represent accretion and negative values represent erosion trends.

The waves influence on the bathymetric changes is almost restricted to the adjacent coastal zone; however for higher wave heights also the inlet area is affected. For smaller waves, smaller bathymetric changes are obtained. For example, Wave #2 induces bathymetric changes between +2 m (accretion) and -2 m (erosion) for the 60 days numerical simulations while Wave #6 induces higher bathymetric changes, in particular near the head of the North breakwater. These changes are induced by the residual fluxes also illustrated in these figures. It should be pointed out the differences in magnitude of the fluxes induced by these two waves. For all waves, a longshore southward net sediment flux is found, attached to a littoral current which is characteristic of the study area. The width of the longshore residual current, northern of

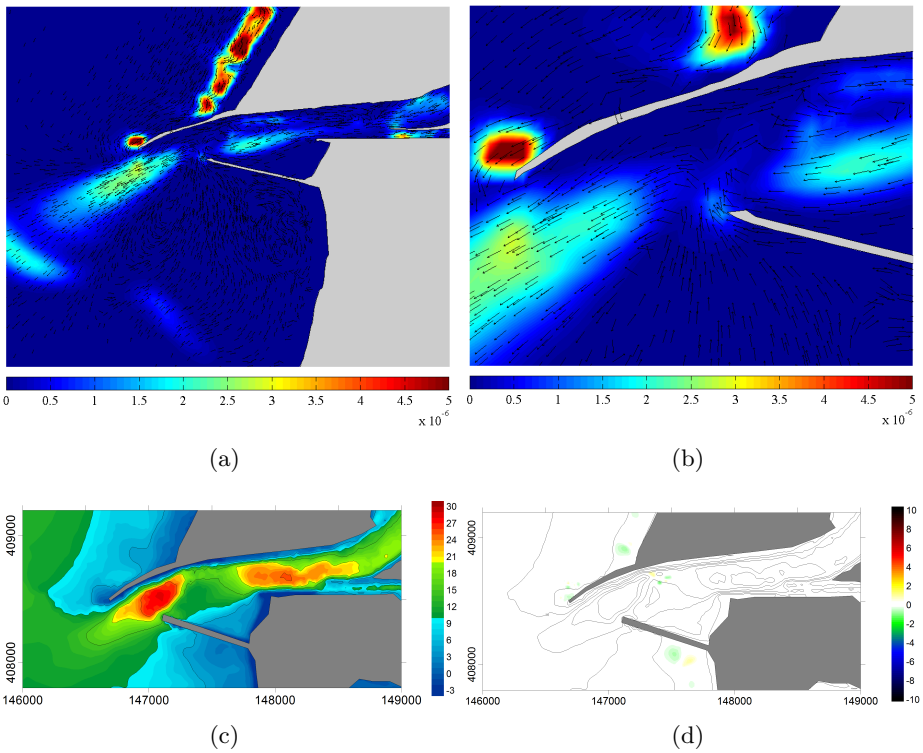

Figure 6.5: (a) and (b) Residual sediment flux (m^2s^{-1}) for Wave #1. (c) Final bathymetry (metre) of the Ria de Aveiro lagoon inlet computed after 60 days. (d) Difference between the computed final and initial bathymetries (metre) for a 60 days simulation. In (d) the solid lines illustrate the 2001 bathymetry. The negative (positive) values represent erosion (accretion). The values in axes are in metres.

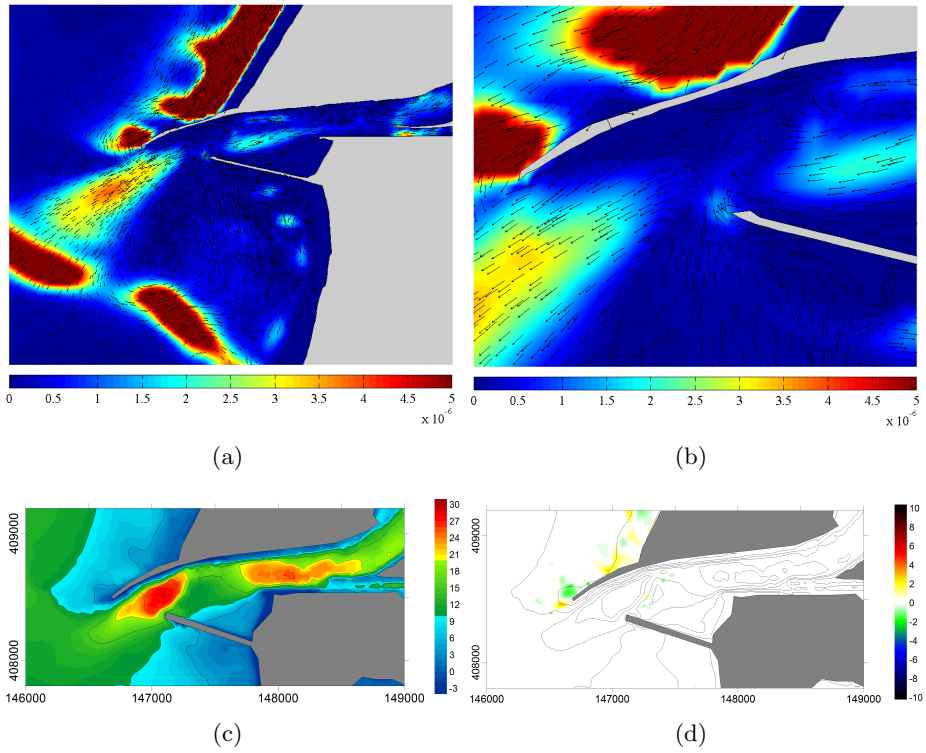

Figure 6.6: Same as Figure 6.5 for Wave #2.

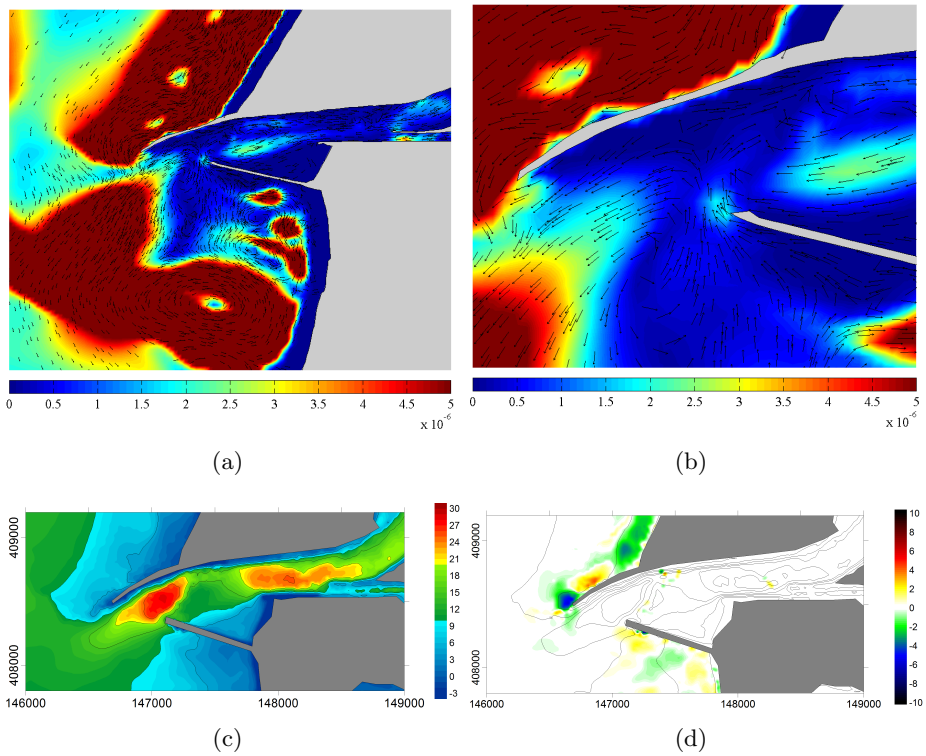

Figure 6.7: Same as Figure 6.5 for Wave #3.

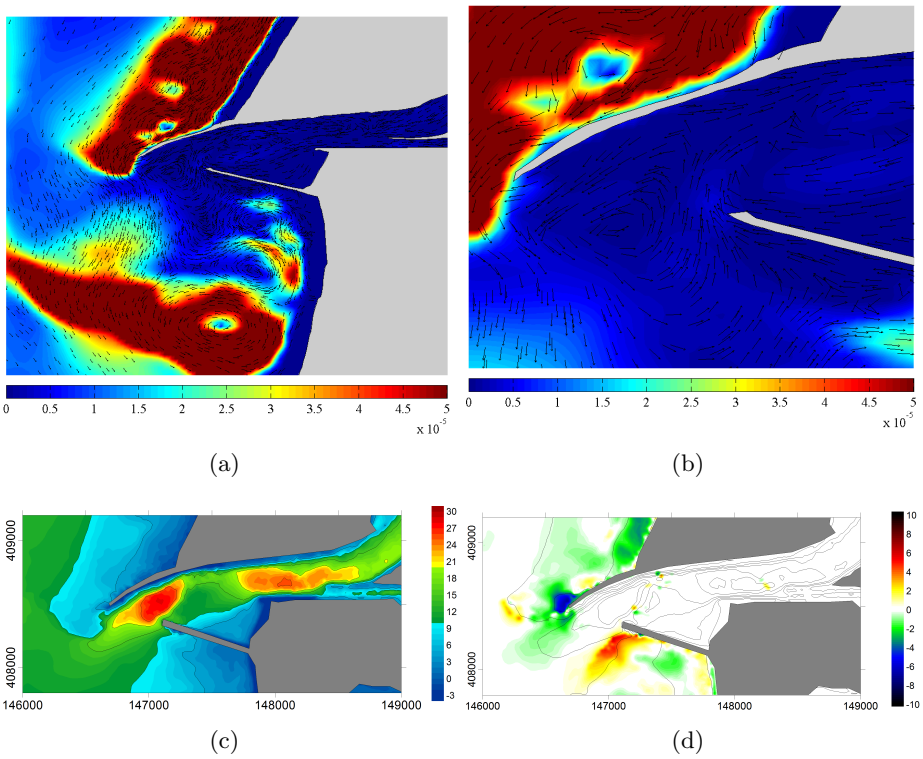

Figure 6.8: Same as Figure 6.5 for Wave #4.

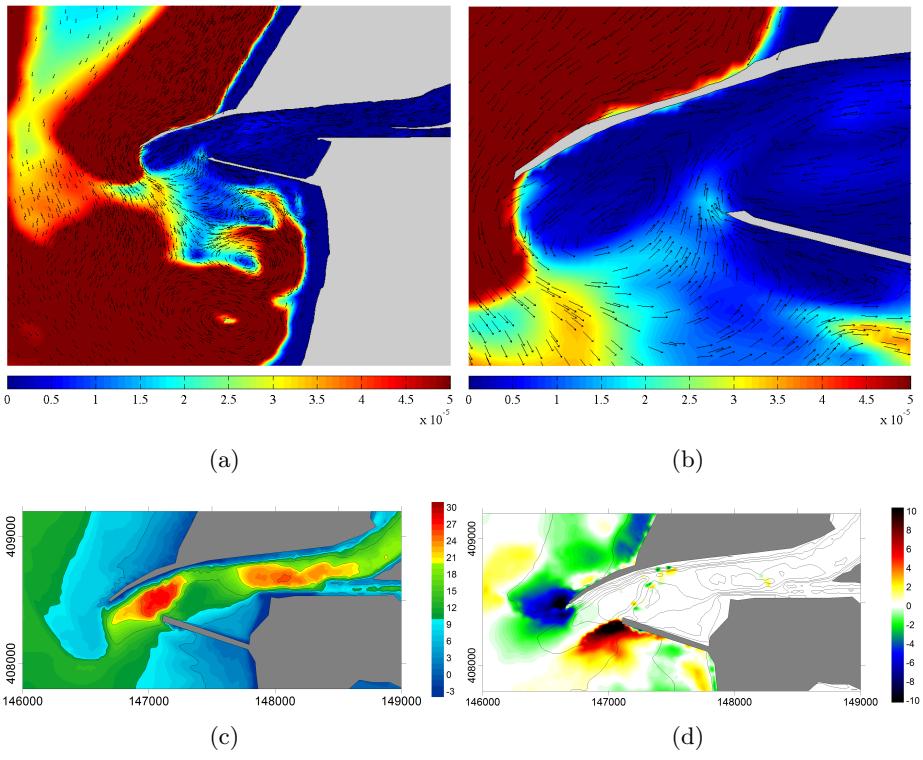

Figure 6.9: Same as Figure 6.5 for Wave #5.

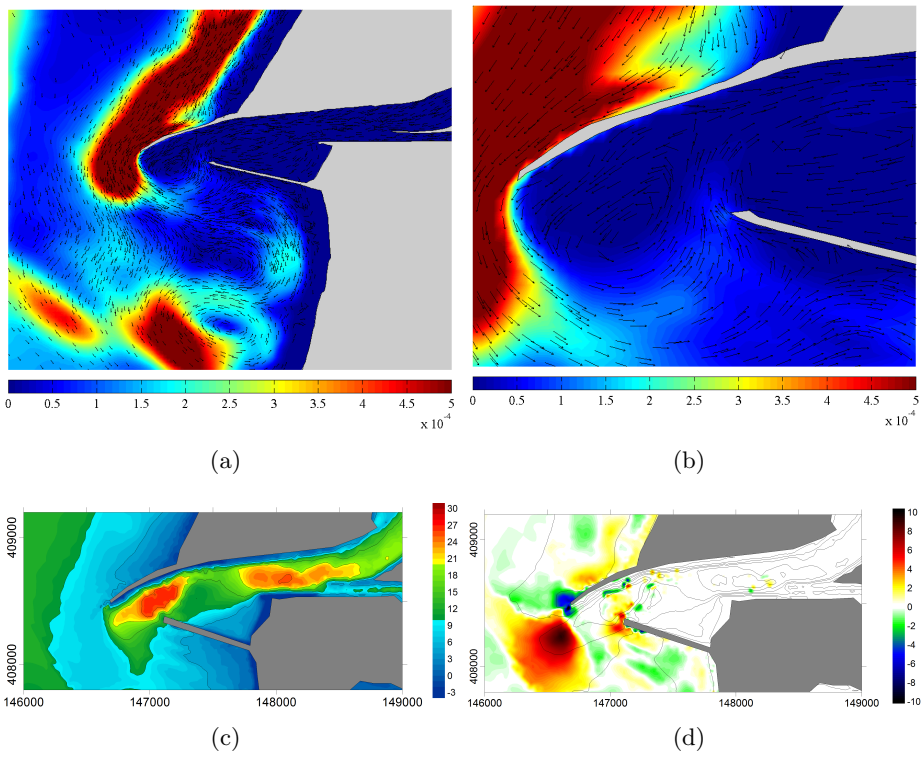

Figure 6.10: Same as Figure 6.5 for Wave #6.

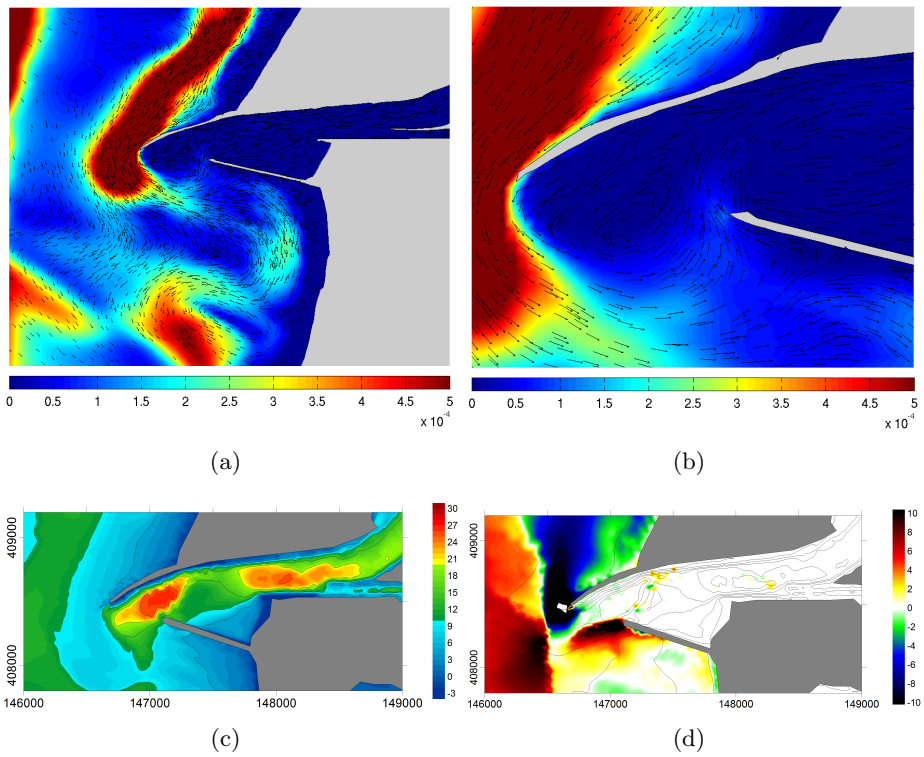

Figure 6.11: Same as Figure 6.5 for Wave #7.

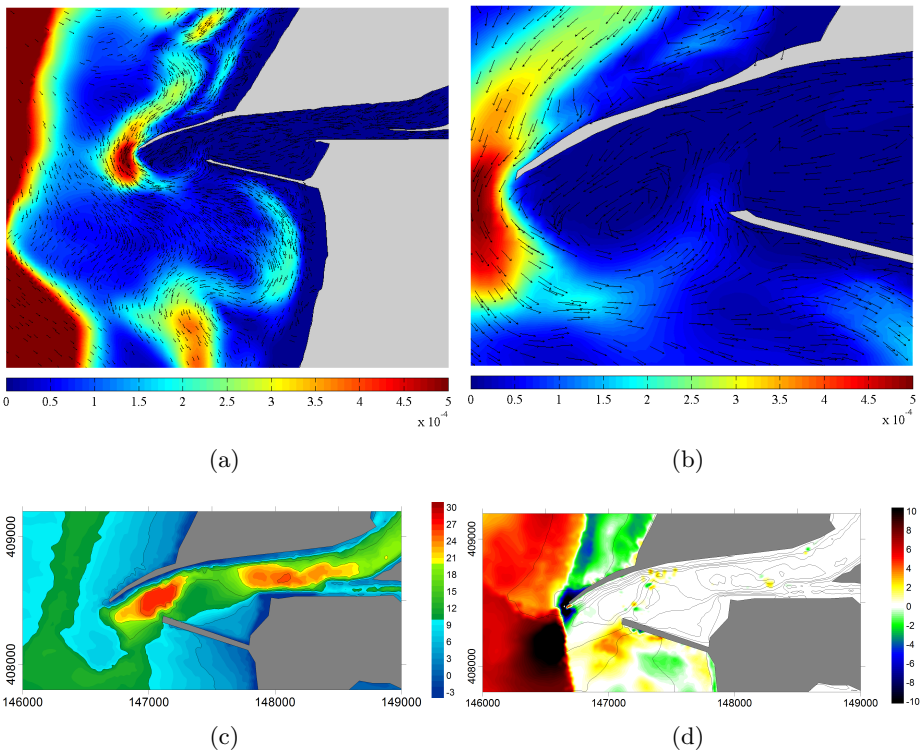

Figure 6.12: Same as Figure 6.5 for Wave #8.

the inlet, depends on the wave height: for instance Wave #2 induces a residual current 300 m wide, while for Wave #6 the width is larger, approximately 500 m.

The residual flux field for smaller waves shows that at the inlet the fluxes are dominated by the seaward tidal currents, due to the small wave height simulated. For storm waves, the longshore sediment transport is continuously southward even across the inlet, which means that the tidally induced residual fluxes at the inlet are surpassed when higher waves are considered. The transport current is clearly identified and interrupted by the presence of the North breakwater. Furthermore, the tidal currents at the inlet are superimposed to the longshore current generated by the wave simulated.

Although storm waves induce considerable changes in the bathymetry they have a smaller frequency of occurrence. Despite the different frequencies of occurrence of the waves, the cumulative effect of the smaller waves is still low when compared with the effect of a storm wave, such as Wave #6.

The residual fluxes in the seven sections chosen are illustrated in Figure 6.13. Negative (positive) values represent sediment flux in the downstream (upstream) directions. At section 3, negative (positive) values mean sediment flux into (out from) region III.

To analyze the residual sediment fluxes generated by different regular monochromatic waves, at the seven sections, the residual fluxes obtained only by the tidal current forcing were

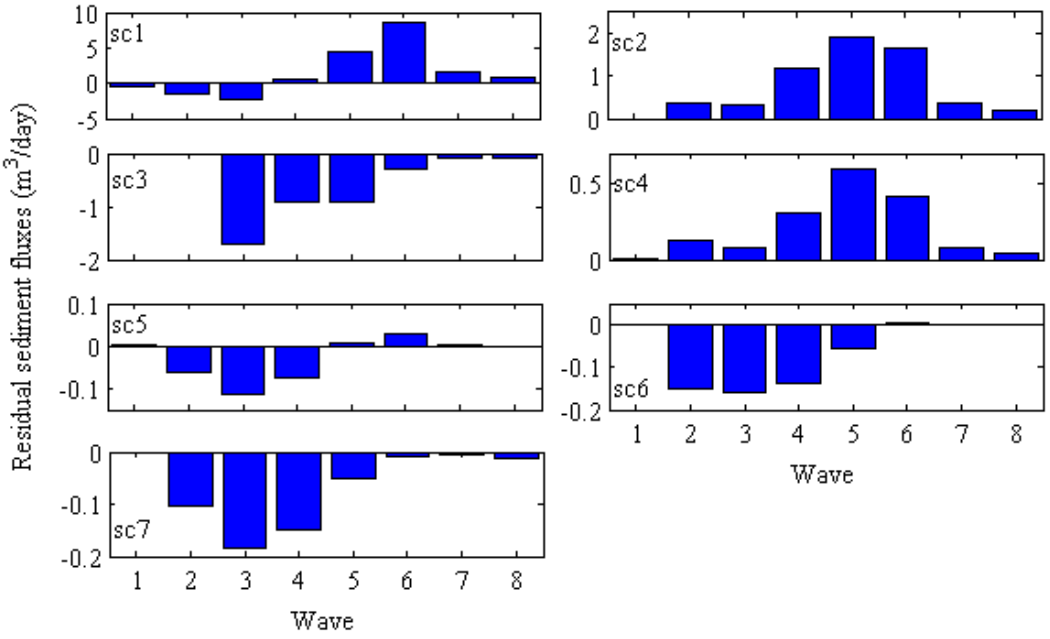

Figure 6.13: Residual sediment flux ($m^3 day^{-1}$) for the 8 representative waves.

removed from the residual fluxes values obtained for the coupled forcing. These computed fluxes are considered to be resultant of the regular monochromatic wave forcing.

The frequency of occurrence of each wave (Table 6.1) was taken into account for the residual sediment fluxes and sedimentation rates computation and was obtained in Subsection 3.7.2. The results for the residual fluxes represented in Figure 6.13 show that the waves influence is very small for the inner sections of the lagoon, with smaller magnitude than at the inlet. Comparing the combined fluxes with those obtained through the simulation performed considering only the tidal currents, it is observed that at the inner sections of the study area (sc5, sc6 and sc7) the fluxes induced by the tidal currents are approximately 100, 30 and 80 times higher, respectively, than those presented in Figure 6.13. For the remaining sections, the fluxes are on average 3 times higher. Consequently, the influence of each wave in the bathymetric changes is essentially restricted to the lagoon mouth and adjacent coastline, as referred earlier.

It is observed in Figure 6.13 that considering the frequency of occurrence of the regular monochromatic waves, the two highest waves, Wave #7 and #8, with 0.36% of frequency of occurrence, have almost a null influence in the sediment fluxes for all cross-sections. Nevertheless, it is interesting to recognize that, in the inlet cross-section, the third highest wave (Wave #6) with Hb=5.39 m, even though with a low frequency of occurrence of 1.19%, induce almost twice the flux corresponding to the sum of the first four waves, with a combined frequency of occurrence of 94.49%. Also Wave #5 has a large influence in the residual sediment flux.

The sediment flux in section 1 is seaward (negative values) but small, for simulations with the lower wave heights. For higher wave heights the residual sediment flux is upstream, transporting sediments inside the lagoon. Comparing the residual fluxes in the upstream (sc6 and sc7) and downstream (sc1) sections (sections that delimit the study area) for each wave, it is observed that high wave height induces accretion at the domain, since the flux at the inlet is always positive and higher in magnitude than at upstream sections (e.g. Waves #4 to #8). On the other hand, small wave height induces erosion at the study area, with higher and negative flux values (pointing seaward) at the inlet section than at the upstream sections. Considering the case of tidal currents only, accretion is observed, however with higher values than those obtained herein.

Thus, the analysis of the net residual fluxes at selected sections (1-7) give information about the morphological changes at the regions that they delimit (I-V), which are illustrated in Figure 3.7.

To analyze the erosion or accretion tendency for each region, the sedimentation rates (in m^3day^{-1}) for the five regions defined and presented in Figure 3.7 were computed and are illustrated in Figure 6.14. Positive values indicate accretion trends and negative values erosion. As before, the tidal current signal was filtered.

The results show that sedimentation rates obtained for region I are higher than those obtained for the remaining regions. For almost all regions and waves studied accretion was found for the study area. The highest waves (except Wave #8), despite their low frequency of occurrence, induce higher sedimentation rates (accretion) than the first four waves.

In conclusion, it was observed that the wave induced residual sediment fluxes in the cross sections upstream the lagoon mouth are smaller in magnitude than at the inlet, restricting the influence of the waves to the lagoon mouth and adjacent coastline.

For the sections located at and near the inlet (sc1 and sc2), Wave #5 and #6 are those that

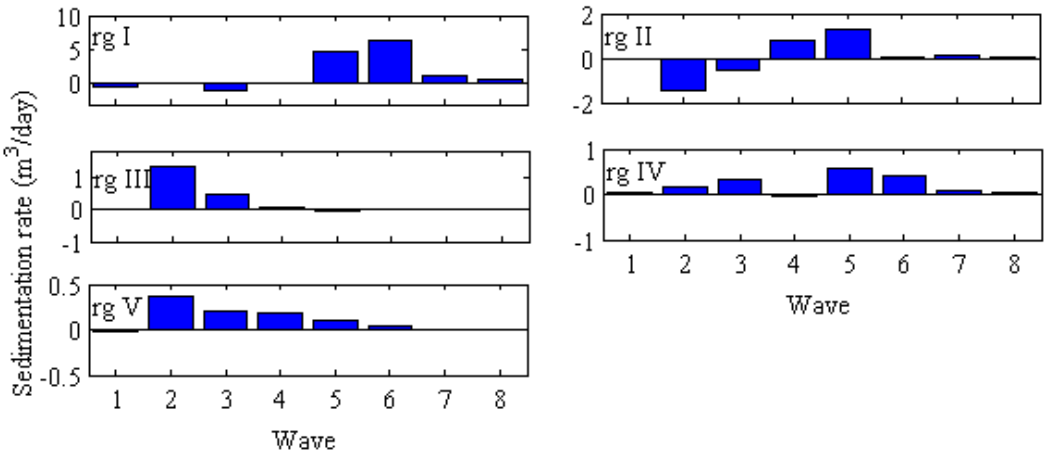

Figure 6.14: Sedimentation rate m^3day^{-1} for 60 days obtained for the 8 representative waves.

mostly contribute to the residual sediment fluxes. Despite the importance of each one of the 8 regular monochromatic waves to the accurate reproduction of the longshore sediment transport, it can be considered that Waves #1, #7 and #8 are those with the lower contribute to the sediment balance in the study area.
This analysis in terms of residual sediment fluxes and sedimentation rates revealed that each wave has more influence at a given section or region.

6.3 Simulations forced with a wave regime

6.3.1 Storm events

In this subsection the influence of a storm event on the morphodynamic changes of the inlet is analyzed. The changes induced by the storm event are expected to be more significative when compared with the predicted annual changes.
Considering the period of 1 year studied in Section 6.1.1, comprised between June 2001 and 2002, three storms occurred in the West coast of Portugal, according to the records of the WaveWatchIII model run at NCEP/NOAA [Tolman et al., 2002]. This value is in agreement with the reference values published in the literature: according to Pita and Santos [1989] on average 3 storms per year occur in the Portuguese coast and, according to Andrade et al. [1996], 2.7 per year with mean duration of approximately 4 days [Ferreira, 1998].
To analyze the influence of storm events, numerical simulations for a period of 1.5 months are performed, comprised between 1 October and 15 November 2001, enclosing the storm events illustrated in Figure 6.15. The offshore wave heights at this storm period reach 6.15 m with predominantly directions NW-NNW.
The significant wave height and wave orbital velocities are illustrated in Figure 6.16 for two

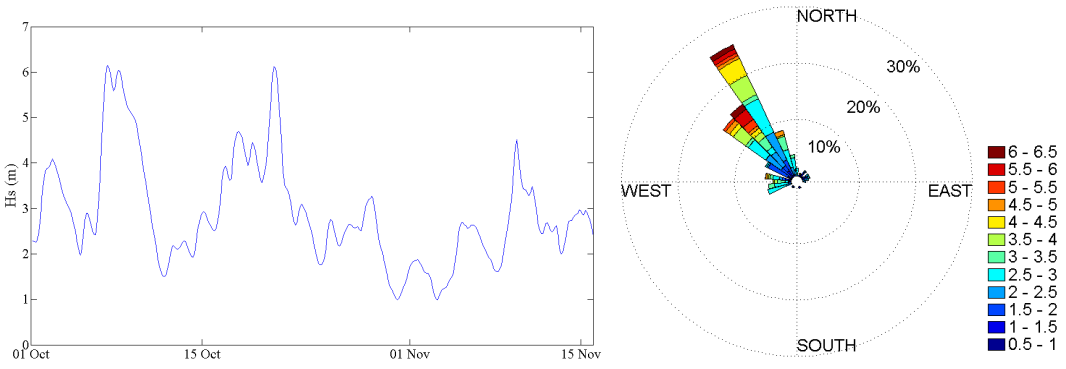

(a) (b)

Figure 6.15: Characteristics of the period chosen enclosing a storm event: from 1 October to 31 December 2001. Offshore (a) waves height (metre) and (b) distribution of wave height and direction.

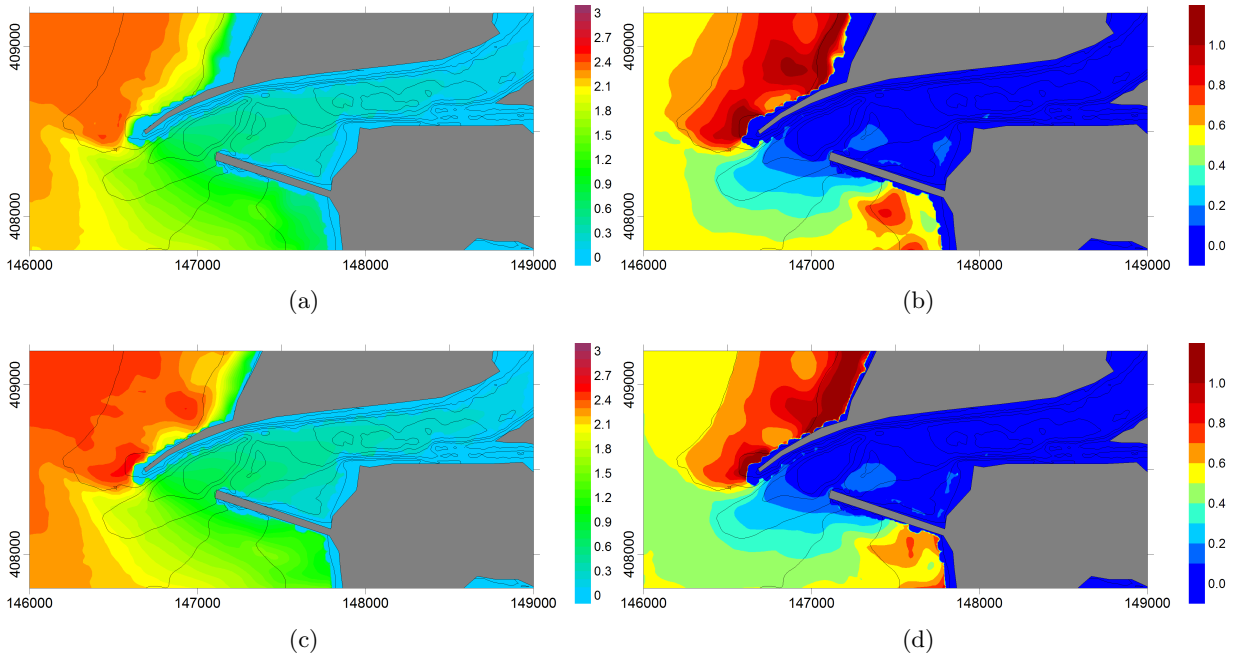

Figure 6.16: (a),(c) Significant wave height and (b),(d) wave orbital velocity for a day in normal conditions (01 Oct, top panel) and in a storm event (09 Oct, bottom panel).

distinct days: one day with offshore wave height of approximately 2 m (1^{st} October) and other with wave height of 6 m (8^{th} October). The analysis of the significant wave height shows that, in the navigation channel, the waves have small heights and therefore small influence on the dynamics of the inner sections of the study area, for both conditions. The higher wave heights, observed in a storm day, reach closer to the North breakwater than in normal conditions, subjecting this structure to highly energetic conditions. The orbital velocities at storm events are larger closer to the adjacent coastal area and breakwater at the North side of the inlet, than for wave heights of 2 m. Also, the width of the region with high orbital wave velocities decreases, inducing a stretching of the width of the nearshore sediment transport.

To analyze the influence of the storm event on the morphodynamics of the Ria de Aveiro inlet, the bathymetric changes for the 1.5 month period are computed and illustrated in Figure 6.17. The predictions show trends of erosion and accretion in equal magnitude, with maximum values of approximately 4 m.

Comparing these changes with those predicted for the 1 year period (Figure 6.1) the patterns are coincident, with the development of an erosion trend near the head of the North breakwater and accretion slightly further South. However, the magnitude of the bathymetric changes induced by the storm event are smaller than those predicted for the 1 year period.

According to Teixeira [1994] the amount of wave transported sediments is function of the wave height and period ($Q \propto H^2T$). For the period of 1 year between June 2001 and 2002,

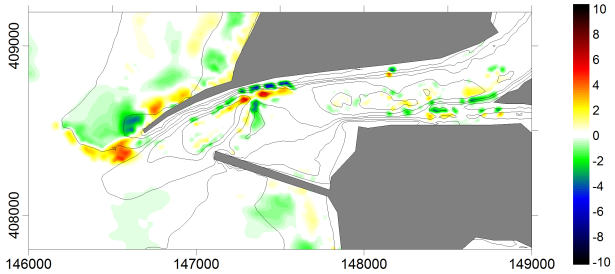

Figure 6.17: Bathymetric changes (metre) computed after 1.5 months simulation enclosing a storm event, for simulations forced by tidal currents coupled with a wave regime. The solid lines illustrate the initial bathymetry. The negative (positive) values represent erosion (accretion). The values in axes are in metres.

the relative frequencies of H, H^2 and H^2T are illustrated in Figure 6.18. The results considering the storm wave height limit (H=5 m) show that the group of waves with wave height lesser than 5 m has frequency of occurrence of 90% and is responsible for 3/4 of the sediment transport. The storm waves, defined by wave heights higher than 5 m, with only 10% of frequency of occurrence, are responsible for 1/4 of the sediment transport.
The distribution of the square height is similar to the obtained for H^2T, illustrating that the influence of the high wave periods, characteristic of the storm waves, is surpassed by the lower wave periods, which occur with higher frequency of occurrence. Therefore, the majority of the potential sediment transport occurs for wave heights smaller than the limit for storm wave height. In summary, it was observed that the storm waves, defined by wave heights higher than 5 m and with only 10% of frequency of occurrence, are responsible for 1/4 of the sediment transport, while the group of waves with wave height lower than 5 m,

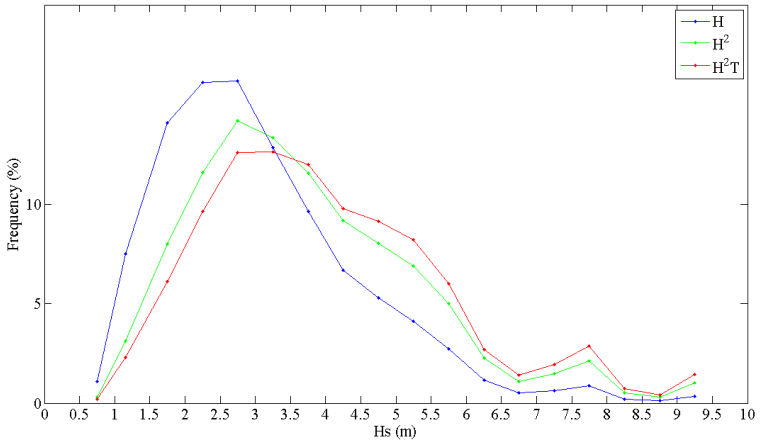

Figure 6.18: Relative frequency of H, H^2 and H^2T, considering the wave data between June 2001-2001.

with frequency of occurrence of 90%, is responsible for 3/4 of the sediment transport. It is then concluded that the majority of the potential sediment transport occurs for wave heights smaller than the limit for storm wave height. However, the storm waves have also strong influence on the sediment transport, transporting 25% of sediment in only 10% of occurrence.

6.3.2 Period June 2001 - March 2003

The influence of the full wave climate on the inlet morphodynamics is analyzed by comparing the numerical results obtained through simulations forced only by tidal currents and by tidal currents coupled with the wave regime.

The 2001 bathymetry presented in Figure 4.3 is considered as the initial condition for the morphodynamic simulations. The bathymetric changes and sedimentation rates obtained for 1.75 years simulations (between June 2001 and March 2003) induced by the wave regime coupled with the tidal currents, are computed and analyzed. From this analysis, areas with erosion and accretion trends are identified and the influence of the wave climate in these changes is understood.

The residual fluxes induced by the combination between tidal currents and wave regime are illustrated in Figure 6.4 and were already analyzed in Section 6.1.1.

To access the relative importance of tidal currents and wave regime in the sediment balance at the inlet, the residual sediment fluxes for the sections 1-7 defined in Figure 3.7 were computed, and are illustrated in Figure 6.19(a), as well as the results obtained when considering only the tidal currents forcing.

The sediment fluxes for the simulations forced by tidal currents and wave regime are very similar to those obtained forced only by tidal currents: as mentioned above, the sediment fluxes are outward for almost the cross-sections; the waves influence is very small for the inner sections analyzed. The comparison between the tidally induced flux and the one driven by the combination between the wave regime and tidal currents, shows that at the inner sections of the study area (sc 4-7) the fluxes induced by the tidal currents are approximately 30, 20, 10 and 20 times higher, respectively.

At sections 1, 2 and 3 the influence of the wave regime in the sediment fluxes is more obvious. In order to understand the influence of the wave regime on the residual sediment fluxes, the fluxes obtained for the simulations forced only by tidal currents were removed from those obtained for the simulations forced by tidal currents coupled with the wave regime. For sections 2 and 3, the residual sediment fluxes induced only by tidal currents are approximately 4 and 26 $m^3 day^{-1}$, while those induced by the wave regime are approximately 25% and 63% of these values. The influence of waves surpasses the influence of tides in section 1, where the flux due to the wave regime is approximately 1.5 times higher than the flux generated by tidal currents.

The analysis of the residual fluxes budget between sections provides information about the

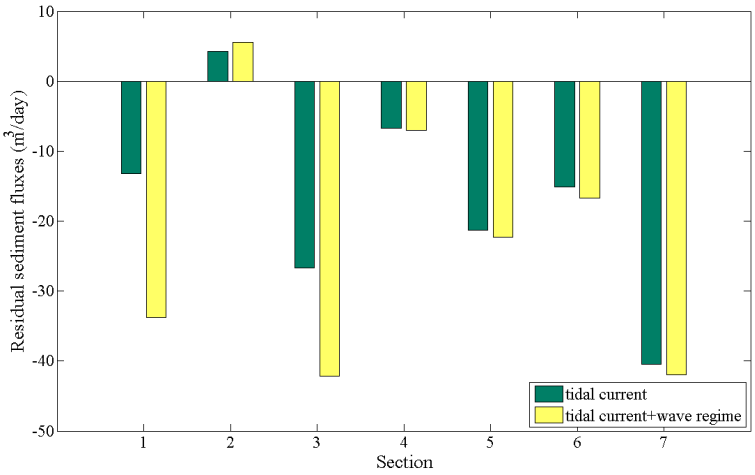

(a)

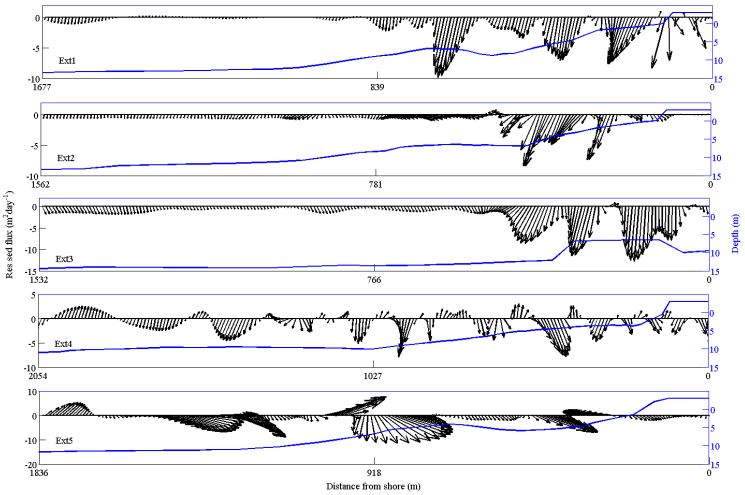

(b)

Figure 6.19: (a) Residual sediment fluxes (m^3day^{-1}) in the seven sections defined at the inlet and navigation channel, only with tidal currents forcing (■) and for tidal currents coupled with a wave regime forcing (■). (b) Residual sediment fluxes (m^2day^{-1}) for the sections located at the offshore area of the inlet Ext1-5.

morphological changes at the regions delimited by them (Figure 3.7). Thus, to analyze the erosion or accretion trend for each region, the sedimentation rates (in m^3day^{-1}) for the regions defined and presented in Figure 3.7 were computed and are illustrated in Figure 6.20(a).

The results show that for region I, which is the deeper area of the inlet, the observed erosion is predicted by the numerical model. This means that this region is deepening at a rate of about 20 m^3day^{-1}. Region III also has an erosion trend but with a smaller rate, even for the simulations forced by the tidal currents and wave regime. For the remaining sections is predicted accretion at rates between 10 and 40 m^3day^{-1}. The higher sedimentation rate

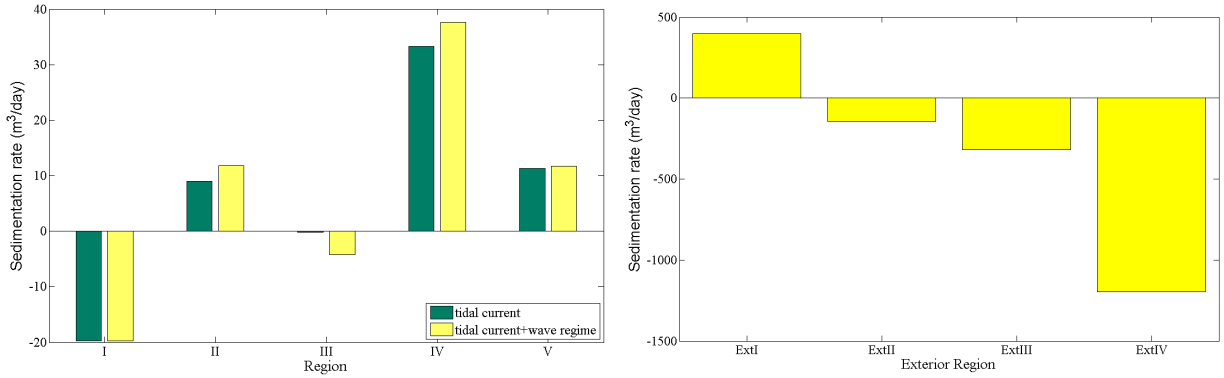

(a) (b)

Figure 6.20: Sedimentation rate ($m^3 day^{-1}$) in the nine regions defined (a) at the inlet and navigation channel and (b) nearshore region.

values in region IV indicate that exists an infilling of the deeper area located between the *tidal gauge* and the channel bifurcation at a rate of approximately 33 and 38 $m^3 day^{-1}$, for simulations forced only by tidal currents and by tidal currents coupled with a wave regime, respectively. The accretion rates in region II and V are approximately 10 $m^3 day^{-1}$.
Analyzing the residual sediment fluxes and the sedimentation rates for the inlet and navigation channel, it is concluded that the wave regime influence diminishes from the inlet up to the navigation channel and channel bifurcation, being negligible in this upstream region.

Figure 6.19b illustrates the cross-shore distribution of the residual sediment fluxes and the bathymetry for the five exterior sections (Ext1-Ext5) located in Figure 3.7.
The residual fluxes North of the inlet (Ext1-3) are directed from North to South and parallel to the shoreline. They are related to the drift currents generated by the breaking waves. The higher fluxes are observed at the section located close to the North breakwater, where the influence of this structure is experienced.
The residual sediment transport North of the inlet is limited to a partial extent of the section (approximately 800 m for Ext1, 510 m for Ext2 and 450 m for Ext3). This limited extent can be related to the depth of closure, which is the most landward depth offshore of which there is no significant change in bottom elevation and no significant net sediment exchange between the nearshore and the offshore [Kraus et al., 1988]. Different estimations of the depth of closure nearshore of the study area are found in literature, although the value is not known precisely: Ferreira [1993] suggested the range 14-17 m, Teixeira [1994] 12.2-14.8 m and Coelho [2005] 12.1-16.8 m. Coelho [2005] illustrated the cross-shore distribution of the longshore sediment transport as a function of the width of the active profile and concluded that the integrated flux reaches almost 90% of the net volume at just half of the width of the section. Figure 6.19b reveals that the zone where the longshore fluxes are significant is

close to the previous estimation.
An evaluation of the annual longshore transport at sections Ext1-3 was also performed. For sections Ext1 the longshore transport obtained is 1.17×10^6 m^3year^{-1}, for section Ext2 is 0.77×10^6 m^3year^{-1} and 1.68×10^6 m^3year^{-1} for Ext3, all directed North-South. Comparing these values to those published in literature and cited in Sections 3.6 and 3.7: 1×10^6 m^3year^{-1} [Larangeiro and Oliveira, 2003] and 1-2×10^6 m^3year^{-1} [Andrade et al., 2002] was found their agreement. Thus, it can be concluded that the numerical model MORSYS2D is accurately reproducing the littoral sediment transport.
The "uniformity" observed northward of the inlet is not found at the southward sections. The re-circulations observed are induced by the breakwaters that define the artificial inlet and by the existence of local submerged sandbanks. Thus, the inlet substantially influences the extension and magnitude of the residual fluxes. These re-circulations are also observed in Figures 6.19.
For the outward sections, the sedimentation rates obtained for the simulations forced only by tidal currents are always lower than 12 m^3day^{-1}, which is negligible when compared with the rates obtained for the simulations forced by tidal currents coupled with the wave regime. Consequently, in Figure 6.20b only the rates obtained for the later simulations are presented. The analysis of the residual sediment fluxes of Figure 6.19b give information about the trends of the exterior regions: the lower value of the longshore transport at Ext2 when compared with Ext1 and Ext3 might induce accretion in the region delimited by Ext1 and Ext2 sections (region Ext I); and erosion by the one delimited by Ext2 and Ext3 (region ExtII). The results obtained for the sedimentation rates (Figure 6.20(b)) show accretion in region ExtI, at a rate of approximately 400 m^3day^{-1}. In the remaining exterior regions, erosion is observed at rates of approximately 140, 300 and 1000 m^3day^{-1}. Grouping the northern and southern regions of the inlet, is found accretion at North and erosion at South, at rates of approximately 250 and 1500 m^3day^{-1}, respectively. These trends are in agreement with the observations along the years since the construction of the breakwaters [Dias et al., 1994].

The bathymetry predicted and the bathymetric changes are illustrated in Figure 6.21. The numerical results, for simulations forced only by tidal currents and tidal currents coupled with a wave regime, for the inner part of the lagoon and for the time period studied are similar. Higher changes are found at the mouth and at the offshore adjacent area. The wave climate changes the dynamics of the study area, pushing the sediments towards the inlet, as shown by the South inflection of the bathymetric contour lines for the area outside the inlet. These results demonstrate the local North-South littoral drift induced by the wave climate. Near the northern breakwater head the predictions reveal a strong erosion trend.
The comparison between the bathymetric changes predictions considering the coupled forcing of tides and waves (Figure 6.21), the tidal currents forcing only (Figure 5.13) and the bathymetric changes observed (Figure 3.5) shows that the inclusion of the wave regime

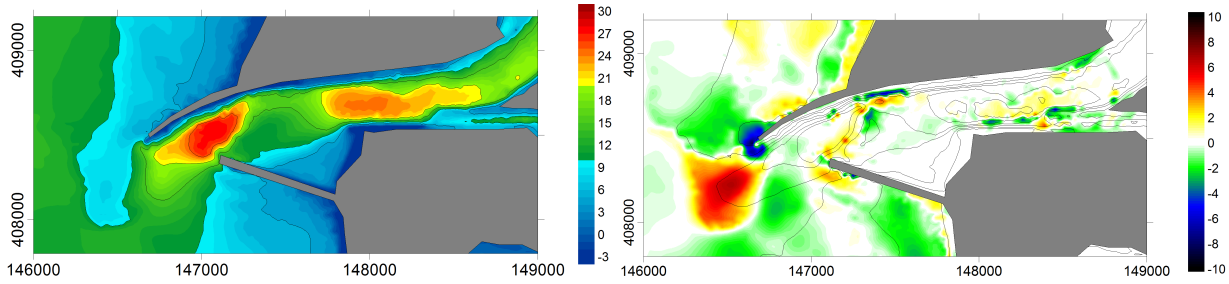

(a) (b)

Figure 6.21: (a) Final bathymetry (metre) of the Ria de Aveiro lagoon inlet computed after 1.75 years and (b) Difference between the computed final and initial bathymetries (metre) for a 1.75 years simulation for simulations forced by tidal currents coupled with a wave regime. In (b) the solid lines illustrate the initial bathymetry. The negative (positive) values represent erosion (accretion). The values in axes are in metres.

in the numerical simulations improves the accuracy of the predictions. Thus, the results obtained through simulations forced by tidal currents and wave regime confirm that the model reproduces the trends observed in the collected data, but slightly underpredicts the amplitudes of the bathymetric changes.
It is important to realize that the strong erosion pattern observed at the head of the North breakwater is now reproduced by the model, but slightly closer to the structure. The accretion trend found offshore this structure can not be compared to the observed pattern because it lies out of the area where the surveys were performed.

In Figure 6.22 the depths along the sections represented in Figure 3.7 observed in June 2001 (o) and March 2003 (+) surveys and simulated with the AW formulation for tidal currents and wave regime forcing are illustrated. The set of figures at the top panel correspond to sections 1-7 and the figure at the bottom panel corresponds to the longitudinal section.
In Sections 5, 6 and 7 data was not collected in the 03/2003 survey, thus only the initial and predicted depths are illustrated.
At the remaining sections, the depths predicted are very similar to those observed, with exception to the areas close to the structures, where slightly accretion trends are observed while the numerical model predict erosion trends. The erosion trends at the center of Sections 1,2 and 3 and the accretion trend at Section 4 are predicted by the model. However, their magnitude is slightly underestimated.
The longitudinal section, illustrated at the bottom panel of Figure 6.22, reveals that the erosion trend observed at the seaside of the inlet is predicted, but underestimated in magnitude. The center of the deepest area is characterized by a slight accretion trend, overestimated by the model. In the shallower area is observed erosion at the side walls and accretion at its center, narrowing this bottom feature. However, the model predicted erosion at the

center and a slightly accretion at the side walls, stretching this shallower feature. With this simulation it is noticeable the improvements in the morphodynamic predictions when the wave regime is added as sediment transport forcing. The observed offshore migration and inflection of the deeper area between the breakwaters and the erosion trend at the head of the northern jetty, are reproduced in this case.

6.3.3 Period June 2001 - September 2005

The period between June 2001 and September 2005 was also studied through numerical simulations considering the coupled sediment transport forcing between tidal currents and a real wave regime. In Figure 6.23 the bathymetry predicted after 4.25 years and the bathymetric changes induced by the coupled forcing are illustrated. These results are compared to the data observed (Figures 3.3 and 3.6) and with the simulations forced by tidal currents only (Figure 5.16).

The results show that the wave regime typical of the coastal zone adjacent to this study area generate a strip of shallower depths, induced by the sediments transported by the longshore currents. These currents push the bathymetric lines to South, inflecting the deepest bottom feature located at the inlet. The North breakwater is also subject to the influence of these strong currents resulting in a strong erosion trend at its head of more than 9 m.

Inside the inlet, at the navigation channel and channel bifurcation, the trends observed are very similar to those obtained in the previous chapter, when only tidal currents were considered. This is also observed when comparing the depth along Sections 3 to 7 in Figure 6.24 with those illustrated in Figure 5.17. These patterns were expected, since the influence of the waves inside the lagoon inlet is negligible when compared with the tidal currents.

The comparison between model results and the data shows that the predicted accretion trend located offshore the inlet is not observed, as well as the accretion at the navigation channel (both with predicted changes of approximately 5 m). These accretion trends predicted and not observed might be justified with the regular dredging activities that are performed offshore the inlet and at the navigation channel in order to guaranty the secure navigation.

To compare these results with observations, the sedimentation rates ($m^3 day^{-1}$) in the nine regions defined at the inlet and navigation channel and nearshore region are computed and are illustrated in Figure 6.25.

The analysis of Figure 6.25(a) reveals erosion at most of the overall domain. The erosion trends predicted at the inlet (Region I) and near the tidal gauge (Region IV) are consistent to those observed, however the model underestimate these trends, with rates of approximately 8 and 5 $m^3 year^{-1}$, respectively. At outward regions (Figure 6.25(b)) the model reproduces the observed erosion trends, however with minor magnitude.

The differences between observations and predictions may be explained by several factors.

Near the head of the North breakwater the differences can be justified, as referred in the

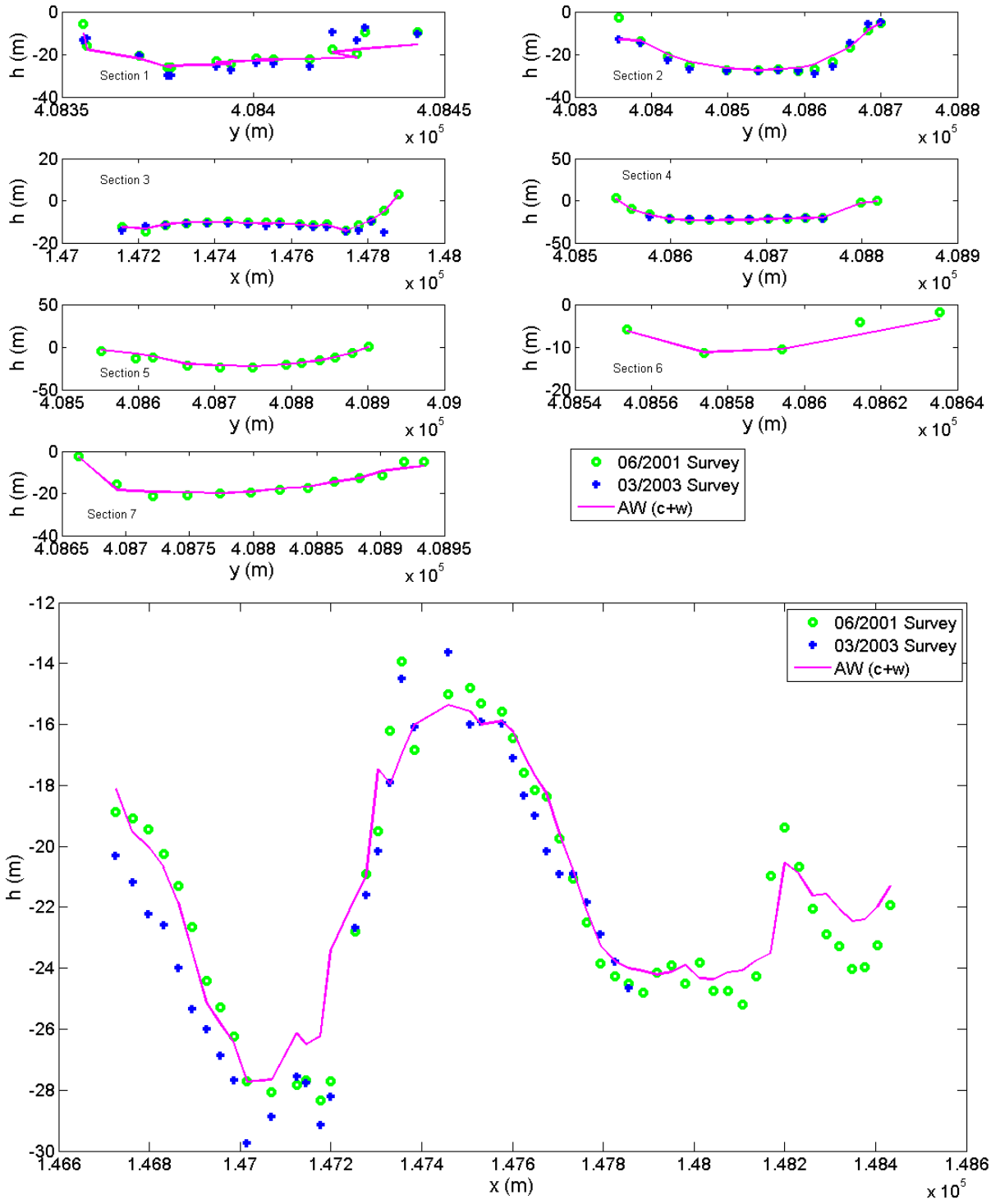

Figure 6.22: Depth along the sections illustrated in Figure 3.7 observed in June 2001 (o) and March 2003 (+) surveys and simulated with the AW formulation for tidal currents and wave regime forcing. The set of figures at the top panel correspond to the sections 1-7 and the figure at the bottom panel correspond to the longitudinal section (dashed line in Figure 3.7). The y (x) values in the x-axis increases from South to North (West to East).

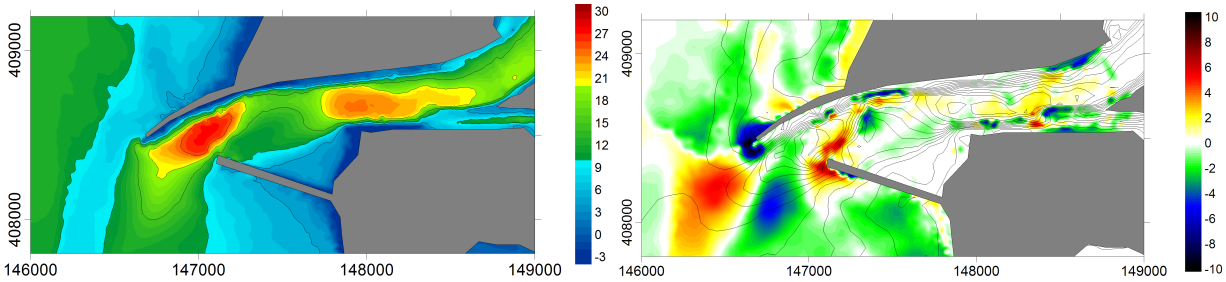

(a) (b)

Figure 6.23: (a) Final bathymetry (metre) of the Ria de Aveiro lagoon inlet computed after 4.25 years and (b) Difference between the computed final and initial bathymetries (metre) for a 4 years simulation forced by tidal currents coupled with a wave regime. In (b) the solid lines illustrate the initial bathymetry. The negative (positive) values represent erosion (accretion). The values in axes are in metres.

previous chapter, by the presence of structural rocks that collapsed from the breakwater and by the emergency works performed in 2004 to repair this structure, that deposited large amount of rocks at the breakwater and near its bottom. Also the scarce survey data close to the structures does not allow reliable analysis.

Considering the analysis performed in Section 4.4.1, where it was observed that the imposed wave height regime is overestimated and recalling the analysis of the results obtained with the numerical model forced by tidal currents and a regular monochromatic wave (Section 6.2.2), a probable justification for the predicted trends near the North and South breakwaters can be made. Considering that the yearly mean wave height is 2-2.5 m and considering that the overestimation of the wave regime imposed is of about 0.7 m, it is possible to perform an analogy between the morphodynamic changes originated by the Wave #3 (H =2.23 m) and Wave #4 (H =3.13 m). Comparing the bathymetric changes illustrated in Figures and , it is observed that the wave regime overestimation induce overpredictions on the erosion trends located North of the North breakwater and on the accretion trends located South of the South breakwater head.

Offshore the inlet is predicted a strong accretion trend which is not observed in the surveys. In fact the wave height overprediction of the imposed regime can generate stronger sediment fluxes directed North-South (approximately one order magnitude), inducing a longshore sediment transport continuously southward even across the inlet. Additionally to this, the absence of this predicted accretion trend in the surveys, can be eventually justified by the regular maintenance dredging works performed by the Aveiro Harbour Administration (due to sand accumulation in the inlet) that remove an unknown amount of sediments.

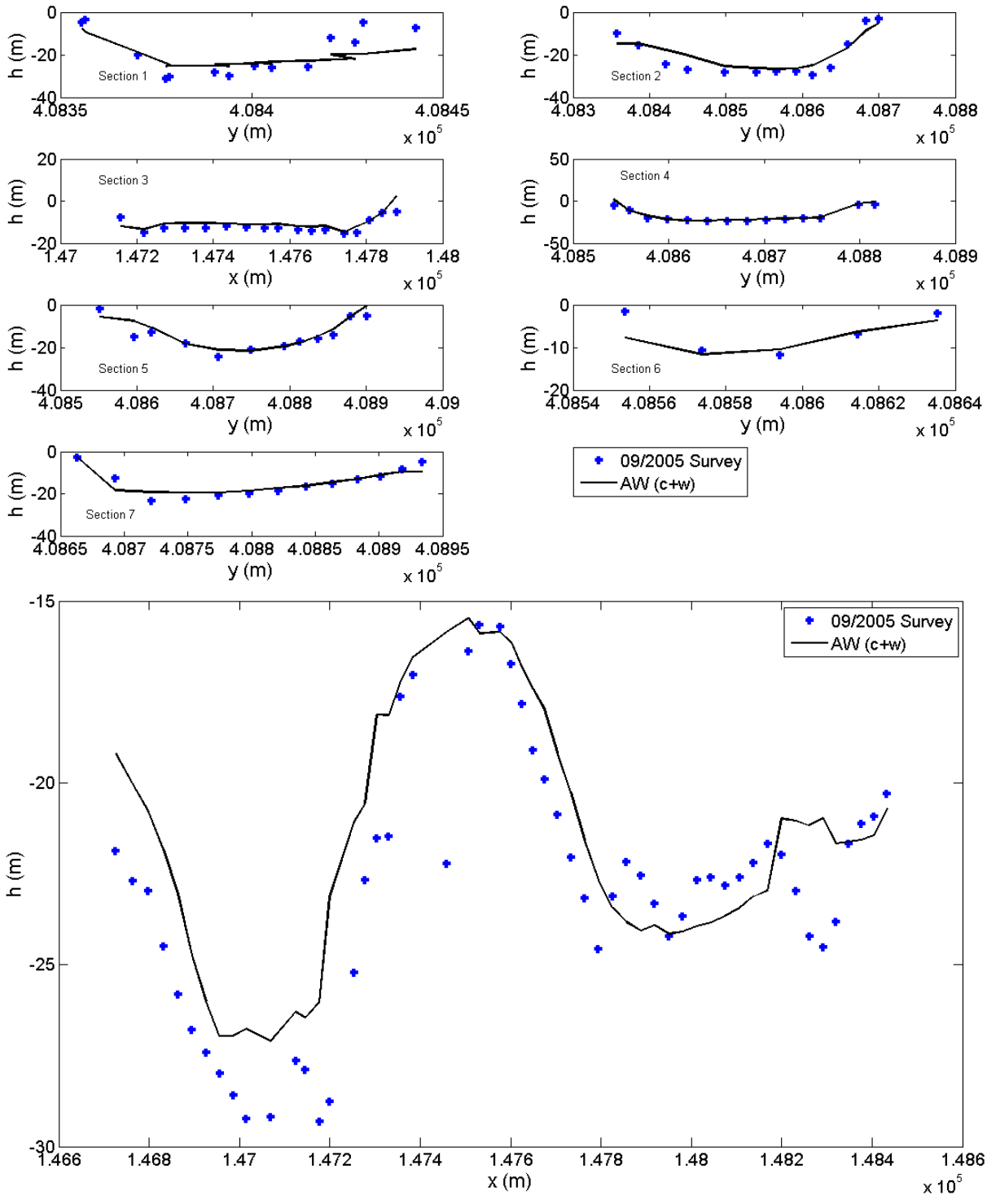

Figure 6.24: Depth along the sections illustrated in Figure 3.7 observed in September 2005 (+) and predicted using AW formulation for coupled forcing of tidal currents and wave regime(-). The set of figures at the top panel correspond to the sections 1-7 and the figure at the bottom panel correspond to the longitudinal section (dashed line in Figure 3.7). The y (x) values in the x-axis increases from South to North (West to East).

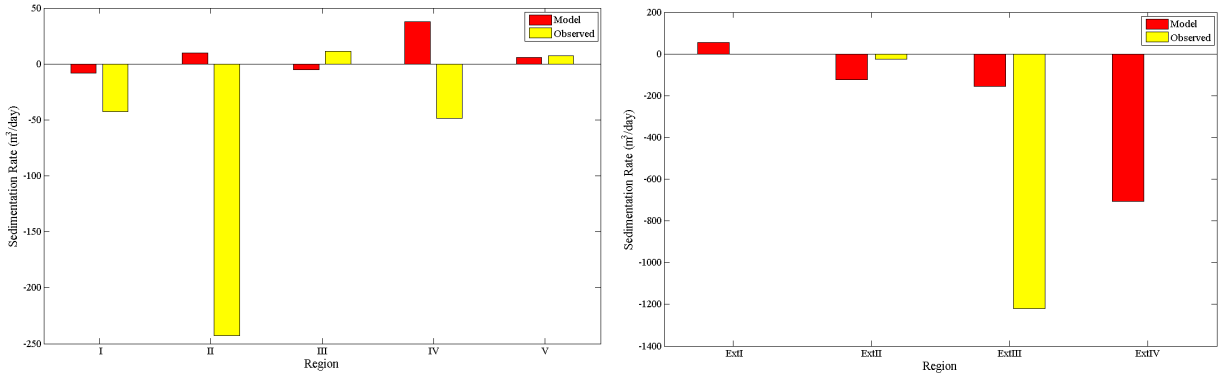

(a) (b)

Figure 6.25: Sedimentation rate ($m^3 day^{-1}$) in the nine regions defined (a) at the inlet and navigation channel and (b) nearshore region.

6.4 Discussion

In this Chapter the waves were considered as coupled forcing with tidal currents in the sediment transport in order to improve the bathymetric predictions accuracy and understand their influence in the morphodynamics of the study area.

The numerical simulations performed considering the Ackers and White [1973], Bijker [1967] and Soulsby [1997] formulations to compute the sediment transport in simulations forced by tidal currents coupled with a wave regime, revealed similar results. The residual fluxes predicted by the SvR formulation are more intense than those obtained by the AW formulation, which are similar to the results obtained with the Bi formulation. However, considering the high sensitivity to sediment size d_{50} of the Bi formulation and the transport overestimation with the SvR formulation, the AW formulation was chosen to compute the sediment transport.

Considering a regular monochromatic wave forcing in the sediment fluxes, the numerical results revealed that waves with heights between 4 m and 5 m are those that mostly contribute to the residual sediment fluxes. Despite the importance of each one of the 8 regular monochromatic waves simulated to the accurate reproduction of the longshore sediment transport, it can be considered that the waves with heights below 1 m and above 5 m are those with the lower contribution to the sediment balance in the study area. This conclusion was enhanced by the analysis of the influence of a storm period in the sediment transport. This simulation revealed that the group of waves with wave height lower than 5 m has a frequency of occurrence of 90% and is responsible for 3/4 of the sediment transport. The storm waves, defined by wave heights higher than 5 m, with only 10% of frequency of occurrence, are responsible for 25% of the sediment transported.

The sediment fluxes in the navigation channel are mainly induced by the seaward tidal cur-

rents, dominating the long term transport in this zone. At the inner sections of the lagoon mouth the fluxes induced by the tidal currents are higher than those produced only by the wave regime, restricting the influence of the waves to the lagoon mouth and adjacent shoreline. At the inlet, the fluxes are still dominated by the seaward tidal currents, however near the northern breakwater, they are affected by the longshore currents, which are generated by the wave regime. At the inlet and adjacent shoreline, the wave regime in addition with the tidal currents forcing induces sediment fluxes magnitudes five times higher than those obtained with only the tidal currents forcing. At the nearshore area, the sediment fluxes are generated by the wave regime and their residual patterns are modified by the northern breakwater.

The residual fluxes patterns and the values for the sedimentation rates illustrate accretion at the northern shoreline of the inlet, whereas erosion was found at the southern shoreline. This pattern is characteristic of this kind of structures along the Portuguese coast, due to the North-South littoral drift.

Through the comparison among the final predicted and observed bathymetric changes between 2001 and March 2003, it was concluded that the wave climate forcing coupled with tidal currents provide better predictions of the trends observed than those obtained considering only the tidal forcing. It were reproduced the offshore migration and inflection of the deeper area between the breakwaters and the erosion trend at the head of the northern jetty, in agreement with the patterns observed in surveyed data.

Comparing the bathymetric changes observed and predicted between June 2001 and September 2005, a few differences were observed and are probably justified by some factors such as the presence of structural rocks that collapsed from the breakwater emergency works performed in 2004 to repair this structure, that deposited large amount of rocks at the breakwater and near its bottom. Also the amounts of sediment that are removed from the offshore inlet area and at the navigation channel by the Aveiro Harbour Administration, due to sand accumulation and that are unknown, contribute to the differences observed.

Considering all the analysis performed in this chapter, it is concluded that the predicted bathymetric changes are in agreement with the erosion and deposition trends observed for the predictions of 1.75 years, which were not rigourously reproduced by the previous numerical simulations, that considered only the tidal currents forcing in the sediment transport fluxes. For longer simulations the overprediction of the wave height regime and therefore the overpredicted sediment fluxes, reveals erosion in regions where the numerical simulations predict accretion.

In conclusion, the inclusion of a wave regime in the numerical simulations increases the accuracy of the morphological predictions. These simulations provided knowledge of the Ria de Aveiro lagoon inlet morphodynamics and could be useful in future studies concerning this study area.

Chapter 7

Conclusions and Future Work

The morphological changes of the *Ria de Aveiro* lagoon inlet and it's relation with the hydrodynamic processes were weakly studied before this study. It was the aim of this work to give a contribution to the knowledge of this lagoon inlet morphodynamic characteristics and dominant processes, through a combination of data analysis and numerical model application. To achieve this goal several information published in literature concerning historical records, bathymetric data collected from surveys and data concerning the bottom sediment size distribution were collected and analyzed. Additionally, the numerical modeling system MORSYS2D was implemented and applied to the *Ria de Aveiro* lagoon inlet in order to understand the processes governing the sediment transport at the inlet and nearshore area.
The historical records of the *Ria de Aveiro* lagoon inlet give the information about the morphological evolution of the inlet and surrounding areas along the years. These data shows that the bathymetric configuration of the lagoon inlet and navigation channel is composed by two deeper areas, with the deepest located between the head of the breakwaters and the other located between the tidal gauge and the *triângulo das marés*. The analysis of the bathymetric data collected between 1987/88 and 2010 by the Administration of the *Ria de Aveiro* lagoon (A.P.A.), revealed an offshore and southward movement of the former deeper area and an infilling of the latter. However, the analysis of the bathymetric changes based on data analysis alone turned out to be very difficult due to the unknown information concerning dredging activities and data collection.
The study area is also characterized by a heterogeneous distribution of the bottom sediment size, with coarser sediments near the North breakwater, which decrease in size up to the *Meia Laranja* Beach. Despite this heterogeneity had been used in the numerical simulations, it was concluded that its influence on the sediment transport fluxes is negligible, being mandatory the navigation channel and breakwaters configuration at the study area. However, the hydrodynamics of the lagoon and the bottom sediment size can be related to the erosion and accretion trends observed: areas with finer sediment correspond to shallow accretion zones characterized by small flow velocities while areas with coarser sediment correspond to

deeper zones where higher flow velocities are observed.

The hydrodynamic model results of this study revealed that the magnitudes of the tidal currents velocity in neap tide conditions are lower than in spring tide conditions. These results also revealed that the *Ria de Aveiro* lagoon has ebb dominance at the inlet and central area and flood dominance at the upstream regions of the lagoon. This tidal asymmetry is characterized by the higher duration of flood currents when compared with the ebb currents.

Additionally to tidal forcing in the sediment transport, the adjacent coast of the *Ria de Aveiro* lagoon inlet is subjected to a highly energetic wave climate, that induces a littoral drift evaluated in a range of 1-2$\times 10^6$ $m^3 year^{-1}$. To study the influence of a single wave in the sediment transport, eight regular monochromatic waves were derived taking into account the principles of conservation of wave power and longshore sediment transport capacity, constituting a simplified wave regime. This simplified wave regime was obtained by grouping the waves by the corresponding incident height or angle. In the present study, wave height classes of intervals of 1 m were grouped and were obtained eight equivalent waves with different heights, periods and directions, having different frequencies of occurrence. This equivalent regime induce a littoral sediment transport of 1.90×10^6 $m^3 year^{-1}$.

The numerical results show that the sediment fluxes observed in the overall study area are not generated by a single forcing, revealing that the tide and the wave regime have different importances on distinct parts of the system. The tidal currents are responsible for the sediment fluxes and consequently bathymetric changes at the navigation channel, also contributing for bottom changes at the inlet, while the influence of the waves is restricted to the lagoon mouth and adjacent shoreline. The tidal sediment fluxes, stronger at the inlet and offshore zone than at the navigation channel, are directed offshore (characteristic of the ebb-dominated coastal systems), exporting sediments and promoting the observed offshore migration of the bedforms. The fluxes at the inlet, near the North breakwater, are also affected by the longshore currents which are generated by the wave regime. At the nearshore area, the presence of the North breakwater interrupts the longshore sediment fluxes.

Additionally, the numerical results show that the waves contributing most for the residual sediment fluxes are those within 4 m and 5 m height. The waves higher than 5 m height, considered storm waves, have approximately 10% of frequency of occurrence and are responsible for 1/4 of the sediment that is transported. The smaller waves are responsible for 75% of the sediment transport, having a frequency of occurrence of 90%.

The sediment fluxes generated by the tide and the wave regime induce different bathymetric changes at the study area: changes at the navigation channel are promoted by the tide, at the inlet are promoted by the coupled effect of tide and waves and at the nearshore area are promoted exclusively by the wave regime. The trends of erosion and accretion observed in the navigation channel were reproduced by the numerical simulations considering the tides as the only sediment transport forcing. When the wave regime is included through coupled forcing, trends at the nearshore area are predicted, consisting in accretion at the North side

of the inlet and erosion at the South side, which is consistent with the observations. Also, the offshore migration and inflection of the deeper area between the breakwaters and the erosion trend at the head of the northern jetty, were numerically reproduced and are in agreement with the patterns observed in the surveyed data.
These numerical results, obtained with the inclusion of the wave regime in the sediment transport forcing improved the accuracy in the predictions of the trends observed, when compared to those obtained when the tidal currents is considered as single forcing. However, the longer simulations showed considerable differences between the observed and the predicted changes.

The differences between the trends predicted and those observed might have several sources such as uncertainties in measurements and numerical errors.
Concerning the data observed, it is known that structural rocks that collapsed from the breakwater are located near the head of the North breakwater. Additionally the data used to validate the numerical predictions have several gaps. The initial bathymetry used in numerical simulations was obtained by coupling surveys from different periods, 1987/88 and 2001, consequently there are regions where the bathymetric evolutions concerns changes from 1987/88 and not from 2001. The regions close to the structures are not sampled in all surveys illustrating trends that doesn't occur in reality. Additionally, the surveyed data is interpolated generating errors in the numerical bathymetries and consequently in the numerical predictions. A very relevant uncertainty lies in the lack of information about the dredging activities performed in the study area. In fact, the periods, areas and amounts of sediments removed from the study area are not known, increasing the difficulty of the bathymetric changes analysis disregarding anthropogenic actions.
Numerically, despite the errors induced by neglecting physical processes (e.g. effect of the wave interaction with currents, the energy generation and dissipation by wind and the effect of wave diffraction), each model component induce errors in the predictions.
Hydrodynamically it is considered that the tidal dynamics is quite well reproduced by the model since the errors in the SSE reproduction are considered small and similar to the works published in the literature. However, it was observed that the amplitude of the M_2 first harmonic (M_4) is underestimated by the model predictions. This underestimation might induce a reduction of the amount of sediments that are exported due to the attenuation of the tidal distortion and consequently the lower residual currents and the lower sediment transport fluxes towards the adjacent ocean. When performing long period morphodynamic simulations, the M_4 amplitude underestimation in the hydrodynamic model may result in the underestimation of the erosion trend observed in the region between the head of the south breakwater and the *tidal gauge*, and in the overestimation of the accretion trends between the *tidal gauge* and the *triângulo das marés*.
Concerning the wave model, the simplifications performed by neglecting non-linear and

generation terms (enumerated in the models setup section) induce inaccuracies in the reproduction of the observed wave regime characteristics and processes. It was also observed that the wave regime imposed is an overestimation of the regime observed at the Leixões buoy. Indeed, an overestimation of approximately 70 cm of wave height might induce an overestimation of the sediment fluxes of almost one order of magnitude. This overestimation induces not only higher bathymetric changes at the nearshore area of the Ria de Aveiro lagoon inlet but also in the region within the lagoon closer to the inlet. Indeed the wave regime overestimation may induce overpredictions on the erosion trends located North of the North breakwater, and on the accretion trends located South of the South breakwater head. Additionally, the predicted strong accretion trend offshore the inlet (not observed in the surveys), might be generated by the overestimated longshore sediment transport across the inlet. Furthermore, the absence of this predicted accretion trend in the surveys, can be eventually justified by unknown amounts of sediments removed through regular maintenance dredging works performed by the Aveiro Harbour Administration, due to sand accumulation in the inlet.
These uncertainties are inputs of the formulations that evaluate the sediment transport and consequently the morphodynamic predictions. Additionally, the formulations are very sensitive to small variations in the sediment size, the velocity or tidal constituents. Therefore, a small error in these characteristics is amplified in the sediment fluxes computation. These formulations, on the other hand, were developed and calibrated for specific environments, inducing inaccuracies on the sediment transport evaluation in a real and complex system as the Ria de Aveiro lagoon inlet.

In summary and considering the main research questions of this work (Chapter 1.1) it is concluded that in the *Ria de Aveiro* lagoon inlet and nearshore area the bathymetric trends at the navigation channel are originated by the tidal currents, at the nearshore area originated by the wave regime and at the inlet by both forcings. The configuration of the lagoon's inlet controls the sediment fluxes pattern, which are directed offshore at the navigation channel, where accretion is observed and leads to an infilling of the deeper area located between the tidal gauge and the *triângulo das marés*. At the inlet the sediment fluxes are dominated by the tidal currents when the wave heights are small and surpassed at the offshore region by the influence of the wave regime when storm waves occur. In this region is observed erosion and an offshore and southward propagation of the deeper area. At the nearshore area it is observed accretion at the North side of the inlet and erosion at South as a result of the North-South longshore sediment fluxes generated by the wave regime. These sediment fluxes are interrupted by the North breakwater originating a strong erosion pattern near its head. In this study area the storm waves, despite the low frequency of occurrence, have an important influence on the rate of the sediment transport when compared with the most frequent and lower height waves, reaching 25% of the total transport.

Considering the numerical results obtained it is believed that if dredging operations weren't performed, a strip of shallower depths would be observed offshore the inlet. Also a strong erosion near the head of the North breakwater would approach the bathymetric contour of 15 m depth to this structure, endangering its stability.

The conclusions presented in this thesis are restricted by the limitations of the work itself, namely those concerning the amount and quality of the data available. In fact, the basis of an accurate modeling study lies in the knowledge of good quality data to define the initial conditions and to calibrate the numerical predictions. The study performed herein would benefit if there was a wave directional buoy near Aveiro to provide the characteristics of the wave regime at the *Ria de Aveiro* lagoon inlet, in spite of using wave records from buoys located far from the study area. Also, the accuracy of the predictions could improve if regular bathymetric surveys data were available in the overall domain as well as the knowledge of the exact amount of sediment that is withdrawn at dredging activities, in order to reproduce accurately the sedimentation rates observed. Additionally, a good knowledge of the bottom sediment size distribution, despite its low influence in the sediment transport, might improve the predictions. Future works would benefit if these data were available.

Concerning the numerical model, the sediment transport was computed using formulations that evaluate the bottom transport and estimate the suspended load, however the total transport would be more accurate if a description of the sediment fluxes above the bed was implemented in the model.

The research developed in this study opens new avenues of investigation for the future. On the numerical modeling side, the morphodynamic modeling system MORSYS2D can be further improved through the integration of a suspended sediment transport module, rather than just using a total transport empirical formulae. This improvement will allow an accurate estimation of the suspended sediment transport, important in the case of non steady effects resulting from phase lags between the sediment and the flow regimes.

The current application of MORSYS2D to the Aveiro lagoon can also improved, through more complete set of forcings. For instance, previous studies [Dias et al., 2011b,c] showed that the occurrence of storm surges at the Aveiro coast produce an increase in the water level and in the tidal amplitude in Ria de Aveiro lagoon, influencing the tidal currents and the tidal prism. These modifications in the hydrodynamics induce changes in the sediment transport, that could modify the inlet bathymetry and therefore constitute an interesting challenge to evaluate through future morphodynamic simulations. This work can also constitute the basis to study the influence of hydrodynamic changes or modifications at the study area morphology on the sediment transport and consequently on the bathymetric trends and changes, essential to understand and predict the future evolution of the Ria de Aveiro lagoon.

As consequence of the climate changes, a sea level rise is expected at the Portuguese coast, as well as modifications on the wave regime, such as a clockwise rotation of 5^o to 15^o in the

future wave climate direction, relative to present conditions [Dodet et al., 2010]. Previous studies [Lopes et al., 2011; Dias et al., 2011c] on the Ria de Aveiro hydrodynamics show that the sea level rise will increase the tidal amplitude and velocity, inducing an increase in the tidal prism. The rotation of the wave regime has a direct influence on the longshore transport, enlarging the future coastal erosion by 15 to 25%. These changes in the tide and wave regime characteristics modify the forcing agents of the sediment transport fluxes. Consequently the study of the impact of the climate change in the bathymetry of the lagoon should be considered as research to perform in the future.

Other example of future applications of the products developed in this thesis lies in the study of possible long term morphologic changes of the inlet channel induced by anthropogenic interventions. The modification of its geometry and bathymetry, due for instance to the intent of the Aveiro Harbor Administration to extend the North breakwater and perform dredging works outside the inlet, in order to allow the navigation of larger ships to the inner harbour, will have an impact on the morphology of the system that needs to be quantified. Previous studies [WW - Consultores em Hidráulica e Obras Marítimas SA, 2009; Dias and Mariano, 2011; Dias et al., 2011c] concerning the influence of these works in the hydrodynamics of the lagoon revealed that the differences found are not very large. In fact, minor changes were predicted for the tidal propagation along the lagoon or for the tidal amplitude, but some differences on the tidal currents close to the North breakwater were identified. However, these studies did not take into account the long period morphological changes. Despite the fact that expected hydrodynamic changes are small, they may modify the sediment transport and intensify the accretion and erosion trends observed, changing the inlet bathymetry along the next years. Furthermore, previous studies [Araújo et al., 2008; Dias et al., 2011a] on Ria de Aveiro lagoon concluded that changes at the inlet water depth have influence in the entire lagoon hydrodynamics. Additionally, changes at the breakwaters configuration will interfere with the longshore sediment transport and consequently with the sedimentation rates observed, possibly increasing the accretion at the North side of the inlet and the erosion problems at the beaches South of the inlet lagoon

The study of all these processes should be considered as challenging topics to research in the near future.

Chapter 8

Appendix

In this Appendix the bathymetries of the Ria de Aveiro lagoon inlet obtained through surveys and interpolated through the Nearest Neighbor method are presented.

Figure 8.1: Bathymetry in meters of the Ria de Aveiro lagoon inlet corresponding to the interpolated surveys of (from left to right, top to bottom): 1987/88, June 2001, March 2003, July 2003, September 2003, November 2003, March 2004, September 2004 and October 2004. The values in the axis are in metres.

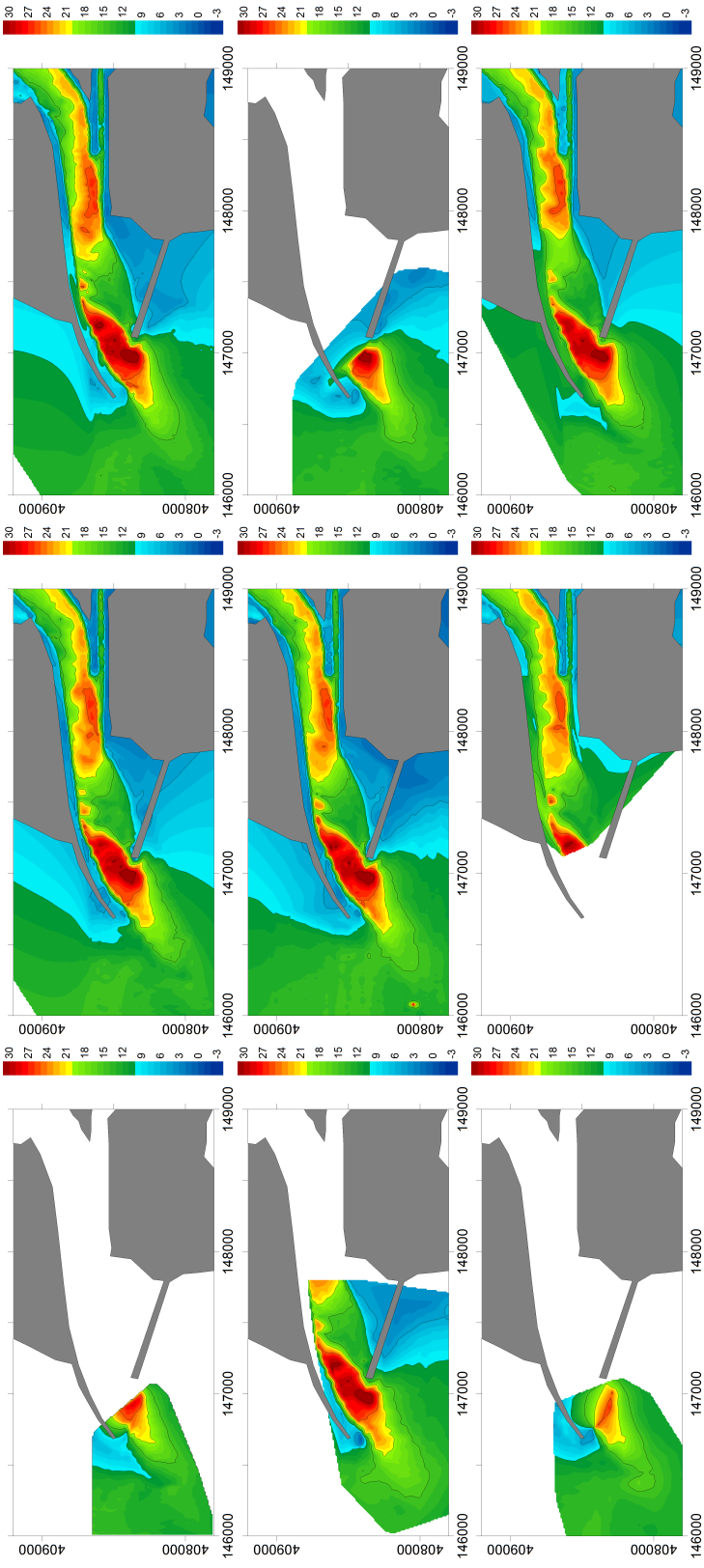

Figure 8.2: Bathymetry in meters of the Ria de Aveiro lagoon inlet corresponding to the interpolated surveys of (from left to right, top to bottom): March 2005, September 2005, October 2006, May 2007, September 2007, January 2008, June 2008, December 2008 and June 2010. The values in the axis are in metres.

Bibliography

Abrantes I., Dias J.M. and Rocha F. (2006). Spatial and temporal variability of suspended sediments concentration in Ria de Aveiro lagoon and fluxes between the lagoon and the ocean. *Journal of Coastal Research*, SI39:718–723.

Ackers P. and White W.R. (1973). Sediment transport: a new approach and analysis. *Journal of the Hydraulics Division*, 99:2041–2060.

Aires J.P., Nogueira J. and Martins H. (2005). Survival of sardine larvae off the Atlantic Portuguese coast: a preliminary numerical study. *ICES Journal of Marine Science*, 62:634–644.

Andrade C., Freitas M.C., Cachado C., Cardoso A.C., Monteiro J.H., Brito P. and Rebelo L. (2002). *Coastal zones. Climate change in Portugal. Scenarios, impacts and adaptation measures. SIAM Project.* Tech. Rep., 173–219.

Andrade C., Teixeira S., Reis R. and Freitas C. (1996). *The Record of Storminess of the Portuguese NW Coast in Newspaper Sources.* Partnership in Coastal Zone Management, Samara Publishing, 159–166.

Araújo I., Dias J.M. and Pugh D. (2008). Model simulations of tidal changes in a coastal lagoon, the Ria de Aveiro (Portugal). *Continental Shelf Research*, 28:1010–1025.

Araújo I.G.B. (2005). *Sea Level Variability: Examples from the Atlantic Coast of Europe.* PhD Thesis, School of the National Oceanography Centre, Southampton, UK.

Aubrey D.G. and Speer P.E. (1985). A study of non-linear tidal propagation in shallow inlet/estuarine systems, part 1: observations. *Estuarine Coastal and Shelf Science*, 21:185–205.

Barnes R.S.K. (1980). *Coastal Lagoons.* Cambridge: Cambridge University Press, 106 pp.

Bastos M.R. (2009). On the track of salt: Adding value to the history of saltponds exploration in the coastal management scene of Aveiro lagoon. *Journal of Integrated Coastal Zone Management*, 9(3):25–43.

Bertin X., Fortunato A.B. and Oliveira A. (2007). Sensitivity analysis of a morphodynamic modeling system applied to a Portuguese tidal inlet. In *5th IAHR Symposium on River, Coastal and Estuarine Morphodynamics*. Netherlands, 11–17.

Bertin X., Fortunato A.B. and Oliveira A. (2009a). A modeling-based analysis of processes driving wave-dominated inlets. *Continental Shelf Research*, 29(5):819–834.

Bertin X., Fortunato A.B. and Oliveira A. (2009b). Morphodynamic modeling of the Ancão inlet, South Portugal. *Journal of Coastal Research*, SI56:10–14.

Bertin X., Oliveira A. and Fortunato A.B. (2009c). Simulating morphodynamics with unstructure grids: Description and validation of a modeling system for coastal applications. *Ocean Modelling*, 28:75–87.

Bhattacharya B., Price R.K. and Solomati D.P. (2007). A machine learning approach to modeling sediment transport. *Journal of Hydraulic Engineering*, 133(4):440–450.

Bijker E.W. (1967). *Some considerations about scales for coastal models with moveable bed.* PhD dissertation, Delft University of Technology, Netherlands, 150 pp.

Bijker E.W. (1971). Longshore transport computations. *Journal of Waterway, Ports, Harbor, Coastal and Ocean Engineering*, 97(4):687–703.

Booij N., Ris R. and Holthuijsen L. (1999). A third-generation wave model for coastal regions. 1. Model description and validation. *Journal of Geophysical Research*, 104(7):7649–7666.

Brown J.M. and Davies A.G. (2010). Flood/ebb tidal asymmetry in a shallow sandy estuary and the impact on net sand transport. *Geomorphology*, 114:431–439.

Bruneau N., Fortunato A.B., Oliveira A., Bertin X., Costa M. and Dodet G. (2010). Towards long-term simulations of tidal inlets: performance analysis and application of a partially parallelized morphodynamic modeling system. In *XVIII International Conference on Water Resources*. Spain.

Bruun P. and Gerritsen F. (1959). Natural by-passing of sand at coastal inlets. *Journal of the Waterways and Harbours Division*, 75–107.

Bruun P. and Gerritsen F. (1960). *Stability of Coastal Inlets.* North Holland Publishing Co., Amsterdam, The Netherlands, 123 pp.

Bruun P., Mehta A.J. and Jonsson I.G. (1978). *Stability of Tidal Inlets: Theory and Engineering*, Vol. 23 of *Developments in Geotechnical Engineering.* Elsevier Scientific Publishing Co., Amsterdam, The Netherlands, 510 pp.

Capitão R.P., Fortes C.J. and Carvalho M.M. (1997). *Análise da dinâmica costeira no troço Cabo Mondego - Estuário do Mondego. Erosões em Buarcos. Estudo de agitação marítima.* Tech. Rep. 167/97 NPP, LNEC, Lisbon, Portugal, 28 pp.

Carmo J.S.A. (1995). *Contribuição para o Estudo dos Processos Morfodinâmicos em Regiões Costeiras e Estuarinas.* PhD dissertation, University of Coimbra, Portugal, 238 pp.

Cayocca F. (2001). Long-term morphological modeling of a tidal inlet: the Arcachon Basin, France. *Coastal Engineering*, 42:115–142.

CEM (2002). *Coastal Engineering Manual.* US Army Corps of Engineers.

Chonwattana S., Weesakul S. and Vongvisessomjai S. (2005). 3D Modeling of morphological changes using representative waves. *Coastal Engineering Journal*, 47(4):205–229.

Coelho C.D.B. (2005). *Riscos de Exposição de Frentes Urbanas para Diferentes Intervenções de Defesa Costeira.* PhD dissertation, University of Aveiro, Portugal, 404 pp.

Coli A.B. (2003). Estimação de regimes de agitação marítima em locais onde não existam dados. In *3as Jornadas Portuguesas de Engenharia Costeira e Portuária.* Aveiro, Portugal.

Costa M., Baptista R. and Rusu L. (2003). Vinte anos de dados de agitação marítima na costa Portuguesa. In *3as Jornadas Portuguesas de Engenharia Costeira e Portuária.* Aveiro, Portugal.

Cunha M.A., Dias J.M., Almeida M.A., Lopes J.F. and Alcântara F. (2003). Fluxes of bacterioplankton between a tidal estuary and the sea: returning to the "outwelling hypothesis". *Aquatic Ecology*, 37:45–54.

Davidson M.A., Morris B.D. and Turner I.L. (2009). A simple numerical model for inlet sedimentation at intermittently open-close coastal lagoons. *Continental Shelf Research*, 29:1975–1982.

de Vriend H.J. (1996). Mathematical modelling of meso-tidal barrier island coasts. part I and II: Empirical and semi-empirical models. *Advances in Coastal and Ocean Engineering*, 2:115–197.

Dias J.A., Ferreira .M.F.C. and Pereira A.P.R.R. (1994). *Estudo Sintético da Geomorfologia e da Dinâmica Sedimentar dos Troços Costeiros entre Espinho e a Nazaré.* Estudos de Ambiente e Informática, Lda, 261 pp.

Dias J.M. (2001). *Contribution to the Study of the Ria de Aveiro Hydrodynamics.* PhD dissertation, University of Aveiro, Portugal, 288 pp.

Dias J.M., Abrantes I. and Rocha F. (2007). Suspended particulate matter sources and residence time in a mesotidal lagoon. *Journal of Coastal Research*, SI50:1034–1039.

Dias J.M., Araújo I. and Picado A. (2011a). Dinâmica da maré na Ria de Aveiro. In *Jornadas da Ria de Aveiro*. University of Aveiro, 169–177.

Dias J.M., Fonseca A., Picado A., Lopes C.L., Silva J., Vaz L., Sousa M., Vaz N., Mendes R. and Plecha S. (2011b). *Estudos da Evolução e da Dinâmica Costeira e Estuarina da Ria de Aveiro in the scope of Polis Litoral da Ria de Aveiro*. Tech. Rep. 2, University of Aveiro, Portugal, 147 pp.

Dias J.M. and Lopes J.F. (2006). Implementation and assessment of hydrodynamic, salt and heat transport models: the case of Ria de Aveiro lagoon (Portugal). *Environmental Modelling and Software*, 21:1–15.

Dias J.M., Lopes J.L. and Dekeyser I. (1999). Hydrological characterisation of Ria de Aveiro, Portugal, in early Summer. *Oceanologia Acta*, 22(5):473–485.

Dias J.M., Lopes J.L. and Dekeyser I. (2000). Tidal propagation in Ria de Aveiro lagoon, Portugal. *Physics and Chemistry of the Earth*, 25(4):369–374.

Dias J.M., Lopes J.L. and Dekeyser I. (2003). A numerical model system application to the study of the transport properties in Ria de Aveiro lagoon. *Ocean Dynamics*, 53(3):220–231.

Dias J.M. and Mariano S. (2011). Numerical modelling of hydrodynamic changes induced by a jetty extension – the case of Ria de Aveiro (Portugal). *Journal of Coastal Research*, SI64:1008–1012.

Dias J.M. and Picado A. (2011). Impact of morphologic anthropogenic and natural changes in estuarine tidal dynamics. *Journal of Coastal Research*, SI64:1490–1494.

Dias J.M., Picado A., Lopes C.L., Silva J., Vaz L., Sousa M., Vaz N., Mendes R. and Plecha S. (2011c). *Estudos da Evolução e da Dinâmica Costeira e Estuarina da Ria de Aveiro in the scope of Polis Litoral da Ria de Aveiro*. Tech. Rep. 5, University of Aveiro, Portugal, 246 pp.

Dias J.M., Sousa M.C., Bertin X., Fortunato A.B. and Oliveira A. (2009). Numerical modeling of the impact of the Ancão inlet relocation (Ria Formosa, Portugal). *Environmental Modeling and Software*, 24:711–725.

Dodet G., Bertin X. and Taborda R. (2010). Wave climate variability in the North-East Atlantic Ocean over the last six decades. *Ocean Modeling*, 31(3-4):120–131.

Dronkers J. and van de Kreeke J. (1986). Experimental determination of salt intrusion mechanisms in the Volkerak Estuary. *Netherlands Journal of Sea Research*, 20:1–19.

Dyer K.R. (1997). *Estuaries. A Physical Introduction.* John Wiley & Sons, 195 pp.

Engelund F. and Hansen F. (1967). *A Monograph of Sediment Transport in Alluvial Channels.* 168 pp.

Ferreira O. (1993). *Caracterização dos Principais Factores Condicionantes do Balanço Sedimentar e da Evolução da Linha de Costa entre Aveiro e o Cabo Mondego.* MSc dissertation, University of Lisbon, 168 pp.

Ferreira O., Dias J.A. and Taborda R. (2008). Implications of sea-level rise for Continental Portugal. *Journal of Coastal Research*, 24(2):317–324.

Ferreira O.M.F.C. (1998). *Morfodinâmica de Praias Expostas: Aplicação ao Sector Costeiro Aveiro - Cabo Mondego.* PhD dissertation, University of Algarve, Portugal, 337 pp.

Fitzgerald D.M. (1988). *Shoreline Erosional-depositional Processes Associated with Tidal Inlets*, Vol. 29 of *Lecture notes on coastal and estuarine studies. Hydrodynamics and Sediment Dynamics of tidal inlets.* D.G. Aubrey, L.Weishar (Eds), 186–225.

Fitzgerald D.M., Hubbard D.K. and Nummedal D. (1978). Shoreline Changes Associated with Tidal Inlets along the South Carolina Coast. In *Proceedings Coastal Zone '78.* American Society of Civil Engineers, New York, 1973–1994.

Fortunato A.B. (2006). *Modelação numérica da dinâmica sedimentar em embocaduras.* Thesis presented to obtain the title to performing scientific coordinations, LNEC.

Fortunato A.B., Bertin X. and Oliveira A. (2009). Space and time variability of uncertainty in morphodynamic simulations. *Coastal Engineering*, 56:886–894.

Fortunato A.B. and Oliveira A. (2000). On the representation of bathymetry by unstructured grids. In *Computational Methods in Water Resources XIII* (*et al.* L.R.B., ed.), Vol. 2. Balkema, 889–896.

Fortunato A.B. and Oliveira A. (2003). A modeling system for tidally driven long-term morphodynamics. *Journal of Hydraulic Research*, 42(4):426–434.

Fortunato A.B. and Oliveira A. (2004). Um modelo morfodinâmico para estuários baseado em malhas não-estruturadas. *Applied Computing Engineering Journal*, 3(2):87–93.

Fortunato A.B. and Oliveira A. (2006). Uma comparação de métodos para melhorar a estabilidade de um sistema de modelos morfodinâmico. In *Conferência Nacional de Métodos Numéricos em Mecânica dos Fluidos e Termodinâmica.* Portugal.

Fortunato A.B. and Oliveira A. (2007). Improving the stability of a morphodynamic modeling system. *Journal of Coastal Research*, SI50:486–490.

Fortunato A.B., Pinto L., Oliveira A. and Ferreira J.S. (2002). Tidally generated shelf waves off the western Iberian coast. *Continental Shelf Research*, 22:1935–1950.

Fredsøe J. and Deigaard R. (1992). *Mechanics of Coastal Sediment Transport*, Vol. 3 of *Advanced Series on Ocean Engineering*. World Scientific Publishing Co Pte Ltd, 369 pp.

Freitas R., Sampaio L., Rodrigues A. and Quintino V. (2005). Sea-bottom classification across a shallow water bar channel and near-shore shelf, using single-beam acoustics. *Estuarine Coastal and Shelf Science*, 65:625–632.

Friedrichs C.T. and Aubrey D.G. (1988). Non-linear tidal distortion in shallow well-mixed estuaries: a synthesis. *Estuarine Coastal and Shelf Science*, 27:521–545.

Grunnet N.M., Walstra D.J.R. and Ruessink B.G. (2004). Process-based modelling of a shoreface nourishment. *Coastal Engineering*, 51:581–607.

Guerreiro M., Fortunato A.B., Oliveira A., Bertin X., Bruneau N. and Rodrigues M. (2010). Simulation of morphodynamic processes in small coastal systems: application to the Aljezur coastal stream (Portugal). In *Geophysical Research Abstracts*, Vol. 12.

Hayes M.O. (1979). *Barrier Island Morphology as a Function of Tidal and Wave Regime*. Leatherman, S.P. (ed) Barrier Islands. New York, Academic Press, 1–28.

Heap A., Bryce S., Ryan D., Radke L., Smith C., Smith R., Harris P. and Heggie D. (2001). *Australian estuaries and coastal waterways: A geoscience perspective for improved and integrated resource management*. Tech. Rep. AGSO Record 2001/07, National Land and Water Resources Audit, 118 pp.

Hibma A. (1999). *Process-based Modelling of Tidal Inlet Dynamics. Evaluation of Frisian Inlet Data*. MSc thesis, Delft University of Technology, 177 pp.

Hibma A., Stive M.J.F. and Wang Z.B. (2004). Estuarine morphodynamics. *Coastal Engineering*, 51:765–778.

Hidroprojecto (1995). *Estudos especializados de modelação matemática para a barra de Aveiro*. Tech. Rep. Final, Hidroprojecto, JAPA, Lisbon, Portugal, 56 pp.

Kamphuis J.W. (1991). Alongshore sediment transport rate. *Journal of Waterway Port Coastal and Ocean Engineering (ASCE)*, 117(6):624–641.

Kamphuis J.W., Davies M.H., Nairn R.B. and Sayao O.J. (1986). Calculation of littoral sand transport rate. *Coastal Engineering*, 10(1):1–21.

Karim M.F. and Kennedy J.F. (1990). Menu of coupled velocity and sediment discharge relation for rivers. *Journal of Hydraulic Engineering*, 116(8):978–996.

Komar P.D. and Inman D.L. (1970). Longshore sand transport on beaches. *Journal of Geophysical Research*, 75(30):5514–5527.

Kraus N.C., Gingerich K.J. and Rosati J.D. (1988). Towards an improved empirical formula for longshore sand transport. In *Proceedings of the 21st International Conference on Coastal Engineering* (ASCE, ed.). New York, 1183–1196.

Laboratoire d'Hydraulique de France (1997). *Telemac System — Presentation document.*

Larangeiro S.H.C.D. and Oliveira F.S.B.F. (2003). Assessment of the longshore sediment transport at Buarcos beach (West coast of Portugal) through different formulations. In *CoastGis'03*. Genova.

Larangeiro S.H.C.D., Oliveira F.S.F.B. and Taborda R.P.M. (2005). Application of formulations and models to estimate the longshore sediment transport between Praia da Vieira and Praia Velha, West coast of Portugal. In *International Conference on Coastal Conservation and Management 2005*. Tavira, Portugal, 309–310.

LNEC (1989). *Caracterização de Aspectos Fisiográficos de Praias da Costa Portuguesa. Orla Litoral da Ria de Aveiro.* Tech. Rep. 244/94 NET, LNEC, Lisbon, Portugal.

Longuet-Higgins M.S. and Stewart R.W. (1964). Radiation stress in water waves; a physical discussion, with applications. *Deep-Sea Research*, 11:529–562.

Lopes C.B., ad P. Pato A.I.L., Dias J.M., Rodrigues S.M., Pereira E. and Duarte A.C. (2008). Inputs of organic carbon from Ria de Aveiro coastal lagoon to the Atlantic Ocean. *Estuarine, Coastal and Shelf Science*, 79:751–757.

Lopes C.L., A.Silva P., Dias J.M., Rocha A., Picado A., Plecha S. and Fortunato A.B. (2011). Local sea level changes cenarios for the end of the 21st century and potential physical impacts in the lower Ria de Aveiro (Portugal). *Continental Shelf Research*, 31:1515–1526.

Lopes C.L., Silva P.A., Dias J.M., Rocha A., Picado A. and Plecha S. (2010). Impacts of sea level rise in Ria de Aveiro lagoon during 21st century. In *First International Conference on Coastal Zone Management of River Deltas and Low Land Coastlines*. Alexandria, Egypt.

Lopes J.F. and Dias J.M. (2007). Residual circulation and sediments transport in Ria de Aveiro lagoon, Portugal. *Journal of Marine Systems*, 68:507–528.

Lopes J.F., Dias J.M. and Dekeyser I. (2001). Influence of tides and river inputs on suspended sediment transport in the Ria de Aveiro lagoon, Portugal. *Physics and Chemistry of the Earth*, 26(9):729–734.

Lopes J.F., Dias J.M. and Dekeyser I. (2006). Numerical Modelling of Cohesive Sediments Transport in the Ria de Aveiro Lagoon. *Journal of Hydrology*, 319:176–198.

Martins V., Grangeia C., Jesus C.C., Martins P., Laut L.M., Sequeira C., Dias J.M., Silva P.A., Abrantes I., da Silva E.F. and Rocha F. (2011). Erosion and accretion in the Ria de Aveiro inlet (N Portugal) and exportation of fine–grained sediments to the shelf. *Journal of Iberian Geology*, 37(2):215–230.

Martins V., Jesus C.C., Abrantes I., Dias J.M. and Rocha F. (2009). Suspended particulate matter vs. bottom sediments in a mesotidal lagoon (Ria de Aveiro, Portugal). *Journal of Coastal Research*, SI36:1370–1374.

Martins V., Rodrigues S., Grangeia C., Bernardes C., Silva P., Dias J.M. and Rocha F. (2007). Sediments erosion/deposition in the Ria de Aveiro inlet. In *Book of Abstracts ISMS07, International Symposium in Marine Sciences*. Spain.

Meyer-Peter E. and Muller R. (1948). Formulas for bed-load transport. In *Proceedings of the 3^{rd} Meeting IAHR*. Sweden, 39–64.

Moore R.D., Wolf J., Souza A.J. and Flint S.S. (2009). Morphological evolution of the Dee Estuary, Eastern Irish Sea, UK: a tidal asymmetry approach. *Geomorphology*, 103:588–596.

Moreira E. and Gomes E. (2001). Reabilitação do molhe Norte do porto de Aveiro. In *2^{as} Jornadas Portuguesas de Engenharia Costeira e Portuária*. Sines, Portugal.

Moreira H.M., Queiroga H., Machado M.M. and Cunha M.R. (1993). Environmental gradients in a southern estuarine system: Ria de Aveiro, Portugal, implication for soft bottom macrofauna colonization. *Netherlands Journal of Aquatic Ecology*, 27:465–482.

Neves R.J.J., Leitão P.C., Braunschweig F., Martins F., Coelho H., Santos A. and Miranda R. (2000). The advantage of a generic coordinate approach for ocean modeling. In *Proceedings of Hydrosoft 2000 Conference*. Lisbon, Portugal, 25–34.

Nicholson J., Broker I., Roelvink J.A., Price D., Tanguy J.M. and Moreno L. (1997). Intercomparison of coastal area morphodynamic models. *Coastal Engineering*, 31(1):97–123.

O'Brien M.P. (1969). Flow Areas of Inlets on Sandy Coasts. *Journal of the Waterways and Harbours Division*, 95:43–52.

Oliveira A., Fortunato A.B. and Dias J.M. (2007). Numerical modeling of the Aveiro inlet dynamics. In *Proceedings of the 30^{th} International Conference on Coastal Engineering* (Co W.S.P., ed.), Vol. 4. 3282–3294.

Oliveira A., Fortunato A.B. and Rego J.R.L. (2006). Effect of morphological changes on the hydrodynamics and flushing properties of the Óbidos lagoon (Portugal). *Continental Shelf Research*, 26(8):917–942.

Oliveira A., Fortunato A.B. and Sancho F.E.P. (2005). Morphodynamic modeling of the Óbidos lagoon. In *Proceedings of the 29th International Conference on Coastal Engineering* (ASCE, ed.), Vol. 3. 2506–2518.

Oliveira I.M., Valle A.F. and Miranda F. (1982). Litoral problems in the portuguese west coast. In *Coastal engineering 1982 Proceedings*, Vol. III. 1951–1969.

Parker B.B. (1991). *The Relative Importance of the Various Non-linear Mechanisms in a Wide Range of Tidal Interactions.* Parker B. B. (Ed.), Tidal Hydrodynamics. Wiley, New York, USA, 237–268.

Pato P., Lopes C., Válega M., Lillebø A.I., Dias J.M., Pereira E. and Duarte A.C. (2008). Mercury fluxes between an impacted coastal lagoon and the Atlantic Ocean. *Estuarine Coastal and Shelf Science*, 76(4):787–796.

Phillips O.M. (1977). *The Dynamics of the Upper Ocean.* 2nd ed, Cambridge University Press.

Picado A. (2008). *Degradation of the salt pans in Ria de Aveiro: An Hydrodynamical Study.* MSc Thesis, University of Aveiro, 68.

Picado A., Dias J.M. and Fortunato A.B. (2010). Tidal changes in estuarine systems induced by local geomorphologic modifications. *Continental Shelf Research*, 30(17):1854–1864.

Pinto L., Fortunato A.B. and Freire P. (2006). Sensitivity analysis of non-cohesive sediment transport formulae. *Continental Shelf Research*, 26:1826–1829.

Pinto L.L.M.A. (2010). *Modelação da Morfodinâmica de Estuários.* PhD dissertation, University of Coimbra, Portugal, 188 pp.

Pires A.R., Freitas M.C., Andrade C., Taborda R., Ramos R., Pacheco A., Ferreira O., Bezerra M. and Cruces A. (2011). Morphodynamics of an ephemeral tidal inlet during a life cycle (Santo Andr'e lagoon, SW Portugal). *Journal of Coastal Research*, SI64:1565–1569.

Pita C. and Santos J.A. (1989). *Análise dos Temporais da Costa Oeste de Portugal Continental.* Tech. Rep. Report $PO-WAVES$ $1/89-A$, $IH/LNEC$, 29 pp.

Plecha S., Lopes C.L., Silva P.A., Oliveira A. and Dias J.M. (2011a). Evolução morfodinâmica da embocadura da Ria de Aveiro. In *Jornadas da Ria de Aveiro.* University of Aveiro, 187–196.

Plecha S., Rodrigues S., Silva P., Dias J.M., Oliveira A. and Fortunato A.B. (2007). *Trends of bathymetric variations at a tidal inlet.* Taylor & Francis, Netherlands, River, Coastal and Estuarine Morphodynamics: RCEM2007 ed., 19–23.

Plecha S., Silva P., Vaz N., Bertin X., Oliveira A., Fortunato A.B. and Dias J.M. (2010). Sensitivity analysis of a morphodynamic modeling system applied to a coastal lagoon inlet. *Ocean Dynamics*, (60):275–284.

Plecha S., Silva P.A., Oliveira A. and Dias J.M. (2011b). Establishing the wave climate influence on the morphodynamics of a coastal lagoon inlet. *Ocean Dynamics*. Submitted.

Plecha S., Silva P.A., Oliveira A. and Dias J.M. (2011c). Evaluation of single waves effects on the morphology evolution of a coastal lagoon inlet. *Journal of Coastal Research*, SI64:1155–1559.

Plecha S., Silva P.A., Oliveira A. and Dias J.M. (2011d). Modelação morfodinâmica da embocadura da Ria de Aveiro. In *Conferência sobre Morfodinâmica Estuarina e Costeira*. Lisbon, Portugal.

Plecha S., Silva P.A., Oliveira A. and Dias J.M. (2011e). *Sediment Transport Modelling and Morphological Trends at a Tidal Inlet*. 8, INTECH, 163–186.

Pugh D.T. (1987). *Tides, Surges and Mean-Sea Level*. John Wiley and Sons, 472 pp.

Ranasinghe R. and Pattiaratchi C. (1999). The seasonal closure of tidal inlets: Wilson inlet—a case study. *Coastal Engineering*, 37:37–56.

Ranasinghe R. and Pattiaratchi C. (2003). The seasonal closure of tidal inlets: causes and effects. *Coastal Engineering Journal*, 45(4):601–627.

Ranasinghe R., Pattiaratchi C. and Masselink G. (1999). A morphodynamic model todmulate the seasonal closure of tidal inlets. *Coastal Engineering*, 37:1–36.

Robins P.E. and Davies A.G. (2010). Morphological controls in sandy estuaries: the influence of tidal flats and bathymetry on sediment transport. *Ocean Dynamics*, 60:503–517.

Rodrigues M., Oliveira A., Queiroga H., Fortunato A.B. and Zhang Y.J. (2009). Three-dimensional modeling of the lower trophic levels in the Ria de Aveiro (Portugal). *Ecological Modelling*, 220:1274–1290.

Roelvink J.A. and Banning G.K.F.M. (1994). Design and development of Delf3D and application to coastal morphodynamics. *Hydroinformatics*, 94:451–455.

Rosa J., Gonçalves D., Silva P.A., Pinheiro L.M., Rebêlo L., Fortunato A.B. and Bertin X. (2011). Estudo da evolução de uma área de extracção de sedimentos ao largo de Vale de Lobo (Algarve - Portugal) - Comparação entre resultados numéricos e dados batimétricos adquiridos. *Revista de Gestão Costeira Integrada*, 11(3):369–377.

Schwartz M.L. (1973). *Barrier islands*, Vol. 9. Stroudsburg, 451 pp.

Silva A.J.R., Leitão J.C. and Abecassis C. (2004). Improving the navigability and safety conditions in Douro estuary inlet. In *Proceedings of International Conference in Coastal Engineering 2004* (ASCE, ed.). 3277–3289.

Silva J. and Duck R.W. (2001). Historical changes of bottom topography and tidal amplitude in the Ria de Aveiro, Portugal - trends for future evolution. *Climate Research*, 18:17–24.

Silva P., Bertin X., Fortunato A.B. and Oliveira A. (2009). Intercomparison of sediment transport computations in current and combined wave-current conditions. *Journal of Coastal Research*, SI56:559–563.

Silva P., Temperville A. and Santos F.S. (2006a). Sand transport under combined current and wave conditions: A semi-unsteady, practical model. *Coastal Engineering*, 53:897–913.

Silva P.A., Ramos M., Almeida M. and Dubert J. (2006b). Water exchange mechanisms between Ria de Aveiro and the Atlantic Ocean. *Journal of Coastal Research*, SI39:1622–1626.

Silvio G.D., Dall'Angelo C., Bonaldo D. and Fasolato G. (2010). Long-term model of planimetric and bathymetric evolution of a tidal lagoon. *Continental Shelf Research*, 30:894–903.

Sistermans P. and van der Graaff J. (2001). *Intercomparison of Model Computations.* 2nd ed, Aqua Publications, SEDMOC-sediment transport modelling in marine coastal environments ed., CK 1–10.

Smith J.M., Sherlock A.R. and Resio D.T. (2001). *Steady-state Wave Model User's Manual for STWAVE. V3.0.* U.S Army Engineer Research and Development Center, Vicksburg.

Soulsby R. (1997). *Dynamics of Marine Sands - A Manual for Pratical Applications.*

Soulsby R.L. and Damgaard J.S. (2005). Bedload sediment transport in coastal waters. *Coastal Engineering*, 25:673–689.

Sousa M. and Dias J.M. (2007). Hydrodynamic model calibration for a mesotidal lagoon: the case of Ria de Aveiro (Portugal). *Journal of Coastal Research*, SI50:1075–1080.

Teixeira S.L.R.B. (1994). *Dinâmica Morfosedimentar da Ria de Aveiro (Portugal).* PhD dissertation, University of Lisbon, Portugal, 396 pp.

Tolman H.L., Balasubramaniyan B., Burroughs L.D., Chalikov D.V., Chao Y.Y., Chen H.S. and Gerald V.M. (2002). Development and implementation of wind generated ocean surface wave models at ncep. *Weather and Forecasting*, 17:311–333.

Tomás J.M.V. (1995). *Caracterização Morfológica e Textural do Litoral entre Espinho e Cabo Mondego (Portugal).* Tese de Mestrado, University of Lisbon, 195 pp.

Tung T.T., Walstra D.J.R., van de Graaff J. and Stive M.J. (2009). Morphological modeling of tidal inlet migration and closure. *Journal of Coastal Research*, SI56:1080–1084.

Valle R., Medina R. and Losada M.A. (1993). Dependence of coeficient K on grain size. *Journal of Waterways, Port, Coastal and Ocean Engineering (ASCE)*, 119(5):568–574.

van de Graaff J. and van Overeem J. (1979). Evaluation of sediment transport formulae in coastal engineering practice. *Coastal Engineering*, 3:1–32.

van Rijn L.C. (1984a). Sediment transport — part 1: bed load transport. *Journal of Hydraulic Engineering*, 110(10):1431–1456.

van Rijn L.C. (1984b). Sediment transport – part 2: suspended load transport. *Journal of Hydraulic Engineering*, 110(11):1613–1641.

van Rijn L.C. (1984c). Sediment transport – part 3: bed forms and alluvial roughness. *Journal of Hydraulic Engineering*, 110(12):1733–1754.

Vaz N. and Dias J.M. (2008). Hydrographic characterization of an estuarine tidal channel. *Journal of Marine Systems*, 70:168–181.

Vaz N., Dias J.M. and Leitão P.C. (2009). Three-dimensional modelling of a tidal channel: the Espinheiro Channel (Portugal). *Continental Shelf Research*, 29:29–41.

Vaz N., Dias J.M., Leitão P.C. and Nolasco R. (2007). Application of the Mohid-2D model to a mesotidal temperate coastal lagoon. *Computers and Geosciences*, 33:1204–1209.

Wai O.W.H., Chen Y. and Li Y.S. (2004). A 3-D wave-current driven coastal sediment transport model. *Coastal Engineering Journal*, 46(4):385–424.

Warner J.C., Geyer W.R. and Lerczak J.A. (2005). Numerical modelling of an estuary: a comprehensive skill assessment. *Journal of Geophysical Research*, 110:C05001.

Warren I.R. and Bach H.K. (1992). MIKE21: a modelling system for estuaries, coastal waters and seas. *Environmental Software*, 7:229–240.

Woodroffe C.D. (2002). *Coasts: Form, Processes and Evolution*. Cambridge University Press, Cambridge, 623 pp.

Work P.A., Guan J., Hayter E.J. and Elçi S. (2001). Mesoscale model for morphological change at tidal inlet. *Journal of Waterway Port Coastal and Ocean Engineering*, 127(5):282–289.

WW - Consultores em Hidráulica e Obras Marítimas SA (2009). *Projecto de Reconfiguração da Barra do Porto de Aveiro - Estudo de Impacte Ambiental*. Tech. Rep., Administração do Porto de Aveiro, S.A., 420 pp.

Xie D., Wang Z., Gao S. and de Vriend H.J. (2009). Modeling the tidal channel morphodynamics in a macro-tidal embayment, Hangzhou Bay, China. *Continental Shelf Research*, 29:1757–1767.

Zhang Y., Baptista A.M. and Myers E.P. (2004). A cross-scale model for 3D baroclinic circulation in estuary-plume-shelf systems: I. Formulation and skill assessment. *Continental Shelf Research*, 110(10):1431–1456.